ISSN 2618-9992

Energy Systems Research

Volume 8, Number 3, 2025

International scientific peer-reviewed journal since 2018

Available online: http://esrj.ru

About the journal

Energy Systems Research is an international peer-reviewed journal addressing all the aspects of energy systems, including their sustainable development and effective use, smart and reliable operation, control and management, integration and interaction in a complex physical, technical, economic and social environment.

Within this broad multi-disciplinary scope, topics of particular interest include strategic energy systems development at the international, regional, national and local levels; energy supply reliability and security; energy markets, regulations and policy; technological innovations with their impacts and future-oriented transformations of energy systems. The journal welcomes papers on advances in heat and electric power industries, energy efficiency and energy saving, renewable energy and clean fossil fuel generation, and other energy technologies.

Energy Systems Research is also concerned with energy systems challenges related to the applications of information and communication technologies, including intelligent control and cyber security, modern approaches of systems analysis, modeling, forecasting, numerical computations and optimization.

The journal is published by Melentiev Energy Systems Institute of Siberian Branch of Russian Academy of Sciences. The journal's ISSN is 2618-9992. There are 4 issues per year (special issues are available). All articles are available online on English as Open access articles.

The journal is indexed in the international database Scopus and included in the Unified Russian List of Scientific Journals ("White List") - level 2. The journal is included in the list of peer-reviewed scientific publications (VAK) in which the main scientific results of dissertations should be published in scientific specialties:
1.2.2. Mathematical modeling, numerical methods and software packages (technical sciences),
2.4.3. Electrical power engineering (technical sciences),
2.4.5. Energy systems and complexes (technical sciences).

Indexed by: Scopus, RSCI, CyberLeninka, Google Scholar, Crossref.

The journal is registered with Roskomnadzor. Certificate Эл № ФС77-84526 January 16, 2023

Topics

- Energy production, conversion, transport and distribution systems
- Integrated energy systems
- Energy complexes
- National, regional, international and global energy systems
- Energy system protection, control and management
- Smart energy systems, smart grids
- Energy systems reliability and energy security
- Electric, gas, oil and heat supply systems
- Energy system development and operation
- System problems of energy consumers
- Energy economics and policy
- Renewable energy and clean fossil fuel-based systems
- Distributed energy systems
- Sustainable energy transitions
- System problems of power and thermal engineering
- Artificial intelligence in energy systems
- Information and communication technologies in energy systems
- Energy system analysis and modelling
- Computational methods and optimization in energy systems

Contacts
Scientific secretary: Alexey Mikheev, Dr. of Eng.
E-mail: info@esrj.ru
Tel: +7 (914) 8950980 (English, Russian)
Address: 130, Lermontov str., Irkutsk, 664033, Russia

CONTENTS

Incorporating System Reliability Criteria into Unit Commitment Models for Electric Power Systems

Yu.E. Dobrynina[1,*], D.S. Krupenev[1]

[1] Melentiev Energy Systems Institute of Siberian Branch of Russian Academy of Sciences, Irkutsk, Russia

***Abstract* — The study aims to analyze unit commitment models and mechanisms within the wholesale electricity and capacity market in Russia and other countries, considering the methodology and criteria for assessing system reliability. The object of the study is the wholesale electricity and capacity markets in Russia, the United Kingdom, the European Union, Australia, and the United States of America. The main principles that govern the electricity markets and regulatory mechanisms within the unit commitment optimization problem are examined and the regulatory framework is analyzed. The main areas for the wholesale electricity and capacity market development with regard to unit commitment are outlined, highlighting the strengths and weaknesses of the regulatory framework that influence this process.**

***Index Terms* — Energy system, unit commitment, system reliability, wholesale electricity and capacity market.**

I. Introduction

In a dynamically developing society, all components undergo changes, and the energy sector is no exception. Finding a solution to the unit commitment optimization problem within the framework of the wholesale energy and capacity market is aimed at maintaining efficient, uninterrupted, and reliable operation of the energy system.

In the Russian Federation, the wholesale electricity and capacity market (WECM) is divided into the electricity market, the capacity market, and the system services market. The electricity market includes the balancing market (BM), the day-ahead market (DAM), and free and bilateral contract markets.

The unit commitment model is applied within the framework of the DAM. According to the regulatory documents, the mathematical model of unit commitment is aimed at minimizing costs (given economic parameters), meeting the constraints (technical parameters). This study involves analyzing the unit commitment model existing on the wholesale electricity market and formulating requirements (areas) for improving the process.

The main objectives of the study are to analyze the unit commitment procedures used in different countries and existing theoretical developments in this area, as well as to formulate proposals that will facilitate adjusting the solution to the UC optimization problem, considering system reliability criteria.

The approaches applied in various countries to solve the UC optimization problem were examined, including the current domestic UC model. Additionally, a comparative analysis was conducted and further areas for the research were identified.

The paper consists of four parts. The main parameters of the current UC model in Russia, given its constraints, are described in the first part. The second part delves into domestic and international experience in organizing the UC process, focusing on the system reliability criteria on the example of the United Kingdom, European Union countries, Australia, and the United States of America. The third part provides a comparative analysis of the current UC models in various countries. The fourth part of presents

* Corresponding author.
E-mail: yulia071294@mail.ru

DOI: 10.25729/esr.2025.03.0001

Received June 16, 2025. Accepted August 19, 2025. Available online November 28, 2025.

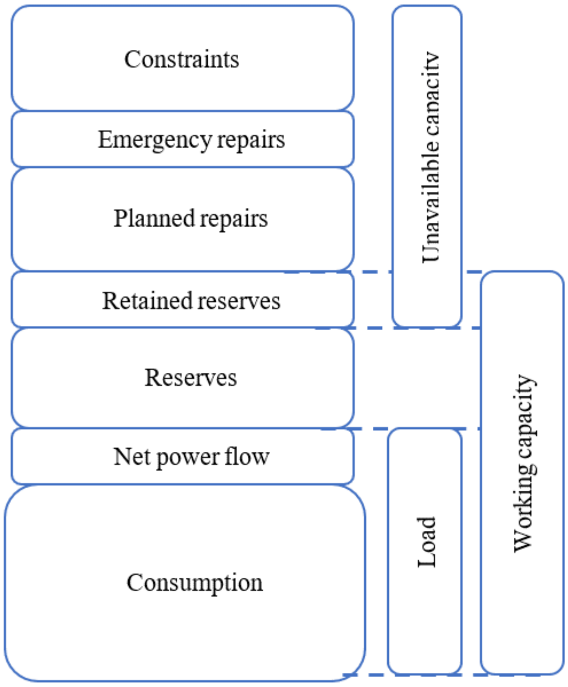

Fig. 1. Structure of capacity balances during peak demand hours.

the conclusions, formulating the main principles and areas for further research.

II. Analysis of Domestic and International Experience in Unit Commitment to Meet the System Reliability Criteria

The WECM in Russia is a mechanism for interaction between numerous entities in the electric power industry, namely, DAM, BM, and market of free and bilateral contracts [1]. Electricity within the WECM price zones can be sold at regulated prices under regulated contracts and at competitive (unregulated) prices under DAM and BM.

Let us consider the structure of balance capacity during peak consumption hours (Fig. 1). Balance capacity is "a system of indicators that shows whether the sum of the power system load values and the required reserve capacity values corresponds to the amount of available capacity."

There are two types of reserves in the capacity balance structure:

– Reserve capacity, which is backup electrical capacity

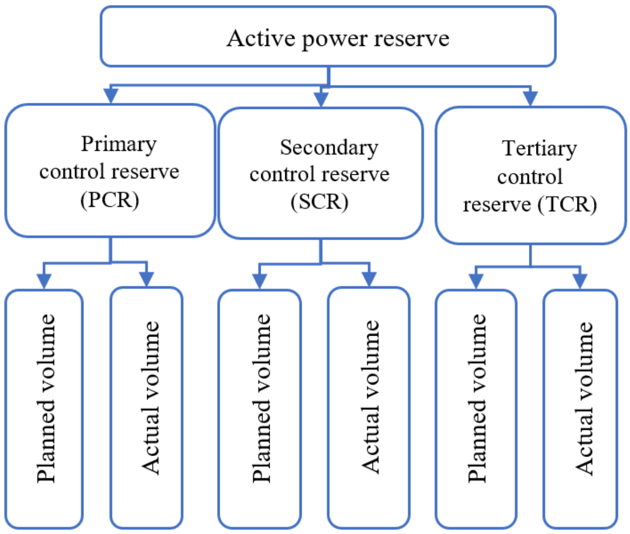

Fig. 2. Active power reserve structure.

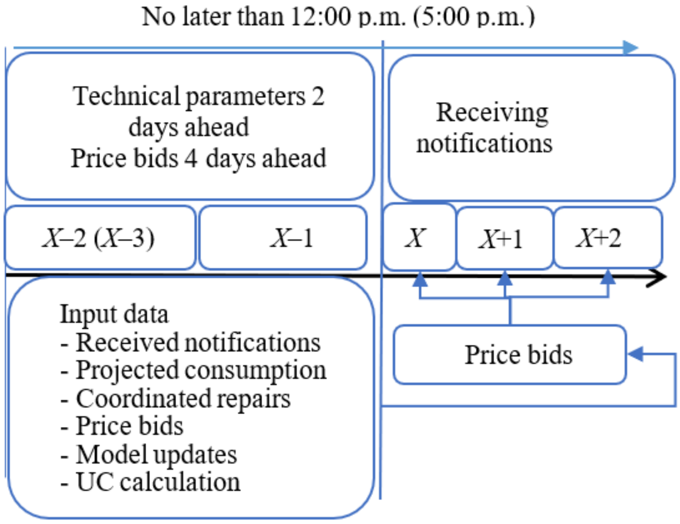

Fig. 3. UC model (daily UC calculation).

considered in design to cover potential changes or additional loads in the future.

– Non-used capacity reserve, which is part of the spinning reserve for loading, supplemental reserve for loading, and cold reserve that cannot be utilized due to network limitations in the electrical network cutsets controlled by the System Operator (SO).

The UC procedure implies the availability of equipment in reserve. At the same time, within the framework of WECM and the current standard, the reserve is divided into three control components and includes primary control reserve (PCR), secondary control reserve (SCR), and tertiary control reserve (TCR). Let us consider the structure of the reserve in detail based on the standard (Fig. 2).

In accordance with the information provided above, the UC procedure accommodates the requirements for maintaining tertiary power reserves (including their geographical location in the Russian Unified Energy System) for the UC period.

The system operator (SO) accumulates information on the minimum parameters of the TCR in accordance with the Methodological Guidelines for Determining the Volumes and Location of Active Power Reserves in the Russian Unified Energy System during Short-Term Power Flow Planning.

The UC optimization problem is solved relying on the regulatory documents governing the WECM activities. From the participants' perspective, the UC process for WECM takes place as shown in Fig. 3.

Based on the input data and using the mathematical model, the SO solves the UC optimization problem, considering power generation forecast schedules, power supply reliability, and reduction in the cost of electrical energy [2]. Based on the results of the UC optimization calculation, the SO determines the unit commitment for day X and makes projection for the period from day $X + 1$ to day $X + 2$ (inclusive) [3].

Following the UC optimization calculation, the SO forms a list of generation equipment to be switched on/off in accordance with the specified power system parameter.

The existing mathematical model uses the following parameters:

Constraints on power flow parameters (system-wide), i.e., on active and reactive power parameters, power flows in network branches depending on voltage, cross-section, reserve level (tertiary control reserve);

Constraints considered by the SO when assigning operating generators, i.e., constraints on electricity generation equipment in terms of minimum required and maximum permissible operating capacity, minimum number of operating generator units, minimum and maximum permissible load;

Constraints related to the power plant process parameters, specified by the WECM participant, i.e., equipment state (non-optimized state, forced state, optimized state, number of generation equipment startups, number of equipment starts and shutdowns at each station on specific operating days).

The UC model optimization problem was previously explored by many authors as an economic problem [4, 5]. The priority area of research was solving the optimization problem from the perspective of company's behavior [3, 6] in WECM. This paper proposes solving the UC problem considering the criteria of system reliability.

In this context, we examine and analyze approaches applied in other countries to solve the UC optimization problem.

The United Kingdom. The UK wholesale electricity market model is aimed at covering costs and maximizing profits.

Adequacy is analyzed within the existing structure of the electricity market, which factors in the adequacy indices (power reserves, regulatory shutdowns of networks and generation equipment).

The new British Electricity Trading and Transmission Arrangements (BETTA) system is a procedure for calculating “imbalance,” which involves comparing the contracted electricity purchased and sold with the measured physical electricity production and consumption [7]. An additional difficulty in regulating the energy system is the location of generation capacities in the northern part of the UK, while the main consumers are located in the southern part.

One of the BETTA activities suggests the Balancing Mechanism according to which System operator identifies the strategy (actions) to maintain balance between producers and consumers [7].

The electrical energy supplied in a specific half-hour interval is sold until the so-called “gate closure,” which occurs one hour before the start of that interval. These data are called the final physical notification and determine the actual energy demand during a given half-hour interval. No further changes to these positions are permitted.

The permanent reserve service preceded the service of Short-Term Operating Reserve (STOR) [8], which is aimed at maintaining and protecting the system (within 20 minutes) in the event of demand shift when suppliers with a short response time enter the market. As part of the STOR action, the response time for electric energy suppliers (reserves) increased from 20 to 240 minutes, resulting in a greater variability among players.

A distinctive characteristic of the UK energy market is a structured and systematic approach to the energy system operation, which factors in the strengths and weaknesses of the special territorial location of generation equipment, transport logistics, and alternative energy sources in the balancing market.

European Union. The European Union's energy markets constitute a structure integrated into the European Energy Exchange (EEX). EEX AG develops, manages, and connects safe, liquid, and transparent markets, promoting emissions regulation in Europe.

European Power Exchange (EPEX) SPOT operates the most liquid day-ahead market through a blind auction with trades on an hourly basis for the day following the settlement day and intraday market, which is a continuous trading platform [9].

According to current legislation, when changing (increasing) capacities, the EU Member States should follow the current reliability standard, while calculating the value of lost load (VoLL).

VoLL is the value attributed by consumers to unused energy [10]. It represents the maximum price that consumer is willing to pay for energy supply at the established price for consumers: when electricity is supplied, they pay the established price; when there is no supply, consumers pay nothing [11].

The analysis of the power system reliability in the EU is carried out within the framework of the European Network of Transmission System Operators for Electricity (ENTSO-E) [12]. The System Operator acts as the main regulator of resource adequacy assessment through the national reliability assessment [13].

The European energy system includes both traditional and alternative energy sources, which makes it much more difficult to ensure reliable and sustainable operation of the energy system. A centralized approach to energy system management used in the European Union is shifting to an integrated one, with bids submitted simultaneously.

Australia. Australia has a Wholesale Electricity Market (WEM) and the National Electricity Market (NEM). NEM is Australia's main electricity market, serving 88% of the population.

The Australian energy market operator (AEMO) regulates activities in the energy market in Australia. In the current architecture of the energy system, it is essential to maintain a balance between production and consumption in order to prevent emergency shutdowns.

Generators send bids every 5 minutes on a daily basis [14]. AEMO solves the UC optimization problem based on the principle of minimizing costs and choosing the most efficient generator.

AEMO distributes the load by sending automatic generation control signals, while considering the technical parameters of each generation unit. Within the framework of the AEMO, there is a Reliability and Emergency Reserve Trader (REPT), which provides reserves at

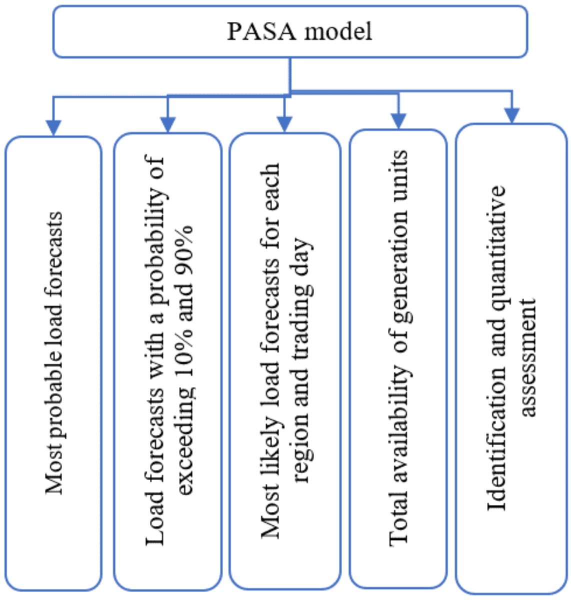

Fig. 4. Publication settings within a short-term PASA.

various time intervals (from 3 hours to 7 days).

The RERT panel allows AEMO to conduct an accelerated tender process in short- and medium-term notification situations [15].

NEM reliability standards are set by the Reliability Panel of Australian Energy Market Commission. In accordance with current standards, the energy unserved should not exceed 0.002% of the region's annual consumption. At the same time, it is necessary to ensure the transfer of 850 MW as a reserve, within the framework of NEM [16].

Reliability level is measured through the energy unserved, i.e., the amount of energy required by consumers, which cannot be supplied due to a lack of capacity.

Projected Assessment of System Adequacy (PASA) model/mechanism is presented in Fig. 4. PASA is a comprehensive program that collects, analyzes, and provides information on the medium- and short-term security of the power system and the reliability of supply prospects [17].

The PASA mechanism aids in strengthening system reliability within the established regulatory framework and sends notifications to AEMO in the event of detected deviations.

The energy market is structured to provide the confidentiality of data sent by AEMO participants, which is outlined in the relevant regulatory documents, while market participants have the opportunity to adjust the submitted applications (daily, every 5 minutes). In turn, the Russian System Operator regulates the time for submitting a bid 3 days before the model calculation, allows adjustments before a set time *X*, and publishes the calculated (selected) data on the website.

The United States of America. The energy market in the United States of America is geographically decentralized and is divided by states, each with its state-specific regulatory frameworks that govern their activities, UC approaches, structures of market players, and other indicators.

There are 2 types of operators in the United States: Independent System Operator (ISO) and Regional Transmission Organization (RTO).

In the event of poor service (poor performance of obligations to consumers) in maintaining the agreed load, penalties are imposed to ensure the required volume.

Let us consider the features of the Pennsylvania-New Jersey-Maryland (PJM) Interconnection energy market in terms of reliability. The market provides reliability through quick-response reserve options: frequency control (the decision must be made within 5 minutes after the signal is received), rotating frequency reserve (the decision must be made within 10 minutes after the signal is received), and a day ahead (the decision must be made within 30 minutes after the signal is received in real time).

California Independent System Operator (CAISO)

TABLE 1. Analysis of Wholesale Electricity Markets in Various Countries

Indicators	Russian Federation	United Kingdom	EU	Australia	USA
Number of price zones	2+non-price zones	3 zones combined into 1	28	1	21
SO role	Central control, strong regulator	Central control, single regulator	Central control, single regulator	Central control, strong regulator	Energy exchange operator, close interconnection among participants, while maintaining independence
Planning features	Approved forecasts, key indicators	Energy system performance targets	–	–	–
Transparency:					
Information disclosure, regulations	+ Structured information available on the relevant portals	+ Structured information available on the main portal	+ General information available on a single portal, no access to some sources	+ Structured information available on relevant portals, information disclosure upon request	+ General information available on a single portal, structured information available on relevant portals
Calculation mechanism disclosure	+/– The main model (basic equation) is publicly available, but there is a lack of transparency in the final decision formation	– Lack of freely available basic UC calculation model (basic equation)	– Lack of freely available basic UC calculation model (basic equation)	+/– Lack of freely available basic UC calculation model (basic equation) Regulations contain a descriptive section	– Lack of freely available basic UC calculation model (basic equation)
Disclosure of input, intermediate, and final information	+/– No information on input and intermediate data is available; the portal provides final calculation results	+/– No information on input and intermediate data is available; the portal provides final calculation results	+/– No information on input and intermediate data is available; the portal provides final calculation results	+/– Partial information is available on the portal, by area of activity; disclosure of information mainly upon request	+/– No information on input and intermediate data is available; the portal provides final calculation results
Reserve volume regulation	Standard, TCR	STOR	No data	RERT	Operational reserve a day ahead
Bid submission	4 (3) days before each hour of the day until time *X* and 2 days ahead	Every 30 minutes, one hour before time *X*	Blind auction once a day on the following day	Daily, every 5 minutes	In advance

operates the wholesale electricity market and ancillary services market in 80% of California territory and a small part of Nevada in the United States [18, 19].

Based on the data selection, relying on the submitted bids, a customized consumption schedule is generated for each territory within the CAISO. The price and offer are calculated and entered into the software for further processing, while also considering technical constraints. Based on the available data, the program calculates the maximum price level at various nodes.

Reliability within CAISO is ensured by the Reliability Demand Response Resource (RDRR), which supplies electricity within 40 minutes and in the amount of at least 0.5 MW at the command of the system operator.

The level of reliability in the US power grid is considered through the N-1 reliability criteria, factoring in the aspect of redundancy determined by the territorial features. The energy market model and reliability criteria find a response in the domestic energy system.

III. COMPARISON OF THE UC PROCESS IN DIFFERENT COUNTRIES

The analysis of the energy markets reveals the different approaches used to solve the UC optimization problem. The main features of each energy market are presented in Table 1.

Solving the UC optimization problem involves considering additional criteria of system reliability.

Recent years has seen a significant leap forward in solving optimization problems, including the UC problem, new approaches and methodologies have been developed, and various hypotheses have been put forward, which are currently being investigated. The UC optimization problem is solved by selecting the generator units, focusing on the optimal load curve and production level (capacities involved) in the power system at a specific time span to meet power system constraints [20, 21]. A wide range of methodologies can be employed to solve the UC optimization problem. Traditional approaches include stochastic, software, and numerical methods, while more sophisticated methods encompass exhaustive enumeration (the enumeration of all possible outcomes or truth values for a given set of statements); expert system (expert assessment) [22] based on an algorithm for collecting information and determining a behavior strategy; priority lists; fuzzy logic; and neural networks.

The search for an optimal solution to the UC optimization problem takes into consideration not only the initial technical conditions, the specifics of the power system, and territorial parameters, but also climatic features [23–25], along with the established practice in addressing emergencies and measures to prevent them. Emergencies are inevitable, and the nature of their occurrence suggests different solutions, but solving the UC optimization problem in terms of the system reliability indices facilitates avoiding critical moments and, in some cases, managing without disconnection and load shedding.

The UC optimization problem has been relevant for many decades. Current realities suggest unifying the problem-solving approach, i.e. combining several methods and techniques, which will expand the research methods variability.

IV. Conclusion

1. The UC optimization problem stands as a challenge within the energy sector and addressing it is both practical, because it allows real-time assessment of the outcomes, and scientifically significant. The variety of approaches and methods enriches our understanding of this issue, which contributes to the search for a solution to the UC optimization problem within different (related) scientific domains.

2. A structured approach to the study of the energy market fosters the optimal distribution of the price burden, accommodating the strengths and weaknesses of the energy system for the competent distribution of the opportunities available to players.

3. The study conducted reveals the need to introduce additional criteria for considering system reliability to achieve the optimal unit commitment.

4. Solving the UC optimization problem based on system reliability enables each player to assess their capabilities alongside the potential of other players (technical capabilities, economic component). Further in-depth study in this area is required across all levels of the energy system.

References

[1] V. V. Lebedev, “Development of the electricity market in Russia – history and statistics of reform results,” Russian Online Economic Magazine, no. 1, Art. no. 10, 2022. [Online] Available: https://www.elibrary.ru/item.asp?id=48367467. Accessed on: Feb. 15, 2025. (In Russian).

[2] Official website of the System Operator of the Unified Energy System. Available: https://www.so-ups.ru. Accessed on: Feb. 12, 2025. (In Russian)

[3] E. K. Arakelyan, A. V. Andryushin, S. V. Mezin, et al, “Problems of accounting for the reliability factor when selecting the composition of generating equipment of the CHPP in the wholesale electricity market and ways to solve them,” Automat. Remote Control, vol. 83, no. 5, pp. 792–804, 2022. DOI: 10.1134/S0005117922050101.

[4] A. Yu. Amelina, E. M. Lisin, Yu. A. Anisimova, W. Strielkowsky, “The optimal strategic choice of generating company behavior on the day-ahead market in conditions of market regulation,” Science Vector of Tolyatti State University, vol. 4, pp. 63–68, 2013. (In Russian)

[5] A. V. Seleznev, “Software package for solving the unit commitment problem in a competitive electricity market environment in Russia,” in Proc. the 7th International Conference “Management of the development of large-scale systems (MLSD'2015),” September 29 – October 1, 2015, Moscow, Trapeznikov Institute of Control Sciences of the Russian Academy of Sciences, 2015, vol. 1, pp. 281–290. (In Russian)

[6] O. V. Pastukhov, “Increasing the accuracy of optimal unit commitment,” in Proc. the VII International Youth Scientific and Technical Conference “Electric Power Industry through the Eyes of Youth – 2016,” September 19–23, 2016, Kazan', Kazan State Energy University, 2016, vol. 2, pp. 347–350. (In Russian)

[7] Official website of Balancing and Settlement Code (BSD). Available: https://bscdocs.elexon.co.uk. Accessed on: Jan. 5, 2025.

[8] Official website of National Energy System Operator (NESO). Available: https://www2.nationalgrideso.com. Accessed on: Jan. 12, 2025.

[9] G. Fridgen, A. Michaelis, M. Rinck, M. Schöpf, M. Weibelzahl, “The search for the perfect match: aligning power-trading products to the energy transition,” Energy Policy, vol. 144, Art. no. 111523, 2020. DOI: 10.1016/j.enpol.2020.111523.

[10] ACER Security of EU electricity supply in 2021: Report on Member States approaches to assess and ensure adequacy October 2022. Available: https://emissions-euets.com/european-resource-adequacy-assessment-eraa?highlight=WyJlcmFhIl0=. Accessed on: Jan. 25, 2025.

[11] Official portal of the European Union Emissions Trading System – legal point of view. Available: https://emissions-euets.com. Accessed on: Feb. 12, 2025.

[12] Official website of ENTSO-E. Available: https://www.entsoe.eu/. Accessed on: Jan. 27, 2025.

[13] G. Ragosa, J. Watson, M. Grubb, "The political economy of electricity system resource adequacy and renewable energy integration: a comparative study of Britain, Italy, and California," Energy Research & Social Science, vol. 107, Art. no. 103335, 2024. DOI: 10.1016/j.erss.2023.103335

[14] C. Cornell, N. T. Dinh, S. A. Pourmousavi, "A probabilistic forecast methodology for volatile electricity prices in the Australian national electricity market," International Journal of Forecasting, vol. 40, no. 4, pp. 1421–1437, 2024. DOI: 10.1016/j.ijforecast.2023.12.003

[15] A. Prakash, R. Ashby, A. Bruce, I. MacGill, "Quantifying reserve capabilities for designing flexible electricity markets: An Australian case study with increasing penetrations of renewables," Energy Policy, vol. 177, Art. no. 113551, 2023. DOI: 10.1016/j.enpol.2023.113551.

[16] International Energy Agency World Energy Outlook 2023. Available: https://www.iea.org/contact. Accessed on: Jan. 12, 2025.

[17] Official website of Australian Energy Market Operator. Available: https://aemo.com.au/. Accessed on: Jan. 12, 2025.

[18] E. Wachs, B. Engel, "Reliability versus renewables: modeling costs and revenue in CAISO and PJM," The Electricity Journal, vol. 33, no. 10, Art. no. 106860, 2020. DOI: 10.1016/j.tej.2020.106860.

[19] S. Westgaard, S.-E. Fleten, A. Negash, A. Botterud, K. Bogaard, T. H. Verling, "Performing price scenario analysis and stress testing using quantile regression: a case study of the Californian electricity market," Energy, vol. 214, Art. no. 118796, 2021. DOI: 10.1016/j.energy.2020.118796.

[20] A. F. Castelli, I. Harjunkoski, J. Poland, M. Giuntoli, E. Martelli, I. E. Grossmann, "Solving the security constrained unit commitment problem: Three novel approaches," International Journal of Electrical Power & Energy Systems, vol. 162, Art. no. 110213, 2024. DOI: 10.1016/j.ijepes.2024.110213.

[21] A. I. Cohen, V. R. Sherkat, "Optimization-Based Methods for Operations Scheduling," IEEE Transactions, vol. 75, no. 12, pp. 1574–1590, 1987. DOI: 10.1109/PROC.1987.13928.

[22] Appendix No. 3.1 to the Agreement on Accession to the Wholesale Market Trading System Regulations for Unit Commitment Calculation with amendments dated by April 23, 2025 (Minutes No. 12/2025 of the meeting of the Supervisory Board of the NP Market Council Association). (In Russian)

[23] Policy Paper of Department for Energy Security & Net Zero UK (2025, Mar. 28). NESO review into the North Hyde Substation outage: terms of reference. [Online]. Available: https://www.gov.uk/government/publications/review-into-the-north-hyde-substation-outage-terms-of-reference/neso-review-into-the-north-hyde-substation-outage-terms-of-reference. Accessed on: Mar. 30, 2025.

[24] V. Yu. Elpidiforov, "A blackout in the UK power grid that led to a large-scale power outage in August 2019," Electric Power. Transmission and Distribution, no. 1(58), pp.152–159, 2020. (In Russian)

[25] N. I. Voropai, D. S. Krupenev, S. V. Podkovalnikov, S. M. Senderov, "Two energy collapses – in Texas, USA and in Primorsky Krai, Russia," Electric Power. Transmission and Distribution, no. 4(67), pp. 166–174, 2021. (In Russian)

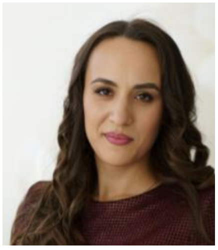

Yulia Dobrynina is currently a postgraduate student at Melentiev Energy Systems Institute SB RAS. Her research interests include wholesale electricity and capacity markets, unit commitment.

Dmitry Krupenev received the Ph. D. degree in Electrical Engineering in 2011. He is currently the Head of a laboratory at the Melentiev Energy Systems Institute of the Siberian Branch of the Russian Academy of Sciences. His research interests include methods for assessing the adequacy of power systems; methods for determining the optimal reserve levels of generation capacity for long-term planning of the development of electric power systems; and modeling the interlinked operation of energy systems to investigate reliability and energy security issues.

A Methodological Approach for Scenario Modeling of the Integrated Wind, Solar, And Small Hydro Power Output to Cost-Effectively Meet the Peak Power Demand in Power Systems

N.R. Rakhmanov[1], G.B. Guliyev[2,*], F.Sh. Ibragimov[2]

[1] Azerbaijan Energy Research and Engineering Design Institute, Baku, Azerbaijan
[2] Azerbaijan Technical University, Baku, Azerbaijan

***Abstract* — This study contributes a methodological framework for identification of a holistic model of power output by multiple renewable power plants integrated into a power system at locations with distinct meteorological and geographical conditions. The scenarios generated based on individual predictions relying on $k-$medoids clustering demonstrate better capturing of the variable nature of the total output from multiple renewable power plants. A case study of the integration of several renewable power plants into a power system is presented to show that the direct prediction of the total output by these green sources proves effective in cutting operational costs of the system, mostly by better serving the peak load demand. The methodological framework proposed in this paper can be used for online management of power systems with several different renewable power plants such as solar power plants, wind farms, and small hydropower plants. This approach also enables the estimation of the contribution of each source to the overall output.**

***Index Terms* — Power system, renewable energy sources, serving electricity demand, online management, load profile, aggregation of renewable power plants.**

* Corresponding author.
E-mail: huseyngulu@mail.ru

DOI: 10.25729/esr.2025.03.0002

Received August 20, 2025. Accepted August 25, 2025. Available online November 28, 2025.

I. Introduction

The drastically increased penetration of renewables is a key factor defining the process of transformation of the power sector. Over the last four decades, the total output of electricity in the world has increased by more than 25% and the global installed capacity of power plants running on renewables reached as much as 3 870 GW in 2023. In 2024, renewables accounted for over 90% of new capacity additions that total about 585 GW [1].

Among all renewables integrated into power systems around the world, wind farms (WF), solar power plants (SPP), and hydropower plants lead in renewable energy production. In 2024, the installed capacity of PV plants was at 1 900 GW, surpassing the capacity of nuclear power plants by a factor of 5 [2]; and that of wind farms reached over 1 000 GW [3]. Unlike conventional electricity sources, wind farms, solar power plants, and small hydropower plants (sHPP) are usually sited in the areas with 'critical' meteorological conditions where winds and solar radiation persist for extended periods of time, thus ensuring the availability of renewable energy potential in these locations. Power output of sHPP, WF, and SPP is indeterminate and stochastic as it depends on meteorological conditions in the areas of their installation. In order to offset the random fluctuations in the power system induced by intermittent renewable generation, the system is provided with an additional source of energy. The choice of the additional source depends on technical and economic capabilities of the system as well as meteorological conditions in given areas [4–7]. Stable and efficient operation of power systems with integrated WF, SPP, and sHPP requires an in-depth analysis of intermittent power generation by these plants. This analysis should be complemented by forecasting models that reflect the current time and factor in meteorological data.

The findings from the scenario analysis of complementarity of wind farms and solar power plants and their use to serve the demand in the power system parts that lack renewable generation are presented in [10–15]. Spatial and temporal changes in climate variables are examined in [16, 17] to prove that the ability to meet the demand in a power system with wind farms and solar power plants can be enhanced by the additional output resulting from complementarity of such plants located in the areas with diverse geographical and climate conditions. The studies [18–20] rely on correlation analysis of different geographical areas with operating wind farms and solar power plants to establish that in areas with higher penetration of wind power than in other areas with lesser penetration of renewables, adding solar power can help meet the demand and offset its intermittency [20–24].

This study presents a methodological framework for identification of scenarios of joint generation for intermittent renewable energy sources placed in the areas with different geographical and weather conditions.

II. Method for Identifying Scenarios of Combined Power Generation in Individual Power System Parts with Wind Farms, Solar Power Plants, and Small Hydropower Plants

A. *Cluster Analysis of Changes in the Output of Wind Farms and Solar PV Power Plants Given Meteorological Conditions of Areas and Their Integration*

At its core, the identification of aggregated generation relies on cluster analysis of stochastic processes governing intermittent output of wind farms, solar power plants, and hydropower plants to extract clusters with identical parameters that meet some specified criteria.

Establishing relationships for the aggregated power output from wind farms, solar power plants, and hydropower plants connected to the power system in its different areas enables the identification of key defining features of models of such relationships. This approach filters out the effects of individual areas with integrated renewable power plants and groups the points of the power grid topology exhibiting similar patterns of power generation.

Identification of scenarios of combined power output from power plants running on renewable energy is a key step in assessing prospective capacity additions of wind farms, solar power plants, and hydropower plants in the power system during the planning horizon. Cluster analysis proves effective in terms of precision and detail in capturing data on intermittency of renewable energy potential and weather conditions in geographical areas.

This study leverages *k*-medoid clustering to identify patterns in power output of wind farms, solar power plants, and hydropower plants installed in the power system. The *k*-medoid clustering model can have the following form [19]:

$$D = \arg\min\left\{\sum_{k=1}^{k}\sum_{n=1}^{k}\left(\left\|x_n - C_k\right\|^2\right)\right\}, \tag{1}$$

$$x_n = \begin{vmatrix} w_{1,1} & w_{1,2} & \cdots & w_{1,i} \\ w_{2,1} & w_{2,2} & \cdots & w_{2,i} \\ \vdots & & & \\ w_{n,1} & w_{n,2} & \cdots & w_{n,i} \end{vmatrix}, \tag{2}$$

where D is the distance between the current values of hourly changes and the medoid of each cluster; C_k is the *k*-th cluster medoid; n is he number of measured parameters; $w_{n,i}$ is power outputs of renewable power plants, power system loads, wind speed, solar radiation, ambient temperature, etc. to be grouped into *k*-clusters $(k < n)$; i is the number of renewable power plants. The clustering algorithm is applied separately to each renewable power plant and the entire area with installed wind farms, solar power plants, and hydropower plants.

B. *Algorithm for Choosing the Scenarios of the Most Cost-Effective Capacity Additions of Wind Farms and Solar Power Plants to Meet the Expected Demand Growth in the Power System*

The optimization technique applied makes use of linear objective functions to evaluate possible expansion scenarios for wind farm, solar power plant, and hydropower plant capacities installed before 2024. The algorithm that relies on the above method proves exceptionally useful because it is simpler than its alternatives based on heuristic search techniques. The function of demand variability is treated as the “net” load N_{net} (the total demand less the total output by all renewable power plants). The subsequent period of the N_{net} increase by ΔN_{net} implies the expansion of wind

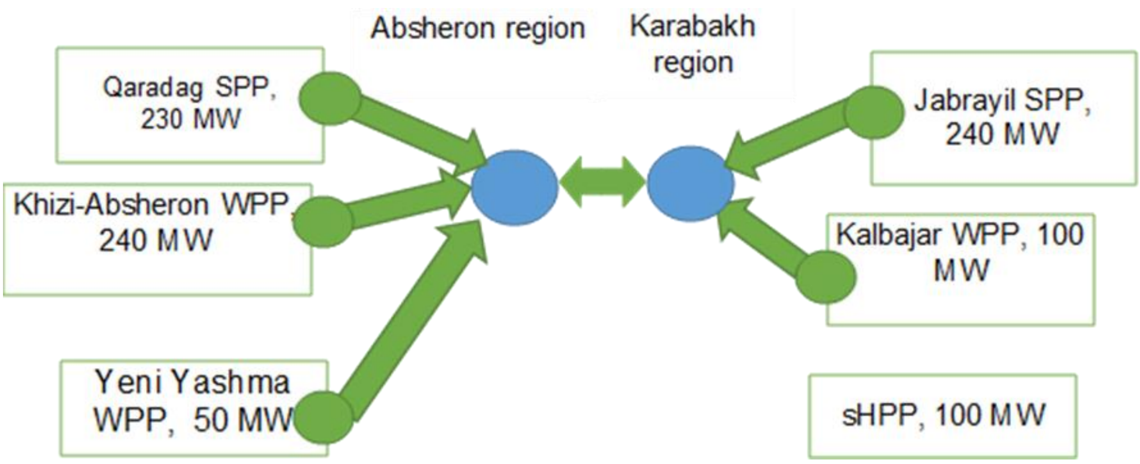

Fig. 1. Overall layout of operating intermittent renewable sources located in two regions of Azerbaijan.

farms, solar power plants, and hydropower plants during the same period combined so as to optimally serve the demand for ΔN_{net}. The objective functions utilized to identify scenarios of expansion for renewable power plants installed in the power system are as follows:

1. The minimum mean square error of the random variable of annual change in the net load (NS_{demand})

$$SO(z) \to \min . \qquad (3)$$

2. The minimum mean square error of the net load by hour during the year:

$$SO(z) = \sqrt{\frac{\sum_{t=1}^{T}\left(z(t)-\bar{z}\right)^2}{T-1}} \to \min \ \forall t \ , \qquad (4)$$

where $z(t) = N_{net}(t_{hour})$ is changes in the net load by hour during a single year; $T = 8760$ h; $\bar{z}$ is the average hourly change in load by hour during a single year. Minimization of functions (3) and (4) has the following solutions:

$$z(t_{year}) = N_{net}(t_{year}) \ \forall t_{year} \qquad (5)$$

and

$$z(t_{hour}) = N_{net}(t_h) - N_{net}(t_{h-1}) \ \forall t_h . \qquad (6)$$

Solutions (5) and (6) meet the constraints on the annual power output of renewable energy plants up to 30% of demand (under the assumption that by 2030 wind farms and solar power plants will serve up to 30% of demand in Azerbaijan's power system):

$$30\left\{\sum_t \frac{P_{(WF+SPP+HPP)}(t)}{N_{net}(t_h)}\right\} \le N_{net\max} \qquad (7)$$

subject to

$$N_{net}(t) = P_{demand}(t) - \left(P_{WF}(t) + P_{SPP}(t) + P_{HPP}(t)\right) \forall t \ , \qquad (8)$$

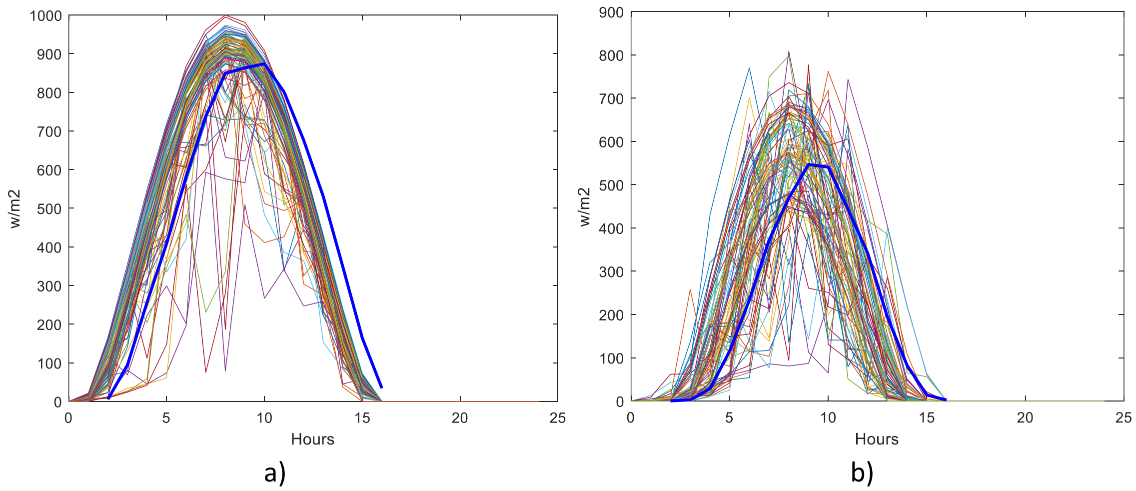

Fig. 2. Clusters of solar radiation in the regions of Absheron (a) and Karabakh (b).

$$\begin{aligned} P_{WF}(t)+P_{SPP}(t) &= \sum_{R}\sum_{it} N_{WF}(it,r_W)P_{WF}(t,r_{WF})+ \\ &+\sum_{r_{SPP}}\sum_{it} N_{SPP}(it,r_{SPP})P_{SPP}(t,r_{SPP})+ \\ &+\sum_{r_{HPP}}\sum_{it} N_{HPP}(it,r_{HPP})P_{HPP}(t,r_{HPP}), \\ &\forall t,\forall it,\forall r_{WF},\forall r_{SPP}\ , \end{aligned} \tag{9}$$

$$VRE_{surplus}(t)=\begin{cases} VRE(t)-S_{demand}(t), & VRE(t)>S_{demand}(t), \\ 0, & VRE(t)\le S_{demand}(t), \end{cases}, \tag{10}$$

$$z, NL, VRE, VRE_{surplus,}\ N_{WF},\ N_{SPP}, N_{HPP}\in NR, \tag{11}$$

where $t\in[t_1,t_2,...,t_{8760}]$ represents indices of the hourly power output from renewables by time; $it\in[it_1,it_2,...,it_m]$ is the number of renewable energy units at power plants; $r_{SPP}\in[r_{SPP1},r_{SPP2},...,r_{SPPM}]$, $r_{WF}\in[r_{WF1},r_{WF2},...,r_{WFN}]$, and $r_{HPP}\in[r_{HPP1},r_{HPP2},...,r_{HPPK}]$ are the number of areas with installed renewable power plants. $VRE_{surplus}$ is surplus output of renewable power plants; $P_{WF}(t)$, $P_{SPP}(t)$, and $P_{HPP}(t)$ stand for hourly generation from wind farms, solar PV power plants, and hydropower plants. In equations (7)–(11), N_{WF} and N_{SPP} are the number of wind farms and solar power plants as determined by the optimization algorithm for wind and solar power output models.

III. Scenario Analysis of Combined Power Output of Wind Farms and Solar Power Plants for Supply and Demand Planning

A. Key Data on Meteorological Conditions and Power Output of Wind Farms, Solar Power Plants, and Hydropower Plants in Individual Regions

The installed capacity of the Azerenergy system is about 7.5 GW, the largest share of which comes from gas turbine

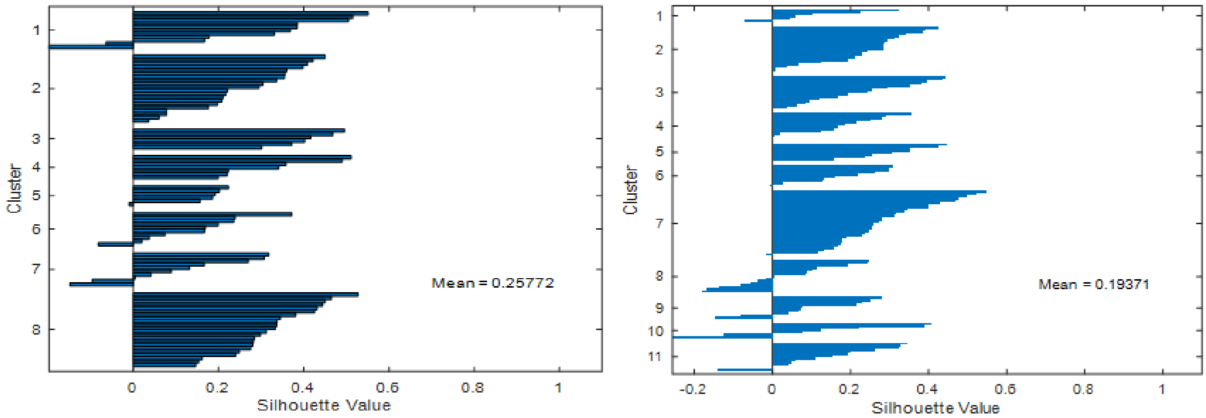

a) b)

Fig. 3. Silhouette values of optimal numbers for clusters of wind speeds: (a) for the 1st cluster of radiation and loads; (b) for the 2nd cluster of radiation and loads.

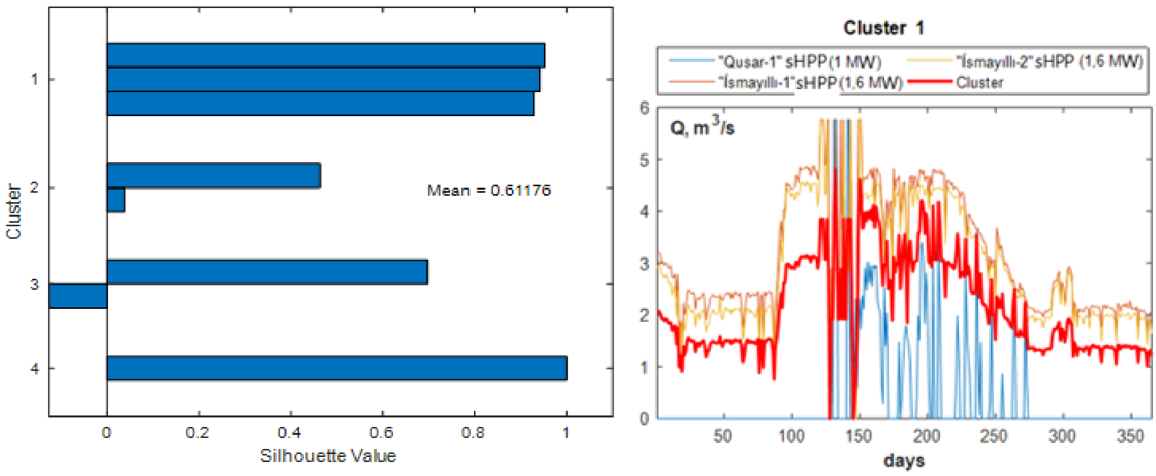

a) b)

Fig. 4. Clustering by the total annual water flow rate (a) and flow rates for individual sHPPs (b).

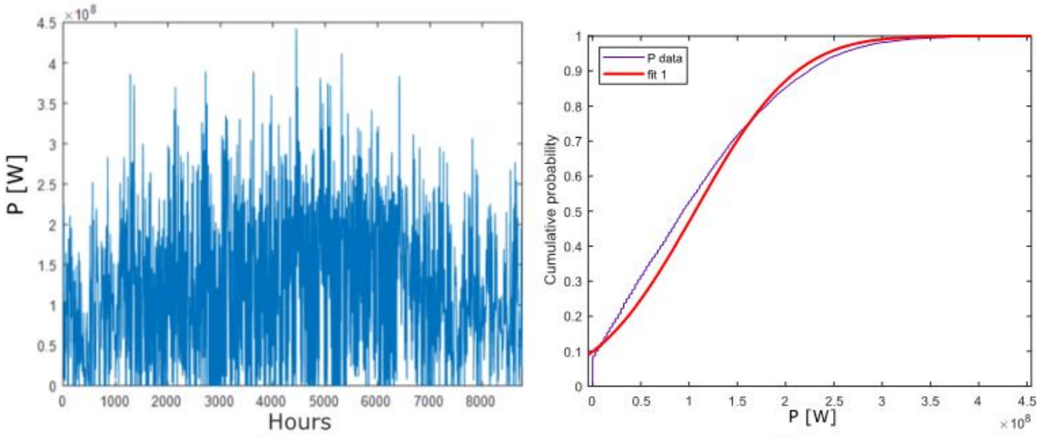

a) b)

Fig. 5. Annual power output of SPP-WF in the Absheron region (a) and probability of distribution of the annual power output (b).

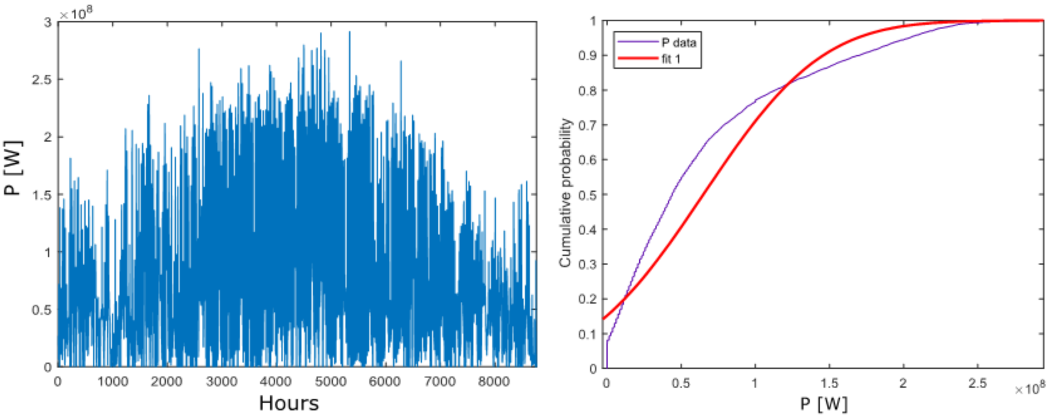

a) b)

Fig. 6. Annual power output of SPP-WF-sHPP in the Karabakh region (a) and probability of annual power output (b).

thermal power plants (about 5.6 GW), followed by hydropower plants (1.4 GW). Wind farms, solar power plants, and small hydropower plants combined contribute 0.5 GW. In 2004, renewable power plants generated 850 mln kWh, of which 6% was generated by wind farms, 67% – by solar power plants, and 27% – by small hydropower plants. Wind and solar power potential is primarily concentrated in two major geographical and economic regions of the country: the Absheron region (including the coastal areas of the Caspian Sea) and the Eastern Zangezur region (including the Karabakh region). This is the reason for the placement of wind farms, solar power plants, and hydropower plants in those regions. Figure 1 shows the overall layout of wind farms and solar power plants in the regions of Absheron and Karabakh. As of 2023, there were two wind farms operating in the Absheron region, including the 240 MW Khizi-Absheron wind farm and the 50 MW Yeni-Yashma wind farm. The Karabakh renewable power plants connected to the power grid include the 240 MW Jabrayil SPP, 100 MW Kalbajar wind farm, and sHPPs with a total capacity of 170 MW.

B. Clustering of Power Output from Renewable Power Plants in the Region Given Meteorological Conditions

Figure 2 shows clusters of solar radiation in the regions. Solar irradiance in the regions makes it possible to generate electric power by solar power plants for most of the day.

The silhouettes in Fig. 3 and 4 show the number of significant clusters of wind and hydro power with the corresponding clusters of system loads.

IV. Results From the Analysis of Scenarios of Combined Power Output from Green Renewable Sources Located in the Areas with Distinct Meteorological and Climate Conditions

The cluster analysis was performed to identify common scenarios of power output in each region as well as cross-regional interactions. The analysis relied on hourly measurements of demand in the power grid and meteorological data. The meteorological data (wind speed, solar radiation, and ambient temperature) were collected hourly during a single year in two regions (see. Fig. 1) with installed renewables.

Figures 5 and 6 show, respectively, the power output and probability of its distribution among wind farms, solar power plants, and hydropower plants located in the Absheron and Karabakh regions in 2024.

The mean-square error of the power output of wind farms is derived from wind power potential. The wind farm output is a key factor to decide on the feasibility of complementarity of wind farms in the region.

V. Conclusion

1. This study proposes a clustering-based algorithm for identification of power output scenarios for wind farms, solar power plants, and hydropower plants that operate within the power system in the areas with distinct climate conditions. An algorithm designed to detect patterns in the power output scenarios of renewable power plants located in different regions of the country is presented.

2. The cluster analysis of data was performed to identify spatial and temporal variability in the power output of wind farms, solar power plants, and hydropower plants in the Azerbaijan power system. The analysis revealed two regions with different wind and solar power profiles as well as availability of hydropower resources. These profiles were utilized to investigate different scenarios of new capacity additions of renewable power plants for operation as part of the power system.

3. The findings suggest that the highest penetration of renewables (in terms of the annual consumption) is achieved when the outputs of wind farms and solar power plants complement each other. Under the WF+SPP scenario, a sustainable way to raise the penetration of renewables up to 30%, given the annual surplus output of 5 to 10% (relative to consumption), is to increase the capacity of solar power plants and small hydropower plants.

References

[1] Renewable Capacity Statistics 2024. IRENA (International Renewable Energy Agency). [Online]. Available: https://www.irena.org/Publications/2024/Mar/Renewable-Capacity-Statistics-2024. Accessed on: Oct. 3, 2025.

[2] Global Solar Power Generation. The Global Energy Association. Available: https://globalenergyprize.org. Accessed on: Oct. 3, 2025.

[3] WWEA Annual Report 2023: Record Year for Windpower. [Online]. Available: https://wwindea.org/AnnualReport2023. Accessed on: Oct. 3, 2025.

[4] P. V. Ilyushin, A. V. Pazderin, “Requirements for power stations islanding automation,” in Proc. the 2018 International Conference on Industrial Engineering, Applications and Manufacturing (ICIEAM), 15–18 May 2018, Moscow, Russia, 2018.

[5] K. Guerra, P. Haro, R. E. Gutierrez, A. Gomez-Borea, “Facing the high share of variable renewable energy in the power system: Flexibility and stability requirements,” Journal of Applied Energy, vol. 310, Art. no. 118561, 2022.

[6] H. Chandler, Harnessing variable renewables: A guide to the balancing challenge. Paris, France: International Energy Agency, 2011.

[7] P. V. Ilyushin, O. V. Shepovalova, S. P. Filippov, A. A. Nekrasov, “The effect of complex load on the reliable operation of solar photovoltaic and wind power stations integrated into energy systems and into off-grid energy areas,” Energy Reports, vol. 8, pp. 1515–1529, 2022.

[8] A. M. Hashimov, N. R. Rahmanov, A. Z. Mahmudova, J. M. B. Morillo, “Assessment of Probability Distribution Sequence for Voltage Stability in a Power system with Large Share Integration of Variable Renewable Sources,” International Journal on Technical and Physical Problems of Engineering (IJTPE), iss. 55, vol. 15, no. 2, pp. 291–296, 2023.

[9] V. A. Stennikov, V. G. Kurbatsky, N. R. Rahmanov, G. B. Guliyev, V. A. Shakirov, Regional Aspects of Wind Power. Irkutsk, Russia: Melentiev Energy Systems Institute SB RAS, 2020. (In Russian)

[10] N. Rahmanov, H. B. Guliyev, F. Sh. Ibrahimov, Z. A. Mammadov, “Determination of optimal dimensions of hybrid AC/DC distributed generation system with renewable sources for autonomous power supply of remote locations,” in Proc. the Rudenko International Conference on Methodological Problems in Reliability Study of Large Energy Systems (RSES 2024), vol. 584, 2024.

[11] G. Niu, Y. Ji, Z. Zhang, W. Wang, J. Chen, P. Yu, “Clustering analysis of typical scenarios of island supply system by using cohesive hierarchical clustering-based K-Means clustering method,” Energy Reports, vol. 7, suppl. 6, pp. 250–256, 2021.

[12] A. L. Kulikov, O. V. Shepovalova, P. V. Ilyushin, S. P. Filippov, S. V. Chirkov, “Control of electric power quality indicators in distribution networks comprising a high share of solar photovoltaic and wind power stations,” Energy Reports, vol. 8. pp. 1501–1514, 2022.

[13] A. Buttler, F. Dinkel, S. Franz, H. Spliethoff, “Variability of wind and solar power – An assessment of the current situation in the European Union based on the year 2014,” Energy, vol. 106, pp. 147–161, 2016.

[14] S. Han, L. Zhang, Y. Liu, H. Zhang, J. Yan, L. Li, X. Lei, X. Wang, “Quantitative evaluation method for the complementarity of wind-solar-hydro power and optimization of wind-solar ratio,” Appl. Energy, vol. 236, pp. 973–984, 2019.

[15] K. Engeland, M. Borga, J.-D. Creutin, B. Francois, M.-H. Ramos, J.-P. Vidal, "Space–time variability of climate variables and intermittent renewably electricity production. A review," Renew. Sustain. Energy Rev., vol. 79, pp. 600–617, 2017.

[16] G. Ren, J. Wan, D. Yu, "Spatial and temporal assessments of complementarity for renewable energy resources in China," Energy, vol. 177, pp. 262–275, 2019.

[17] P. E. Bett, H. E. Thornton, "The climatological relationships between wind and solar energy supply in Britain," Renew. Energy, vol. 87, pp. 96–110, 2016.

[18] J. Peter, "How does climate change affect electricity system planning and optimal allocation of variable renewable energy," Appl. Energy, vol. 252, Art. no. 113397, 2019.

[19] N. R. Rakhmanov, V. G. Kurbatsky, H. B. Guliyev, N. V. Tomin, R. N. Rakhmanov, "Analysis and modeling of harmonic distortions in consumer's distribution networks, containing a powerful non-linear load," E3S Web of Conf., vol. 58, Art. no. 03015, 2018.

[20] A. M. Hashimov, H. B. Guliyev, A. R. Babayeva, "Shunt reactors control algorithm using fuzzy sets theory," International Journal on Technical and physical problems of engineering (IJTPE), iss. 38, vol. 11, no. 1, pp. 10–15, 2019.

[21] A. M. Hashimov, N. M. Rahmanov, N. M. Tabatabaei, H. B. Guliyev, F. Sh. Ibrahimov, "Probabilistic evaluation of voltage stability limit of power system under the conditions of accidental emergency outages of lines and generators," International Journal on Technical and physical problems of engineering (IJTPE), iss. 43, vol. 12, no. 2, pp. 40–45, 2020.

[22] N. R. Rahmanov, V. G. Kurbatskiy, H. B. Guliyev, N. V. Tomin, Z. Mammadov, "Probabilistic assessment of power system mode with a varying degree of wind sources integration," E3S Web of Conf., vol. 25, Art. no. 02003, 2017.

[23] A. Rylov, P. Ilyushin, A. Kulikov, K. Suslov, "Testing Photovoltaic Power Plants for Participation in General Primary Frequency Control under Various Topology and Operating Conditions," Energies, vol. 14, no. 16, Art. no. 5179, 2021.

[24] P. V. Ilyushin, A. L. Kulikov, S. P. Filippov, "Adaptive algorithm for automated undervoltage protection of industrial power districts with distributed generation facilities," in Proc. the 2019 International Russian Automation Conference, RusAutoCon, 08–14 Sep. 2019, Sochi, Russia, 2019.

Nariman R. Rahmanov, D. Sc. in Engineering, Professor, currently heads the Department of Modern Challenges in the Energy Sector and Artificial Intelligence at the Scientific-Research and Design-Prospecting Power Engineering Institute. He also holds the position of Chief Researcher at the Institute of Physics under the Ministry of Science and Education of the Republic of Azerbaijan. N. R. Rahmanov is a Deputy Editor-in-Chief of the Power Engineering Problems Journal. His research interests include long-term sustainable development of the power sector, operational management of power systems, hybrid systems with renewable energy sources, distributed power systems, microsystems, data analysis, and artificial intelligence. N. R. Rahmanov has authored 290 research papers.

Huseyngulu B. Guliyev, D. Sc. in Engineering, Professor at the Department of Mechatronics, currently serves as the Dean of the Department of Energy and Automation at Azerbaijan Technical University. His research interests include power system operation and control, distributed generation systems, artificial intelligence applications in power system control design, power system stability, renewable energy integration, power quality. H. B. Guliyev has authored 310 research papers and a monograph, while also holding 3 patents.

Famil Sh. Ibrahimov, B. Sc. and M.Sc. in Engineering, is currently a Junior Researcher at the Institute of Cyberphysical Systems and Cybersecurity of Azerbaijan Technical University. His research interests include analysis and control of steady states of electrical systems, modern relay protection systems of electrical networks, and fuzzy logic applications in power engineering. F. Sh. Ibrahimov holds 1 patent and is an author of 60 research papers.

An Experimental and Theoretical Study of the Thermal Treatment Stage during Semi-Coke Briquetting from Weakly Caking Coal

I.G. Donskoy[1,*], A.N. Kozlov[1], M.V. Penzik[1], V.G. Galeev[1], Y.M. Isa[2]

[1] Melentiev Energy Systems Institute of Siberian Branch of Russian Academy of Sciences, Irkutsk, Russia
[2] Witwatersrand University, Johannesburg, South Africa

***Abstract* — The paper proposes a method for assessing the state of coal particle packing before pressing. The method is based on a numerical calculation of internal temperature and component composition heterogeneities. The mathematical model developed for this purpose is validated using experimental data. The calculation results are used to predict the quality of briquettes based on the distribution of the coal conversion degree. The obtained dependencies show that the low mechanical strength of briquettes corresponds to conditions where the conversion degree exhibits high heterogeneity. Using the model, a numerical study is conducted to find suitable briquetting conditions (lower temperature, longer heating).**

***Index Terms* — Coal briquettes, semi-coking, pyrolysis, mechanical strength, mathematical modelling.**

I. Introduction

Among coal technologies, those designed for the production of high-carbon materials are the most challenging for reducing emissions. This is due to both the inevitable high energy consumption in the target processes and the continuous deterioration of the quality of fossil fuels [1]. In this context, studies aimed at developing new methods for extracting solid carbon (semi-cokes and cokes) from a wide range of coals, including those lower-grade ones, are highly relevant. It is worth noting that in addition to carbonaceous materials, coal pyrolysis yields a variety of valuable chemical products, including calorific gas, pyro-liquids, and others [2].

Coal matter is a natural porous composite characterized by highly variable physical and chemical properties. In this regard, the main role in the study of coal pyrolysis processes is played by the statistical approach, which requires a large number of experiments to develop prognostic tools. As of now, no universal models exist for describing the set of processes of chemical transformations with heat and mass transfer during heating and decomposition of coals, although over fifty years of research have produced a number of methodological approaches relying on basic models of chemical kinetics, some approximations of the coal macromolecule structure, representation of functional groups in the form of networks, and others [3–7]. The disadvantages of such approaches are the large volume of initial information required for calculations and the empirical nature of the patterns they are based on [8].

The main tool for controlling the pyrolysis process is temperature [9]. The structure of carbon materials depends significantly on the conditions of raw material pyrolysis [10]. Even for coals that are weakly caking at low heating rates, it is possible to select conditions (thermal shock, pressure, particle size) that allow the production of good-quality semi-coke [11]. However, this requires fine (and often completely empirical) adjustment of the apparatus [12]. The temperature at which the plastic state is reached for coals usually ranges from 350 to 550 °C [13], but with

* Corresponding author.
E-mail: donskoy.chem@mail.ru

DOI: 10.25729/esr.2025.03.0003

Received September 15, 2025. Accepted September 27, 2025.
Available online November 28, 2025.

slow heating, secondary reactions (crosslinking of aromatic structures [14], interaction with volatile components [15], and formation of new phases [16]) lead to deterioration in the quality of the carbonaceous material. Controlled heating allows separating the time scales of thermal processes and chemical transformations to control semi-coking processes. For this purpose, both traditional transport devices for dispersed flows and other methods of controlling thermal processes (for example, high-frequency heating [17]) can be used.

Another important factor is the composition of the raw material. Instead of raw coal, individual fractions [18], mixtures of different types of coal or even different types of fuel, such as coal and biomass [19], coal and waste [20–22], can be processed through pyrolysis. The choice of binding additives and the method of mechanical processing of the plasticized mass are also of great significance.

In addition, thermal schemes of semi-coking processes are constantly improved, primarily to enhance their thermodynamic efficiency [23]. To this end, studies are conducted on the interaction of heat transfer and thermal decomposition of coals in pyrolysis apparatuses [24–26], (which often requires at least crude estimates of the chemical reaction rates). Another important area is the use of staged schemes (for example, with the combustion of pyrolysis gas in process furnaces [27, 28] or with partial gasification [29, 30]).

Numerical modeling is usually based on simplified concepts of the pyrolysis mechanism, heat and mass transfer of decomposing particles with the environment and with other decomposing particles, which is associated with high computational costs of detailed mathematical models. The most widely used approaches are the selection of a reference particle [7, 31], spatial averaging [32], and the reduction of kinetic models to one- and two-stage lumped schemes [33]. It is important to note that many of the data required for thermochemical calculations (primarily the thermophysical properties of intermediate compounds) are often unknown due to the complexity involved in experimentally measuring the characteristics of the reacting phases. Selecting methods for assessing such characteristics poses a significant challenge in numerical modeling, which is usually approached only by comparing the calculation results and experimental measurements. In this context, empirical research holds immense value [34].

This paper considers the pyrolysis process of a small coal bed (with a height of several centimeters) in a muffle furnace. Typical heating times are tens of minutes. The study aims to find conditions for producing mechanically strong briquettes. This is achieved using experimental methods and mathematical modeling. The novelty of the study lies in the method proposed for producing semi-coke briquettes from weakly caking coal and in a new mathematical model developed for the pyrolysis process of the coal packing, which determines the degree of heterogeneity of temperature and conversion of coal. The resulting briquettes are semi-products; a higher-quality product is yielded through further high-temperature processing, which ensures complete devolatilization, hardening of the material, and high reactivity. These issues will be considered in subsequent studies.

The paper is organized as follows: Section 2 describes experimental techniques; Section 3 presents the mathematical model; Section 4 compares the measurements and calculated results; and Section 5 focuses on the mathematical model used to identify the optimal conditions for coal pyrolysis for the purpose of briquetting.

II. Experimental Methods

Cheremkhovo coal, characterized by fractions with an average particle size of 6 mm, was used to obtain semi-coke samples. The problems of Siberian coal use are partially covered in the review presented in [35].

The physicochemical properties of coals were determined using macrothermogravimetry, calorimetry, and fuel elemental composition analyzers. A TGA 801 macrothermogravimetric analyzer (LECO, USA) was used to determine moisture (W), ash content (A), volatile matter yield (VM), and the proportion of fixed carbon (FX). The net calorific value (Q) was determined using an AC 500 calorimeter (LECO, USA). The carbon (C) and sulfur (S) content was determined using a Metavac CS20 elemental analyzer (Russia). The equipment employed is part of the High-Temperature Circuit Multi-Access Research Center (MESI SB RAS). The physicochemical properties determined are given in Table 1.

Table 1 also shows the reactivity index (RI). The reactivity of fuels is understood as their chemical activity in the oxidation process. Most often, the reactivity of fuels is expressed through the volatile matter yield index, which characterizes the process of ignition and combustion of the fuel. The reactivity of the fuel (RI) is calculated using the following equation:

$$RI = \frac{FX}{VM} = \frac{100}{VM} - 1 .$$

The higher the value, the lower the reactivity. According to the reactivity value, coals can be divided into several

TABLE 1. Physicochemical Properties of Cheremkhovo Coal (*r* is for Raw Matter)

Property	*W*, %	*VM*, %	*A*, %	*FX*, %	Q^r, MJ/kg	*RI*	C^r, %	S^r, %
Value	10	38.7	30.2	31.2	19.2	1.6	43.4	0.8

TABLE 2. Results of a Semi-Quantitative XRF Analysis of Mineral Matter

Component	Mass fraction, %
Na_2O	<d.t.*
MgO	1.4
Al_2O_3	16.5
SiO_2	74.8
P_2O_5	<d.t.
SO_3	0.57
K_2O	1.87
CaO	1.24
TiO_2	0.30
Cr_2O_3	<d.t.
MnO	<d.t.
Fe_2O_3	2.70
SrO	0.025
ZrO_2	0.015
BaO	0.339

*<d.t. is for "less than detection threshold"

groups: those with a value of *RI* = 0.8 – 1.0 can be classified as subbituminous brown coals, when RI falls between 1.1 and 1.2, they are identified as highly reactive bituminous brown coals. An *RI* of 1.3 indicates medium-reactive bituminous brown coals. An *RI* between 1.4 and 1.5 represents low-reactive bituminous brown coals. For low-reactive hard coals, *RI* = 1.6 – 2.3. Thus, the coal under study is classified as low-reactive hard coal.

To determine the composition of the mineral part of coal, the X-ray fluorescence analysis (XRF) method was used. The coal ash samples were analyzed using an S4 Pioneer wave-dispersive X-ray spectrometer from Bruker AXS, featuring a Soller-type X-ray optical scheme, equipped with an Rh-anode X-ray tube operating at 4 kW.

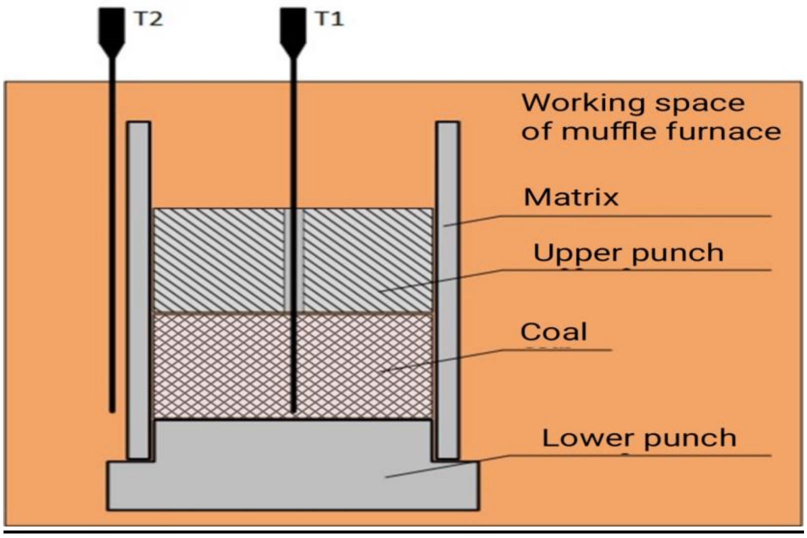

Fig. 1. The scheme of the mold used in experiments.

TABLE 3. Experimental Conditions

	Target temperature, °C	Residence time, min	Coal weight, g	Produced briquette mass, g
1	300	0		67.1
2	300	5		68.7
3	300	10		67.3
4	320	10	80.0	63.9
5	350	10		59.7
6	400	0		55.0
7	375	0		57.1

Table 2 shows the results of the approximate quantitative X-ray fluorescence analysis for the ash of the coal under study.

The packing density of particles was 759 kg/m^3, the swelling index stood at 1.5, and the coking residue type by Gray-King was G1 (sintered, non-melted).

The technique of coal briquette production under laboratory conditions can be represented by the following algorithm:

1) Prepare the coal packing (mass is 80 g);

2) Fill the mold;

3) Install the upper punch with a hole for the thermocouple on the hanger.

4) Place the assembled mold in a muffle furnace. Install a thermocouple (T1) through the hole in the upper punch so that it touches the lower punch.

5) Place the second thermocouple (T2) in the volume of the muffle furnace near the wall of the mold.

6) Turn on the muffle furnace and set the heating temperature to 500–600°C.

7) After reaching the target temperature inside the mold, remove the thermocouple, transfer the mold from the muffle to the platform, and press it with a 5-ton force.

8) Keep the mold under pressure until it cools to room temperature.

9) Remove the lower punch and take out the produced coal briquette.

The influence of residence time (up to 10 min) and temperature (300-400°C) was studied according to the experimental plan presented in Table 3. The obtained briquettes are shown in Fig. 2. The obtained coal briquettes were non-uniform (coal grains are clearly visible on the upper and lower parts) and crumbled. This was especially pronounced for samples 6 and 7 (see Appendix, Fig. 1A), which were processed at higher temperatures relative to the other samples. The non-uniformity of the briquettes and cracks were present across all samples, both on their upper and lower sides.

These phenomena likely result from the non-uniformity of the coal conversion degree along the height of the briquette. To assess the non-uniformity quantitatively, we developed a mathematical model of the physical and chemical processes that occur during the heating of the workpiece. This model is detailed in the next Section.

III. MATHEMATICAL MODEL OF COAL PACKING PYROLYSIS

We consider a quasi-one-dimensional coal packing with an initially uniform distribution of temperature, moisture content, and conversion degree. The packing is placed in a muffle furnace and heated at a given temperature of the furnace walls. Since the shell of the mold is metallic, it can be assumed that the main thermal resistance is related to the convective and radiative heat transfer between the shell surface and the environment. During heating, the organic mass undergoes drying and a two-stage decomposition.

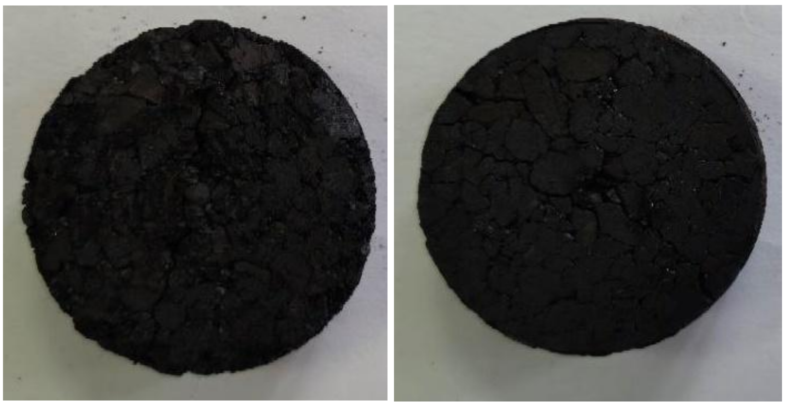

Fig. 2. The appearance of coal briquettes for experiment No. 1 (with the upper view on the left and the bottom view on the right). Other appearances can be found in the Appendix.

The presented model is grounded in the findings of [5, 36–39], which reveal the main physical and chemical features of the processes of thermal decomposition and softening of the coal matter, particularly when subjected to mechanical loading. Chemical transformations of the coal mass involve thousands of organic substances formed during the decomposition of macromolecules. Practical experience, however, demonstrates that despite this diversity, the overall behavior of the coal mass can be described with a small number of variables. These variables do not always correspond to specific organic compounds, but instead represent broader “classes” of decomposition products characterized by their properties such as stages of appearance, phase state, hydrophobicity, and others. In this context, excessive detailing can be an unfavorable factor for the computational model, especially at the stage of the reactor concept testing where identifying qualitative patterns is more crucial than accurate quantitative results.

The propagation of heat is described by a one-dimensional heat conduction equation with the coordinate representing the height of the packing:

$$c\rho\frac{\partial T}{\partial t}=\lambda\frac{\partial^2 T}{\partial x^2}+q\,,$$

where c is the heat capacity, ρ is the density, T is the temperature, t is the heating time, x is the sample height, λ is the thermal conductivity, and q is the heat sink, related to phase transitions and chemical reactions. Thermophysical properties depend on temperature and coal conversion:

$$c\rho=c_W\rho_W+c_C\rho_C+c_A\rho_A\,,$$

$$\lambda=\frac{\lambda_W\rho_W+\lambda_C\rho_C+\lambda_A\rho_A}{\rho}+\lambda_{rad}\,,$$

where c_i is the heat capacity of components (moisture, organic mass, mineral matter), ρ_i is the mass concentration of components (given porosity); λ_i is the thermal conductivity of components, and λ_{rad} is the radiative thermal conductivity (calculated by a formula proposed by Kovenskii and Teplitskii [40]). The thermal conductivity of coal matter (W/(m·K)) linearly increases with temperature [41]:

$$\lambda_C=0.12+0.12\frac{T-273}{1000}\,.$$

The drying rate is determined by a heat balance:

$$\frac{\partial\rho_W}{\partial t}=\begin{cases}0, & T<T_b,\\ -\dfrac{c\rho}{|Q_b|}\dfrac{\partial T}{\partial t}, & T\ge T_b,\end{cases}$$

where, T_b is the water phase transition temperature (373 K) and Q_b is the water phase transition latent heat.

The thermal conductivity of coals ranges from 0.1 to 0.5 W/(m·K) depending on the carbon content (for coals with a carbon content exceeding 80%, the thermal conductivity is higher due to graphitization) [42]. Then, with a heat transfer coefficient of about tens of W/(m^2·K) and a particle size of about a centimeter, the Biot number will be in the range of hundredths to tenths. It can be confidently assumed that the temperature inside the particle relaxes quickly enough to neglect internal gradients [43]. In some cases, intense gas evolution or mechanical abrasion can lead to cracking of particles, additionally intensifying heat transfer.

To describe the lumped kinetics of coal decomposition, we adopt a two-stage model, which is often used to describe coal semi-coking processes. The first stage involves the formation of a multiphase set of products, including organic matter in a plastic state termed metaplast. The second stage corresponds to the degradation of the plastic state, its transformation into a solid product and residual volatile substances. For modeling purposes, it suffices to consider only the phase state of the products and their mass fractions. Therefore, for example, volatile substances are not separated by composition but are included in one macrocomponent.

Gross reaction kinetic equations can be written as follows [39]:

$$\frac{dC}{dt}=-k_1C\,,$$

$$\frac{dM}{dt}=k_1C-k_2M\,,$$

$$\frac{dR}{dt}=k_2M\,,$$

where C is the raw coal organic mass, M is the coal organic mass in its plastic state, R is the solid residue mass (semicoke and ash); k_1 and k_2 are kinetic coefficients for gross reactions. The sum of the components $C + M + R$ is the packing mass. The kinetic coefficients exhibit temperature dependence in accordance with Arrhenius’s law:

$$k_i=k_i^0e^{-\frac{E_i}{R_gT}}\,,$$

where E is the activation energy, k^0 is the pre-exponential factor, and R_g is the gas constant. The mass of the particle at each moment is equal to the sum of masses of the condensed macrocomponents. The kinetic coefficients, holding the highest degree of uncertainty of all the coefficients in the model, are sourced from the

TABLE 4. Numerical Values of the Coefficients Used in the Mathematical Model

Parameter	Dimensions	Value
Specific heat of coal, c_C	J/(kg·K)	1 400
Specific heat of moisture, c_W	J/(kg·K)	4 200
Specific heat of ash, c_A	J/(kg·K)	2 000
Raw coal density, ρ	kg/m^3	1 300
Universal gas constant, R_g	J/(mol·K)	8.314
Preexponent of the first reaction, k_1^0	1/s	245
Activation energy of the first reaction, E_1	kJ/mol	40.7
Preexponent of the second reaction, k_2^0	1/s	2×10^8
Activation energy of the second reaction, E_2	kJ/mol	133
Pyrolysis heat, Q_p	kJ/kg	–300
Water evaporation heat, Q_{ev}	kJ/kg	-2.27×10^3
Heat transfer coefficient, α	W/(m^2·K)	20
Stefan-Boltzmann constant, σ	W/(m^2·K^4)	5.67×10^{-8}
Emissivity, ε	–	0.99
Packing height, H	м	0.044
Packing porosity, Π	–	0.3
Coke-ash residue thermal conductivity, λ_A	W/(m·K)	1

aforementioned literature. The coefficients factoring in the distribution of the products across phases are chosen so that the solid residue is equal to that measured in the laboratory.

With the total yield of volatiles assumed at 42%, we can assume that the yield of condensed organic residue in the first reaction stands at 95%, while in the second reaction, it is 61%. Both reactions are irreversible and have formal first order with respect to the reagent. The integral thermal effect of decomposition Q_p is –300 kJ/kg (in some cases the thermal effect depends on the degree of conversion [8], but we neglect this dependence). Then the term q on the right-hand side of the heat balance equation can be written as follows:

$$q = -Q_b \frac{\partial \rho_W}{\partial t} - Q_p \frac{\partial \rho_C}{\partial t} .$$

The boundary conditions are as follows:

$$-\lambda \frac{\partial T}{\partial x}\left(x \in \Omega\right) = \alpha\left(T - T_g\right) + u\left(t\right)\varepsilon\sigma\left(T^4 - T_w^4\right) ,$$

where, α is the heat transfer coefficient (mainly due to free convection in the muffle furnace space), Ω is the outer surface of the sample, ε is the emissivity of the surface (0.99), and σ is the Stefan-Boltzmann constant. Note that the temperatures of heating through the convective and radiant heating differ. The gas temperature near the surface of the samples is measured by a thermocouple and the wall temperature is set constant. When the gas temperature reaches a given temperature, the experimental technique disables radiant heat exchange. As a result, the second term on the right-hand side contains the control $u(t)$, which equals one during the heating phase and switches to zero when the target temperature is achieved. This condition underlies the control of the thermal state of the muffle furnace. We take these values from the measurements. Table 4 shows the coefficients used in the calculations.

The heat transfer equations with chemical reactions are numerically solved utilizing a combined scheme with splitting by physical process. The drying and pyrolysis processes are considered to occur under a fixed temperature distribution, independently in each grid element. Calculations rely on analytical and balance expressions, which include local temperature as a constant parameter. The process of heat conduction with heat sinks, whose intensity is determined in the previous stage, is considered to occur under fixed physical and chemical properties of the packing. For this purpose, a system of difference equations with implicit approximation is solved using the tridiagonal matrix algorithm. The resulting scheme has the first order of convergence in time and space grid steps [41].

As in the case of other similar systems, the choice of the spatial grid step cannot be based on any highly detailed characteristics of the sample. The coal particle packing is a heterogeneous system, therefore reducing the grid step to a size smaller than that of a single particle generally requires switching to other methods for its description, such as DEM, XDEM, and others [45]. In this paper, we assume that the interpenetrating phase model can still be applied (at least for calculations) even when the grid step is reduced to sizes that are smaller than single particles ($h = 0.4\times10^{-4}$ m). The time step was chosen in accordance with the constraints on the thermal relaxation time of both the grid element and the entire sample ($\tau = 5\times10^{-2}$ s). The calculation results presented below were obtained for these values of the difference scheme parameters.

IV. The Calculation Results and Their Comparison with Experimental Findings

For the experiments from Table 1, the conditions for heating the coal packings before pressing into briquettes were reproduced using the mathematical model. In all cases, the heating temperature varied from 300 to 400°C, the initial mass of the sample was 80 g, and the initial moisture content was about 10% (given the moisture content, the loss of organic mass during decomposition is quite small). At high temperatures, the briquettes are brittle, which may be associated, for example, with a change in the distribution of properties across the packing height.

Figure 3 (see also Fig. A2 in Appendix) shows the calculated temperature dynamics at different points (the

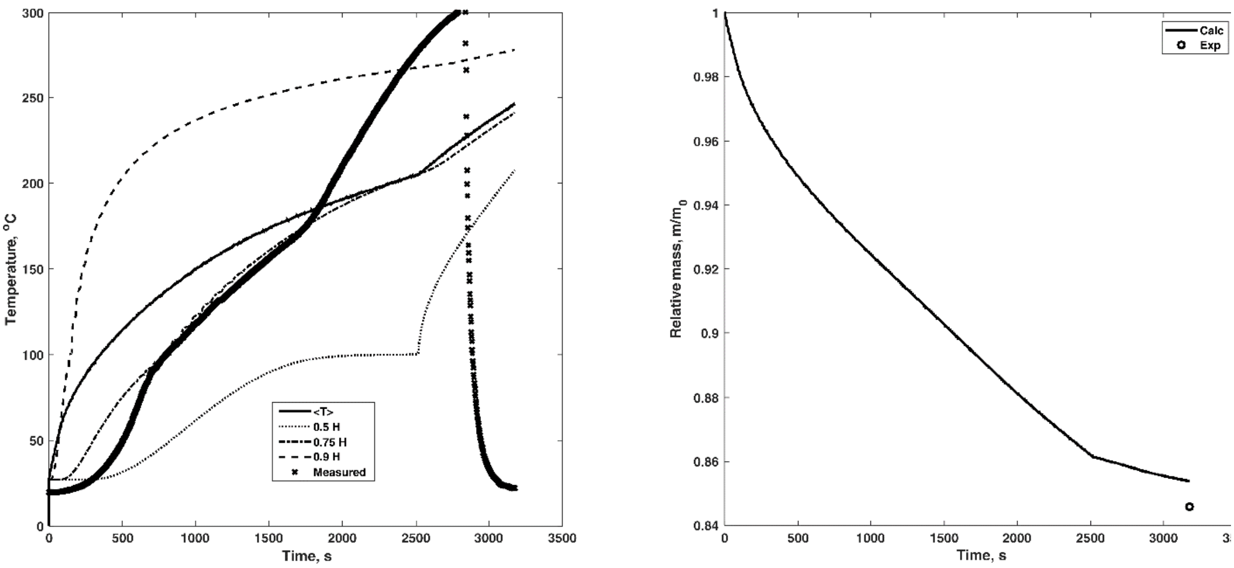

Fig. 3. The dynamics of temperature inside the samples (left) and their mass loss (right) for experiment No. 1 (300°C, no residence time). The markers indicate the measured values.

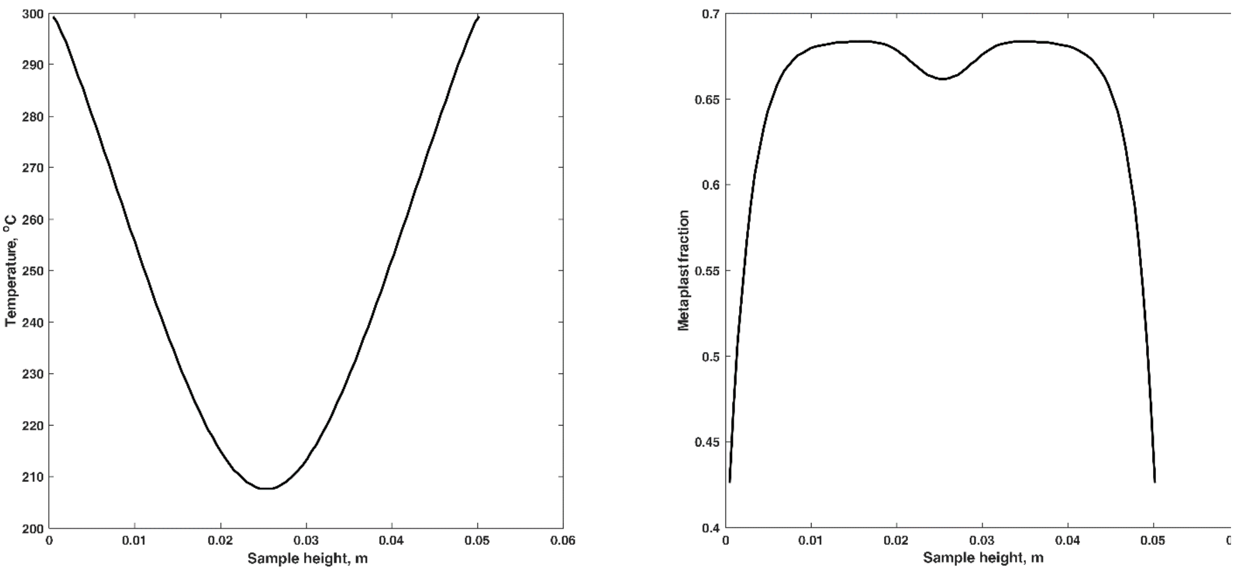

Fig. 4. The calculated distribution of the temperature (left) and softened coal mass fraction (right) along the sample height for experiment No. 1 (300°C).

center of the sample, a quarter of the height, and the near-surface layer) on the left side. The mass average temperature (<*T*>) is also presented. The temperature of the phase transition of water stands out on all the graphs: drying makes a significant contribution to the creation of high temperature gradients in the sample (as well as to the overall mass loss). The sharp decrease in temperature at the end of each experiment is caused by the removal of the thermocouple from the packing before pressing. Due to significant thermal inertia, the temperature distribution inside the packing is "preserved" for a significant time, sufficient to remove the samples from the muffle furnace and obtain briquettes.

Figure 3 shows that the mathematical model reproduces the mass loss of the samples quite accurately. Comparison of temperatures demonstrates a qualitative agreement (which can be attributed to various factors, ranging from neglected convective transfer processes inside the packing to a simplified mechanism of chemical transformations). A major source of error is the uncertainty of the thermophysical properties of the coal organic mass throughout the conversion process. With a rise in heating temperature, the differences between measurements and modeling results decrease.

Despite the differences between the measured and calculated curves, the model proves to be a reliable tool for estimating the thermal state of coal packing. The distribution of temperature and metaplast at the end of the experiment can be seen in Fig. 4 (also see Fig. A3 in Appendix). The general patterns of the packing heating are as follows. The temperature gradient is significant for all cases and ranges from 30 to 90°C per half-height of the

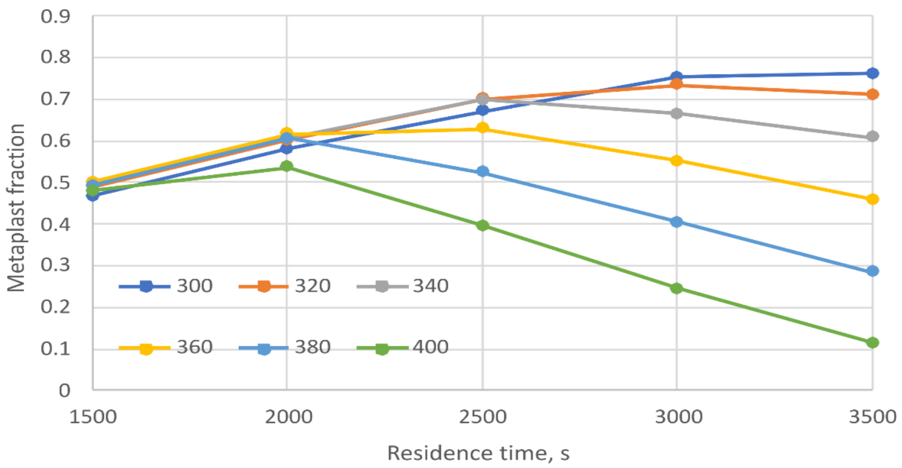

Fig. 5. The dependence of organic mass in plastic state mass fraction on residence time and maximum temperature (numbers in the Figure, °C)

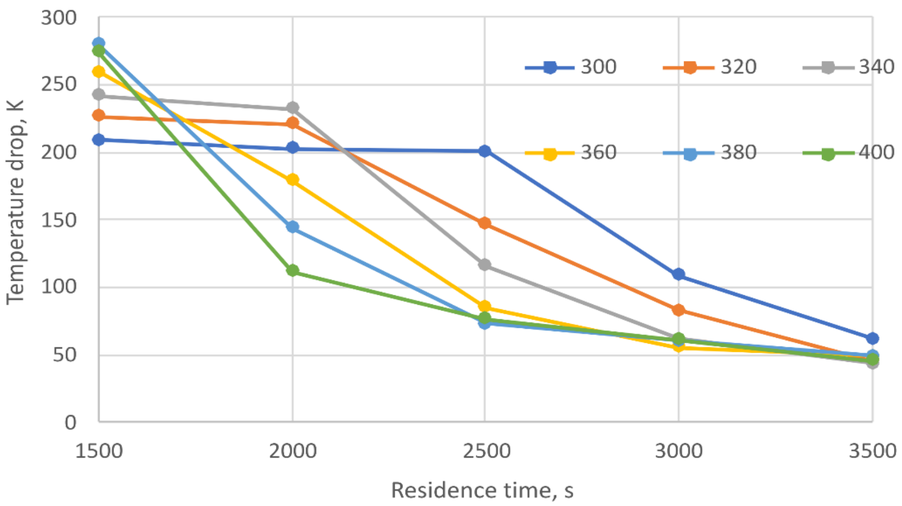

Fig. 6. The dependence of maximum temperature difference across the packing on residence time and maximum temperature (numbers in the Figure, °C).

sample. This variation in temperature entails heterogeneity in the pyrolysis degree. When the heating temperature and residence time increase, the coal mass at the workpiece boundaries almost completely turns into semi-coke, leading to the production of brittle briquettes upon pressing. In contrast, at low temperatures and short residence times, the workpiece may not have sufficient time to achieve the required conversion.

Thus, an optimization problem arises concerning the selection of thermal conditions for heating coal packing prior to the pressing process.

V. Results and Discussion

The model was used to calculate the pyrolysis process of coal packing (with a weight of 80 g and a fixed height) across various maximum temperatures and heating intervals. For simplicity, we assumed that the gas temperature in the muffle furnace rose linearly at a rate of 10 K/min until achieving the maximum temperature, at which point it remained constant. The dependences for the proportion of softened mass and the maximum temperature difference are demonstrated in Fig. 5 and 6. Expectedly, the decomposition degree increases as the maximum temperature rises. With a heating time of up to 2000 s, the curves are close, but a notable decline in the fraction of organic mass in the plastic state occurs at high temperatures. At the same time, as seen in Fig. 6, the temperature difference across the coal particle layer gradually decreases.

The regions with a slightly changing high temperature gradient correspond to the drying stage [46]. The drying stage significantly overlaps with decomposition of the organic matter of coal. The presented model does not factor in possible cross-effects (e.g., the effect of water vapor on the dynamics of release and the composition of the products), therefore, the effect of drying is reduced to the thermal interaction between the phase transition and heat transfer processes. At long heating times, the temperature gradient diminishes, resulting in values around 50–100 K at 3000 s, similar to those observed in the previous Section.

To assess the heterogeneity of the distribution of coal mass in the plastic state across the packing height, the following criterion can be proposed:

$$F = \frac{M\left(t_{end}, x\right) - M\left(t_{end}, x\right)}{E\left[M\left(t_{end}, x\right)\right]},$$

where $M(t, x)$ is the local content of the coal mass in the plastic state and E is the estimate of the mean value. Thus, the heterogeneity criterion is the range of values normalized to the mean value. The dependence of heterogeneity on the pyrolysis conditions is shown in Fig. 7. Heterogeneity increases with temperature, albeit non-monotonically, at heating periods of up to 2000 s. The choice of a high temperature leads to considerable packing heterogeneity, making the briquettes extremely unstable after pressing. However, it is impossible to unambiguously select the optimal conditions from the results of numerical modeling. Even for the maximum heating temperature of 400°C, there can be a range of conditions (at shorter heating times) within which acceptable workpiece homogeneity can be expected. These results need to be verified experimentally.

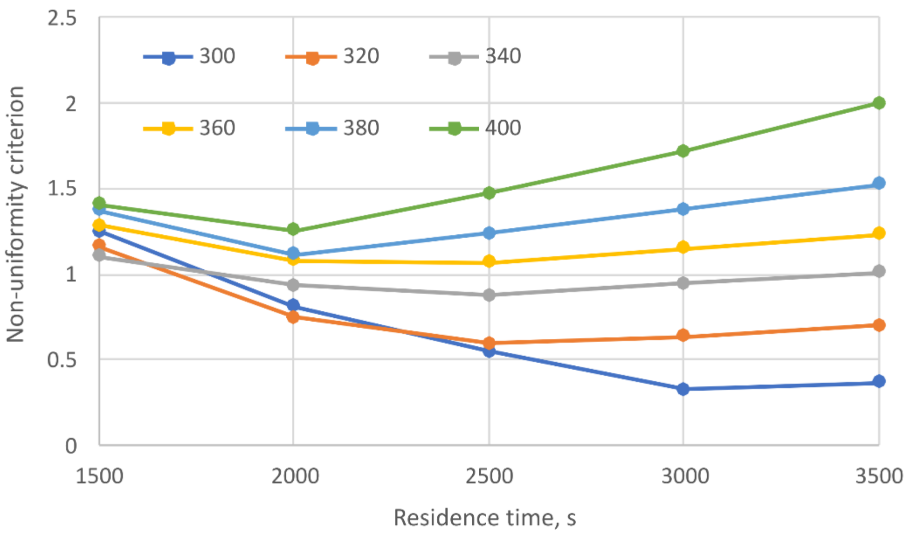

Fig. 7. The dependence of the heterogeneity criterion on residence time and maximum temperature (numbers in the Figure, °C).

A more significant outcome of the study is the development of a mathematical model of heat transfer processes and physicochemical processes in coal packing. This model not only qualitatively reproduces the heating curves but also provides a highly accurate estimation of the final mass. Such a tool (given corrections for the reactive and thermal properties of materials, as well as a more detailed consideration of processes within the packing) can be used to find optimal conditions for thermal briquetting of coals. In addition to mechanical strength, it is also crucial to consider energy consumption, which increases with long heating times. The development of new, highly efficient schemes with coal pyrolysis can become one of the ways to reduce emissions and the carbon footprint of semi-coke production.

VI. Conclusions

The paper presents the results of experimental measurements and numerical calculations achieved when studying the processes of heating and pyrolysis of coal packing before pressing them into briquettes. The findings reveal that briquettes produced at heating temperatures of 375–400°C are brittle. To analyze the causes behind this, a simplified mathematical model was developed to estimate the degree of the composition and temperature heterogeneity within the briquette during laboratory heating. The calculation results indicate that with an increase in temperature and heating time, the degree of coal conversion into semi-coke rises, which deteriorates the quality of the packings. Variant calculations allow us to determine the range of heating conditions for pre-treatment of coal before briquetting.

A crucial strand for further research is the consideration of processes within the particles. The sintering of particles during pressing relies heavily on adhesion, making it essential to have comprehensive information on the surface state. Various modifications of the layer model have been proposed to consider the processes within the particles [47]. Integrating chemical reactions with transfer processes and solid mechanics, especially in coal processing, needs a more detailed analysis, additional experiments, and new theoretical approaches.

VII. Funding

The work was supported by RF Ministry of Science and Higher Education No. 13.2251.21.0254 (contract No. 075-15-2024-651).

References

[1] H. Katalambula, R. Gupta, "Low-Grade Coals: A Review of Some Prospective Upgrading Technologies," Energy & Fuels, vol. 23, pp. 3392–3405, 2009.

[2] M. Granda, C. Blanco, P. Alvarez, J. W. Patrick, R. Menéndez, "Chemicals from Coal Coking," Chemical Reviews, vol. 114, pp. 1608–1636, 2014.

[3] T. H. Fletcher, "Review of 30 Years of Research Using the Chemical Percolation Devolatilization Model," Energy & Fuels, vol. 33, pp. 12123–12153, 2019.

[4] K. Luo, J. Xing, Y. Bai, J. Fan, "Prediction of product distributions in coal devolatilization by an artificial neural network model," Combustion and Flame, vol. 193, pp. 283–294, 2018.

[5] S. Niksa, Process Chemistry of Coal Utilization. Elsevier, 2020. DOI: 10.1016/C2018-0-04246-2.

[6] P. R. Solomon, D. G. Hamblen, R. M. Carangelo, M. A. Serio, G. V. Deshpande, "General model of coal devolatilization," Energy & Fuels, vol. 2, pp. 405–422, 1988.

[7] E. Ranzi, T. Faravelli, F.Manenti, "Pyrolysis, Gasification, and Combustion of Solid Fuels," Advances in Chemical Engineering, vol. 49, pp. 1–94, 2016.

[8] M. Sciazko, B. Mertas, L. Kosyrczyk, A. Sobolewski, "A Predictive Model for Coal Coking Based on Product Yield and Energy Balance," Energies, vol. 13, Art. no. 4953, 2020.

[9] M. F. Vega, E. Díaz-Faes, C. Barriocanal, "Influence of the Heating Rate on the Quality of Metallurgical Coke," ACS Omega, vol. 6, pp. 34615–34623, 2021.

[10] Z. F. Chukhanov, Some problems of fuel and energy science. Moscow, USSR: USSR Academy of Sciences Publ., 1961. (In Russian)

[11] A. L. Perepelitsa, Pyrogenetic briquetting of Irkutsk regions coals. Moscow, USSR: USSR Academy of Sciences Publ., 1963. (In Russian)

[12] M. S. Nyathi, R. Kruse, M. Mastalerz, D. L. Bish, "Nature and origin of coke quality variation in heat-recovery coke making technology," Fuel, vol. 176, pp. 11–19, 2016.

[13] Y. Chen, et al. "A review of the state-of-the-art research on carbon structure evolution during the coking process: From plastic layer chemistry to 3D carbon structure establishment," Fuel, vol. 271, Art. no. 117657, 2020.

[14] L. Xu, et al. "Structural order and dielectric properties of coal chars," Fuel, vol. 137, pp. 164–171, 2014.

[15] Z. Liu, et al. "Reaction of volatiles – A crucial step in pyrolysis of coals," Fuel, vol. 154, pp. 361–369, 2015.

[16] J. Yu, J. A. Lucas, T. F. Wall, "Formation of the structure of chars during devolatilization of pulverized coal and its thermoproperties: A review," Progress in Energy and Combustion Science, vol. 33, pp. 135–170, 2007.

[17] B. Lin, et al. "Sensitivity analysis on the microwave heating of coal: A coupled electromagnetic and heat transfer model," Applied Thermal Engineering, vol. 126, pp. 949–962, 2017.

[18] W. Xie, et al. "Impact of large sized inertinite particles on thermo-swelling and volatile release of coking coals," Fuel Processing Technology, vol. 193, pp. 63–72, 2019.

[19] L. Florentino-Madiedo, E. Díaz-Faes, C. Barriocanal, "Reactivity of biomass containing briquettes for metallurgical coke production," Fuel Processing Technology, vol. 193, pp. 212–220, 2019.

[20] J. Wu, et al. "Coke formation during thermal reaction of tar from pyrolysis of a subbituminous coal," Fuel Processing Technology, vol. 155, pp. 68–73, 2017.

[21] A. Koskela, H. Suopajärvi, T. "Fabritius, Interaction between coal and lignin briquettes in co-carbonization," Fuel, vol. 324, Art. no. 124823, 2022.

[22] I. G. Donskoy, A. N. Kozlov, M. V. Penzik, D. A. Svishchev, L. Ding, "Agglomeration of coal and polyethylene mixtures during fixed-bed co-gasification," International Journal of Coal Science & Technology, vol. 11, Art. no. 21, 2024.

[23] C. Liu, Z. Xie, F. Sun, L. Chen, "Exergy analysis and optimization of coking process," Energy, vol. 139, pp. 694–705, 2017.

[24] Ł. Słupik, et al. "CFD model of the coal carbonization process," Fuel, vol. 150, pp. 415–424, 2015.

[25] Y. Zhuo, C. Li, C. Wu, Y. Shen, "A combined numerical and experimental approach to study the carbonization of low-rank coal ellipsoidal briquettes," Chemical Engineering Science, vol. 204, pp. 76–90, 2019.

[26] K. Xiao, X. Liu, H. Hu, Z. Wen, G. Lou, "Heat and mass transfer analysis of coal coking process in the coking chamber," International Journal of Coal Preparation and Utilization, vol. 44, pp. 1732–1747, 2024.

[27] "ENCOAL mild coal gasification project: ENCOAL project final report," ENCOAL corporation, USA, Rep. DOE/MC/27339-5979, 1997.

[28] M. L. Shchipko, O. P. Potapov, "Possibilities of autothermal pyrolysis use for the stabilization of combustion process," Teploenergetika, vol. 11, pp. 54–58, 1991. (In Russian)

[29] S. R. Islamov, Partial gasification of coal. Moscow, Russia: Gornoe delo, 2017. (In Russian)

[30] X. Zeng, et al. "Pilot verification of a low-tar two-stage coal gasification process with a fluidized bed pyrolyzer and fixed bed gasifier," Applied Energy, vol. 115, pp. 9–16, 2014.

[31] C. B. Nguyen, et al. „A hybrid particle model with advanced conversion parameters and dynamic drag model applied for the CFD modeling of an entrained-flow gasifier," Combustion and Flame, vol. 240, Art. no. 112040, 2022.

[32] X. Ke, et al. "Modeling and experimental investigation on the fuel particle heat-up and devolatilization behavior in a fluidized bed," Fuel, vol. 288, Art. no. 119794, 2021.

[33] J. Mularski, N. Modliński, "Entrained flow coal gasification process simulation with the emphasis on empirical devolatilization models optimization procedure," Applied Thermal Engineering, vol. 175, Art. no. 115401, 2020.

[34] V. M. Strakhov, A. G. Kaliakparov, V. P. Panfilov, S. Sh. Imanbaev, A. M. Aubakirov, "Coke Quality in Medium-Temperature Coking of Fractionated Long-Flame Coal," Coke and Chemistry, vol. 65, pp. 316–334, 2022.

[35] L. Takaishvili, A. Sokolov, G. Agafonov, "Trends and Prospects for Coal Deliveries from Russia's Eastern Regions," Energy Systems Research, vol. 5, pp. 55–66, 2022.

[36] W. S. Fong, W. A. Peters, J. B. Howard, "Kinetics of generation and destruction of pyridine extractables in a rapidly pyrolysing bituminous coal," Fuel, vol. 65, pp. 251–254, 1986.

[37] M. S. Oh, W. A. Peters, J. B. Howard, "An experimental and modeling study of softening coal pyrolysis," AIChE Journal, vol. 35, pp. 775–792, 1989.

[38] K. Matsuoka, J. Hayashi, T. Chiba, "A Model for Softening and Resolidification of Coals Heated at Different Rates," ISIJ International, vol. 37, pp. 566–572, 1997.

[39] M. Sciazko, B. Mertas, L. Stepien, "Kinetic modelling of coking coal fluidity development," Journal of Thermal Analysis and Calorimetry, vol. 142, pp. 977–990, 2020.

[40] V. I. Kovenskii, Yu. S. Teplitskii, "On the thermal conductivity of a blown granular bed," Journal of Engineering Physics and Thermophysics, vol. 81, pp. 998–1005, 2008.

[41] A. A. Agroskin, Thermal and electric properties of coals. Moscow, USSR: Metallurgizdat, 1959. (In Russian)

[42] Q. Shi, Y. Qin, Y. Chen, "Relationship between Thermal Conductivity and Chemical Structures of Chinese Coals," ACS Omega, vol. 5, pp. 18424–18431, 2020.

[43] A. V. Luikov, Analytical heat diffusion theory. NY and London: Academic Press, 1968.

[44] I. G. Donskoy, "Mathematical modelling of woody particles pyrolysis in a fixed bed," Computational Technologies, vol. 23, no. 6, pp. 14–24, 2018. (In Russian)

[45] Q. Wang, E. Wang, "Numerical investigation of the influence of particle shape, pretreatment temperature, and coal blending on biochar combustion in a blast furnace," Fuel, vol. 313, Art. no. 123016, 2022.

[46] B. Atkinson, D. Merrick, "Mathematical models of the thermal decomposition of coal4. Heat transfer and temperature profiles in a coke-oven charge," Fuel, vol. 62, pp. 553–561, 1983.

[47] Yu. V. Sharikov, F. Yu. Sharikov, K. A. Krylov, "Mathematical Model of Optimum Control for Petroleum Coke Production in a Rotary Tube Kiln," Theoretical Foundations of Chemical Engineering, vol. 55, pp. 711–719, 2021.

Igor G. Donskoy, Ph.D., Dr.Sc., currently serves as the Head of the Power Plants Research Laboratory at the Melentiev Energy Systems Institute (ESI) SB RAS, Irkutsk, Russia. His main research interests include mathematical modelling related to fuel processing and thermal engineering.

Alexander N. Kozlov, Ph.D., is a Senior Researcher in the Department of Thermal Power Systems at the ESI SB RAS. His research interests include the combustion of heterogeneous solid fuels (biomass, coal), as well as the development of simple engineering techniques for calculating gasification processes.

Maxim V. Penzik Ph.D., is a Senior Researcher in the Department of Thermal Power Systems at the ESI SB RAS. Since 2022, he has been an Associate Professor at the Faculty of Chemistry at Irkutsk State University. His research interests include the processes of thermal decomposition of biomass, polymers, and organic compounds, as well as their study using the TG-MS method.

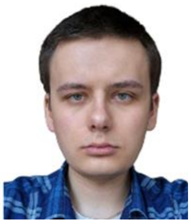

Vladislav G. Galeev is an engineer at the Melentiev Energy Systems Institute SB RAS. He is a second-year master's student at Irkutsk National Research Technical University. His research interests include processes of thermal decomposition of biomass, as well as biochar and supercapacitors based on it.

Yusuf Makarfi Isa is a Professor with a Ph.D. from the School of Chemical and Metallurgical Engineering at the University of the Witwatersrand, South Africa. His research focuses on thermochemical conversion of fuels and carbon-containing materials.

Reliability Challenges of District Heating Systems in the Context of Technological and Organizational Innovations

V.A. Stennikov[1], I.V. Postnikov[1,*]

[1] Melentiev Energy Systems Institute of Siberian Branch of Russian Academy of Sciences, Irkutsk, Russia

Abstract **This paper reviews current trends in the evolution of district heating systems and some emerging areas of their technological transformation related to the reliability of operation. It also contributes insights into advancing the methodology for reliability analysis and synthesis for these systems. The study highlights the issues of the heat network infrastructure health through a case study of the Irkutsk region, which elucidates their severity. We conclude by noticing an imbalance in the reliability issues of evolving district heating systems: on the one hand, the technological changes and structural transformations are irreversible, on the other hand, a range of major unresolved issues hinder and slow down the adoption of innovations and advancement of the systems.**

***Index Terms* — District heating system, transformation of energy systems, energy transition, reliability, reliability analysis and synthesis, equipment health, equipment wear and tear, prosumer, hybrid district and distributed heating system.**

I. Introduction

The reliability of district heating systems (DHSs) becomes an increasingly critical issue with each year. The significant loss of heat, substantial wear of equipment, annual failures of heating mains resulting in prolonged interruptions in heating supply highlight the urgent need to address the issues of heating systems, even in the face of limited resources. The primary areas of confronting the above challenges aim to better equipment health, whereas further evolution of DHS involves the adoption of new technologies, principles of construction, design, and operation; mass digitalization of technological processes; and others.

All these trends, when viewed through the lens of the overall paradigm of transformation of energy systems (ES) as part of the energy transition [1], require more advanced production facilities and up-to-date theoretical foundations. Implementation of technological, structural, and organizational innovations leads to the emergence of new facilities and links, changes in properties, and introduction of new functions of DHSs. These transformations need to be considered in the analysis and synthesis (optimization, assurance) of their reliability and when formulating strategies to ensure it. Based on the literature review [2], we have compiled a systematized list of current methodological research on solving DHS reliability problems [3–34]. This list is shown in Table 1 (it, however, does not claim to be an exhaustive representation of the current research in the field).

The co-occurrence graph of keywords of research papers shown in Fig. 1 provides an overview of the state-of-the-art of DHS reliability studies (received using the service VOSviewer). The cluster that stands out from the rest of the graph links the term *district heating system* to the reliability-related concepts such as *reliability*, *reliability analysis*, *reliability assessment*, and *nodal reliability indices*. The relative isolation of this cluster indicates weak interconnections between reliability issues and other areas of research, in particular, those related to energy efficiency, adoption of renewables, and new principles of systems

* Corresponding author.
E-mail: postnikov@isem.irk.ru

DOI:10.25729/esr.2025.03.0004

Received July 16, 2025. Accepted September 20, 2025. Available online November 28, 2025.

TABLE 1. Published Research On the Design of Methods for Analysis and Synthesis of DHS Reliability (Compiled Based On the Data Reported in [2])

Reliability problem	Level of detail	Methods	References
DHS reliability analysis	System (overall solutions)	Probabilistic, stochastic processes	Valinčius et al., 2015 [3]; Badarai et al., 2018 [4]; Postnikov, 2023 [5]
		Statistical	Rasoulian, 2022 [6]; Gilski et al., 2014 [7]; Marx et al. [8]; Postnikov & Mednikova, 2022 [9]
	Components (node-specific solutions)	Probabilistic	Mortensen et al., 2022 [10]; Ziganshin et al., 2016 [11]; Khoshgoflar Manesh et al., 2018 [12]; Losi et al., 2024 [13]; Mao el al., 2024 [14]; Mao et al., 2022 [15]
		Deterministic	Maliavina et al.,2022 [16]
DHS reliability analysis and risk assessment	Components	Probabilistic	Žutautaite et al., 2017 [17]; Shan et al., 2017 [I8]; Postnikov & Stennikov, 2020 [19]
		Statistical analysis	Sernhed & Jönsson, 2017 [20]
		Hybrid (Weibull model + Monte Carlo methods + failure mode and effects analysis)	Palakodeti, 2016 [21]
		Machine learning methods	Mortensen el al., 2022 [22]
DHS reliability forecasting, predictive analysis	Components	Hybrid (probabilistic + machine learning)	Mortensen & Shaker, 2024 [23]
		Weibull model	Kovacs et al., 2021 [24]; Langroudi & Weidlich, 2020 [25]
		Deterministic	Sun et al., 2009 [26]
DHS reliability optimization	System	Statistical analysis	Dai et al., 2022 [27]; Pan et al., 2024 [28]; Li et al., 2021 [29]
		Machine learning methods	Mao et al., 2021 [30]
	Components	Probabilistic	Postnikov et al., 2017 [31]; Stennikov & Postnikov, 2013 [32]; Postnikov et al., 2018 [33]; I. Postnikov, 2023 [34]

design in general. This situation may result in an inconsistent approach to the overall development of DHSs, lacking well-informed and balanced decisions and failing to consider conflicting multiple criteria for economic performance, efficiency, and reliability. The theory of hydraulic circuits [35] laid out a solid theoretical groundwork for DHS reliability: it contributed a method for *nodal reliability assessment* of consumer heating supply, a system of criteria and requirements for reliability based on the current standards, as well as methods of synthesis of optimal DHSs that consider their reliability [36]. This line of research was further elaborated in [31–34].

II. RELIABILITY OF EMERGING DHS TECHNOLOGIES

The array of modern technologies used for development and transformation of DHS to ensure and enhance their reliability is diverse both in the scope of application (subsystems, facilities, equipment) and in the scale of modernization of the systems. The production level involves the use of efficient heat sources (HSs), secondary thermal energy resources, and renewables. The distribution level focuses on addressing such urgent issues as efficient control of thermal-hydraulic states of heat networks (HNs), reduction in heat loss, reconstruction of pipelines, and, in some systems, transition to low-temperature parameters of heat carrier. It is envisioned that the consumption subsystems will be provided with a set of energy efficient systems and technologies for residential heating, cooling,

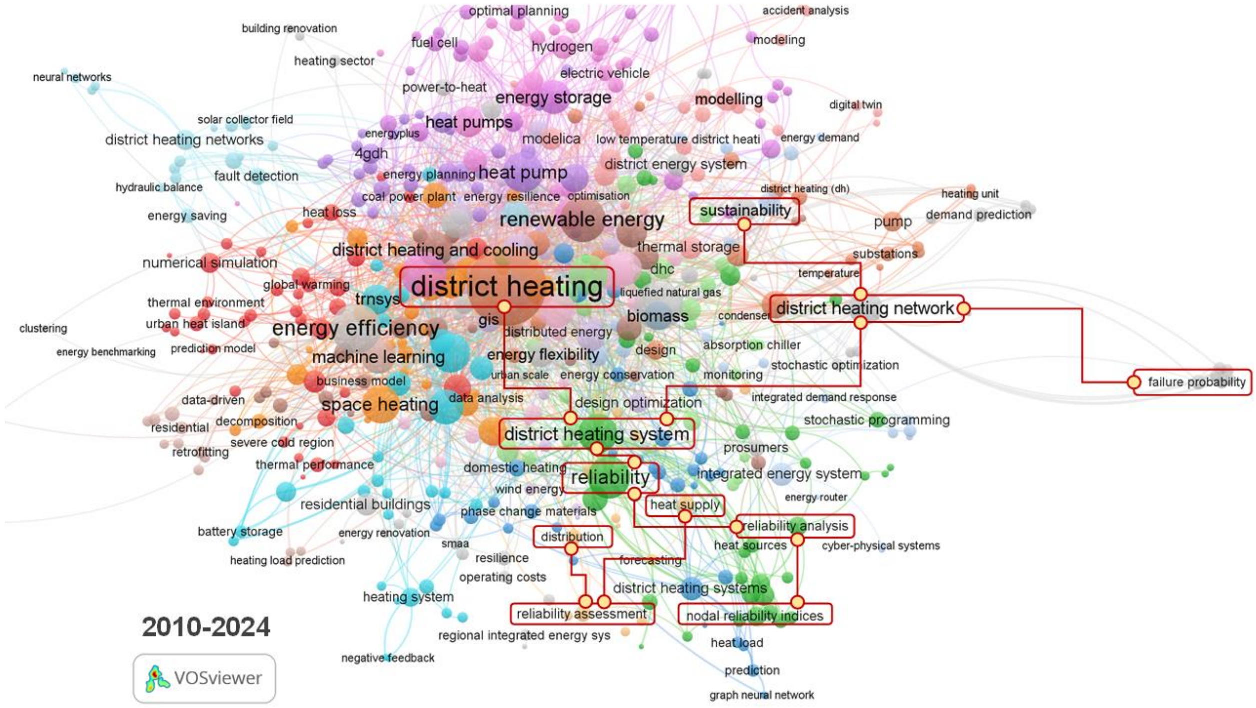

Fig. 1. The co-occurrence graph for reliability studies within research on various aspects of DHS; generated by querying the Scopus database for the search term "district heating + reliability" (based on over 1 000 items published in 2010–2024).

TABLE 2. Reliability Throughout the Stages of Technological Evolution of DHSs

1st generation of DHS (1880–1930)	2nd generation of DHS (1930–1980)	3rd generation of DHS (1980–2020)	4th generation of DHS (2020–2050)
	Key technologies		
Localized steam systems, steam pipes in concrete ducts, condensate lines, expansion joints, pressurized condensate tanks	Hot water pipes in concrete ducts, high pressures, metal-intensive and heavy equipment of heat networks, weak system of monitoring and control of operating conditions	Pre-insulated buried pipelines, efficient compact heating substations, metering and monitoring, control of operating conditions parameters	Integrated energy technologies with intelligent control, full digitalization of processes, prosumers, high energy efficiency, environmental friendliness
	Reliability aspect		
Low reliability due to intensive corrosion damage of condensate piping; high heat loss induced by higher steam parameters, exposure to high risks in case of incidents	Improved reliability due to reduced heal transfer medium parameters, more reliable equipment, energy-saving technologies, as well as systems design with built-in functional and structural redundancy	Still higher reliability due to lower heat transfer medium parameters; integration of various sources (including renewables) which provides a wider safety margin but complicates operating conditions, hence the need for fundamentally new intelligent control systems to back the further evolution	High reliability and controllability of systems; multiple options for multi-resource redundancy due to integration with other energy systems; high level of operational reliability at the level of prosumer-based demand-response subsystems due to optimization of consumption and local thermal capacity redundancy; further improvement of reliability of individual components

and hot water supply, and prosumers will be introduced there to form hybrid district and distributed heating systems (as detailed below).

According to a well-established conception of district heating evolution, the technological change in DHSs is tentatively divided into 4 stages or generations of systems [37] (currently the 5th generation is also being considered). It should be noted that this classification is provisional, which is due to the continuity of the evolutionary process itself and, as a consequence, the impossibility of clearly delimiting the systems of "adjacent" generations by the features unique to them. For example, the DHSs operating

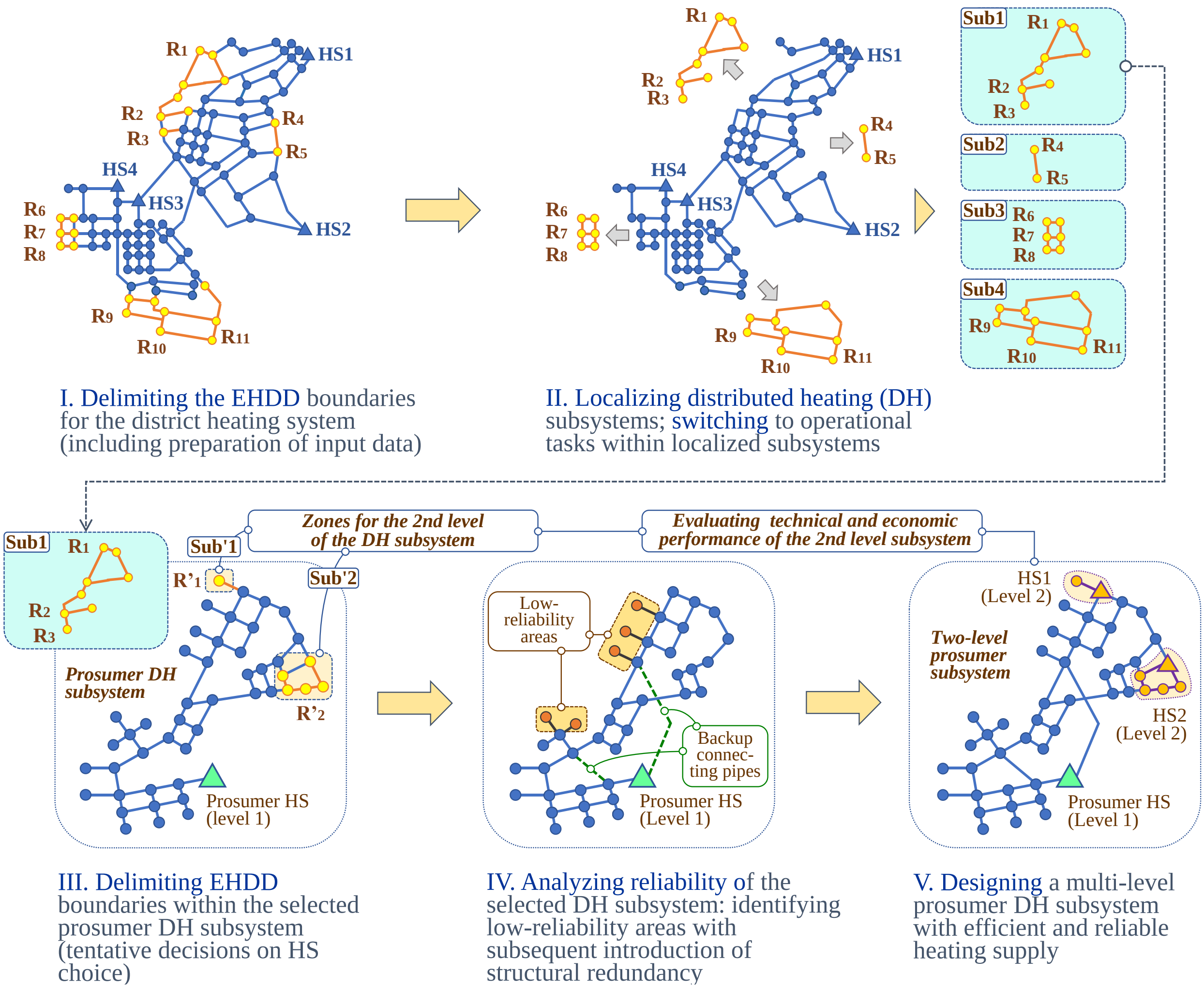

Fig. 2. Formation of reliable hybrid district and distributed heating systems with a multi-level prosumer distributed heating subsystem [35, 39].

in Russia correspond to the 2nd generation, although many of them are unique in scale and structure; most systems in European countries, as well as the new systems operating in China, correspond to the 3rd generation, and only a small number of systems in some European countries (Denmark is a recognized leader in this group) belong to the 4th generation.

An overview of the historical background, structure, and basic properties of these stages is detailed in [37]. Based on the technological features specific to DHSs of different generations we have formulated the corresponding reliability aspects and presented them in Table 2. In the foreseeable future, DHSs will focus on achieving the properties of the 4th and 5th generation systems, which involves: high system reliability and controllability; a variety of options for multi-resource redundancy as part of integration with other ESs; high operational reliability at the level of subsystems run by prosumers due to optimization of consumption and local thermal capacity redundancy at their own DHSs; increased technical reliability of system components, and others. The key parameter that affects the DHS efficiency within the framework of the above conception is the heat carrier temperature, whose decrease leads to a lower heat loss. Furthermore, the transition to low-temperature operating conditions enhances operational reliability, extending service life of pipelines while reducing their thermal stress and deformation. This decreases the thermal expansion of pipelines, enabling the use of more compact compensators and streamlining their installation and replacement. The above factors facilitate cutting costs incurred for maintenance repairs and overhauls of HN equipment, as

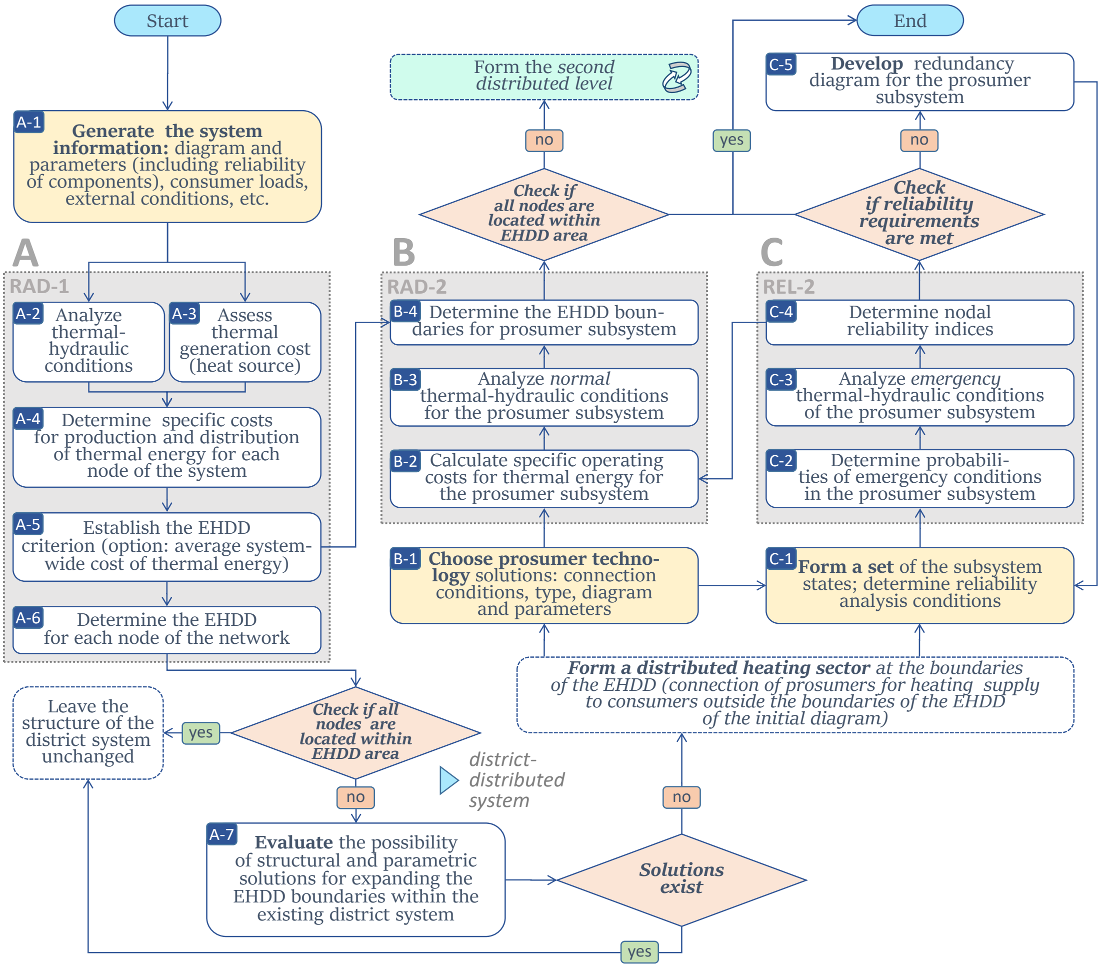

Fig. 3. Algorithm for HDDHS formation (corresponds to the main stages shown in Fig. 2).

well as for the means of rectifying incidents at the facilities that use higher parameters of the heat carrier. However, it is also crucial to consider higher material intensity of HNs due to larger diameters needed to increase the flow rate for compensating for the decrease in the temperature drop.

III. Ensuring Reliability in the Transition to Hybrid District and Distributed Heating

Studies [35, 39] have contributed a promising conception of DHS development that prioritizes reliability assurance. At the core of this conception is the transformation of existing systems or establishment of new ones that are built in line with the principles of synergistic integration of district heating and distributed heating. Such systems, which we refer to as hybrid district and distributed heating systems (HDDHS) have a multi-level hierarchical structure formed by hydraulically independent heating circuits. The circuits implement distributed sources run by prosumers at each level of heat generation to serve the heat load at the nodes of the original layout where reliability goes beyond the acceptable range of nodal reliability indices and efficiency lies outside the acceptable range of economic heat distribution distances (EHDD).

Figure 2 shows the overall flowchart of the algorithm for the design of hybrid district and distributed heating systems with a multi-level structure of distributed heating (DH) subsystems based on HSs run by prosumers. *Stage I* identifies the range of efficient operation of district heating of the original HS layout in terms of its EHDD. *Stage II* localizes DH subsystems so that the problems of their operation are solved within these subsystems. *Stage III* delimits the EHDD boundaries within the selected DH subsystem. If there are consumers outside these boundaries, they are assumed to be connected to the source of the second-level DH: thus, a bi-level (or, generally, multi-level) hierarchical structure is formed with each level having its own prosumers. *Stage IV* focuses on reliability analysis within the efficient operation range obtained for the selected subsystem and identifies low-reliability nodes to ensure their required redundancy. *Stage V* forms a multi-level HDDHS with efficient and reliable heating supply. Figure 3 shows an algorithm for HDDHS formation, including all the main stages discussed above. This algorithm is capable of accomplishing a wide range of scientific and methodological tasks, including stochastic modeling of the studied system operation (to determine the probabilities of emergency states) and thermal-hydraulic modeling of emergency conditions corresponding to failures of system components. The set of reliability problems corresponding to stage C-5 (see Fig. 3) includes, in addition to stochastic modeling of states, the use of optimization procedures to find solutions for structural and parametric redundancy of the system.

A detailed description of the HDDHS formation algorithm, as well as the methods and models used are presented in [38]. The application of the developed methods to the real-life DHS is considered in the paper [39], which also discusses the achieved reliability and economic effects. Thus, the formation of the considered distributed heating subsystem connected to the prosumer source improves reliability by 44%, while structural redundancy in the system increases reliability to 62% (based on the adopted key reliability indices – availability factor and failure-free operation probability). The total economic benefit is estimated at about RUB 94 million per year, or 48% of the operating costs corresponding to the initial heating system diagram. The economic benefit derived from localizing the distributed heating subsystem based on the prosumer can be attributed to two reasons: 1) a reduction in the thermal energy cost through a decrease in operating network costs for pumping at a reduction in the heating supply distance; 2) a reduction in damage from shortages due to increased reliability. An additional economic benefit can be gained in the district system by lowering operating costs through the integration of distributed heat sources to meet part of the heating demand. The optimal distribution of the load of district and prosumer sources over the calculation period demonstrates the economic effect that can be obtained [40]. For example, the effect can be achieved by changing thermal energy output from the prosumer distributed source and the corresponding operating costs. The greater the part of the load covered by the subsystem self-generation, the smaller the correction required to the resulting effect. However, this factor does not affect the value of the economic effect from damage reduction.

IV. Further Development of the Methodology for Analyzing DHS Reliability

As noted above, the transformations of heating systems entail not only the establishment of new facilities and incorporation of additional links but also the development of the theoretical foundations for solving the reliability problems of these systems. Simultaneously, it is crucial to enhance both production facilities and technologies.

For example, modeling the heating systems with a hybrid district and distributed heating structure which assumes parallel operation of district heating sources and distributed heating sources run by prosumers within a single interconnected heat network infrastructure, should be based on the hierarchy of technological processes capturing both physical and stochastic parameters of the

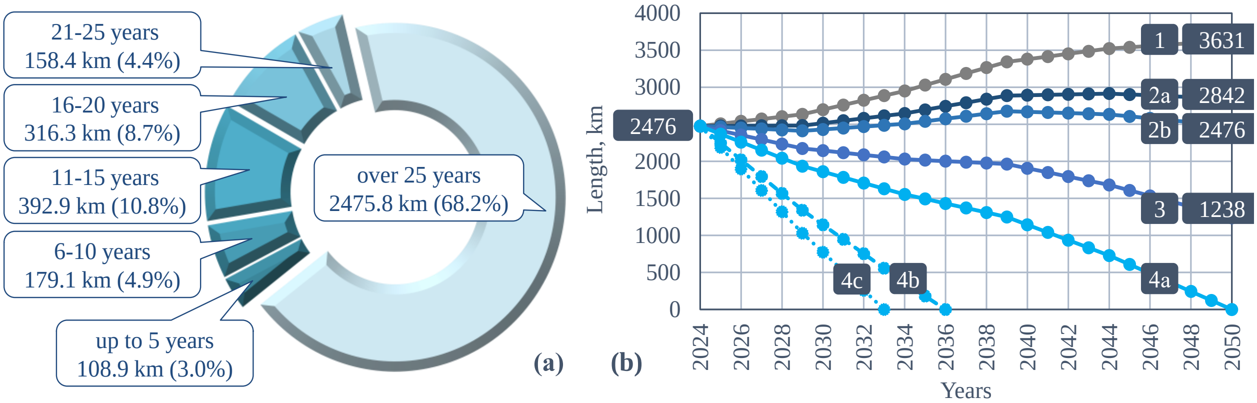

Fig. 4. Current state and projected wear and tear of heat networks in the Irkutsk region to 2050: (a) "age" structure of pipelines; (b) projected wear dynamics under different replacement rates: 1 – no re-laying, 2a – current rate (30.36 km/year), 2b – compensating rate (44.45 km/year), 3 – a 50% reduction in wear (92.06 km/year), 4a, 4b, 4c – complete elimination of wear by 2050 (139.67 km/year), by 2036 (258.97 km/year), and by 2033 (320.81 km/year), respectively.

system and their coordination at the upper level of system control [34]. In this context, the use of logical-probabilistic, stochastic, or statistical models deemed suitable for conventional district heating systems may lead to faulty results that leave out of consideration the concurrent and dependent failures of components operating at different critical facilities and levels of district heating and distributed heating segments of the system. It is important to note that subsystems of different levels are not autonomous, but rather function together to make load redistribution and redundancy possible. On the other hand, this also complicates the failure effects analysis, which relies on emergency thermal-hydraulic conditions in the heat network combined with modeled HSs failures. The design of a hierarchical control system of the heating system with a multi-level generation structure is a research problem in its own right, which involves accomplishing a number of technological (creation of production facilities), theoretical, applied, information-related, and regulatory tasks. The above methodological aspects are equally important for the reliability synthesis of systems being examined and for the establishment of regulatory standards aimed at ensuring high reliability and quality in heating supply.

V. Wear and Tear of the Heat Network Infrastructure in Heating Systems

The key factor hindering the implementation of the majority of promising solutions for heating system development is poor equipment health, mainly that of heat network equipment. For example, there were 4 203 documented incidents in the heating systems operating in Russia in 2022, of which 497 (12%) were in heat sources and 3 706 (88%) were in heat networks [41]. There were 1 327 600 people affected by these incidents in 2022. In this context, the Irkutsk region is an illustrative example (Fig. 4).

The total length of HNs in the region is 3 631 km, whereas the worn out part is 2 476 km (68.2%), of which about 37% is dilapidated, being a priority for replacement to ensure that the incident rate at least does not exceed its current level. Figure 4-b shows projected changes in the length of worn-out HN pipelines for different rates of their restoration. The projection method relies on the following input data: a) the current wear of heat networks (as of 2024); b) the age structure of operating networks in terms of length (Fig. 4-a); c) the current rate of replacement (restoration). These data allow us to estimate the length of pipelines to be worn out annually, according to their service life (over 25 years). Thus, a wear curve is calculated without factoring in renewal. Changing the rate of pipeline replacement can impact the resulting trend either decelerating it or transforming it into a trend of restoration. The existing rate of renovation (curve 2a) fails even to maintain the current level of wear during the projection period. A 50% reduction in wear would require a 3-fold rise in the re-laying rate (curve 3), and more than a 4.5-fold increase to eliminate it completely (curve 4a).

VI. Conclusion

The above review of published research on theoretical and applied reliability problems of heating systems undergoing technological and structural changes has revealed that these problems are either understudied or weakly connected to other lines of research. This may result in inconsistent policies that hinder the development of the systems, as these policies may lack deliberate and balanced decision-making that considers conflicting multiple criteria of economic performance, efficiency, and reliability.

The array of modern technologies used for development and transformation of district heating systems to ensure and enhance their reliability is diverse both in terms of the scope of application (subsystems, facilities, equipment) and the scale of modernization of the systems. As heat generation and distribution technologies continue to evolve, the vision of energy sector development shifts to embracing the trend towards the establishment of integrated multi-energy complexes. These complexes suggest integrating heating systems with various other systems (electricity, gas, and oil systems, as well as those based on renewables), which, along with other effects, leverages interchangeability of energy resources, thereby increasing the redundancy at different levels within the system. In line with this conception, it can be argued that there is much promise in the transition to hybrid district and distributed heating systems with a multi-level hierarchical structure based on prosumer subsystems implemented at each generation level to serve the heat load of the nodes of the original scheme, whose reliability and efficiency go beyond the acceptable limits. In terms of methodological development, a number of assumptions deemed appropriate for modeling conventional district heating systems become restrictive when applied to hierarchical layouts of hybrid district and distributed heating systems, which prompts the development of a methodological framework for reliability analysis and synthesis.

Another important reliability aspect of heating systems is equipment health. The current level of wear and tear of heat networks necessitates a multiple-fold increase in renovation rates, along with a significant rise in funding, which is currently beyond reach. As a result, there is a growing imbalance in ensuring the reliability of heating systems in the process of their evolution: on the one hand, the technological change and structural transformation are irreversible, on the other hand, a number of major unresolved issues greatly hinder the adoption of innovations. Addressing top-priority issues of reliability of the existing systems to achieve, first of all, their normal (i.e., to specifications) and reliable operation is critical for the effective transition to the future stages of their evolution.

The main developments of the study are a methodology and an algorithm for the formation of district-distributed heating systems. The key limitations assumed in the development of the methodology are as follows: a) for stochastic modeling, we assumed the simplest failure flow of components characterized by typical behavior, independence, and an exponential distribution; b) for thermal-hydraulic modeling, we assumed the main parameters of steady-state conditions in the system (temperature, pressure, flow rates, and others) would remain constant. A number of practical limitations associated with the implementation of district-distributed heating facilities concern the technical level of existing heating systems for innovative transformations. First of all, these are current high wear of heat network, system misalignment, as well as a low level of digitalization and process control.

Advancing the proposed methodology involves addressing many scientific, methodological, and applied problems. At this stage, the priority ones are as follows:

1) Determining the feedback loop of solutions obtained at various levels of the district-distributed heating system (achieving an optimal multi-level system structure necessitates an iterative procedure with “floating” efficiency and reliability criteria to be implemented until some equilibrium solution is reached with acceptable accuracy);

2) Developing methods for optimal loading (based on technical and economic criteria) of district and distributed heat sources in accordance with the thermal load curve during the design period (possible approaches include two-level programming methods, game approaches, and others);

3) Improving the methods designed to ensure reliability of the district-distributed heating system by expanding the use of various functional and structural redundancy methods in prosumer subsystems, including the ability to supply thermal energy into the district network to compensate for emergency shortages;

4) Detailing prosumer circuits, considering the technological and operational factors of their connection to the district system, the conditions and requirements for the reliable operation of the system throughout the entire period, and the range of possible emergency states and events.

Acknowledgment

This research was carried out as part of the State Assignment Project (No. FWEU-2021-0002) of the Program for Basic Research of the Russian Federation for 2021–2030.

References

[1] Systems studies in energy: the energy transition, N. I. Voropai, A. A. Makarov, Eds. Irkutsk, Russia: Melentiev Energy Systems Institute, SB RAS, 2022. ISBN 978-5-93908-153-5. (In Russian)

[2] A. Rafati et al., “Data-driven reliability analysis of district heating systems for asset management applications: A review.” Sustainable Cities and Society, vol. 118, Art. no. 106052, 2025.

[3] M. Valinčius et al., “Integrated assessment of failure probability of the district heating network,” Reliability Engineering & System Safety, vol. 133, pp. 314–322, 2015.

[4] M. Badami et al., “Design of district heating networks through an integrated thermo-fluid dynamics and reliability modelling approach,” Energy, vol. 144, pp. 826–838, 2018.

[5] I. Postnikov, “Probabilistic modeling of functioning of district-distributed heating systems for the reliability analysis,” E3S Web of Conf., vol. 397, Art.no. 02004, 2023.

[6] H. Rasoulian, “Reliability, availability and resilience assessment of heating systems using sequential Monte-Carlo simulation and critical load analysis,” M. S. thesis, Concordia University, Montreal, Canada, 2022.

[7] P. Gilski et al., “Probability of failure assessment in district heating network,” in The 14th International Symposium on District Heating and Cooling, Stockholm, Sweden, 2014.

[8] N. Marx et al., “Risk assessment in district heating: Evaluating the economic risks of inter-regional heat transfer networks with regards to uncertainties of energy prices and waste heat availability using Monte Carlo simulations,” Smart Energy, vol. 12, Art. no. 100119, 2023.

[9] I. Postnikov, E. Mednikova, “A reliability analysis of fuel supply for district heating systems based on statistical test method,” Energy Reports, vol. 8, pp. 304–311, 2022.

[10] L. K. Mortensen et al., “A probabilistic approach to reliability analysis of district heating networks incorporating censoring: A report of implementation experiences,” Energy Informatics, vol. 5(3), 2022.

[11] S. G. Ziganshin et al., “Reliability of thermal networks for city development,” Procedia Engineering, vol. 150, pp. 2327–2333, 2016.

[12] M. H. Khoshgoftar Manesh et al., “New procedure for determination of availability and reliability of complex cogeneration systems by improving the approximated Markov method,” Applied Thermal Engineering, vol. 138, pp. 62–71, 2018.

[13] E. Losi et al., “Data-driven approach for the detection of faults in district heating networks,” Sustainable Energy, Grids and Networks, vol. 38, Art. no. 101355, 2024.

[14] D. Mao et al., “Understanding District Heating Networks Vulnerability: A Comprehensive Analytical Approach with Controllability Consideration,” Sustainable Cities and Society, vol. 101, Art. no. 105068, 2024.

[15] D. Mao et al., “Failure consequence evaluation of uncontrollable district heating network,” Sustainable Cities Society, vol. 78, Art, no. 103593, 2022.

[16] O. Maliavina et al., “Development of statistical modeling of the pipelines’ reliability projections of the main heat networks, according to the period of operation and diameter,” EUREKA: Physics and Engineering, vol. 2, pp. 74–81, 2022.

[17] I. Žutautaite et al., “Risk and reliability assessment of the district heating network methodology with case study,” in European safety and reliability conference ESREL 2016, Glasgow, Scotland, Tim Bedford London: CRC Press (Taylor & Francis group), 2017.

[18] X. Shan et al., “The reliability and availability evaluation of repairable district heating networks under changeable external conditions,” Applied Energy, vol. 203, pp. 686–695, 2017.

[19] I. Postnikov, V. Stennikov, “Modifications of probabilistic models of states evolution for reliability analysis of district heating systems,” Energy Reports, vol. 6(2), pp. 293–298, 2020.

[20] K. Sernhed, M. Jönsson, “Risk management for maintenance of district heating networks,” Energy Procedia, vol. 116, pp. 381–393, 2017.

[21] S. R. Palakodeti, “Reliability Assessment in Asset Management – An Utility Perspective,” in Proc. the 10th World Congress on Engineering Asset Management (WCEAM 2015), Cham, Springer International Publishing, 2016, pp 447–457.

[22] L. K. Mortensen et al., “Relative fault vulnerability prediction for energy distribution networks,” Applied Energy, vol. 322, Art. no. 119449, 2022.

[23] L. K. Mortensen, H. R. Shaker, “Data-Driven reliability prediction for district heating networks,” Smart Cities, vol. 7, pp. 1706–1722, 2024.

[24] K. Kovacs et al., “A modified Weibull model for service life prediction and spare parts forecast in heat treatment industry,” Procedia Manufacturing, vol. 54, pp. 172–177, 2021.

[25] P. P. Langroudi, I. Weidlich, “Applicable predictive maintenance diagnosis methods in service-life prediction of district heating pipes,” Environmental and Climate Technologies, vol. 24(3), pp. 294–304, 2020.

[26] Y. Sun et al., “A practical approach for reliability prediction of pipeline systems,” European Journal of Operational Research, vol. 198(1), pp. 210–214, 2009.

[27] P. Dai et al., “Data-driven reliability evaluation of the integrated energy system considering optimal service restoration,” Frontiers in Energy Research, vol. 10, Art. no. 934774, 2022.

[28] C. Pan et al., “Reliability evaluation of integrated energy system based on exergy,” CSEE Journal of Power and Energy Systems, vol. 10, no. 6, pp. 2507–2516, 2024.

[29] Z. Li et al., “Energy supply reliability assessment of the integrated energy system considering complementary and optimal operation during failure,” IET Generation, Transmission & Distr., vol. 15(13), pp. 1897–1907, 2021.

[30] P. Mao et al., “Topology optimization of district heating network based on edge influence degree,” in Proc. the 2021 3rd International Conference on System Reliability and Safety Engineering (SRSE), China, Harbin, 2021. pp. 270–277.

[31] I. Postnikov et al., “A methodology for optimization of component reliability of heat supply systems,” Energy Procedia, vol. 105, pp. 3083–3088, 2017.

[32] V. Stennikov, I. Postnikov, “Methods for comprehensive analysis of heat supply reliability,” International Journal of Energy Optimization and Engineering, vol. 2(4), pp. 120–142, 2013.

[33] I. Postnikov et al., “Methodology for optimization of component reliability of heat supply systems,” Applied Energy, vol. 227, pp. 365–374, 2018.

[34] I. Postnikov, “Methods for the reliability optimization of district-distributed heating systems with prosumers,” Energy Reports, vol. 9, pp. 584–593, 2023.

[35] A. P. Merenkov, V. Ya. Khasilev, The theory of hydraulic circuits. Moscow, USSR: Nauka, 1985. (In Russian)

[36] E. V. Sennova, A. V. Smirnov, A. A. Ionin et al., Reliability of heating systems. Novosibirsk, Russia: Nauka, 2000. (In Russian)

[37] H. Lund et al., “4th Generation District Heating (4GDH): Integrating smart thermal grids into future sustainable energy systems,” Energy, vol. 68, pp. 1–11, 2014.

[38] V. A. Stennikov, I. V. Postnikov, E. E. Mednikova, “Methods and models for designing hybrid district and distributed heating systems and proving the efficiency and reliability of their operation,” Izvestiya RAN. Energetika, no.5, pp. 3–14, 2024. (In Russian)

[39] V. A. Stennikov, I. V. Postnikov, E. E. Mednikova, “Assessment of the efficiency and reliability performance of the existing heating system and proposals for the development of the distributed heating sector with the introduction of prosumers,” Izvestiya RAN. Energetika, no.1, pp. 3–12, 2025. (In Russian)

[40] V. A. Stennikov, I. V. Postnikov, A. V. Penkovskii, “A Methodology for Performance and Reliability Analysis of Prosumers’ Local Heat Sources in District Heating System,” Energy Systems Research, vol. 6(3), pp. 17–27, 2023.

[41] State of the heating sector and district heating in the Russian Federation in 2022. Moscow, Russia: Ministry of Energy of Russia, Russian Energy Agency, 2023. (In Russian)

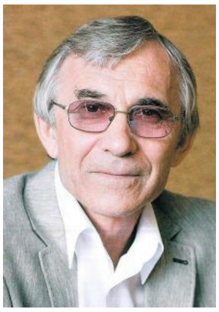

Valery A. Stennikov, Academician of the Russian Academy of Sciences (RAS), Dr. Eng., Professor, serves as Director of the Melentiev Energy Systems Institute of the Siberian Branch of the Russian Academy of Sciences (ESI SB RAS), Irkutsk, Russia. Valery Stennikov has authored and co-authored over 500 scientific publications. His research interests include systems research in the energy industry, theory of hydraulic circuits, mathematical modeling, optimization methods, heating systems, district heating systems, cogeneration, reliability, energy efficiency, energy saving, and intelligent energy systems.

Ivan V. Postnikov, Ph.D., is a Senior Researcher in the Laboratory of Heating Systems of ESI SB RAS, Irkutsk, Russia. He received the Ph.D. degree from ESI SB RAS in 2013. Ivan Postnikov has authored and co-authored over 130 scientific publications. His research interests include energy systems, district heating systems, mathematical modeling, reliability, random processes, optimization, energy efficiency, intelligent energy systems, prosumer, and renewable energy.

Ant Lion Optimization and Grey Wolf Optimizer to Optimally Locate Single and Multiple Distributed Generation Units and Capacitor Shunts in Power Distribution Networks

A.M. Al-Hadeethi[1,*], B.H. Al Igeb[1], P.P. Oshchepkov[1]

[1] People's Friendship University of Russia (RUDN), Moscow, Russia

Abstract **Power supply challenges continue to be a significant issue, necessitating ongoing efforts to enhance power generation, network infrastructure, and system configurations. Notably, the integration of distributed generation (DG) units and capacitor shunts (CSs) has emerged as a key advancement. With the escalating complexity and scale of power systems, optimizing these components to maximize benefits and mitigate drawbacks has become essential. Consequently, optimization has become a crucial element in the development of algorithms. This study proposes the utilization of the Grey Wolf Optimizer (GWO) and Ant Lion Optimization (ALO) methods for determining the optimal sizing of capacitor shunts and distributed generation units within distribution systems. The Reconfiguration Method (RM) is employed to identify the optimal location for single-generation units and capacitor shunts, while the Loss Sensitivity Factor (LSF) is utilized to determine the optimal placement for multiple DG units and CSs. The primary objective is to minimize real power losses across the entire system by selecting the optimal sizes with GWO and ALO, while also optimizing their placement using LSF and RM. The performance of the proposed algorithms, GWO and ALO, was evaluated using the IEEE 33-bus power system. Four distinct scenarios were employed to demonstrate the superiority and effectiveness of these optimization methods.**

Index Terms **— Capacitor shunt, distributed generation, Grey Wolf Optimizer, Ant Lion Optimization, optimal allocation, real power loss minimization, IEEE 33-bus system.**

* Corresponding author.
E-mail: ahmedbohl@gmail.com

DOI:10.25729/esr.2025.03.0005

Received July 16, 2025. Accepted September 20, 2025. Available online November 28, 2025.

I. INTRODUCTION

The increasing global demand for energy, driven by social, economic, and industrial developments, makes efficient power supply a critical concern. Distribution networks, which represent a significant investment and directly connect with consumers, are particularly susceptible to power losses, with approximately 70% of real power losses occurring within these networks [1]. Traditional solutions, such as building new generation stations, are often costly and time-consuming. Consequently, modern approaches focus on optimizing existing infrastructure through network reconfiguration and the strategic integration of devices like distributed generation (DG) units and capacitor shunts (CSs).

DG units, which can be renewable (e.g., solar, wind) or conventional (e.g., fuel cells), are strategically placed near consumption points to enhance system reliability, reduce power losses, improve network performance, and defer the need for new distribution feeders. The integration of DG also transforms traditional unidirectional power flow into bidirectional flow, introducing new complexities and opportunities [2]. However, the unpredictable nature of renewable energy sources necessitates careful planning to avoid negative impacts such as overvoltage or exceeding feeder load limits. Similarly, the installation of CSs is crucial for optimizing voltage profiles, increasing voltage stability, decreasing real power loss, and improving power factor and quality by injecting reactive power into the system. Both DG and CS placement and sizing require meticulous study to maximize their benefits and avoid adverse effects [3]. Various optimization techniques, including heuristic, analytical, and hybrid methods, are proposed for the optimal allocation of DG units and CSs in power systems [4]. For instance, enhanced Ant Lion Optimization (ALO) and Particle Swarm Optimization (PSO) are used for DG allocation in IEEE 69-bus systems [5]. The Grey Wolf Optimizer (GWO) is also widely applied for optimal DG placement and sizing [6, 7]. Other metaheuristic algorithms, such as Harris Hawks Optimization (HHO) [8] and Wild Horse Optimizer (WHO) [9], are explored for similar purposes. The optimal planning of PV sources and D-STATCOM devices, incorporating network reconfiguration using a Modified Ant Lion Optimizer, is investigated in [10]. Similarly, [11] proposes a modified Ant Lion Optimization algorithm for efficient distributed generation allocation in power distribution networks. Furthermore, [12] utilizes an Ant Lion Optimizer-based multi-objective approach for the simultaneous optimal allocation of distributed generations and synchronous condensers in distribution networks. Hybrid approaches combining analytical techniques with optimization algorithms show promise in minimizing power loss and improving voltage profiles [13–16]. A fuzzy genetic approach for network reconfiguration is applied to enhance voltage stability in radial distribution systems [17]. A hybrid of ant colony optimization and artificial bee colony algorithm is employed for probabilistic optimal placement and sizing of distributed energy resources [18].

This paper introduces a novel hybrid optimization strategy for the simultaneous optimal placement and sizing of DG units and CSs in radial distribution networks, specifically targeting the minimization of real power losses. While the application of metaheuristic algorithms to this problem is not new, our work distinguishes itself through a rigorous and direct comparative performance analysis of two prominent nature-inspired algorithms, GWO and ALO, within a unified hybrid framework. We employ a two-step process: the Reconfiguration Method (RM) for single-unit placement and the Loss Sensitivity Factor (LSF) for multiple-unit placement, which effectively streamlines the search space. This allows the powerful GWO and ALO algorithms to focus solely on determining the optimal component sizes, thereby significantly enhancing computational efficiency and the quality of the solution. The study evaluates the performance of this hybrid approach on the IEEE 33-bus system under four distinct and practical scenarios, providing a comprehensive understanding of how these optimization tools perform under various system planning conditions. This direct comparison, coupled with the systematic evaluation across diverse scenarios, offers valuable insights into the strengths and weaknesses of GWO and ALO for real-world power system optimization challenges.

The primary contributions of this study are summarized as follows:

Novel Hybrid Optimization Framework: Development and application of a hybrid methodology that combines deterministic placement strategies (RM for single units, LSF for multiple units) with metaheuristic sizing algorithms (GWO and ALO) to efficiently minimize real power losses in distribution networks.

Direct Comparative Performance Analysis: A rigorous and direct comparison of GWO and ALO for minimizing real power loss through DG and CS integration, tested on the identical IEEE 33-bus system under four distinct and practical scenarios.

Comprehensive Scenario Evaluation: Unlike studies that may focus on a single type of installation, our research evaluates the problem across a comprehensive set of four scenarios (single CS, single DG, multiple CSs and multiple DG units). This provides a broader understanding of how these optimization tools perform under different system planning conditions and demonstrates that the installation of multiple DG units yields the most significant reduction in power losses among the tested configurations.

Improved System Performance: The proposed optimization approach consistently leads to significant reductions in real power losses, alongside improvements in voltage profiles and an enhanced voltage stability index across all evaluated scenarios.

The remainder of this paper is organized as follows: Section 2 details the problem formulation, including objective functions, constraints, the Reconfiguration Method, and the Loss Sensitivity Factor. Section 3 presents the mathematical models and overviews of the proposed GWO and ALO algorithms. Section 4 discusses the simulation results for optimal location and size of single DG units, single CSs, multiple DG units, and multiple CSs on the IEEE 33-bus system. Finally, Section 5 provides the conclusions and outlines avenues for future research.

Convergence Analysis: The convergence characteristics of both algorithms were analyzed by plotting the best fitness value against the number of iterations. The analysis reveals GWO typically converges faster than ALO, reaching near-optimal solutions within 60–70 iterations ALO shows more exploration in the early iterations but may require more iterations to converge. Both algorithms demonstrate good convergence characteristics without premature stagnation. These statistical results provide strong evidence for the effectiveness and reliability of the proposed optimization approach, with GWO showing superior performance in terms of solution quality and consistency.

II. PROBLEM FORMULATION

The proposed approach aims to determine the optimal locations and sizes of DG units and CSs to minimize total real power losses in a multi-constrained radial distribution network (RDN).

A. Power Flow

The radial distribution network (RDN) single-line diagram is shown in Fig. 1. The real and reactive power will be supplied from bus a and received at bus b. The real and reactive powers of buses a and b can be calculated as follows [4]:

$$P_a = P_b + P_{l,b} + R_{ab}\left(\frac{\left(P_{l,a}+P_{l,b}\right)^2+\left(Q_{l,b}+Q_{l,b}\right)^2}{|V_b|^2}\right), \quad (1)$$

$$Q_a = Q_b + Q_{l,b} + X_{ab}\left(\frac{\left(P_{l,a}+P_{l,b}\right)^2+\left(Q_{l,a}+Q_{l,b}\right)^2}{|V_b|^2}\right), \quad (2)$$

$$V_b = \left(V_a^2 - 2\left(P_a R_a + Q_a X_{ab}\right) + \left(R_{ab}{}^2 + X_{ab}{}^2\right)\left(\frac{P_a^2+Q_a^2}{V_a^2}\right)\right), \quad (3)$$

where P_a and P_b are the real powers at buses a and b, respectively; $P_{l,a}$ and $P_{l,b}$ are real load powers at buses a and b, respectively; Q_a and Q_b are the reactive powers at buses a and b, respectively; $Q_{l,a}$ and $Q_{l,b}$ are reactive load powers at buses a and b, respectively; R_a and R_{ab} are the resistance and reactance of lines a and b, respectively; V_b is the voltage at bus b; V_a is the voltage at bus a; X_{ab} is the line impedance.

The real power loss in lines between buses a and b can be computed as follows:

$$P_{loss(a,b)} = R_{a,b}\left(\frac{P_a{}^2 + jQ_a{}^2}{|V_a|^2}\right). \quad (4)$$

The reactive power loss in lines connecting buses a and b is calculated as follows:

$$Q_{loss(a,b)} = X_{a,b}\left(\frac{P_a{}^2 + jQ_a{}^2}{|V_a|^2}\right), \quad (5)$$

where j in this context, is not a variable but the imaginary unit.

Therefore, the total real and reactive power losses in radial distribution network are the following:

$$TP_{loss} = \sum_{a,b}^{Nb_r} P_{loss(a,b)}, \quad (6)$$

$$TQ_{loss} = \sum_{a,b}^{Nb_r} Q_{loss(a,b)}, \quad (7)$$

where TP_{loss} is total real power loss, TQ_{loss} is total reactive power loss, Nb_r is the total number of branches in the network (IEEE 33-Bus system).

B. Objective Function

The primary objective of this study is to minimize the total real power losses in the distribution network. Minimizing real power losses also leads to improved voltage profiles and a higher voltage stability index. The objective function can be expressed in the following

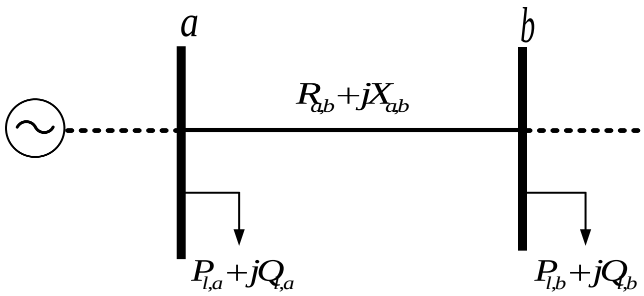

Fig. 1. Single line diagram for two buses of radial distribution network.

manner:

$$P_{loss} = \sum_{a=1}^{N}\sum_{b=1}^{N} \alpha_{ab}(P_a P_b + Q_a Q_b) + \beta_{ab}(Q_a P_b - P_a Q_b), \quad (8)$$

where N represents the total number of busses in the system, α_{ab} and β_{ab} can be calculated as follows:

$$\alpha_{ab} = \frac{R_{ab}}{V_a V_b}\cos(\alpha_a - \alpha_b), \quad (9)$$

$$\beta_{ab} = \frac{R_{ab}}{V_a V_b}\sin(\alpha_a - \alpha_b). \quad (10)$$

Here α_a, α_b are the voltage phase angles (in radians) at bus *a* and *b* respectively.

C. Problem Constraints

The optimization problem is subject to both equality and inequality constraints to ensure a realistic and stable operation of the power system.

1) Equality Constraints

The equality constraints represent the balance between generation and load with the power losses in lines, and can be expressed through as follows:

$$\sum_{i=1}^{N_G} P_{Gen}(i) + \sum_{i=1}^{N_{DG}} P_{DG}(i) - \sum_{i=1}^{N_{load}} P_{Demand}(i) - \sum_{i=1}^{N_{line}} P_{Loss}(i) = 0, \quad (11)$$

$$\sum_{i=1}^{N_G} Q_{Gen}(i) + \sum_{i=1}^{N_{DG}} Q_{DG}(i) + \sum_{i=1}^{N_{CS}} Q_{CS}(i) - \sum_{i=1}^{N_{load}} Q_{Demand}(i) - \sum_{i=1}^{N_{line}} Q_{Loss}(i) = 0, \quad (12)$$

where P_{Gen}, P_{DG}, P_{Demand}, and P_{Loss} denote to real power of generators, distributed generations, demand, and losses, respectively; Q_{Gen}, Q_{DG}, Q_{CS}, Q_{Demand}, and Q_{Loss} refer to reactive power of generators, distributed generations, capacitor shunt, demand, and losses, respectively; N_G, N_{DG}, N_{CS}, N_{load}, and N_{line}, denote to the number of generators, distributed generations, capacitors shunts, loads, and lines, respectively.

2) Inequality Constraints

Inequality constraints provide limits or bounds on specific variables or expressions. Usually, they specify areas or requirements that the variables need to meet. One way to characterize the inequality constraints is as follows:

a) *Bus voltage:* Due to the inequality constraint, voltage at each bus must fall within the given bounds.

$$V_q^{\min} \le V_q \le V_q^{\max}, \quad (13)$$

where $V_q^{\min}$ and $V_q^{\max}$ indicate the lowest and highest voltage values at bus q represented as the range of 0.95 to 1.05.

b) *Line current:* Every branch's current flow cannot exceed its thermal limit due to the inequality constraint

$$I_{ab} \le I_{ab}^{rated}, \quad (14)$$

where I_{ab}^{rated} represents the thermal limit between nodes a and b, and I_{ab} is the line current between nodes a and b.

c) *DG capacity:* A particular percentage of the total feeder load cannot be exceeded by distributed generation capacity, according to the inequality constraint

$$\sum\sqrt{(P_{DG})^2 + (Q_{DG})^2} = \sum\sqrt{(P_L)^2 + (Q_L)^2}. \quad (15)$$

where P_L, Q_L represents the total system active and reactive load demand respectively.

d) *DG capacity:* A particular percentage of the network's total feeder load cannot be exceeded by distributed generation capacity, according to the inequality constraint

$$\sum Q_C = \sum Q_L. \quad (16)$$

where Q_C is the total reactive power compensation from all capacitor shunts.

III. Overview of the Proposed Methodology

System performance in distribution networks is highly dependent on the optimal selection of bus locations for DG and CS integration. This study employs a hybrid approach that combines deterministic methods for identifying candidate locations with metaheuristic algorithms for determining optimal sizing. The Reconfiguration Method (RM) is utilized for the placement of single capacitor shunts (CSs) and distributed generation (DG) units, while the Loss Sensitivity Factor (LSF) guides the placement of multiple units. Subsequently, the Grey Wolf Optimizer (GWO) and Ant Lion Optimization (ALO) algorithms are employed to determine the optimal sizes of these components at the identified locations, with the overarching objective to minimize real power losses.

A. Reconfiguration Method (RM)

Reconfiguration method is the suggested strategy for determining the best placement of single CS and DG connection. By positioning the source (CS or DG) at each bus and figuring out the actual power losses there, the reconfiguration method determines which bus is optimal. The bus that has the lowest real power loss value is the ideal bus, and all of the bus losses combined will be ranked. The primary actions that need to be taken while using distinct single DG unit and CS are:

- Calculating the real power loss at each bus after connecting DG unit and CS, thus selecting the optimal size based on GWO and ALO.
- Identifying the bus that has the lowest real power loss to link the CS and the DG unit.
- Determining the size of DG unit and CS unit according to GWO and ALO.

B. Loss Sensitivity Factor (LSF)

LSF is the indicator used to determine the best location of CSs and DG sources (candidate buses). The bus will be selected by determining which buses have the most sensitive active and reactive power injection. LSFs help minimize the search area and optimize the process by reducing the time required for optimization. Using LSF calculations based on load flow, buses are arranged in declining order. The active power loss in this line can be defined as $I_{ab}^2 R_{ab}$, where:

$$P_{loss(a,b)} = \frac{\left(P_a^2 + Q_a^2\right) R_{ab}}{\left(V_a\right)^2}. \quad (17)$$

LSFs can be computed using the following equation [4]:

$$LSFP(p) = \frac{2P_{loss} R_{ab}}{\left|V_m\right|^2}, \quad (18)$$

$$LSFQ(p) = \frac{2Q_{loss} X_{ab}}{\left|V_m\right|^2}, \quad (19)$$

where Q_{loss}, P_{loss} are the losses on the branch for which the sensitivity is being computed; p denotes the bus number at which the sensitivity factor is being calculated; *LSFP* the loss sensitivity factor with respect to active power injection at bus p; *LSFQ* the loss sensitivity factor with respect to reactive power injection at bus p; P_a the real power flow in the line connected to the bus p; R_{ab}, X_{ab} the resistance and reactance of line connected to bus p; V_m the voltage magnitude at bus p.

C. Grey Wolf Optimizer (GWO)

GWO is a nature-inspired metaheuristic algorithm that mimics the social hierarchy and hunting behavior of grey wolves. The algorithm models the leadership hierarchy among wolves, which consists of alpha (α), beta (β), delta (δ), and omega (ω) wolves. The alpha wolf represents the best solution found so far, guiding the search process. Beta and delta wolves assist the alpha in hunting, while omega wolves follow the dominant wolves. This hierarchical structure facilitates a collaborative search for the optimal solution through iterative updates of wolf positions [19].

The main phases of GWO include:

• **Encircling Prey**: Wolves adjust their positions to encircle the prey, mathematically represented by updating their current positions based on the position of the prey.

• **Hunting**: The hunting process is guided by the three best solutions (alpha, beta, and delta wolves). Other wolves update their positions based on the positions of these three leaders.

• **Attacking Prey** (Exploitation): As the hunting progresses, the wolves converge towards the prey. This phase is characterized by a decreasing parameter that controls the exploration and exploitation balance, allowing the algorithm to narrow down the search to promising regions.

• **Searching for Prey** (Exploration): Wolves also diverge to explore new areas in the search space, preventing premature convergence. This exploration phase is crucial for finding globally optimal solutions.

In the context of this problem, the positions of the wolves correspond to the sizes of the DG units and CSs. The alpha wolf represents the combination of DG and CS sizes that yields the minimum real power loss. The iterative updates of the wolf positions allow the algorithm to efficiently search for the optimal sizing configuration.

D. Ant Lion Optimizer (ALO)

ALO is another metaheuristic algorithm inspired by the hunting mechanism of ant lions in nature. Ant lions dig cone-shaped traps in the sand to catch ants. The algorithm simulates the interactions between ants (representing candidate solutions) and ant lions (representing search agents) in the search space. The movement of ants is modeled as a random walk, while ant lions are responsible for constructing traps and capturing ants [20].

The key stages of ALO are:

• **Random Walks of Ants:** Ants move randomly in the search space, representing the exploration phase. The random walk is influenced by the ant lion's position.

• **Trap Construction:** Ant lions build traps, which are essentially the fitness landscapes around their current positions. Fitter ant lions (better solutions) have larger and more effective traps.

• **Ants Sliding Towards Ant lion:** When an ant falls into an ant lion's trap, its random walk is adjusted to simulate sliding towards the ant lion at the bottom of the cone. This represents the exploitation phase.

• **Catching Prey and Rebuilding the Trap:** Once an

TABLE 1. The Bus and Line Data of IEEE 33-Bus System

Bus Data			Line Data			
	Load		Bus			
Bus	*P*, kW	*Q*, kVAr	From	To	*R*, p.u.	*X*, p.u.
1	0	0	1	2	0.005753	0.002932
2	100	60	2	3	0.030760	0.015667
3	90	40	3	4	0.022836	0.011630
4	120	80	4	5	0.023778	0.012110
5	60	30	5	6	0.051099	0.044112
6	60	20	6	7	0.011680	0.038608
7	200	100	7	8	0.044386	0.014668
8	200	100	8	9	0.064264	0.046170
9	60	20	9	10	0.065138	0.046170
10	60	20	10	11	0.012266	0.004056
11	45	30	11	12	0.023360	0.007724
12	60	35	12	13	0.091592	0.072063
13	60	35	13	14	0.033792	0.044480
14	120	80	14	15	0.036874	0.032818
15	60	10	15	16	0.046564	0.034004
16	60	20	16	17	0.080424	0.107378
17	60	20	17	18	0.045671	0.035813
18	90	40	2	19	0.010232	0.009764
19	90	40	19	20	0.093851	0.084567
20	90	40	20	21	0.025550	0.029849
21	90	40	21	22	0.044230	0.058481
22	90	40	3	23	0.028152	0.019236
23	90	50	23	24	0.056028	0.044243
24	420	200	24	25	0.055904	0.043743
25	420	200	6	26	0.012666	0.006451
26	60	25	26	27	0.017732	0.009028
27	60	25	27	28	0.066074	0.058256
28	60	20	28	29	0.050176	0.043712
29	120	70	29	30	0.031664	0.016128
30	200	600	30	31	0.060795	0.060084
31	150	70	31	32	0.019373	0.022580
32	210	100	32	33	0.021276	0.033081

ant is caught, the ant lion's position is updated to that of the captured ant if it represents a better solution. The ant lion then rebuilds its trap, reflecting the improved solution.

In this study, the ants represent different combinations of DG and CS sizes, and the ant lions represent the potential optimal solutions. The algorithm iteratively refines the sizes by simulating the ant lion's hunting behavior, aiming to find a combination of DG and CS sizes that minimizes real power losses.

E. Algorithm Parameters

For the implementation of the Grey Wolf Optimizer (GWO) and Ant Lion Optimization (ALO) algorithms, specific parameters were carefully selected to ensure optimal performance and fair comparison. The following parameters were used in this study:

Grey Wolf Optimizer (GWO) Parameters: Population Size: 30 wolves. Maximum Iterations: 100. Search Space Dimension: Variable (depends on the

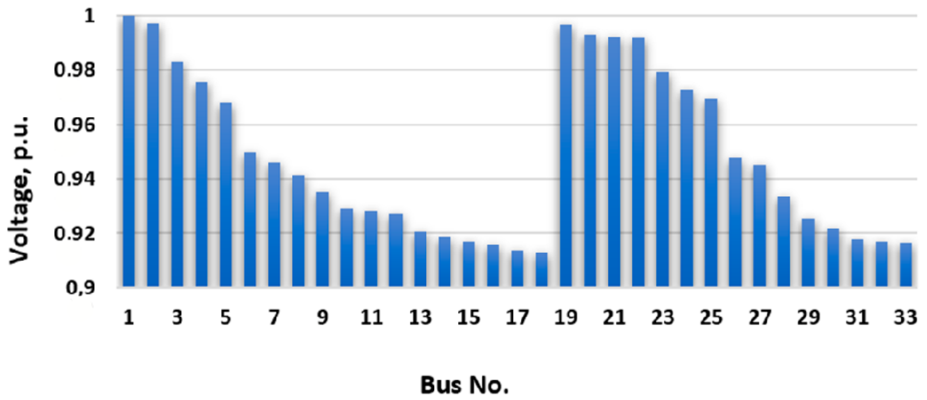

Fig. 3. Voltage profiles for initial case on IEEE 33-bus system.

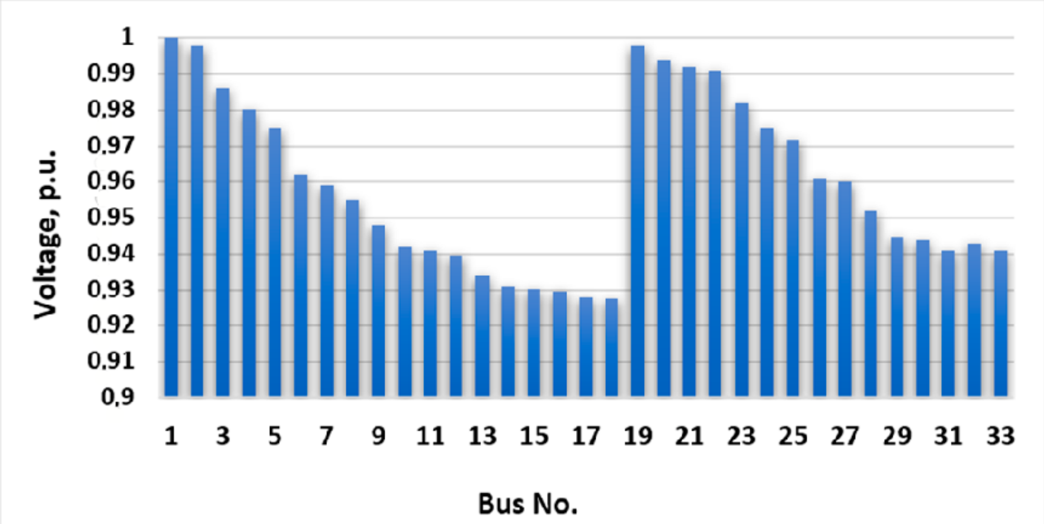

Fig. 4. Voltage profiles for Case 1: a single CS placed in IEEE 33-bus system using the ALO algorithm.

number of DG and CS units to be optimized). Convergence Parameter (a): Linearly decreases from 2 to 0 over the iterations. Random Vectors (r1, r2): Uniformly distributed random numbers in [0, 1]. Position Update Mechanism: Based on alpha, beta, and delta wolves' positions.

Ant Lion Optimization (ALO) Parameters: Population Size: 30 ants. Maximum Iterations: 100. Number of Ant Lions: 30. Random Walk Steps: 500. Elite Selection: Best ant lion is selected as elite. Roulette Wheel Selection: Used for ant lion selection. Random Walk Boundaries: Dynamically updated based on ant lions' positions.

IV. Simulation Results

This section presents the simulation results obtained applying the proposed hybrid optimization methodology to the IEEE 33-bus radial distribution network. The IEEE 33-bus system is a widely recognized benchmark for power system studies. The IEEE 33-bus power system's single line diagram is shown in Fig. 2. The Bus and Line data of IEEE 33-bus system are presented in Table 1.

The system comprises 33 buses and 32 lines, with base voltage and apparent power set at 12.66 kV and 10 MVA, respectively. The objective of these simulations is to demonstrate the efficacy of the GWO and ALO algorithms in minimizing real power losses through optimal placement and sizing of DG units and CSs under various scenarios.

The investigated scenarios include:

- **Initial Case (Base Case):** Represents the system without any DG or CS integration.
- **Case 1: Single source (CS):** Evaluates the impact of optimally placing and sizing a single CS.
- **Case 2: Single source (DG unit):** Assesses the effect of optimally placing and sizing a single DG unit.
- **Case 3: Multiple sources (CSs):** Examines the performance with multiple optimally placed and sized CSs.
- **Case 4: Multiple sources (DG units):** Investigates the impact of multiple optimally placed and sized DG units.

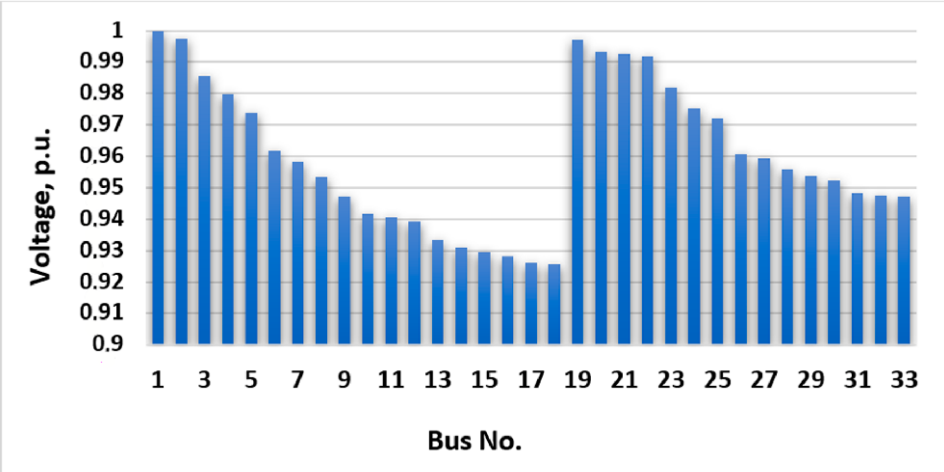

Fig. 5. Voltage profiles for Case 1: a single CS placed in IEEE 33-bus system using the GWO algorithm.

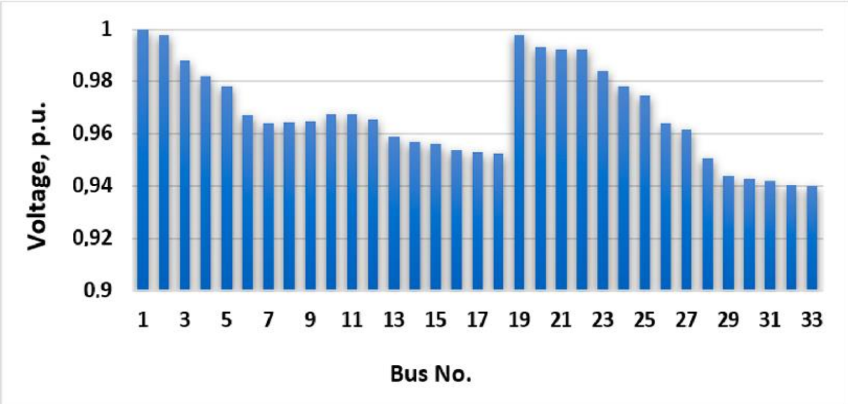

Fig. 6. Voltage profiles for Case 2: a single DG unit placed in IEEE 33-bus system using the ALO algorithm.

A. Initial Case (Base Case)

In this case, power flow calculations are performed using the Newton-Raphson method. The total loads for the active and reactive power are 3.715 MW and 2.3 MVAr, respectively. Reactive power losses total 0.1343 MVAr and active power losses amount to 0.2015 MW. The voltage magnitude reaches its minimum at 0.913 p.u. at bus 18 and its maximum at 0.997 p.u. at bus 2, as shown in Fig. 3. The voltage stability index (VSI) has minimum and highest values of 0.696 and 0.9883 on buses 18 and 2, respectively.

B. Case 1: Single Source (Capacity Shunt)

This case explores the optimal placement and sizing of a single CS unit using both ALO and GWO algorithms in conjunction with the Reconfiguration Method (RM).

1) Use of the ALO algorithm

With the ALO algorithm, the optimal location for the single CS is identified as bus 31, with an optimal size of 1.308 MVAr. This integration reduces the real power losses from the initial 0.2015 MW to 0.1515 MW, representing a 24.81% reduction. Figure 4 shows the voltage profile at each bus after installing a single CS. The minimum VSI at bus 18 improves from 0.6960 to 0.736 and reactive power losses decrease from 0.1343 MVAr to 0.1041 MVAr.

2) Use of the GWO algorithm

When employing the GWO algorithm, the optimal location for the single CS is determined to be bus 30, with an optimal size of 1.2527 MVAr. This results in a decrease in real power losses from 0.2015 MW to 0.1436 MW, achieving a 28.74% reduction. Figure 5 shows the voltage profile at each bus after installing a single CS. The minimum VSI at bus 18 improves from 0.6960 to 0.735 and reactive power losses decrease from 0.1343 MVAr to 0.0959 MVAr.

C. Case 2: Single Distributed Generation (DG) Source

This case investigates the optimal placement and sizing of a single DG unit using ALO and GWO with the

Reconfiguration Method (RM).

1) Use of the ALO algorithm

For the ALO algorithm, the optimal DG placement is at bus 10, with an ideal size of 1.92 MW. This leads to a significant decrease in real power losses from 0.2015 MW to 0.1255 MW, achieving a reduction of 37.73%. Figure 6 illustrates the voltage profile at each bus after installing a single DG unit. The minimum VSI at bus 18 increases from 0.6960 to 0.813 and reactive power losses decrease from 0.1343 MVAr to 0.0867 MVAr.

2) Use of the GWO algorithm

For the GWO algorithm, the optimal DG unit placement is at bus 6, with an ideal size of 2.575 MW. This results in a substantial power loss reduction from 0.2015 MW to 0.1037 MW, achieving a 48.54% reduction. Figure 7 illustrates the voltage profile at each bus after installing a single DG unit. The minimum VSI at bus 18 improves from 0.6960 to 0.8191 and reactive power losses decrease from 0.1343 MVAr to 0.0746 MVAr. Table 2 presents the comparison of the results obtained by GWO and ALO with other methods after installing a single DG unit.

D. Case 3: Multiple Capacitor Shunts (CSs)

This case investigates the optimal placement and sizing of multiple CS units using both ALO and GWO algorithms, guided by the Loss Sensitivity Factor (LSF).

1) Use of the ALO algorithm

Based on LSF values, the optimal candidate buses for multiple CS placement are 25, 2, 9, and 31. The ALO algorithm determines the optimal sizes for these CS units as 0.575 MVAr (bus 25), 0.6 MVAr (bus 2), 0.465 MVAr (bus 9), and 0.575 MVAr (bus 31). This configuration minimizes real power losses to 0.1382 MW, achieving a 31.41% reduction. Figure 8 presents the convergence characteristics of reactive power loss after installing multiple CS units using the ALO algorithm, given the number of populations is 50 and number of iterations is 50. Figure 9 illustrates the voltage profile at each bus after installing multiple CS units. The minimum VSI at bus 18 increases to 0.757.

2) Use of the GWO algorithm

For the GWO algorithm, the LSF also identifies buses 31, 25, 2, and 9 as optimal candidate locations. The optimal

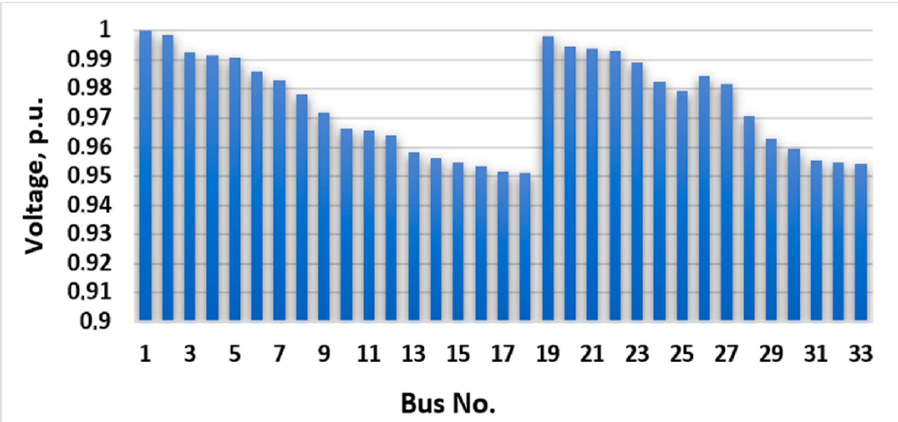

Fig. 7. Voltage profiles for Case 2: a single DG unit placed in IEEE 33-bus system using the GWO algorithm.

TABLE 2. Comparison of the Results Obtained by GWO and ALO with Other Methods after Installing a Single DG Unit

Method	Initial loss, MW	With a DG unit installed			Reduction %
		Loss, MW	Size, MW	Bus	
IWD [21]	0.2112	0.1110	2.49	6	47.46
BB-BC [22]	0.2110	0.1082	2.58	5	48.70
MINLP [23]	0.2110	0.1110	2.59	6	47.39
Analy. [24]	0.2112	0.1112	2.49	6	47.33
PSO [25]	0.2110	0.1153	3.15	6	45.36
PSO [26]	0.2110	0.1188	2.49	6	43.68
GWO	**0.2015**	**0.1037**	**2.575**	**6**	**48.54**
ALO	**0.2015**	**0.1255**	**1.92**	**6**	**37.73**

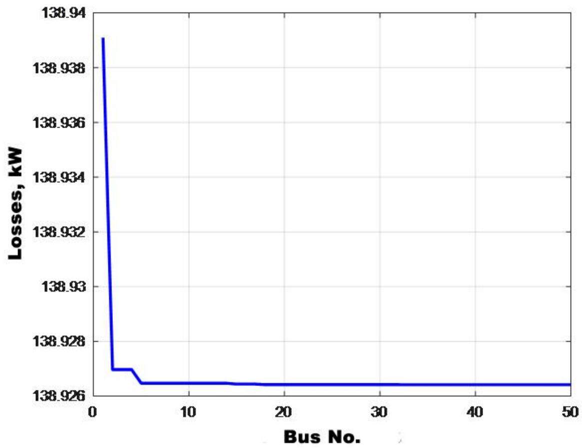

Fig. 10. The convergence characteristics of RPL after installation of multiple CSs using the GWO algorithm.

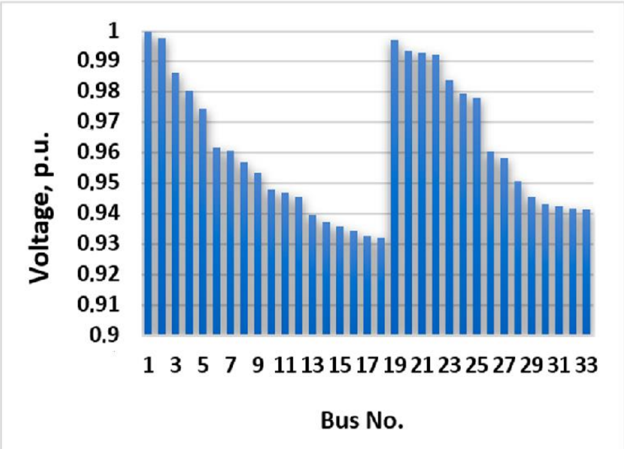

Fig. 11. Voltage profiles for Case 3: multiple CSs placed in IEEE 33-bus system using the GWO algorithm.

sizes for the multiple CS units are determined as 0.575 MVAr (bus 31), 0.4703 MVAr (bus 25), 0.575 MVAr (bus 2), and 0.575 MVAr (bus 9). This configuration results in real power losses minimized to 0.1384 MW, with a 31.31% reduction. Figure 10 presents the convergence characteristics of RPL after installing multiple CSs using the GWO algorithm, given the number of populations is 50 and the number of iterations is 50. Figure 11 presents the voltage profile at each bus. The minimum VSI at bus 18 increases to 0.755.

E. Case 4: Multiple Distributed Generation (DG) Sources

This case examines the optimal placement and sizing of multiple DG units using the ALO and GWO algorithms based on the Loss Sensitivity Factor (LSF).

1)Use of the ALO algorithm

Based on LSF values, the optimal candidate buses for placing multiple DG units are 25, 2, 9, and 31. The ALO algorithm determines the optimal sizes for these DG units as 0.9288 MW (bus 25), 0.9288 MW (bus 2), 0.8456 MW (bus 9), and 0.8994 MW (bus 31). This configuration minimizes real power losses to 0.0754 MW, achieving a substantial 62.59% reduction. Figure 12 presents the convergence characteristics of RPL after installation of multiple DG units using the ALO algorithm, given the number of populations is 50 and number of iterations is 50. Figure 13 presents the voltage profile at each bus. The minimum VSI at bus 18 increases to 0.8374.

2) Use of the GWO algorithm

For the GWO algorithm, the LSF also identifies buses 25, 2, 9, and 31 as optimal candidate locations. The optimal sizes for the multiple DG units are determined as 0.8558 MW (bus 25), 0.9288 MW (bus 2), 0.9288 MW (bus 9), and 0.9093 MW (bus 31). This configuration results in real power losses minimized to 0.0754 MW, with a 62.6% reduction. Figure 14 presents the convergence characteristics of RPL after installation of multiple DG units using the GWO algorithm, with a population size of 50 and 50 iterations. The voltage profiles at each bus are illustrated in Figure 15. The minimum VSI at bus 18 increases to 0.839.

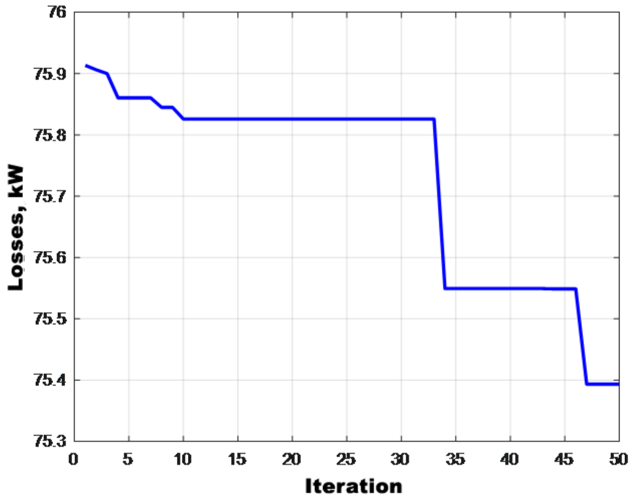

Fig. 12. The convergence characteristics of RPL after installation of multiple DG units using the ALO algorithm.

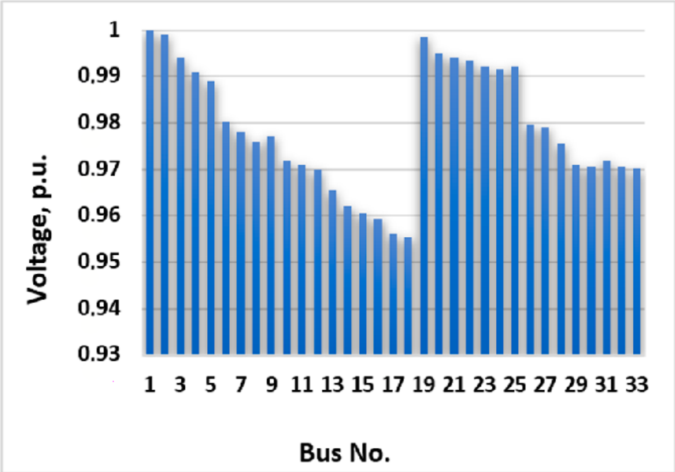

Fig. 13. Voltage profiles for Case 4: multiple DG units placed in IEEE 33-bus system using the ALO algorithm.

Table 3 represents the optimal results achieved through the application of the proposed Grey Wolf Optimizer (GWO) and Ant Lion Optimization (ALO) algorithms to the IEEE 33-bus system. Figures 16 and 17 further illustrate a comparative analysis of real and reactive power losses across the initial case and four distinct scenarios: installation of 1) a single capacitor shunt (CS), 2) a single distributed generation (DG) unit, 3) multiple CSs, and 4) multiple DG units, utilizing both ALO and GWO algorithms. Complementing these findings, Table 4 provides a comprehensive statistical analysis of GWO and ALO performance across these four scenarios, based on 30 independent runs. This analysis evaluates the best, worst, and mean power loss (in kW), alongside the standard deviation (σ) and coefficient of variation (CV), to rigorously assess the reliability and consistency of the generated solutions. The statistical findings consistently demonstrate the superior performance of the GWO algorithm across all evaluated scenarios, achieving lower mean power loss compared to ALO. This research introduces a hybrid optimization strategy for the integration of Distributed Generation (DG) and Capacitor Shunt (CS) into power systems, primarily aimed at minimizing real power loss. The methodology employs deterministic approaches, specifically the Reconfiguration Method (RM) for single-unit placement and the Loss Sensitivity Factor (LSF) for multiple-unit placement, which are then coupled with the metaheuristic GWO and ALO algorithms to determine optimal sizing. This two-step process significantly enhances computational efficiency by streamlining the search space. The study rigorously compares the performance of GWO and ALO algorithms when applied to the IEEE 33-bus system under four diverse

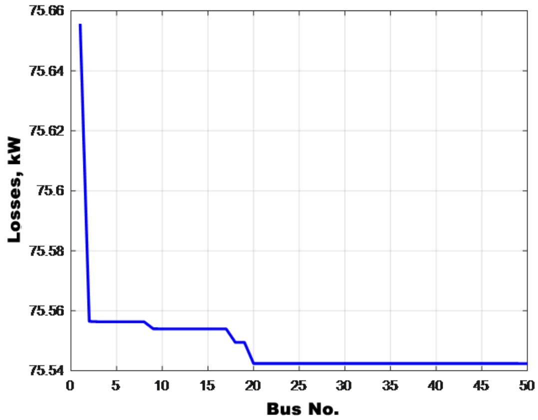

Fig. 14. The convergence characteristics of RPL after installation of multiple DG units using the GWO algorithm.

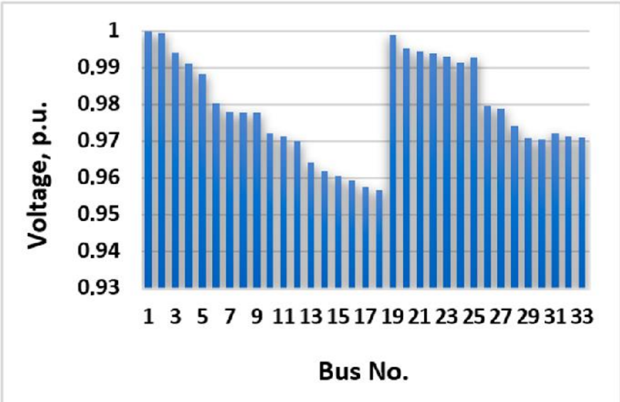

Fig. 15. Voltage profiles for Case 4: multiple DG units placed in IEEE 33-bus system using the GWO algorithm.

TABLE 3. The Optimal Results Obtained for IEEE 33-Bus System with the Proposed ALO and GWO Algorithms

Items	Initial	Using ALO (After Installation)				Using GWO (After Installation)			
		Single CS	Single DG unit	Multiple CSs	Multiple DG units	Single CS	Single DG unit	Multiple CSs	Multiple DG units
Total RPL, MW	0.2015	0.1515	0.1255	0.1382	0.0754	0.1436	0.1037	0.1384	0.0754
Total QPL, MVar	0.1343	0.1041	0.0867	0.0925	0.0517	0.0959	0.0746	0.0959	0.0518
RPL loss reduction rate %	-	24.81	37.73	31.41	62.59	28.74	48.54	31.31	62.6
Minimum VSI	0.696	0.736	0.813	0.757	0.835	0.735	0.819	0.755	0.839
Sum of VSI	27.155	27.273	28.72	27.32	28.15	27.166	28.87	27.30	29.36
Optimal size of CSs, MVAr	-	1.308		0.575 0.6 0.465 0.575		1.253		0.575 0.4703 0.575 0.575	
Optimal size of DG, MW			1.92		0.9288 0.9288 0.8456 0.8994		2.575		0.8558 0.9288 0.9288 0.9093
Location (bus No.)		31	10	25,2,9,31	25, 2, 9, 31	30	6	31, 25, 2, 9	25, 2, 9, 31

TABLE 4. Statistical Analysis Results for Different Scenarios

CV %	Std Dev (σ)	Mean (kW)	Worst (kW)	Best (kW)	Algorithm	Scenario
0.77	1.23	159.87	162.15	158.42	GWO	Single CS
1.03	1.67	161.45	164.33	159.12	ALO	Single CS
0.76	1.08	141.22	143.21	139.55	GWO	Single DG unit
1.01	1.45	142.89	145.67	140.33	ALO	Single DG unit
1.08	1.56	144.78	147.89	142.67	GWO	Multiple CSs
1.29	1.89	146.12	149.23	143.45	ALO	Multiple CSs
1.05	1.34	127.45	129.67	125.34	GWO	Multiple DG units
1.30	1.67	128.89	131.45	126.78	ALO	Multiple DG units

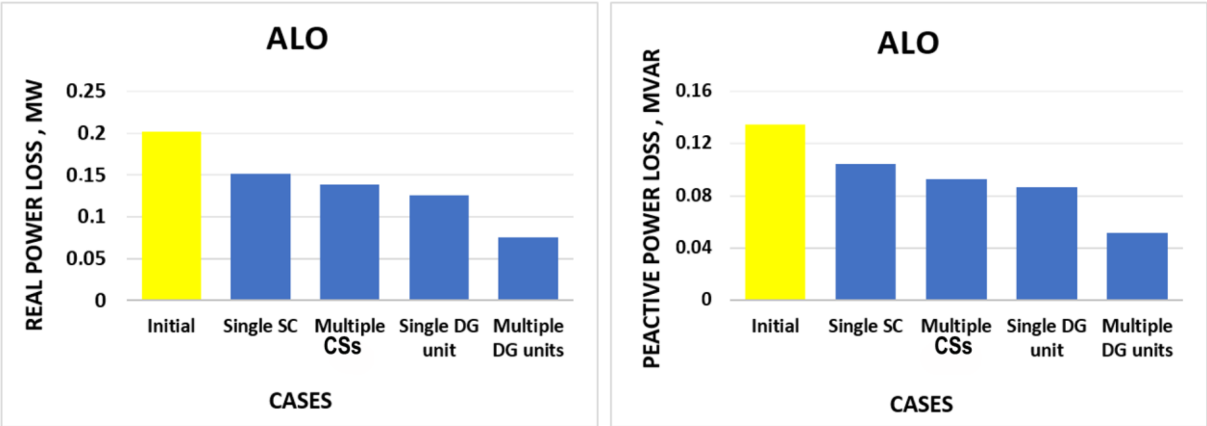

Fig. 16. Comparison results of real power losses and reactive power loss using the ALO for each case.

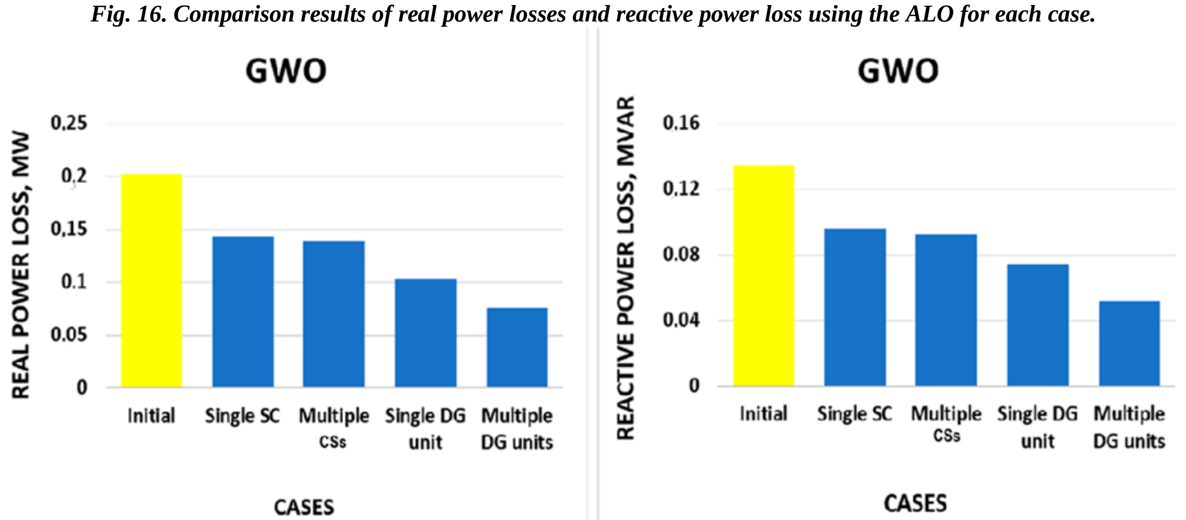

Fig. 17. Comparison results of real power losses and reactive power loss using GWO for each case.

scenarios, confirming that the installation of multiple DG units yields the most substantial reduction in power losses. Key limitations identified for future research include the imperative to incorporate the inherent uncertainty of load demands and renewable energy generation; to adopt a multi-objective optimization framework encompassing economic costs, environmental emissions, and system reliability; and to conduct a comprehensive techno-economic analysis to provide a more pragmatic basis for decision-making in utility planning.

V. CONCLUSION

In this study, we successfully developed and applied a novel hybrid optimization technique for determining the optimal size and location of Distributed generation (DG) units and Capacitor shunts (CSs) within the IEEE 33-bus radial distribution system. The proposed methodology effectively combines deterministic placement strategies – the Reconfiguration Method (RM) for single units and the Loss Sensitivity Factor (LSF) for multiple units – with two powerful metaheuristic algorithms, the Grey Wolf Optimizer (GWO) and Ant Lion Optimization (ALO), for optimal sizing. The primary objective was to minimize the total real power losses, which, as demonstrated, concurrently led to significant improvements in voltage profiles and an enhanced voltage stability index across the system.

Our comprehensive evaluation across four distinct scenarios (single CS, single DG unit, multiple CSs, and multiple DG units) provided valuable insights into the performance of both GWO and ALO. The results consistently indicated that the integration of distributed generation (both single and multiple units) yields a more substantial reduction in real power losses compared to the installation of capacitor shunts. This highlights the significant potential of DG units in enhancing the efficiency and stability of distribution networks. Furthermore, while both GWO and ALO proved to be highly effective in identifying optimal solutions for the sizing of CS and DG units, the Grey Wolf Optimizer consistently demonstrated a more favourable balance of computational efficiency and robustness. GWO often achieved faster convergence and produced results that were more consistent across multiple runs, as evidenced by its lower standard deviation and coefficient of variation in the statistical analysis. Although ALO can find highly competitive solutions and, in some specific instances, might even attain a slightly lower absolute minimum, the superior consistency and reliability of GWO make it a preferable choice for practical applications where rapid and dependable decision-making is paramount.

Building upon the findings of this study, future research endeavours can further enhance the proposed optimization framework by addressing several key areas. These include incorporating the inherent uncertainties of load demands and renewable energy generation through probabilistic or possibility models; expanding the optimization to a multi-objective framework that considers economic costs, environmental impacts, and system reliability; and conducting comprehensive techno-economic analysis to provide a more practical basis for decision-making.

References

[1] M. G. Hemeida, A. Ahmed, A. A. Mohamed, S. Alkhalaf, A. M. B. El-dine, "Optimal allocation of distributed generators DG based Manta Ray Foraging Optimization algorithm (MRFO)," Ain Shams Eng. J., vol. 12, no. 1, pp. 609–619, 2021. DOI: 10.1016/j.asej.2020.07.009.

[2] K. S. Sambaiah, "A Review on Optimal Allocation and Sizing Techniques for DG in Distribution Systems," International Journal of Renewable Energy Research, vol. 8, no. 3, pp. 1236–1256, 2018.

[3] M. M. Sayed, M. Y. Mahdy, S. H. E. A. Aleem, H. K. M. Youssef, T. A. Boghdady, "Simultaneous Distribution Network Reconfiguration and Optimal Allocation of Renewable-Based Distributed Generators and Shunt Capacitors under Uncertain Conditions," Energies, vol. 15, no. 6, Art. no. 2299, 2022. DOI: 10.3390/en15062299.

[4] A. Selim, S. Kamel, A. A. Mohamed, E. E. Elattar, "Optimal Allocation of Multiple Types of Distributed Generations in Radial Distribution Systems Using a Hybrid Technique," Sustainability, vol. 13, no. 12, Art. no. 6644, 2021. DOI: 10.3390/su13126644 2021.

[5] A. R. Ali, A. Abdul, R. Altahir, S. Alwash, M. Al-Kaabi, "Investigation Study of Injecting Numerous DGs in IEEE 69 – bus Radial Networks Using Enhanced PSO and Ant Lion Optimization Algorithms," in 2023 3rd International Conference on Electrical Machines and Drives (ICEMD), Tehran, Iran, Islamic Republic of, 2023, pp. 1–7. DOI: 10.1109/ICEMD60816.2023.10429267.

[6] B. Hussein, A. Igeb, M. Al-Kaabi, P. P. Oshchepkov, M. Muhssin, "Grey Wolf Optimizer Algorithm to Solve Optimal Placement and Sizing of the Distributed Generation Sources in Distribution Radial Networks," in 2023 International Symposium on Fundamentals of Electrical Engineering (ISFEE), Bucharest, Romania, 2023, pp. 1–6. DOI: 10.1109/ISFEE60884.2023.10637122.

[7] J. Al Hasheme, M. Al-Kaabi, L. Toma, "Optimal allocation of distribution generator for radial distribution network using grey wolf optimizer," U.P.B. Sci. Bull., ser. C, vol. 86, no. 3, pp. 371–390, 2024.

[8] A. Naeem, A. Saheb, D. Nazarpour, M. Al-kaabi, "Economic Dispatch Using Harris Hawks Optimization with Renewable Energy Source and Capacitor Shunt," in *2024 16th International Conference on Electronics, Computers and Artificial Intelligence (ECAI)*, Iasi, Romania, 2024, pp. 1–8. DOI: 10.1109/ECAI61503.2024.10607530.

[9] Almoataz Y. Abdelaziz, Mirna Fouad Ali, Eman Beshr, "Hybrid Siting and Sizing of Distributed Generators and Shunt Capacitors with System Reconfiguration using Wild Horse Optimizer," J. Adv. Res. Applied Sciences and Eng. Technol., vol. 38, no. 2, pp. 196–213, 2024.

[10] B. C. Sujatha, A. Usha, R. S. Geetha, "Optimal Planning of PV Sources and D-STATCOM Devices with Network Reconfiguration Employing Modified Ant Lion Optimizer," Energies, vol. 17, no. 10, Art. no. 2238, 2024. DOI: 10.3390/en17102238.

[11] B. P. Nanda, D. P. Mishra, S. R. Salkuti, “A modified ant lion optimization algorithm for efficient distributed generation allocation in power distribution networks,” Electric Power Systems Research, vol. 246, Art. no. 111705, 2025. DOI: 10.1016/j.epsr.2025.111705.

[12] A. R. A. Wafa, “Ant-lion optimizer-based multi-objective optimal simultaneous allocation of distributed generations and synchronous condensers in distribution networks,” Int. Trans. Electr. Energy Syst., vol. 29, pp. 1–14, 2019. DOI: 10.1002/etep.2755.

[13] R. A. Lone, S. J. Iqbal, A. S. Anees, “Optimal location and sizing of distributed generation for distribution systems: An improved analytical technique,” Int. J. Green Energy, vol. 21, no. 3, pp. 682–700, 2024. DOI: 10.1080/15435075.2023.2207638.

[14] M. Alqahtani, P. Marimuthu, V. Moorthy, B. Pangedaiah, C. R. Reddy, M. K. Kumar, M. Khalid, “Investigation and Minimization of Power Loss in Radial Distribution Network Using Gray Wolf Optimization,” Energies, vol. 16, no. 12, Art. no. 4571, 2023. DOI: 10.3390/en16124571.

[15] M. K. Das, “Optimal Placement of Distributed Generation in Distribution Networks Using Grey Wolf Optimization,” Master's Thesis, Dept. of Electrical Engineering, Tribhuvan University, Pulchowk Campus, Lalitpur, Nepal, Jun. 2023.

[16] M. Varan, A. Erduman, F. Menevşeoğlu, “A Grey Wolf Optimization Algorithm-Based Optimal Reactive Power Dispatch with Wind-Integrated Power Systems,” Energies, vol. 16, no. 13, Art. no. 5021, 2023. DOI: 10.3390/en16135021.

[17] N. C. Sahoo, K. Prasad, “A fuzzy genetic approach for network reconfiguration to enhance voltage stability in radial distribution systems,” vol. 47, pp. 3288–3306, 2006. DOI: 10.1016/j.enconman.2006.01.004.

[18] M. Kefayat, A. L. Ara, S. A. N. Niaki, “A hybrid of ant colony optimization and artificial bee colony algorithm for probabilistic optimal placement and sizing of distributed energy resources,” Energy Conversion and Management, vol. 92, pp. 149–161, 2015. DOI: 10.1016/j.enconman.2014.12.037.

[19] S. Mirjalili, S. Mohammad, A. Lewis, “Advances in Engineering Software Grey Wolf Optimizer,” Adv. Eng. Softw., vol. 69, pp. 46–61, 2014. DOI: 10.1016/j.advengsoft.2013.12.007.

[20] A. S. Assiri, A. G. Hussien, M. Amin, “Ant Lion Optimization: Variants, Hybrids, and Applications,” IEEE Access, vol. 8, pp. 77746–77764, 2020. DOI: 10.1109/ACCESS.2020.2990338.

[21] D. R. Prabha, T. Jayabarathi, R. Umamageswari, S. Saranya, “Optimal location and sizing of distributed generation unit using intelligent water drop algorithm,” Sustainable Energy Technologies and Assessments, vol. 11, pp. 106–113, 2015.

[22] M. M. Othman, W. El-Khattam, Y. G. Hegazy, A. Y. Abdelaziz, “Optimal Placement and Sizing of Distributed Generators in Unbalanced Distribution Systems Using Supervised Big Bang-Big Crunch Method,” IEEE Transactions on Power Systems, vol. 30, no. 2, pp. 911–919, 2015.

[23] S. Kaur, G. Kumbhar, J. Sharma, “A MINLP technique for optimal placement of multiple DG units in distribution systems,” Electrical Power and Energy Systems, vol. 63, pp. 609–617, 2014.

[24] N. Acharya, P. Mahat, N. Mithulananthan, “An analytical approach for DG allocation in primary distribution network,” Electrical Power and Energy Systems, vol. 28, no. 10, pp. 669–678, 2006.

[25] S. Kansal, V. Kumar, B. Tyagi, “Optimal placement of different type of DG sources in distribution networks,” Electrical Power and Energy Systems, vol. 53, pp. 752–760, 2013.

[26] M. P. Lalitha, V. C. V. Reddy, V. Usha, “Optimal DG placement for minimum real power loss in radial distribution systems using PSO,” Journal of Theoretical and Applied Information Technology, vol. 13, no. 2, pp. 107–114, 2010.

A. M. Al-Hadeethi is a Senior Electrical Engineer at Iraqi Ministry of Electricity. Currently he is a Ph.D. student of the Department of Electrical and Heat Power Engineering at RUDN, Moscow, Russia. His research interests include power system stability, control, and renewable energy integration.

B. H. AL Igeb is a Chief Engineer at Iraqi Ministry of Construction and Housing. Currently he is a Ph.D. student of the Department of Electrical and Heat Power Engineering at RUDN, Moscow, Russia. His research interests include smart grids, power system optimization, and metaheuristic algorithms.

P.P. Oshchepkov, Ph.D. (Engineering), is an Associate Professor of the Department of Electrical and Heat Power Engineering at RUDN, Moscow, Russia. His research interests include power system plants, control, and turbomachines.

Temperature-Dependent Pyrolysis of Wood Chips in a Fixed-Bed Reactor: Effects on Syngas and Charcoal Yield and Quality

V.V. Badenko[1,*], M.V. Penzik[1], E.V. Gubiy[1], A.N. Kozlov[1]

[1] Melentiev Energy Systems Institute of Siberian Branch of Russian Academy of Sciences, Irkutsk, Russia

***Abstract* — In the context of the global challenge of reducing greenhouse gas and pollutant emissions from thermal and power generation systems, the utilization of secondary fuels, particularly biomass waste, is gaining increasing importance. A promising approach is the thermochemical conversion of wood waste via pyrolysis, which enables the production of energy carriers (syngas and charcoal) with minimal environmental impact. This paper presents a series of various experiments conducted with wood chips at temperatures ranging from 360 to 520 °C. The optimal pyrolysis temperature is found to be 480 °C, resulting in the highest syngas heating value of 12.69 MJ/m³, mechanical gas efficiency of 84.9%, and cold gas efficiency of 25.8 %. The findings also reveal that as temperature increases, charcoal yield decreases from 36% to 27.5%, gas yield rises from 11.1% to 19.5 %; meanwhile the yield of liquid products remains relatively stable (~30%). Notably, that at temperatures above 250 °C, the pyrolysis process involves the self-gasification of charcoal by pyrolytic gas. Additionally, the physicochemical and morphological characteristics of the resulting charcoal, including elemental composition, ash content, porosity, and surface structure, are investigated. The results contribute to the systematic understanding of how temperature affects the distribution of pyrolysis products and their properties under fixed-bed conditions and can be applied in the development of energy-efficient and environmentally safe technologies for wood waste utilization.**

***Index Terms*— Biomass, charcoal, fixed-bed reactor, pyrolysis, self-gasification, tar.**

* Corresponding author.
E-mail: badenko@isem.irk.ru

DOI:10.25729/esr.2025.03.0006

Received October 20, 2025. Accepted October 26, 2025. Available online November 28, 2025.

I. INTRODUCTION

A key priority in today's research landscape is addressing the reduction in emissions of harmful substances (NO_x, SO_x, etc.) and greenhouse gases (CO_2, H_2O, etc.) from thermal and power generation systems. A highly effective strategy for mitigating these emissions is the integration of biomass resources into the energy balance [1, 2]. According to [3], global biomass consumption for energy production amounts to approximately 1 billion tonnes of oil equivalent, with projections indicating a several-fold increase by 2040. This growth will primarily be driven by the utilization of forestry residues, which are generated annually in vast quantities. As reported in the World Food and Agriculture Statistical Yearbook 2023 [4], 4 billion cubic meters of wood were harvested globally in 2021. Nearly half of this volume, 1.95 billion m³ (equivalent to 410 million tonnes of oil equivalent), was used as biofuel. This biofuel includes residues generated during both the harvesting operations in forests and the wood-processing stages.

Pyrolysis is one of the key thermochemical conversion processes for biomass, and its outcomes strongly depend on process conditions. By adjusting pyrolysis parameters, the process can be steered toward maximizing the yield of liquid products, charcoal, or syngas with tailored characteristics [5, 6]. Among these products, syngas and

TABLE 1. Physicochemical Characteristics of Wood Waste

Proximate analysis (wt%, dry basis)	*Values*
Volatile matter (*VM*)	86.80
Fixed carbon (*FC*)	13.03
Ash content (*AC*)	0.17
Ultimate analysis (wt%, dry basis, ash free)	*Values*
Carbon (*C*)	46.60
Hydrogen (*H*)	6.32
Oxygen (*O**)	47.08
Higher heating value (*Q*, MJ/kg)	18.84
Empirical formula of waste wood	$CH_{1.63}O_{0.76}$

*By difference

charcoal are of particular interest due to their broad applications in energy generation, metallurgy, agriculture, and environmental technologies [7].

Temperature is the critical process parameter governing the yield, composition, and energy properties of pyrolysis products. At lower temperatures (300–700 °C), charcoal formation predominates, yielding a carbon-rich solid with limited degradation of the lignocellulosic structure. As temperature increases (>1100 °C), thermal decomposition of cellulose and hemicellulose intensifies, leading to a higher gas-phase yield, while diminishing the solid residue [8, 9]. Concurrently, the composition of syngas undergoes significant changes: concentrations of H_2, CO, and CH_4 increase, enhancing its heating value and suitability for use in internal combustion engines or fuel cells [10].

Fixed-bed reactors represent one of the most widely used laboratory- and pilot-scale systems for fundamental pyrolysis studies. Their simple design, high reproducibility, and precise temperature control make them an ideal platform for systematically investigating the influence of temperature on product distribution [11].

Despite extensive literature on biomass pyrolysis, gaps remain in the quantitative and qualitative understanding of how product characteristics depend on temperature under fixed-bed conditions, particularly regarding localized heat and mass transfer phenomena specific to this reactor type. Moreover, data correlating pyrolysis temperature with charcoal properties, such as specific surface area, porosity, fixed carbon, and ash content, require further systematic analysis across different biomass types, especially wood waste [12].

This paper aims to determine the optimal pyrolysis parameters for wood chips that maximize process efficiency while minimizing the formation of tar compounds. A series of various experiments were conducted at different pyrolysis temperatures.

II. PROCESS MATERIALS AND EXPERIMENTAL METHOD

A. Feedstock

The study utilized pine wood chips (Pinus silvestris) sized to approximately $(30–40) \times 10 \times 10$ mm^3, which were obtained using an electric garden shredder (Viking GE 135). Table 1 presents the details on appearance, as well as proximate and ultimate analysis data. Characteristics of the source wood were determined using standard analytical methods (see section D) and correspond to data obtained by other researchers, for example [13, 14].

B. Laboratory Bench Setup

The laboratory pyrolysis setup for woody biomass (Fig. 1) comprises a reaction chamber, a pyrolysis gas cleaning system, and a tar removal system. The reaction chamber is a fixed-bed thermochemical conversion reactor equipped with a grate (1′), an electrical heating system (1″), thermal insulation (1‴), and thermocouples. The reactor has an internal diameter of 15 cm and a height of 31 cm, with a 5 cm distance between the bottom of the reactor and the grate. The electrical heating system consists of nichrome wire wound around ceramic insulators. Controlled heating is achieved using a voltage regulator and a temperature controller, maintaining precisely the desired pyrolysis temperature. Thermal insulation is provided by fire-resistant glass-ceramic fiber (Cerablanket).

The absence of thermal insulation on the gas outlet pipe facilitates partial condensation of liquid pyrolysis products, which are then returned to the reactor for further cracking.

The reactor is fitted with four Type K thermocouples: the first and second (T1, T2) are positioned within the biomass bed, the third (T3) is located above the bed, and the fourth (T4) measures the temperature of the evolved

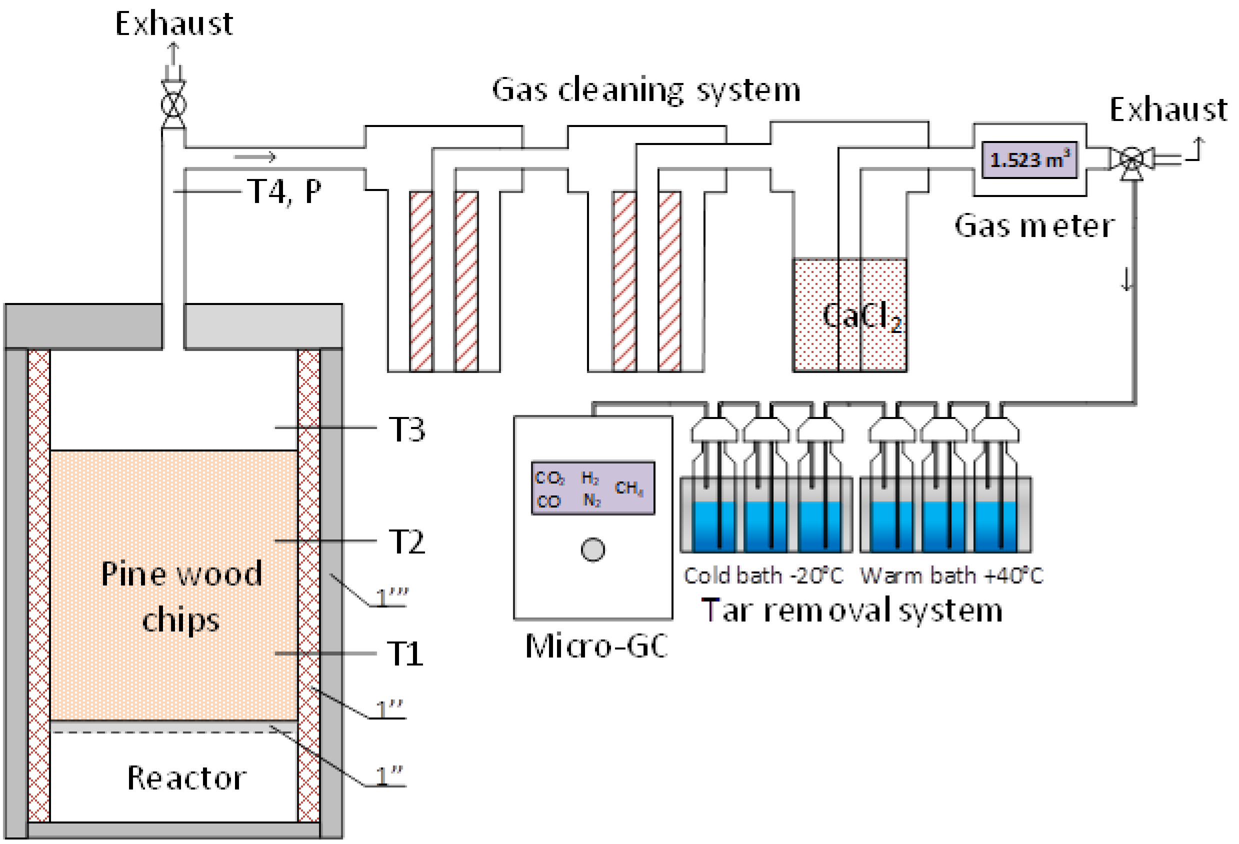

Fig.1 The laboratory bench for pyrolysis of waste wood chips.

gases. Additionally, a differential manometer is installed to monitor pressure drop across the bed. Two relief valves are provided to release excess pressure if necessary.

The gas cleaning system consists of three filters: the first is made of stainless steel, while the second and third are fabricated from transparent polycarbonate. The first two filters are equipped with standard polypropylene foam water filters (PP5-10SL), designed to capture tar and water vapor. The third filter is half-filled with granular calcium chloride ($CaCl_2$) for complete gas drying.

The fine tar removal system follows the method proposed by J.P.A. Neeft and colleagues, as described in [15, 16]. In this approach, syngas passes through a series of impinger bottles filled with isopropanol. Some impingers are immersed in a warm water bath (+40 °C), while others are placed in a cold bath (−20 °C). This technique enables complete tar removal from syngas and is widely adopted by researchers, for example, in [17].

The laboratory setup is also equipped with a gas meter, and the composition of syngas components is analyzed in real time using an INFICON Micro GC Fusion gas chromatograph.

C. Operational Procedures

Approximately (465 ± 1) g of wood waste was loaded into the pyrolysis reactor and gradually heated to the target temperature (360, 400, 440, 480, or 520 °C), which was then maintained constant throughout each experiment. The heating rate was consistent across all tests at approximately

Fig.2 Charcoal agglomerate with tar.

10 °C/min. Upon initiation of pyrolysis, pressure inside the reactor increased, forcing the generated syngas out of the reactor and driving it through the gas duct and subsequent filtration and cleaning systems.

The syngas produced during pyrolysis passes through the layer of charcoal formed in the reactor and then enters an uninsulated gas outlet pipe, which is heated by the hot gas itself. As the gas travels toward the cleaning system, it undergoes reforming. This reforming process reduces tar yield while simultaneously increasing gas yield. As demonstrated in [18], reforming of pyrolytic gas also enhances the hydrogen content in the syngas.

During passage through the gas cleaning system, tar and water vapor are captured, and the gas is fully dried. The cleaned syngas then flows through a gas meter and enters the fine tar removal system before being directed to the gas chromatograph. The INFICON Micro GC Fusion gas chromatograph, operating in online mode, automatically sampled the gas every 3 minutes. It is equipped with Microelectromechanical Systems (MEMS)-based microThermal Conductivity Detectors (TCDs), calibrated to measure the relative concentrations of CO, H_2, CO_2, CH_4, N_2, and hydrocarbons. The total absolute measurement error for all gas components does not exceed 1%.

The experiment was terminated when the gas meter readings stabilized (indicating no further gas evolution) and the excess pressure dropped below the threshold required to transport syngas from the reactor to the chromatograph. Since no external inert gas was supplied to the reactor, the gas meter recorded only the volume of gas generated during wood waste pyrolysis. At the end of each run, heating was switched off, and the reactor was allowed to cool to ambient temperature. The wood charcoal was then extracted.

Char located in the upper part of the reactor formed agglomerates with condensed tar flowing down into the reactor (Fig. 2). Tar was subsequently separated from the char particles using a utility knife and weighed. The mass of the resulting charcoal was also determined. Thereafter, the physicochemical properties and surface morphology of the charcoal were analyzed using scanning electron microscopy (SEM).

The volume of liquid products collected in the gas cleaning system was measured. Tar content was determined by drying a representative liquid sample in a drying oven at 70 °C for 40–50 minutes and weighing the residual solid. This procedure is described in detail in [19]. Subsequently, the elemental composition of the tar was analyzed.

The quantities of tar and water were quantified by measuring the mass difference of the filters before and after drying in an oven at 105 °C. The initial mass of the filters containing both tar and water was recorded immediately after the experiment ended.

D. Analytical Methods

The solid and tar products obtained from the waste wood pyrolysis experiments were characterized using the following analytical methods.

Proximate analysis was performed in accordance with the following ASTM standards:

- ASTM E871 (Standard Test Method for Moisture Analysis of Particulate Wood Fuels),
- ASTM D1102-84(2013) (Standard Test Method for Ash Content (AC) in Wood),
- ASTM E872 (Standard Test Method for Volatile Matter (VM) in the Analysis of Particulate Wood Fuels).

Fixed carbon (*FC*, wt%) was calculated by difference using equation

$$FC = 100 - VM - AC. \quad (1)$$

Ultimate analysis for carbon (*C*, %) and hydrogen (*H*, %) was carried out using a CHNS elemental analyzer (Flash EA 1112, Thermo Finnigan, Italy). The total oxygen (*O*, %) content was determined by difference according to equation

$$O = 100 - AC - C - H. \quad (2)$$

The higher heating value (*Q*, MJ/kg) was calculated from the ultimate analysis data using following equation, originally proposed and validated by Channiwala [20]:

$$Q = 0.3491C + 1.1783H - 0.1034O - 0.0151N - 0.0211AC, \quad (3)$$

where *C, H, S, O, N,* and *AC* represent the mass percentages of carbon, hydrogen, sulfur, oxygen, nitrogen, and ash in the fuel, respectively.

The surface morphology of the pyrolyzed wood samples was examined using scanning electron microscopy (SEM). Chemical microanalysis was performed via energy-dispersive X-ray spectroscopy (EDS) using a Hitachi TM3000 tabletop SEM equipped with an SDD XFlash 430H X-ray detector. Imaging was conducted under low-vacuum conditions (5 kV), which are standard for non-conductive and low-contrast samples. No conductive coating was applied to the samples prior to analysis.

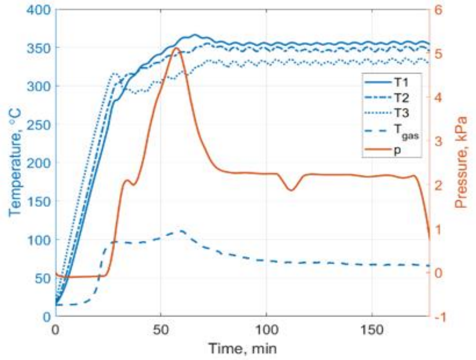

a) 360°C

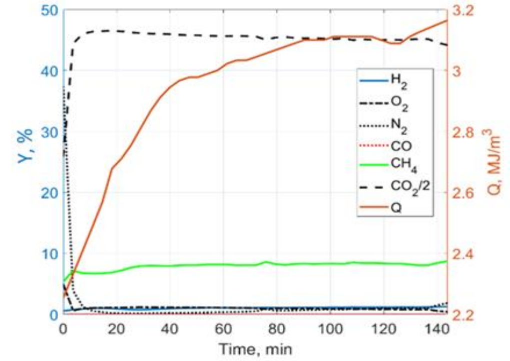

b) 360°C

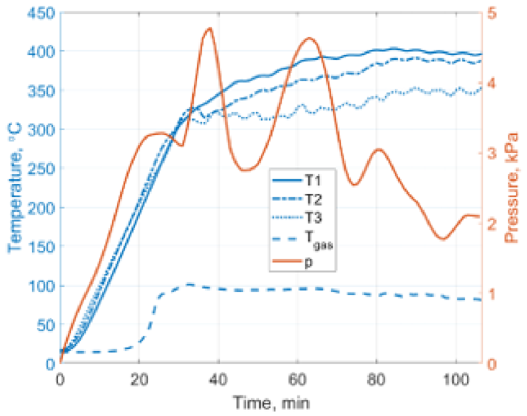

a) 400°C

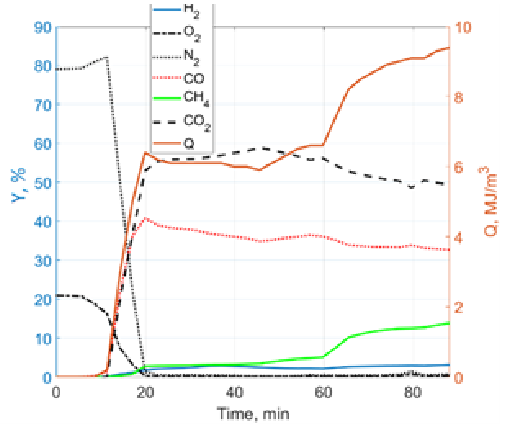

b) 400°C

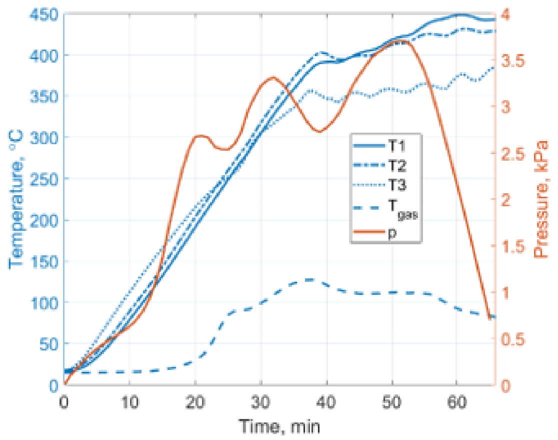

a) 440°C

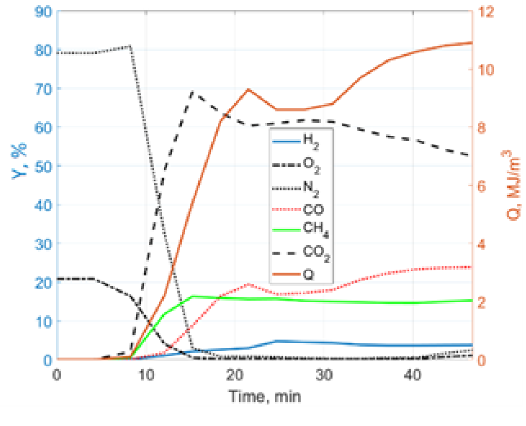

b) 440°C

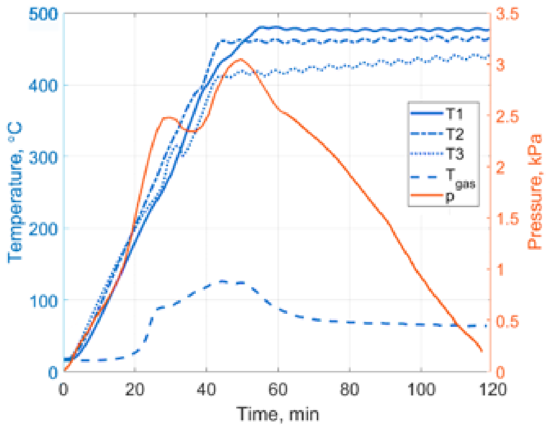

a) 480°C

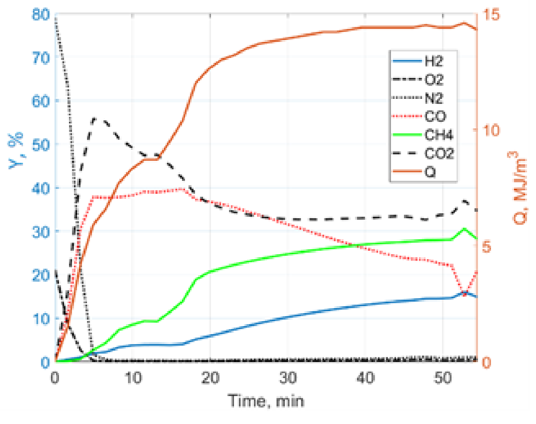

b) 480°C

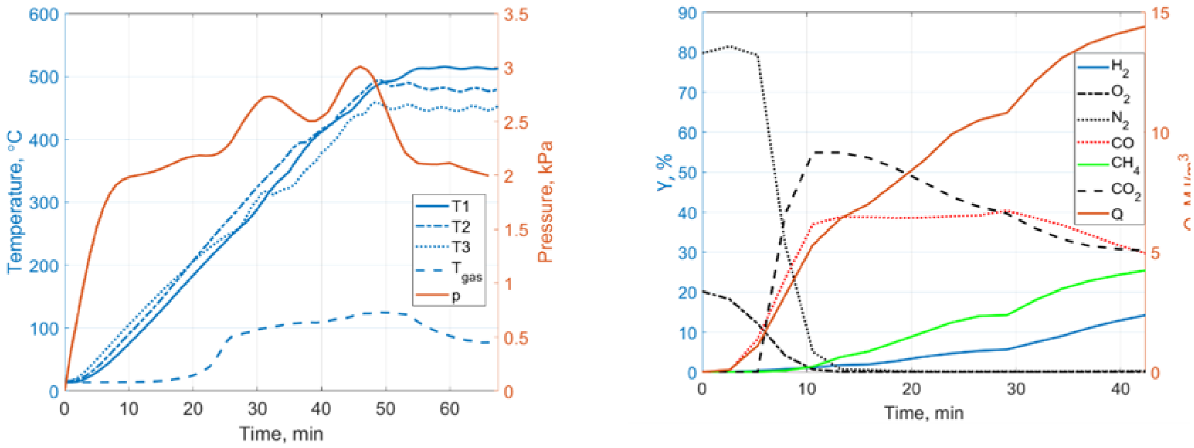

a) 520°C b) 520°C

Fig.3. Profiles of temperature in the bed (T1, T2), above the bed (T3), within fuel and gas (Tgas), as well as pressure curve, depending on the process time (a); Changes in the composition of gas (expressed through the volume fractions Y) and its lower heating value across various pyrolysis temperatures (b).

Pyrolysis of wood chips can be represented by reaction

$$Wood\ chips \rightarrow Char + Liquid\ products\ (tar + water) + Producer\ gas. \quad (4)$$

Based on (4), the yields of pyrolysis products were calculated.

The yields of pyrolysis products Y_j (%) were determined using a mass balance approach according to equation

$$Y_j = \frac{m_j}{m_{wood}} \cdot 100, \quad (5)$$

where m_j and m_{wood} are the masses (kg) of the individual product j (char, liquid, or producer gas) and the initial feedstock, respectively.

Carbon conversion (*CC*) was calculated according to following equation:

$$CC = 1 - \frac{m_{char}\left(y_{CO_2}\frac{12}{44} + y_{CO}\frac{12}{28} + y_{CH_4}\frac{12}{16}\right)}{m_{wood}Y_{char}} \cdot 100, \quad (6)$$

where y_i is the content of components in the producer gas (CO_2, CO, CH_4, H_2). The mechanical gas efficiency (*MGE*) was calculated according to equation

$$MGE = \frac{Q_{gas}}{Q_{wood}} \cdot 100, \quad (7)$$

where Q_{gas} and Q_{wood} are lower heating value of producer gas and wood chips.

The cold gas efficiency (*CGE*) was calculated according to equation

$$CGE = \frac{m_{char}\left(y_{H_2}Q_{H_2} + y_{CO}Q_{CO} + y_{CH_4}Q_{CH_4}\right)}{m_{wood}Q_{wood}} \cdot 100, \quad (8)$$

where Q_i is the heating value of component in the producer gas (CO, CH_4, H_2). The experimental studies were carried out using the resources of the High-Temperature Circuit Multi-Access Research Center at the Melentiev Energy Systems Institute of the Siberian Branch of the Russian Academy of Sciences.

III. Results and Discussion

A. Changes in Producer Gas Composition at Different Temperature

Figure 3a (for pyrolysis temperatures of 360, 400, 440, 480, and 520 °C) presents the time-dependent evolution of temperatures within the biomass bed (T1, T2), above the bed (T3), and in the produced gas (Tgas), as well as the pressure profile during the pyrolysis process. Figure 3b (for the same temperatures) illustrates the variation in composition of syngas (expressed through the volume fractions Y) and its calorific value as a function of pyrolysis temperature.

Analysis of Fig. 3a shows that the initial pressure increase (0–20 min) is caused by thermal expansion of the residual air inside the reactor and by drying of the wood chips, accompanied by evaporation of physically adsorbed moisture. Pyrolysis starts approximately 20 minutes after heating begins, when the temperature within the wood layer reaches 190–210 °C. This is evidenced by a noticeable rise in gas temperature (Tgas), indicating the onset of the active devolatilization phase driven by chemical reactions associated with thermal decomposition.

It is well established that the main macromolecular components of wood undergo thermal decomposition under inert conditions in the following temperature ranges: 225–325 °C for hemicellulose, 305–375 °C for cellulose, and 150–500 °C for lignin [21].

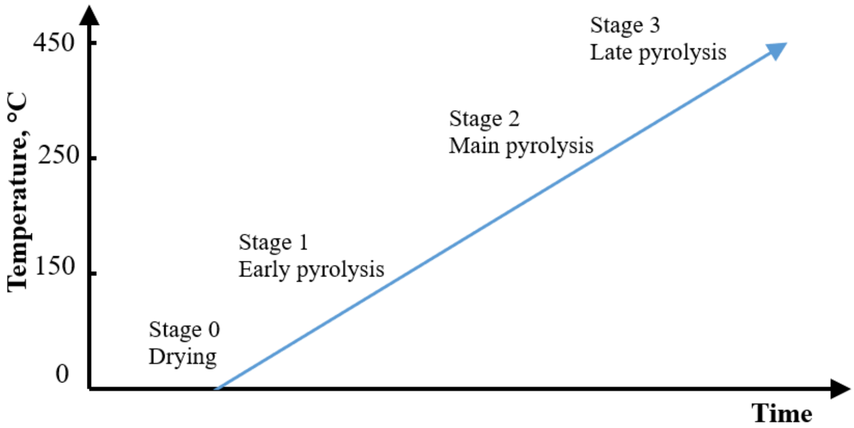

Fig.4. The stages in pyrolysis of wood chips.

TABLE 2. Proximate and Ultimate Analysis of Char Coal

Temperature of pyrolysis, °C	*VM*, %	*AC*, %	*FC*, %	*Q*, MJ/kg	*C*, %	*H*, %	*O*, %	*H/C*	*O/C*
360	36.44	1.07	62.49	31.08	76.53	5.32	18.16	0.83	0.18
400	28.55	1.82	69.63	32.26	80.59	4.82	14.60	0.72	0.14
440	26.71	1.08	72.21	32.80	83.05	4.36	12.60	0.63	0.11
480	16.52	0.95	82.53	34.49	87.34	4.16	8.51	0.57	0.07
520	14.35	1.27	84.38	33.68	92.09	1.85	6.06	0.24	0.05

Analysis of Fig. 3b reveals that the CO_2 concentration in the syngas decreases as pyrolysis temperature rises, while the concentrations of combustible components (CO, CH_4, H_2) and the gas calorific value increase. This trend can be attributed to the self-gasification of char by CO_2 at elevated temperatures, the process described in [22]. Moreover, it is widely accepted that under inert pyrolysis conditions, the oxygen required for CO_2 formation originates primarily from cellulose [23].

It should also be noted that the syngas achieves its maximum calorific value toward the end of the process, which is associated with elevated methane content. Methane is mainly generated from the demethoxylation (–OCH_3) of lignin units in the temperature range of 350 to 450 °C [24].

Carbon monoxide (CO) is produced during thermal decomposition of both cellulose and lignin [23, 25]. As a result, the concentration of CO is relatively stable during the process.

Thus, the pyrolysis process can be described by the scheme presented in Fig. 4:

- Stage 0 (up to 150 °C): Drying of the feedstock.
- Stage 1 (150–250 °C): Initial, low-intensity pyrolysis stage, primarily involving hemicellulose decomposition and formation of light hydrocarbons.
- Stage 2 (250–450 °C): Main pyrolysis stage, characterized by high reaction rates and the generation of the majority of gaseous products. During this stage, residual hemicellulose and cellulose decompose, and lignin degradation begins.
- Stage 3 (>450 °C): Pyrolysis of the remaining, unreacted lignin.

Notably, char self-gasification by CO_2 may occur during both Stage 2 and Stage 3, contributing to the observed increase in H_2 and CO concentrations and the overall enhancement of syngas quality at higher temperatures.

TABLE 3. Ultimate Analysis of Tar

Temperature of pyrolysis, °C	*C*, %	*H*, %	*O*, %
360	53.5	6.7	46.5
400	49.2	6.2	50.8
440	57.1	7.3	42.9
480	51.0	6.7	49.0
520	52.3	5.6	47.7

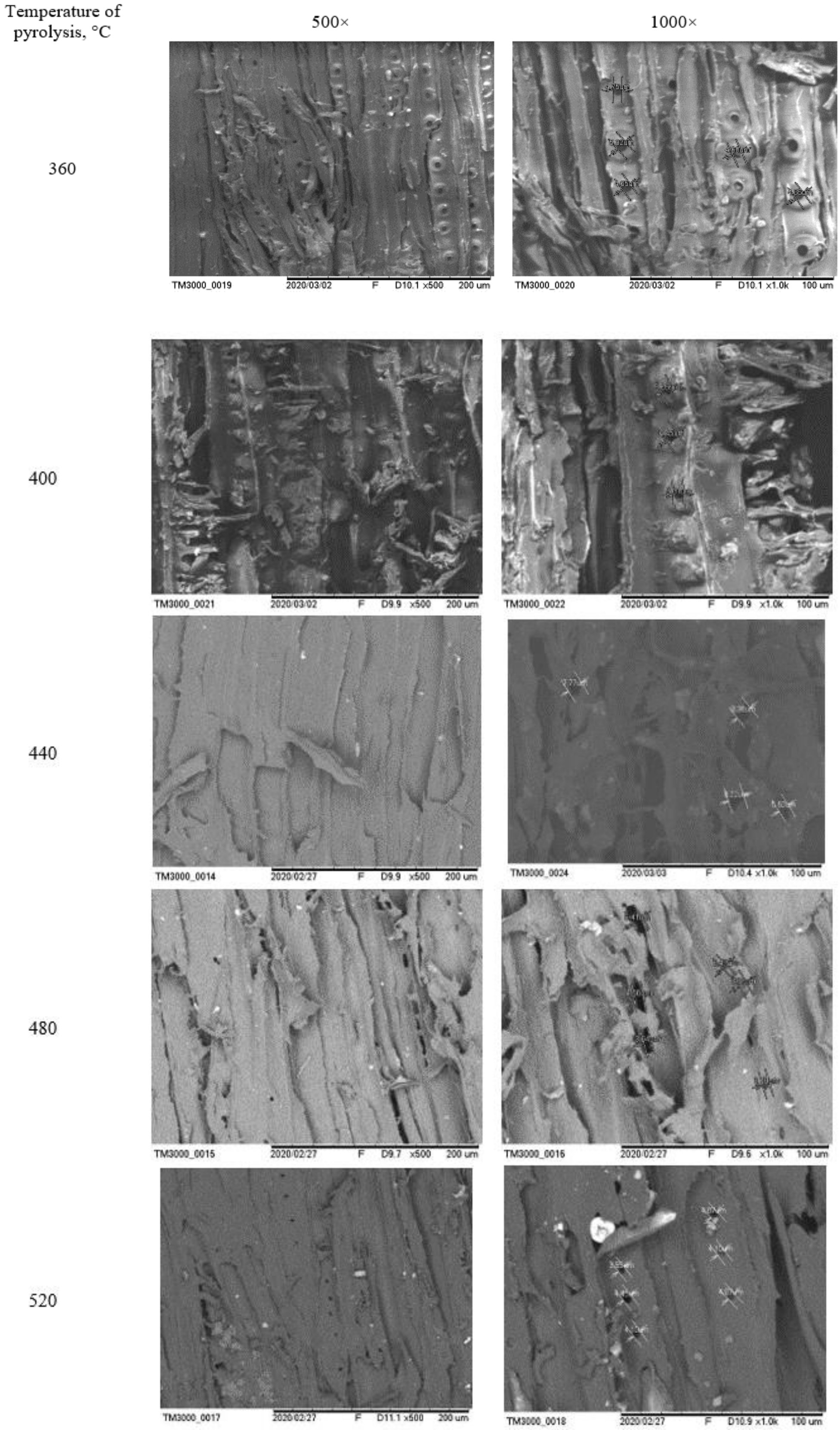

Fig.5. SEM images of charcoal samples at different temperatures of pyrolysis.

B. Proximate and Ultimate Analysis of Charcoal and Tar

After each experiment, samples of the produced charcoal were collected and analyzed. The results of the analysis are presented in Table 2.

Proximate analysis includes standard parameters for charcoal: volatile matter (*VM*), ash content (*AC*), and fixed carbon (*FC*). According to Table 2, increasing the pyrolysis temperature resulted in a decrease in volatile matter and a corresponding rise in fixed carbon content. The slight variation in ash content across samples is attributed to the experimental uncertainty inherent in the determination method.

Elevated pyrolysis temperatures led to a reduction in hydrogen (*H*) and oxygen (*O*) content, while carbon (*C*) concentration increased. This trend is explained by two concurrent processes: (i) enhanced carbonization (aromatization and condensation of carbon structures) and (ii) more extensive cleavage of oxygen- and hydrogen-containing functional groups originally present in the wood biopolymers. This progressive deoxygenation and dehydrogenation also account for the observed increase in the higher heating value of the charcoal with rising pyrolysis temperature peaking at 34.49 MJ/kg at 480 °C.

The atomic ratios *H*/*C* and *O*/*C* decrease monotonically with increasing pyrolysis temperature, reflecting the progressive breakdown of polar and aliphatic bonds in the biomass structure. As reported in [26, 27], this decline is also indicative of increasing aromaticity and structural ordering in the charcoal produced at higher temperatures.

Table 3 shows the ultimate analysis of the tar obtained at different temperatures. There is not a clear dependence of the elemental composition on the pyrolysis temperature. The tar is characterized by a high content of oxygen and hydrogen, which can be explained by the fact that the tar contains a large number of chemical compounds, such as aromatic compounds with one to five rings, polycyclic aromatic hydrocarbons, and some oxygen-containing hydrocarbons [28].

C. Scanning Electron Microscopy Observation

Figure 5 presents scanning electron microscopy (SEM) images of the surface morphology of wood charcoal samples produced at different pyrolysis temperatures. The images were acquired at magnifications of 500× and 1000×. Higher magnifications resulted in significant charge accumulation on the non-conductive sample surfaces, hindering the acquisition of high-quality images.

For the sample pyrolyzed at 360 °C, a relatively dense fibrous structure largely preserved from the original wood is still evident. This structure is primarily composed of lignin and residual carbohydrates. As the pyrolysis temperature increases, the structure becomes progressively less dense due to partial thermal degradation of lignin. Notably, according to literature data [29–31], complete decomposition of cellulose and hemicellulose in pine wood during pyrolysis occurs at temperatures close to 400 °C.

Microscopic pores formed by the evolution of pyrolysis gases are clearly visible in the samples obtained at 360,

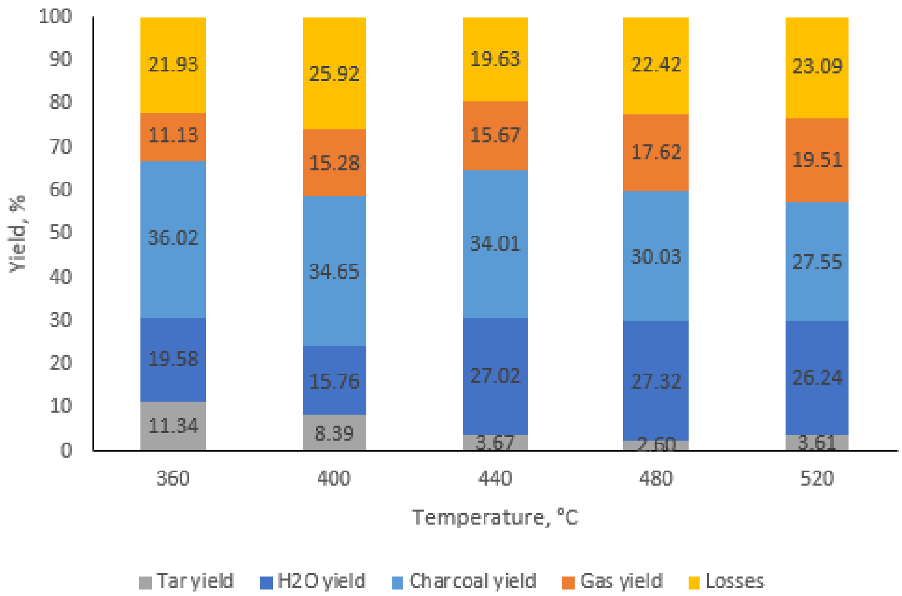

Fig.6. The yields of charcoal, gas, and liquid produced from wood chips at different temperatures.

TABLE 4. Summary of Pyrolysis of Wood Chips at Different Temperatures

Input	Wood chips, kg	0.46				
	Q of wood chips, MJ/kg	18.8				
	Temperature, °C	360	400	440	480	520
Output	[H2], %	1.1	2.6	3.6	9.6	6.7
	[CO], %	0.0	35.5	15.2	30.7	37.0
	[CH4], %	8.1	6.9	19.2	21.7	14.8
	[CO2], %	91.0	54.3	59.8	37.2	41.1
	Q, MJ/m^3	3.0	7.2	9.2	12.7	10.7
	Gas yield, %	11.1	15.3	15.7	17.6	19.5
	Charcoal yield, %	36.0	34.6	34.0	30.0	27.5
	Water yield, %	19.6	15.8	27.0	27.3	26.2
	Tar yield, %	11.3	8.4	3.7	2.6	3.6
	Carbon conversion (*CC*), %	69.4	64.4	63.1	60.0	61.4
	Cold gas efficiency, (*CGE*) %	9.2	19.5	20.7	25.8	20.0
	Mechanical gas efficiency (*MGE*), %	25.9	55.6	61.5	84.9	71.7

400, and 440 °C. The average pore diameter increases with the temperature reaching 4.65–5.32 µm at 360 °C, 5.01–6.45 µm at 400 °C, and 5.62–8.36 µm at 440 °C. In the first two samples (360 °C and 400 °C), these pores are arranged in regular rows aligned with the original fiber orientation. However, this ordered arrangement is no longer discernible at 440 °C due to the progressive breakdown of the fibrous architecture.

At 480 °C, longitudinal fiber fractures appear, with widths ranging from 2.47 to 5.41 µm and varying lengths, resulting in a more developed and irregular surface morphology. Upon further temperature increase to 520 °C, devolatilization is essentially complete, leading to a noticeable reduction in both the number of pores and structural fractures compared to the 480 °C sample.

D. Pyrolysis Efficiency

Figure 6 shows the yields of pyrolysis products as a function of pyrolysis temperature, along with the corresponding mass balance closure error (losses).

With the increasing pyrolysis temperature, the charcoal yield decreases from 36% to 27.5%, while the syngas yield rises from 11.1% to 19.5%. In contrast, the liquid product yield remains relatively constant at approximately 30% across most temperatures, with the exception of the run conducted at 400 °C, where it drops to 24.2%. This deviation is attributed to experimental uncertainties in accurately quantifying the liquid fraction particularly due to collection losses, adhesion to system surfaces, and incomplete separation of tar from water.

The same uncertainty in liquid product measurement is the primary contributor to the observed mass balance discrepancy, which amounts to approximately 22%. This unaccounted fraction likely includes unrecovered condensable vapors, aerosolized tars retained in the gas lines, and minor measurement errors in solid and gas quantification.

Table 4 summarizes the key results of wood chip pyrolysis as a function of temperature. The syngas composition shown in Fig. 3b is averaged over the period after residual air has been fully purged from the reactor. Analysis of the gas composition reveals that the concentration of combustible components (H_2, CO, CH_4) increases with rising pyrolysis temperature, although the relative distribution among these components varies non-uniformly.

The findings indicate that the pyrolysis temperature of 480 °C is optimal, resulting in the maximum lower heating value of syngas (12.7 MJ/m³) and consequently the highest values of Mechanical Gas Efficiency (*MGE*) and Cold Gas Efficiency (*CGE*), which reach 84.9% and 25.8%, respectively.

Analysis of *MGE* and *CGE* trends shows that both efficiencies improve as temperatures climb to 480 °C, but then decline at 520 °C. The relatively low CGE values across all tests are attributed to the inherent energy inefficiency of the laboratory-scale pyrolysis setup, primarily due to significant heat losses to the environment.

Notably, the lowest efficiency values were observed at 360 °C, despite this run exhibiting the highest carbon conversion (69.4%). This apparent contradiction arises because, at this low temperature, the pyrolysis reactions proceed slowly and with low intensity, requiring the longest residence time of the feedstock in the reactor to achieve near-complete carbon conversion. In contrast, at the optimal temperature of 480 °C, carbon conversion is slightly lower (60%) but occurs more rapidly and produces a syngas of significantly higher energy quality, resulting in superior overall process efficiency.

IV. Conclusion

The paper proposes a novel fixed-bed reactor concept designed to minimize tar formation while simultaneously enhancing syngas yield. The reactor's performance was investigated across a range of pyrolysis temperatures, including 360, 400, 440, 480, and 520 °C. The findings demonstrate that 480 °C is the optimal pyrolysis temperature, resulting in the highest syngas heating value (12.69 MJ/m³) and peak efficiency metrics: a Mechanical Gas Efficiency of 84.9% and a Cold Gas Efficiency of 25.8%.

The study has established that as pyrolysis temperature increases, the solid char yield decreases from 36% to 27.5%, while syngas yield rises from 11.1% to 19.5%. In contrast, the liquid product yield remains relatively stable at approximately 30%, with the exception of the 400 °C run, where it dropped to 24.2%, likely due to experimental uncertainties in liquid collection and quantification. The overall mass balance closure error of approximately 22% is primarily attributed to unmeasured condensable vapors, tar deposition in gas lines, and minor measurement inaccuracies.

Additionally, the physicochemical properties and surface morphology of the resulting wood charcoal are characterized, offering valuable insights into structural transformation across various temperatures. These findings contribute to the development of energy-efficient, low-tar pyrolysis technologies for sustainable wood waste valorization.

Acknowledgment

The research was funded by the Russian Science Foundation, Grant No. 24-29-00596 (https://rscf.ru/project/24-29-00596/).

References

[1] J. Popp, Z. Lakner, M. Harangi-Rákos, M. Fári, "The effect of bioenergy expansion: Food, energy, and environment," Renewable and Sustainable Energy Reviews, vol. 32, pp. 559–578, 2014. DOI: 10.1016/j.rser.2014.01.056.

[2] Y. Kang, Q. Yang, P. Bartocci, H. Wei, S. S. Liu, Z. Wu, H. Zhou, H. Yang, F. Fantozzi, H. Chen, "Bioenergy in China: Evaluation of domestic biomass resources and the associated greenhouse gas mitigation potentials," Renewable and Sustainable Energy Reviews, vol. 127, Art. no. 109842, 2020. DOI: 10.1016/j.rser.2020.109842.

[3] M. S. Roni, S. Chowdhury, S. Mamun, M. Marufuzzaman, W. Lein, S. Johnson, "Biomass co-firing technology with policies, challenges, and opportunities: A global review," Renewable and Sustainable Energy Reviews, vol. 78, pp. 1089–1101, 2017. DOI: 10.1016/j.rser.2017.05.023.

[4] "World food and agriculture – statistical yearbook 2023," FAOSTAT, 2023. [Online] Available: https://openknowledge.fao.org/server/api/core/bitstreams/6e04f2b4-82fc-4740-8cd5-9b66f5335239/content. Accessed on: Jun. 07, 2025.

[5] X. Hu, M. Gholizadeh, "Biomass pyrolysis: A review of the process development and challenges from initial researches up to the commercialisation stage," Journal of Energy Chemistry, vol. 39, pp. 109–143, 2019. DOI: 10.1016/j.jechem.2019.01.024.

[6] J. R. Lesme, F. R. M. Nascimento, O. J. Venturini, E. E. S. Lora, "Chapter Five – Biomass energy conversion: Routes and products," in From Crops and Wastes to Bioenergy, Woodhead Publishing, 2025, ch. 5, pp. 139–190. DOI: 10.1016/B978-0-443-16084-4.00018-3.

[7] A. de Oliveira Vilela, E. S. Lora, Q. R. Quintero, R. A. Vicintin, T. Pacceli da Silva e Souza, "A new technology for the combined production of charcoal and electricity through cogeneration," Biomass and Bioenergy, vol. 69, pp. 222–240, 2014. DOI: 10.1016/j.biombioe.2014.06.019.

[8] J. Li, K. Xu, X. Yao, J. Liu, "Investigation of biomass slow pyrolysis mechanisms based on the generation trends in pyrolysis products," Process Safety and Environmental Protection, vol. 183, pp. 327–338, 2024. DOI: 10.1016/j.psep.2024.01.027.

[9] A. Gao, K. Zou, Y. Wang, G. Gao, M. V. Penzik, A. N. Kozlov, Y. M. Isa, Y. Huang, S. Zhang, "The core factors in determining product distributions during pyrolysis: The synergistic effect of volatile-char interactions and temperature," Renewable Energy, vol. 218, Art. no. 119359, 2023. DOI: 10.1016/j.renene.2023.119359.

[10] N. Ungureanu, N.-V. Vladut, S.-S. Biris, N.-E. Gheorg, M. Ionescu, “Biomass Pyrolysis Pathways for Renewable Energy and Sustainable Resource Recovery: A Critical Review of Processes, Parameters, and Product Valorization,” Sustainability, vol. 17, no. 17, 2025. DOI: 10.3390/su17177806.

[11] M. Alam, I. Sarkar, N. Chanda, S. Ghosh, C. Loha, “Enhancing syngas production and hydrogen content in syngas from catalytic slow pyrolysis of biomass in a pilot scale fixed bed reactor,” Biomass Conversion and Biorefinery, vol. 15, no. 4, pp. 6237-6249, 2025. DOI: 10.1007/s13399-024-05453-0.

[12] F. Mahmood, M. Ali, M. Khan, C. F. Mbeugang, Y. M. Isa, A. Kozlov, M. Penzik, X. Xie, H. Yang, S. Zhang, B. Li, “A review of biochar production and its employment in synthesizing carbon-based materials for supercapacitors,” Industrial Crops and Products, vol. 227, Art. no. 120830, 2025. DOI: 10.1016/j.indcrop.2025.120830.

[13] Z. Sun, B. Xu, A. H. Rony, S. Toan, S. Chen, K. A. M. Gasem, H. Adidharma, M. Fan, W. Xiang, “Thermogravimetric and kinetics investigation of pine wood pyrolysis catalyzed with alkali-treated CaO/ZSM-5,” Energy Conversion and Management, vol. 146, pp. 182–194, 2017. DOI: 10.1016/j.enconman.2017.04.104.

[14] K. H. Kim, J.-Y. Kim, T.-S. Cho, J. W. Choi, “Influence of pyrolysis temperature on physicochemical properties of biochar obtained from the fast pyrolysis of pitch pine (Pinus rigida),” Bioresource Technology, vol. 118, pp. 158–162, 2012. DOI: 10.1016/j.biortech.2012.04.094.

[15] J. P. A. Neeft, H. A. M. Knoef, U. Zielke, K. Sjostrom, P. Hasler, P. A. Simell, M.A. Dorrington, L. Thomas, N. Abatzoglou, S. Deutch, “Guideline for sampling and analysis of tar and particles in biomass producer gases,” Progress in thermochemical biomass conversion, vol. 1, pp. 162–175, 2001.

[16] J. P. A. Neeft, “Tar Guideline: A standard method for measurement of tars and particles in biomass producer gases,” in Proc. 12th EUBCE, Amsterdam, Netherlands, 2002, pp. 469–472.

[17] T. Sharma, D. M. Yepes Maya, F. R. M. Nascimento, Y. Shi, A. Ratner, E. E. Silva Lora, L. J. Mendes Neto, J. C. Escobar Palacios, R. Vieira Andrade, “An Experimental and Theoretical Study of the Gasification of Miscanthus Briquettes in a Double-Stage Downdraft Gasifier: Syngas, Tar, and Biochar Characterization,” Energies, vol. 11, no. 11, Art. no. 3225, 2018. DOI: 10.3390/en11113225.

[18] K. Shi, J. Yan, J. A. Menendez, X. Luo, G. Yang, Y. Chen, E. Lester, T. Wu, “Production of H2-Rich Syngas From Lignocellulosic Biomass Using Microwave-Assisted Pyrolysis Coupled With Activated Carbon Enabled Reforming,” Frontiers in Chemistry, vol. 8, 2020. DOI: 10.3389/fchem.2020.00003.

[19] D. A. Svishchev, A. N. Kozlov, I. G. Donskoy, A. F. Ryzhkov, “A semi-empirical approach to the thermodynamic analysis of downdraft gasification,” Fuel, vol. 168, pp. 91–106, 2016. DOI: 10.1016/j.fuel.2015.11.066.

[20] S. A. Channiwala, P. P. Parikh, “A unified correlation for estimating HHV of solid, liquid and gaseous fuels,” Fuel, vol. 81, no. 8, pp. 1051–1063, 2002. DOI: 10.1016/S0016-2361(01)00131-4.

[21] N. Labbe, L. M. Kline, L. Moens, K. Kim, P. C. Kim, D. G. Hayes, “Activation of lignocellulosic biomass by ionic liquid for biorefinery fractionation,” Bioresource Technology, vol. 104, pp. 701–707, 2012. DOI: 10.1016/j.biortech.2011.10.062.

[22] A. Dominguez, Y. Fernandez, B. Fidalgo, J. J. Pis, J. A. Menendez, “Bio-syngas production with low concentrations of CO2 and CH4 from microwave-induced pyrolysis of wet and dried sewage sludge,” Chemosphere, vol. 70, no. 3, pp. 397–403, 2008. DOI: 10.1016/j.chemosphere.2007.06.075.

[23] R. Laryea-Goldsmith, C. Woolard, “Thermal with Mass Spectroscopic Analysis of Wood and Cereal Biomass Torrefaction,” International Scholarly Research Notices, no. 1, Art. no. 508965, 2013.

[24] E. Jakab, O. Faix, F. Till, “Thermal decomposition of milled wood lignins studied by thermogravimetry/mass spectrometry,” Journal of Analytical and Applied Pyrolysis, vol. 40–41, pp. 171–186, 1997. DOI: 10.1016/S0165-2370(97)00046-6.

[25] Y. Chen, J. Duan, Y. Luo, “Investigation of agricultural residues pyrolysis behavior under inert and oxidative conditions,” Journal of Analytical and Applied Pyrolysis, vol. 83, no. 2, pp. 165–174, 2008. DOI: 10.1016/j.jaap.2008.07.008.

[26] S. Wei, M. Zhu, X. Fan, J. Song, P. Peng, K. Li, W. Jia, H. Song, “Influence of pyrolysis temperature and feedstock on carbon fractions of biochar produced from pyrolysis of rice straw, pine wood, pig manure and sewage sludge,” Chemosphere, vol. 218, pp. 624–631, 2019. DOI: 10.1016/j.chemosphere.2018.11.177.

[27] S. Li, S. Harris, A. Anandhi, G. Chen, “Predicting biochar properties and functions based on feedstock and pyrolysis temperature: A review and data syntheses,” Journal of Cleaner Production, vol. 215, pp. 890–902, 2019. DOI: 10.1016/j.jclepro.2019.01.106.

[28] F. Guo, X. Jia, S. Liang, N. Zhou, P. Chen, R. Ruan, "Development of biochar-based nanocatalysts for tar cracking/reforming during biomass pyrolysis and gasification," Bioresource Technology, vol. 298, Art. no. 122263, 2020. DOI: 10.1016/j.biortech.2019.122263.

[29] X. Hu, H. Guo, M. Gholizadeh, B. Sattari, Q. Liu, "Pyrolysis of different wood species: Impacts of C/H ratio in feedstock on distribution of pyrolysis products," Biomass and Bioenergy, vol. 120, pp. 28–39, 2019. DOI: 10.1016/j.biombioe.2018.10.021.

[30] C.H. Pang, E. Lester, T. Wu, "Influence of lignocellulose and plant cell walls on biomass char morphology and combustion reactivity," Biomass and Bioenergy, vol. 119, pp. 480–491, 2018. DOI: 10.1016/j.biombioe.2018.10.011.

[31] W. Cai, R. Liu, "Performance of a commercial-scale biomass fast pyrolysis plant for bio-oil production," Fuel, vol. 182, pp. 677–686, 2016. DOI: 10.1016/j.fuel.2016.06.030.

Vladislav Badenko is a Junior Researcher in the Department of Thermal Power Systems at the Melentiev Energy Systems Institute of the Siberian Branch of the Russian Academy of Sciences (ESI SB RAS). His research interests include thermochemical conversion of biomass, numerical modeling of combustion processes, and combined energy facilities for biomass decomposition.

Maxim Penzik, Ph.D., is a Senior Researcher in the Department of Thermal Power Systems at the ESI SB RAS. Since 2022, he has been an Associate Professor at the Faculty of Chemistry at Irkutsk State University. His research interests include the study on the processes of thermal decomposition of biomass, polymers, and organic compounds using the TG-MS method.

Elena V. Gubiy, Ph.D., is a Research Associate in the Department for Complex and Regional Energy Problems at the ESI SB RAS. Her research interests include the analysis of the efficiency of biofuels and the assessment of the bioenergy expansion potential.

Alexander Kozlov, Ph.D., is a Senior Researcher in the Department of Thermal Power Systems at the ESI SB RAS. His research interests include the combustion of heterogeneous solid fuels (biomass, coal) and the development of simple engineering techniques for calculating gasification processes.

Automating Computations for the Digital Twin-based Design of an Integrated Energy System

E.A. Barakhtenko[1,*], D.V. Sokolov[1], G.S. Mayorov[1]

[1] Melentiev Energy Systems Institute of Siberian Branch of Russian Academy of Sciences, Irkutsk, Russia

Abstract — **Integrated energy systems (IESs) based on traditional energy systems operating separately provide higher efficiency and reliability of energy supply to consumers. However, designing such systems poses significant complexity due to their intricate structure. A digital twin combines all the tools necessary for design in a single information space. To effectively simulate diverse equipment and integrate numerous methodologies alongside advanced mathematical models, software solutions supporting the digital twin paradigm must exhibit exceptional computational versatility. Automation of the computational subsystem development represents a promising strategy for addressing these challenges. This paper introduces a methodological approach for automating the development of the computational subsystem for a digital twin of an IES. The approach relies on advanced metaprogramming tools based on a software platform to automate the development process. Throughout the process, the Model-Driven Engineering concept is implemented, utilizing knowledge formalized in the form of ontologies. The digital twin, constructed using the presented methodological approach, facilitates computer-based and mathematical modeling of an IES in a virtual environment, enabling the exploration of its various configurations.**

* Corresponding author.
E-mail: barakhtenko@isem.irk.ru

DOI:10.25729/esr.2025.03.0007

Received September 17, 2025. Accepted October 20, 2025. Available online November 28, 2025.

Index Terms **— Digital twin, automation of computing process, automation of programming, Model-Driven Engineering, ontology, integrated energy system.**

I. Introduction

Modern cities and industrial centers can boast a developed energy infrastructure, including fuel, electricity, heating, and refrigeration systems. These systems are of high social and economic importance. The creation of a new technological structure in the form of an integrated energy system (IESs) on the basis of several separately functioning energy systems can significantly expand their functionality, ensure the interchangeability of energy carriers, and implement a synergistic effect, thereby ensuring reliable, safe, cost-effective, and environmentally friendly energy supply.

IESs are sophisticated technical systems with extended networks and complex structural configuration. These systems include numerous energy systems, each incorporating subsystems that perform their functions: generation, transportation, distribution, and consumption of energy. Each of these subsystems consists of components with their sets of equipment.

Designing IESs is rather challenging because of their highly complex configuration, a wide range of equipment used, and a diverse set of mathematical models utilized to model it. Designing an IES often involves modeling all the subsystems, sets of their components and equipment, given technical and technological solutions for the integration of systems of various types. It is impossible to solve the problem of IES design without dedicated software, which creates conditions for increasing the efficiency of design, the quality of design solutions, and the automation of labor-intensive computational operations.

A high quality software tool for designing an IES should combine methodological, mathematical, and software support within a single information space where information links with the designed object are implemented. At present, a tool with the specified characteristics corresponds to the concept of a Digital Twin (DT).

In order to effectively incorporate a digital twin into the design process, it is essential to ensure a high level of flexibility in its construction. This is mainly because it enables accurate modeling of a diverse array of equipment. It is also crucial to adjust the methods and algorithms used to a specific problem in the context of solving it. The approaches aimed at automating the construction of a digital twin of for integrated energy systems make it possible to overcome the described difficulties.

The paper proposes an original methodological approach to the automation of computations grounded in the digital twin representation of an IES. The structure of this approach is given. Additionally, we provide a technique for automated development of the computational subsystem of the digital twin and illustrate its utility via an example.

II. Description of the Problem and Formulation of Research Objectives

Mathematical modeling of integrated energy systems, which is carried out to design them, involves solving the subproblems that have common content and mathematical formulations. The methods, algorithms, and dedicated software used to solve them can therefore be of a universal nature. The software tools used however do not provide universality, which is due to the following reasons. Preparation for computation and the computation process encounter difficulties associated with the use of a whole host of mathematical models of equipment for the IES components. Software implementations of methods and algorithms are not separated from software implementations of models of IES components. As a result, it is arduous to adapt them to a specific set of equipment when solving practical problems since it is necessary to change the software components that describe the modeled equipment. Difficulties also arise in the development of methods and algorithms since they are not separated from the software implementation of equipment models. It is challenging to keep up to date the entire set of necessary software components that implement mathematical models of equipment for various IES subsystems.

The use of a component approach to create a digital twin of IES provides universal implementations of software components that can be reused in software development. To successfully apply this approach, it is crucial to establish clear principles for implementing the software components. These principles need to provide the segregation of methods and models, as well as their adaptability and seamless integration into a unified software system. This is essential to effectively solve applied problems.

The process of IES design involves the use of a wide range of methods and algorithms, each of which must be implemented as a software component. The IES consists of subsystems that perform various energy functions, each formed by components from a standard set of equipment. To model this equipment, it is necessary to develop software components that implement its models. As a result, we will obtain a set of components that must be organized into libraries. It will also be essential to give their universal description and develop a methodology for their automated integration into a single software system when solving an applied problem.

The digital twin combines the entire set of methodological, mathematical, and software support for designing an IES and modeling it in a virtual environment, while ensuring the coordination of the characteristics with the real-world IES. The implementation of the IES digital twin requires developing a unified methodological approach to the automation of computations. This approach must consider the above-described difficulties in modeling these systems and deliver the following possibilities:

- Modeling the integrated energy systems with various types of energy systems included in them and sets of equipment;
- Accomplishing a range of tasks for designing IES on the basis of a single software platform;
- Automating computations on the basis of a digital twin of a IES when designing it;
- Separating the software implementations of methods (algorithms) and models of IES components to ensure their versatility and reusability.

III. Overview of Scientific Literature Related to the Research Topic

First presented by Grieves [1], the concept of digital twin included three components: the digital (virtual) part, the real physical product, and their connection. An overview of the history of digital twin development, its modern definitions and models, alongside six types of key enabling technologies are provided in [2]. Tao et al. [3]

expanded the concept of digital twin to five components, including data and service. In general, components of a product or product life cycle can be considered as digital twins. The difference between Product Lifecycle Management (PLM) technology and digital twin is explored in [4], where PLM is more focused on managing company components, products, and systems throughout their entire life cycle, while digital twin can represent a set of models for monitoring and processing data in real time. In some cases, it may be more appropriate to break the product or product lifecycle components into subcomponents, create several digital twins and establish relations between them [5]. The paper [6] is concerned with a 6-layer interoperability architecture in which low-level digital twins are combined into large high-level digital twins.

The study [7] discusses a five-dimensional digital twin model, which, according to the authors, has good applicability and scalability, and can also serve as a general model for applying digital twins in various fields. The same work attempts to explore and summarize commonly used digital twin technologies and tools. The paper notes that due to differences in formats, protocols, and standards, existing tools cannot be integrated and simultaneously used to solve a specific problem. The paper [8] addresses the problem of data standardization within the digital twin and proposes an approach to solving it.

Various scientific and industrial developments are examined in [9], identifying the implementation problems facing digital twin technology. One of the main disadvantages is the differences in the definitions and components of the digital twin. The work concludes that the development of machine learning and big data technologies has significantly influenced the formulation of the digital twin concept.

Currently, research is being actively conducted to develop a methodology for the creation and utilization of digital twins. The paper [10] proposes an approach to building an IT infrastructure for establishing intelligent systems to control the expansion and operation of energy systems. The approach relies on the results of systems studies for the energy industry and uses modern concepts such as digital twins and digital images. The paper [11] examines the state-of-the-art research into digital twins, with a focus on the key components, current developments, and main applications of digital twins in industry. The most important requirements for the digital twins of industrial power systems are identified in [12]. There is a growing number of works exploring the distinct characteristics of digital twin technology when applied to IES. In [13], the technical basis of the technology of digital twins of IES is discussed and its application is analyzed. The authors of [14] investigate an approach to the use of digital twin technologies in IES and propose an infrastructure for digital twin solutions based on hardware. In [15], the structure of the digital twin is proposed to solve the problems of the IES control. The paper also presents the process of automating the generation of a model to ensure that the digital model reflects the physical system in a virtual environment. The paper [16] explores the use of digital twin technology to model a regional integrated energy system when implementing the concept of “smart cities.” The specific examples demonstrate that the practical implementation of digital twin technology not only optimizes the energy system but also brings a significant economic effect. In [17], a combination of digital modeling and real-time simulation technology is used to construct a digital twin intelligent architecture for an integrated energy system. In [18], the most important requirements for digital twins of IES in industrial energy systems are identified.

Some researchers propose the use of semantic networks to create a digital twin [19–21]. Ontologies can serve as a basis for the development of digital twins. Some papers focus on the examples of ontology application in implementation of digital twins. The authors of [22] analyze the control problems for the digital twin data. They propose using ontologies to solve these problems. This approach provides the flexibility of knowledge storage throughout the digital twin life cycle. The work [23] delivers a general architecture of digital twins of the industrial energy systems to ensure flexibility of these systems and optimize their operation. Ontologies are used to store information about resources and services. The researchers make use of a hierarchical design approach, which involves both a top-level ontology and a domain ontology. In [24], an ontology is considered as a representation of a digital twin in the context of cyber-physical systems. In [25], consideration is given to the prerequisites for applying the ontological approach to the construction of a digital twin, given the available results in the field of ontological engineering of energy systems.

Since the major entities expressed their interest in digital twin technologies, the advancement of these technologies has accelerated significantly. As a result, new approaches and software tools have emerged to facilitate the development of digital twins. Some of them will be discussed below. General Electric develops and implements industry-oriented digital twin technology based on the PREDIX platform [26]. Microsoft has proposed the Azure Digital Twins platform, which provides the construction of a digital twin [27]. The Paladin DesignBase platform [28] offers an exceptional opportunity to create a digital twin that enables the modeling, intricate analysis, and optimization of energy systems. An architecture proposed in [29] serves as the basis for the development of a digital twin platform.

Implementing digital twins involves complex software systems whose implementation requires the use of advanced approaches to software development. Such approaches are the subject of research by many specialists and are widely represented in the literature. The basis for modeling modern software is an object-oriented approach [30, 31]. The works [32–35] propose a methodology of Model-Driven Engineering (MDE) to automate the stages of software construction. This methodology is a set of approaches to the automated construction of complex software systems based on pre-developed models [36]. The MDE approach remains an area of ongoing innovation and intensive advancement today. Applying the MDE-based methods enables successful development of intricate software systems [37–40]. Approaches to automating the stages of software construction based on metaprogramming are described in [41–43].

IV. Methodological Approach and Its Components

This paper proposes a methodological approach to the automation of computations based on digital twins for solving a variety of IES design problems. The approach includes the following components:

- Principles of software platform development;
- Architecture of a software platform;
- Technique for automated construction of the computational subsystem of digital twins;
- Principles of ensuring the universality of software components.

A specific feature of the approach proposed to solve the IES design problems is the use of a single universal mathematical tool developed on the basis of mathematical models, methods, and algorithms of the theories of hydraulic and electrical circuits. In the methodological approach at issue, the mathematical tool is implemented in the form of libraries of software components that can be reused when constructing digital twins of various IESs. This makes it possible to overcome the challenges that come with a wide variety of IES equipment and numerous mathematical models used to describe it. Libraries of software components are part of the software platform developed in our study as a single basis for the automated construction of the IES digital twin.

The development of this software platform relies on the following principles.

- Automated construction of a digital twin based on the software platform in the context of IES design problems.
- Separation of software implementations of methods (algorithms) and models of IES components to ensure their universality and reusability.
- Standardization (within the platform) of interfaces of software components that implement methods (algorithms) and models of IES components, and their arrangement in the form of component libraries.
- Application of the MDE methodology and modern metaprogramming technologies within the software

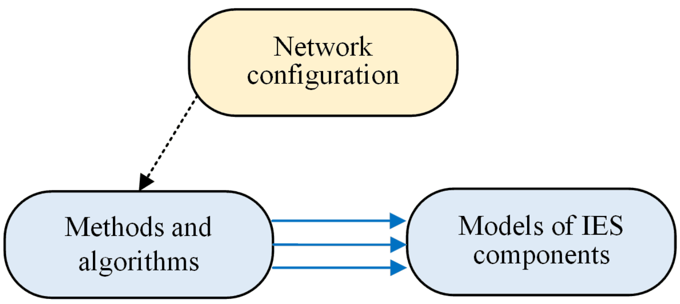

Fig. 1. Illustration of a system construction principle.

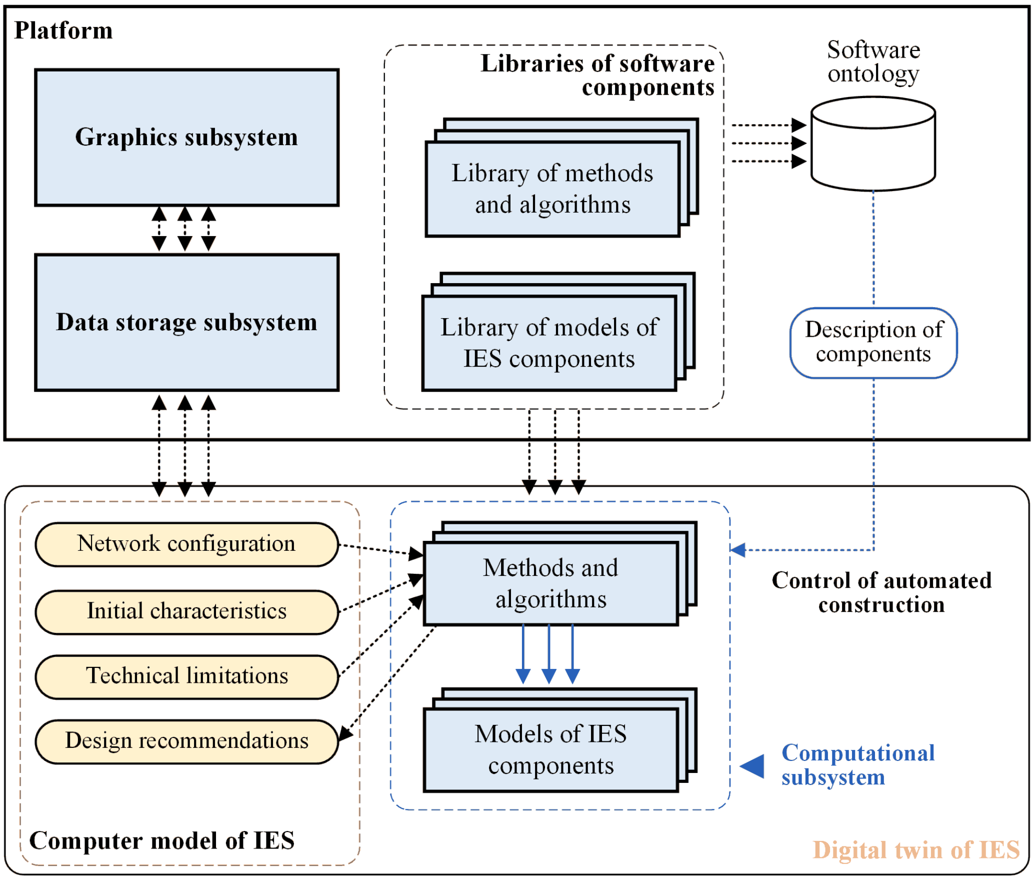

Fig. 2. Architecture of the software platform.

platform to automate the construction of a digital twin.

- Integration of methods for solving problems and models of IES components performed in the context of IES design problems, with this process controlled by knowledge organized in the form of a software ontology.

The universality of software implementation of the problem-solving methods and models of IES components is ensured by separating their software implementations. Their integration is performed in the context of solving an applied problem (see Fig. 1). Automated construction of the digital twin computational subsystem, within which the methods and models are integrated, leverages the concepts of the MDE approach. The specific feature of this approach is that the construction relies on a description of the structural configuration of the modeled system and a universal description of software components contained in the software ontology.

A software platform developed in the Java programming language is proposed for using as a single basis for automated construction. Its architecture, as shown in Fig. 2, includes the following components:

- Graphics subsystem;
- Data storage subsystem;
- Libraries of software components;
- Software ontology.

The graphics subsystem enables the development of a computer model of the IES, which reflects the structural configuration of the system, the initial characteristics of the components, technical limitations, and design recommendations for IES construction. This subsystem allows the user to view data in a readable form and make the necessary changes.

The data storage subsystem ensures the organization of work with various databases, which are used for storing and reusing computer models of IES, initial data and computation results, data on urban development projects.

The libraries of software components of the instrumental platform are categorized into the following functional groups.

1. The library of components, which contains

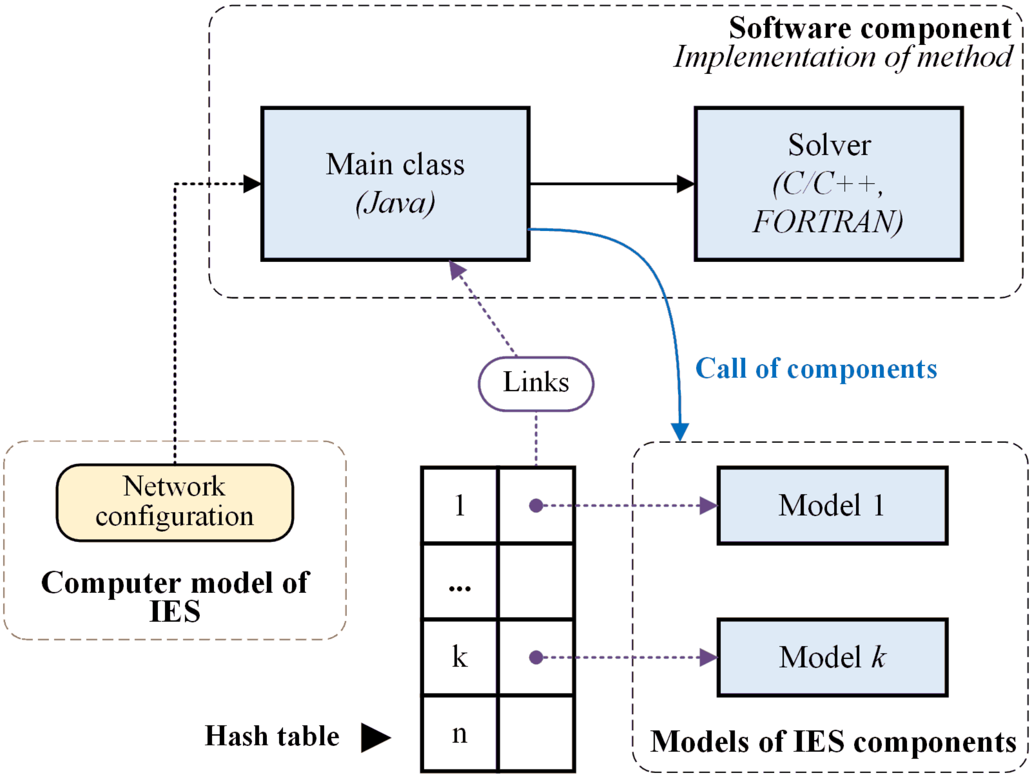

Fig. 3. Diagram of method and model integration.

implementations of mathematical methods and algorithms for solving the IES design problems.

2. The library of models of IES components, which includes software components implementing the models of components of various energy systems that constitute the IES.

The software ontology is designed to store the knowledge necessary to automate the development and use of the software. This ontology contains the description of:

- Software components that implement mathematical methods and algorithms for solving the IES design problems;
- Software components that implement the models of the IES components;
- Metadata (input and output parameters, description of data formats);
- Technologies and interfaces for access to program components.

The platform is used to build the IES digital twin in an automated mode. The digital twin includes (see Fig. 2):

- Computer model of IES;
- Software components that contain implementations of mathematical methods and algorithms for solving the IES design problems;
- Software components that implement the models of IES components.

To enable the dynamic integration of software components, a set of principles was formulated to ensure their universality. These principles are illustrated in Fig. 3. The solution proposed to provide a unified method for accessing the software components that are loaded into memory and implement the models of the IES components is as follows. Each IES component model has its unique identifier. The storage of the models is organized in a hash table, where the model identifier is used as a key, by which you can get a link to the software component that implements the corresponding model.

A software component that implements a method for solving a specific applied problem includes the main class in the Java language, which provides a single standardized access to the component (Fig. 3). In this case, it is possible to use auxiliary classes or computational modules implemented in compiled programming languages (C, C++, FORTRAN). During the computational process, the software component that implements the method for solving a specific applied problem receives the network configuration of the modelled system from the computer model. When calculating the parameters of a particular

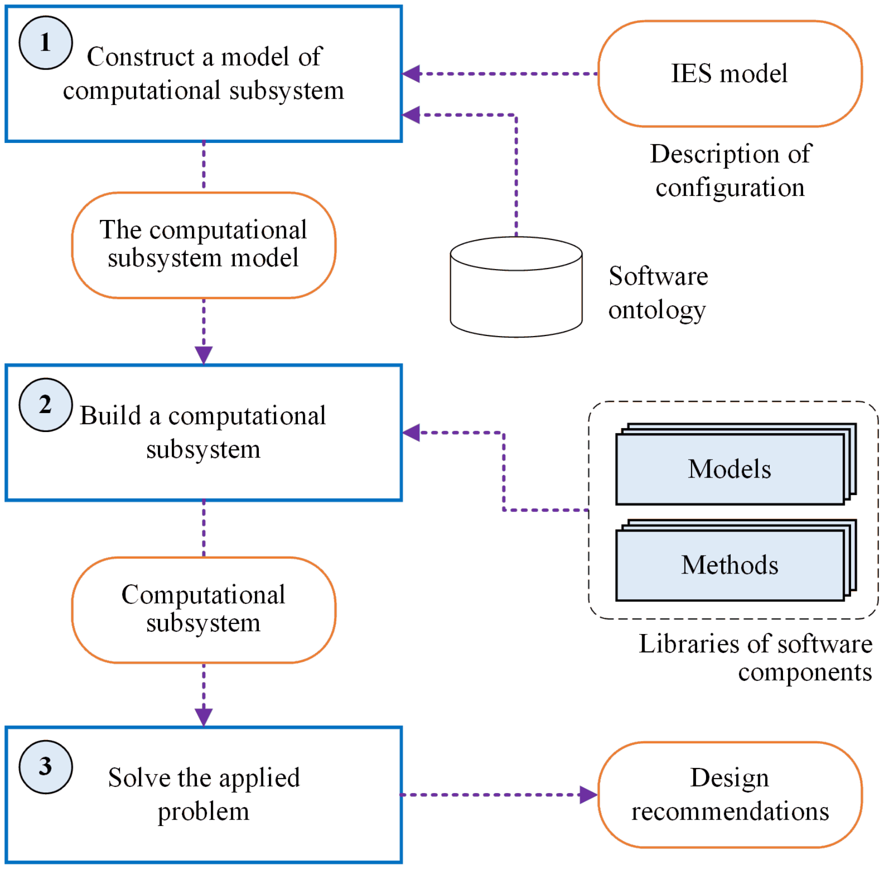

Fig. 4. The technique for the automated construction of the computational subsystem for the digital twin.

component, access to its model is performed from the hash table by its identifier.

V. Technique for Automated Development of a Digital Twin Computational Subsystem

In order to conduct calculations, it is first necessary to develop a computer model of a specific IES. This model must capture the properties of the network, including its structure, a set of equipment used and its properties, alongside parameters of the system components. This model is stored in the database for reuse. The applied problem is formalized, the set of equipment allowed for installation and the conditions for solving the applied problem are specified.

Automated construction of the computational subsystem for the digital twin is carried out in accordance with the technique proposed in this paper, which includes the following steps (see Fig 4).

Stage 1. Automated construction of a model of the computational subsystem. This stage involves building a model in an automated mode. This model describes the computational subsystem of the IES digital twin and represents a set of data structures that describe the computational subsystem.

The subproblems solved during this process are as follows:

1. Establishing a general problem-solving technique based on the description of the design problem, relying on the IES digital twin.
2. Identifying the software component that implements the problem-solving technique based on the software ontology.
3. Determining the methods and algorithms necessary for solving the problem according to the description of the technique.
4. Determining the software components that implement the necessary methods and algorithms, based on the software ontology.
5. Making a list of modeled equipment based on the description of the network configuration of the IES digital twin.
6. Determining software components that implement

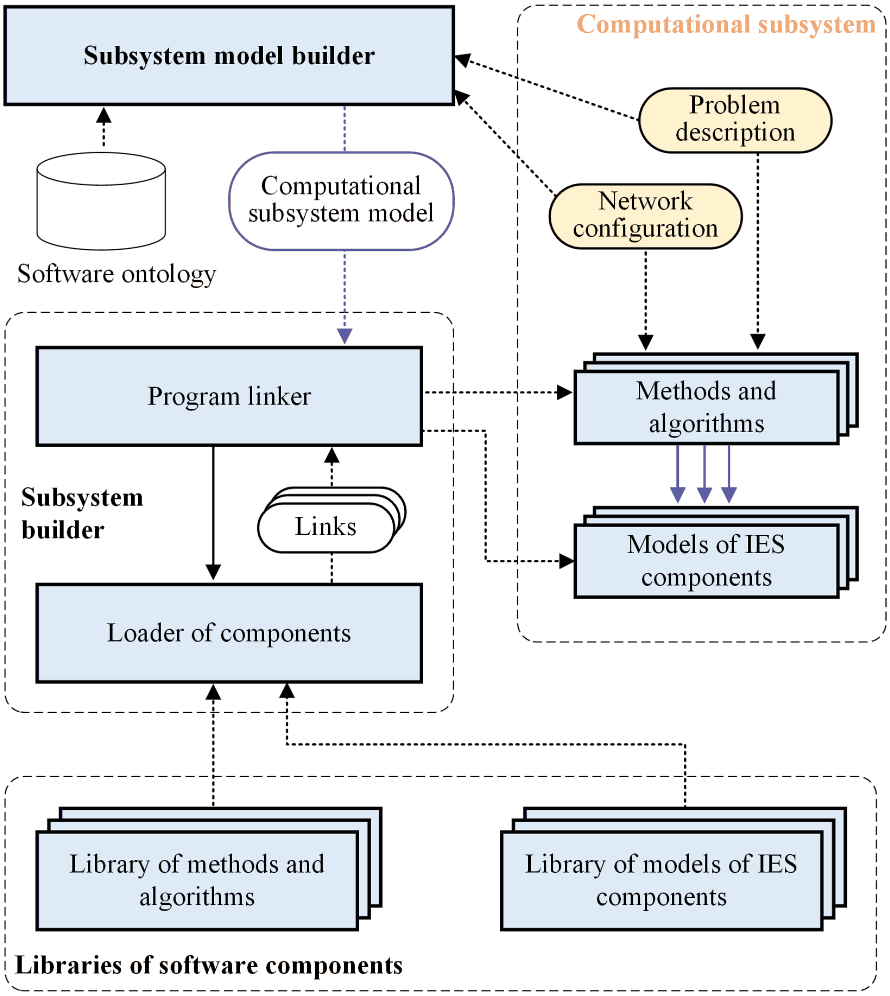

Fig. 5. General diagram of constructing the computational subsystem of the digital twin.

models of the necessary IES components based on the software ontology.

7. Loading the description of the necessary software components from the software ontology.

8. Building the data structures that describe the necessary software components.

9. Developing a general model of the computational subsystem under construction.

Stage 2. Automated construction of the computational subsystem for the digital twin based on its model using modern metaprogramming tools.

This stage involves solving the following subproblems:

1. Configuring the software component loader to work with the required libraries of components.

2. Loading software components that implement the general problem-solving technique, mathematical methods and algorithms.

3. Building the data structures for storing the software components loaded at the previous step.

4. Loading software components that implement the models of IES components.

5. Building the data structures for storing the software components loaded at the previous step.

Stage 3. Application of the digital twins in the development of recommendations for designing IESs.

This stage suggests solving the applied problems. In the course of this process, the methods and models of IES components are integrated.

The diagram of the software components interacting during the automated construction of the digital twin computational subsystem in accordance with the proposed technique is shown in Fig. 5.

The automated construction of the IES digital twin computational subsystem relies on advanced metaprogramming tools. Reflection is used, which is a type of metaprogramming and is an extension of the object-

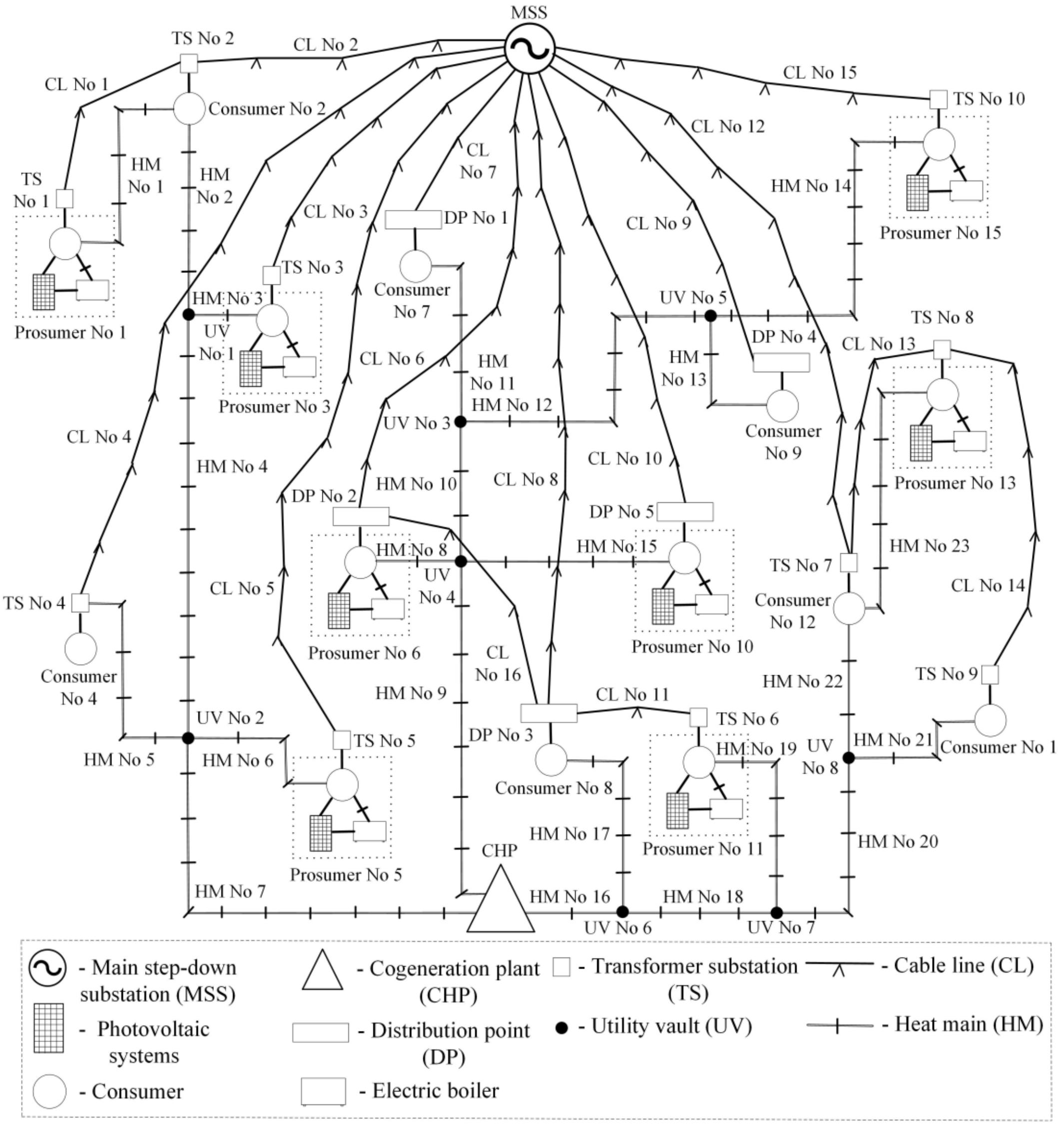

Fig. 6. Scheme of the Irkutsk microdistrict IES.

oriented programming paradigm. Reflection allows operations that cannot be performed in the classical object-oriented programming. The most important of them are studying classes during program execution; determining their fields, methods, and constructors; creating new instances of objects by class name using constructors; setting and getting values of fields by their name; calling methods by their name and argument description; working flexibly with arrays and containers (collections). With the help of reflection, the components are dynamically connected to the designed software system and configured to solve the applied problem.

VI. Testing the Methodological Approach

The methodological approach proposed in this paper is used for the software implementation of a software platform prototype to solve the IES design problems. The digital twin for the IES of an Irkutsk microdistrict was constructed based on the platform. The calculated scheme of the system is shown in Figure 6. The currently functioning electricity and heating systems are taken as a basis. Additionally, to address one of the possible options for their expansion, prosumers with their electrical and thermal energy sources are also added. The presented scheme includes the following entities: seven traditional consumers; eight prosumers; eight electric boilers for heat generation; eight photovoltaic systems for generating electrical energy; sixteen cable lines; twenty-three heat mains; one centralized electrical energy source, and one district thermal energy source.

The developed software platform prototype was used to carry out a computational experiment on the IES expansion. Based on the calculations, a compromise solution was found to allocate power between centralized and distributed energy sources in the IES. The capacity of centralized sources in the electricity and heating systems was 35 MW and 54 Gcal/h, respectively. With these values, there is no increase in the cost of supplying centralized energy to consumers. In this case, the total costs will be USD 21 715 for heating, and USD 18 168 for electricity supply.

The conducted computational experiment shows the operability and efficiency of the proposed solutions, which helped reduce the total cost of energy supply to consumers by redistributing power between the centralized and distributed generation sources in the course of the IES expansion.

VII. CONCLUSION

Integrated Energy Systems (IESs) grounded in the conventional energy systems operating separately ensure higher efficiency and reliability of energy supply to the consumer. Designing them, however, can be a challenging task due to their complexity. Digital twins enable the integration of all the essential design tools within a single information space. The software tools that implement the IES digital twins and are developed to design them require high flexibility in organizing computations. This requirement is crucial for modeling various types of equipment, necessitating a wide range of methods and mathematical models. Automating the development of the computational subsystem emerges as an effective solution for addressing the identified challenges. The paper proposes a methodological approach to automate the development of the computational subsystem for the IES digital twin. The proposed approach leverages the advanced metaprogramming tools based on a software platform. Throughout the development process, the MDE concept is implemented, utilizing formalized knowledge represented through ontologies.

The key components of the proposed methodological approach aimed at automating the development of the computational subsystem for the digital twin are presented. They encompass the principles for building a software platform and designing its architecture; devising a technique for automated construction of the computational subsystem for the digital twin; and ensuring the adaptability of the software components.

The digital twin generated by applying the proposed methodological approach facilitates computer and mathematical modeling of the integrated energy system in a virtual environment, enabling the exploration of its various configurations. This modeling, relying on the digital twin of IES, makes it possible to adopt adaptable and efficient IES design approaches, offering design recommendations to guide the construction of real-world IESs.

ACKNOWLEDGMENT

The research was performed at Melentiev Energy Systems Institute of Siberian Branch of the Russian Academy of Sciences under the support of Russian Science Foundation (Grant number 24-29-00823).

REFERENCES

[1] M. Grieves, “Digital twin: manufacturing excellence through virtual factory replication,” Florida, USA, Florida Institute of Technology: White paper, pp. 1–7, 2015.

[2] W. Hu, T. Zhang, X. Deng, et al., “Digital twin: a state-of-the-art review of its enabling technologies, applications and challenges,” J. Intell. Manuf. Spec. Equip., vol. 2, pp. 1–34, 2021. DOI: 10.1108/JIMSE-12-2020-010.

[3] F. Tao, J. Cheng, Q. Qi, et al., “Digital twin-driven product design, manufacturing and service with big data,” Int. J. Adv. Manuf. Technol., vol. 94, pp. 3563–3576, 2018. DOI: 10.1007/s00170-017-0233-1.

[4] D. Adamenko, S. Kunnen, A. Nagarajah, “Digital twin and product lifecycle management: What is the difference?”, in Product Lifecycle Management Enabling Smart X. PLM 2020, IFIP Advances in Information and Communication Technology, F. Nyffenegger, J. Ríos, L. Rivest, A. Bouras, Eds., Cham, Germany: Springer, vol. 594, pp. 150–162, 2020. DOI: 10.1007/978-3-030-62807-9_13.

[5] S. Malakuti, J. Schmitt, M. Platenius-Mohr, et al., “A four-layer architecture pattern for constructing and managing digital twins,” in Software Architecture, ECSA 2019, Lecture Notes in Computer Science, T. Bures, L. Duchien, P. Inverardi, Eds., Cham, Germany: Springer, vol. 11681, pp. 231–246, 2019. DOI: 10.1007/978-3-030-29983-5_16.

[6] A. J. H. Redelinghuys, K. Kruger, A. Basson, “A six-layer architecture for digital twins with aggregation,” in Service Oriented, Holonic and Multi-agent Manufacturing Systems for Industry of the Future, SOHOMA 2019, Studies in Computational Intelligence, T. Borangiu, D. Trentesaux, P. Leitão, A. Giret Boggino, V. Botti, Eds., Cham, Germany: Springer, vol. 853, pp. 171–182, 2020. DOI: 10.1007/978-3-030-27477-1_13.

[7] Q. Qi, F. Tao, T. Hu, et al., "Enabling technologies and tools for digital twin," J. Manuf. Syst., vol. 58, pp. 3–21, 2021. DOI: 10.1016/j.jmsy.2019.10.001.

[8] Í. A. Fonseca, H. M. Gaspar, P. C. Mello de, et al., "A Standards-Based Digital Twin of an Experiment with a Scale Model Ship," Comput.-Aided Des., vol. 145, Art. no. 103191, 2022. DOI: 10.1016/j.cad.2021.103191.

[9] A. Sharma, E. Kosasih, J. Zhang, et al., "Digital Twins: State of the art theory and practice, challenges, and open research questions," J. Ind. Inf. Integr., vol. 30, Art. no. 100383, 2022. DOI: 10.1016/j.jii.2022.100383.

[10] N. I. Voropai, L. V. Massel, I. N. Kolosok, et al., "IT-Infrastructure for Construction of Intelligent Management Systems of Development and Functioning of Energy Systems Based on Digital Twins and Digital Images," Izv. Ross. Akad. Nauk. Energ., no. 1, pp. 3–13, 2021. DOI: 10.31857/S0002331021010180. (In Russian)

[11] F. Tao, H. Zhang, A. Liu, et al., "Digital Twin in Industry: State-of-the-Art," IEEE Transactions on Industrial Informatics, vol. 15, pp. 2405–2415, 2019. DOI: 10.1109/TII.2018.2873186.

[12] L. Kasper, F. Birkelbach, P. Schwarzmayr, et al., "Toward a Practical Digital Twin Platform Tailored to the Requirements of Industrial Energy Systems," Appl. Sci., vol. 12, Art. no. 6981, 2022. DOI: 10.3390/app12146981.

[13] H. Li, T. Zhang, Y. Huang, "Digital Twin Technology for Integrated Energy System and Its Application," in Proc. the 1st International Conference on Digital Twins and Parallel Intelligence, Beijing, China, 15 July–15 August 2021, USA, NY, New York: IEEE, pp. 422–425, 2021. DOI: 10.1109/DTPI52967.2021.9540160.

[14] Y. Chen, Q. Chen, J. Gao, et al., "Hardware-in-loop based Digital Twin Technology for Integrated Energy System: A Case Study of Guangyang Island in Chongqing," in Proc. the 5th International Electrical and Energy Conference, Nangjing, China, 27–29 May, 2022, New York, NY, USA: IEEE, pp. 4956–4962, 2022. DOI: 10.1109/CIEEC54735.2022.9846475.

[15] H. Bai, Z. Yuan, X. Tang, et al., "Automatic Modeling and Optimization for The Digital twin of a Regional Multi-energy System," in Proc. the Power System and Green Energy Conference, Shanghai, China, 25-27 August 2022, New York, NY, USA: IEEE, pp. 214–219, 2022. DOI: 10.1109/PSGEC54663.2022.9881075.

[16] W. Huang, Y. Zhang, W. Zeng, "Development and application of digital twin technology for integrated regional energy systems in smart cities," Sustainable Comput. Inf. Syst., vol. 36, Art. no. 100781, 2022. DOI: 10.1016/j.suscom.2022.100781.

[17] J. Xing, S. Sun, P. Yu, et al., "Multi-energy Simulation and Optimal Scheduling Strategy Based on Digital Twin," in 2022 Power System and Green Energy Conference (PSGEC), Shanghai, China, 2022, pp. 96–100. DOI: 10.1109/PSGEC54663.2022.9881079

[18] M. You, Q. Wang, H. Sun, et al., "Digital twins based day-ahead integrated energy system scheduling under load and renewable energy uncertainties," Appl. Energy, vol. 305, Art. no. 117899, 2022. DOI: 10.1016/j.apenergy.2021.117899.

[19] A. M. M. Sharif Ullah, "Modeling and simulation of complex manufacturing phenomena using sensor signals from the perspective of Industry 4.0," Advanced Engineering Informatics, vol. 39, pp. 1–13, 2019. DOI: 10.1016/j.aei.2018.11.003.

[20] K. Kannan, N. Arunachalam, "A Digital Twin for Grinding Wheel: An Information Sharing Platform for Sustainable Grinding Process," J. Manuf. Sci. Eng., vol. 141, no. 2, Art. no. 021015, 2019. DOI: 10.1115/1.4042076.

[21] A. Moreno, G. Velez, A. Ardanza, et al., "Virtualisation process of a sheet metal punching machine within the Industry 4.0 vision," Int. J. Interact. Des. Manuf., vol. 11, pp. 365–373, 2017. DOI: 10.1007/s12008-016-0319-2.

[22] S. Singh, E. Shehab, N. Higgins, et al., "Data management for developing digital twin ontology model," in Proc. Inst. Mech. Eng., Part B: J. Eng. Manuf., vol. 235, pp. 2323–2337, 2020. DOI: 10.1177/0954405420978117.

[23] G. Steindl, M. Stagl, L. Kasper, et al., "Generic Digital Twin Architecture for Industrial Energy Systems," Appl. Sci., vol. 10, no. 24, Art. no. 8903, 2020. DOI: 10.3390/app10248903.

[24] C. Steinmetz, A. Rettberg, F. G. C. Ribeiro, et al., "Internet of Things Ontology for Digital Twin in Cyber Physical Systems," in Proc. the VIII Brazilian Symposium on Computing Systems Engineering, Salvador, Brazil, 5–8 Nov., 2018, New York, NY, USA: IEEE, pp. 154–159, 2018. DOI: 10.1109/SBESC.2018.00030.

[25] L. Massel, T. Vorozhtsova, "An ontological approach to the construction of digital twins of energy objects and systems," Ontol. Proekt., vol. 10, pp. 327–337, 2020. DOI: 10.18287/2223-9537-2020-10-3-327-337. (In Russian)

[26] GE, PREDIX. [Online]. Available: https://www.ge.com/digital/iiot-platform. Accessed on: Sep. 05, 2023.

[27] Azure Digital Twins. [Online]. Available: https://docs.microsoft.com/en-us/azure/digital-twins/. Accessed on: Sep. 05, 2023.

[28] Paladin DesignBase. [Online]. Available: https://www.easypower.com/products/paladin-designbase. Accessed on: Sep. 05, 2023.

[29] A. A. H. Dani, S. H. Supangkat, F.F. Lubis, et al., "Development of a Smart City Platform Based on Digital Twin Technology for Monitoring and Supporting Decision-Making," Sustainability, vol. 15, Art. no. 14002, 2023. DOI: 10.3390/su151814002

[30] G. Booch, J. Rumbaugh, I. Jacobson, The Unified Modeling Language User Guide, 2nd. ed. Boston, USA: Addison Wesley, 2005, 475 p.

[31] G. Booch, Object-Oriented Analysis and Design with Applications, 3rd. ed. Boston, USA: Addison Wesley, 2007, 720 p.

[32] A. R. Silva da, "Model-driven engineering: A survey supported by the unified conceptual model," Comput. Lang. Syst. Struct., vol. 43, pp. 139–155, 2015. DOI: 10.1016/j.cl.2015.06.001.

[33] M. Brambilla, J. Cabot, M. Wimmer, "Model-driven software engineering in practice," in Synthesis Lectures on Software Engineering. USA, CA, Kentfield: Morgan & Claypool, 2012, 191 p.

[34] J. Seixas, A. Ribeiro, A. Rodrigues da Silva, "A Model-Driven Approach for Developing Responsive Web Apps," in Proc. the 14th International Conference ENASE 2019, SciTePress, Setubal, 2019, pp. 257–264. DOI: 10.5220/0007678302570264.

[35] D. Akdur, V. Garousi, O. Demirörs, "A survey on modeling and model-driven engineering practices in the embedded software industry," J. Syst. Archit., vol. 91, pp. 62–82, 2018. DOI: 10.1016/j.sysarc.2018.09.007.

[36] V. A. Stennikov, E. A. Barakhtenko, D. V. Sokolov, "Development of Information and Technology Platform for Optimal Design of Heating Systems," in Proc. the 7th Scientific Conference on Information Technologies for Intelligent Decision Making Support, Ufa, Russia, 28–29 May 2019, France, Paris: Atlantis Press, 2019. DOI: 10.2991/itids-19.2019.48.

[37] I. Boussaïd, P. Siarry, M. Ahmed-Nacer, "A survey on search-based model-driven engineering," Automated Software Engineering, vol. 24, pp. 233–294, 2017. DOI: 10.1007/s10515-017-0215-4.

[38] I. Al-Azzoni, J. Blank, N. Petrović, "A Model-Driven Approach for Solving the Software Component Allocation Problem," Algorithms, vol. 14, no. 354, 2021. DOI: 10.3390/a14120354.

[39] E. Araújo Silva, E. Valentin, J. R. H. Carvalho, et al., "A survey of Model Driven Engineering in robotics," J. Comput. Lang., vol. 62, Art. no. 101021, 2021. DOI: 10.1016/j.cola.2020.101021.

[40] V. Stennikov, E. Barakhtenko, D. Sokolov, et al., "Principles of Building Digital Twins to Design Integrated Energy Systems," Computation, vol. 10, no. 12, Art. 222, 2022. DOI: 10.3390/computation10120222.

[41] K. Hazzard, J. Bock, Metaprogramming in NET. Shelter Island, NY, USA: Manning Publications, 2013, 360 p.

[42] R. Lämmel, Software Languages: Syntax, Semantics, and Metaprogramming. Cham, Switzerland: Springer, 2018, 454 p.

[43] V. A. Stennikov, E. A. Barakhtenko, D. V. Sokolov, "A Methodological Approach to the Software Development for Heating System Design," in Proc. the International Multi-Conference on Industrial Engineering and Modern Technologies, Vladivostok, Russia, 3–4 Oct. 2018, New York, NY, USA: IEEE, 2018. DOI: 10.1109/FarEastCon.2018.8602533.

Evgeny Barakhtenko, Ph.D., is the Scientific Secretary of the Melentiev Energy Systems Institute of the Siberian Branch of the Russian Academy of Sciences (ESI SB RAS). E. Barakhtenko is a Winner of the Prize of the Government of the Russian Federation in the Field of Science and Technology for Young Scientists (2016). His scientific interests include mathematical models and methods for expansion planning of energy pipeline systems and integrated energy systems; and digital design. E. Barakhtenko has authored and coauthored over 150 scientific papers. His RSCI Author ID is 670523, Scopus Author ID is 55229371000, and WoS Researcher ID is Q-7173-2016. He can be contacted at barakhtenko@isem.irk.ru.

Dmitry Sokolov, Ph.D., is a Senior Researcher at the ESI SB RAS. D. Sokolov is a Winner of the Prize of the Government of the Russian Federation in the Field of Science and Technology for Young Scientists (2016). His scientific interests include the development of algorithms for optimization of pipeline systems and automation of programming. He has authored over 100 scientific papers. His RSCI Author ID is 710020, Scopus Author ID is 57190607698, and WoS Researcher ID is K-6737-2018. He can be contacted at sokolov_dv@isem.irk.ru

Gleb Mayorov, Ph.D., is a Research Associate at the ESI SB RAS. His research interests include integrated energy systems and methods for solving their design problems, multi-agent approach and its application. G. Mayorov has authored over 40 scientific papers. His RSCI Author ID is 1001072, Scopus Author ID is 57211071672, and WoS Researcher ID is HJZ-2977-2023. He can be contacted at mayorovgs@isem.irk.ru.

Deep Recurrent Convolutional Neural Network for Fault Identification in Photovoltaic Panels using Thermal Imaging

K. Subha[1,*], S.Sharanya[1]

[1] SRM Institute of Science & Technology, Kattankulathur, India

Abstract **— Faults that are often invisible to existing inspection methods can significantly impact the reliability and efficiency of Photovoltaic (PV) systems. This study introduces an innovative framework for identifying PV panel faults using advanced machine learning algorithms and thermal images captured by unmanned aerial vehicles. The proposed Deep Recurrent Convolutional Neural Network (DRCNN) combines the strengths of Recurrent Neural Networks (RNNs) for learning temporal sequences and Convolutional Neural Networks (CNNs) for feature extraction. The DRCNN is designed to analyze thermal images of PV panels by capturing spatial and temporal patterns associated with fault-induced anomalies, such as hot spots, cracked cells or broken electrical connections. By leveraging CNN layers to extract critical features from thermal images and RNN layers to model the temporal dependencies and variations in thermal processes over time, the proposed approach integrates thermal image data collected under diverse environmental conditions. This dual strategy not only identifies faults based on spatial features but forecasts potential fault progression or the End-of-Life (EoL) for the panels by analyzing the evolution of thermal anomalies. The research aims to develop a highly accurate and efficient system for preventive maintenance and early problem detection, thereby improving the efficiency and durability of PV systems. The results demonstrate the DRCNN model's effectiveness in detecting various types of defects and delivering highly accurate real-time fault detection. By incorporating both spatial and temporal information, the proposed model significantly outperforms existing methods providing more robust and reliable defect identification.**

Index Terms **— Deep Recurrent Convolutional Neural Network, fault identification, hot spot detection, end-of-life prediction, proactive maintenance, predictive maintenance.**

I. Introduction

In modern society, electricity systems must operate reliably and efficiently. Key components of electricity systems, including generators, fuses, transmission lines, and PV panels, play a critical role in ensuring the smooth operation of these systems. Malfunctions in these components can lead to significant equipment damage and power outages, causing inconvenience and disruption [1]. Early detection of component failures is essential to mitigate the impact of outages on the electrical system [2]. Rapid identification and resolution of component issues are vital for the reliable and continuous operation of power systems. Early fault detection minimizes downtime, enhances system reliability, and improves customer satisfaction by enabling timely repairs and scheduled maintenance. Existing methods for identifying faults in power system components primarily rely on manual diagnostic techniques and periodic visual inspections [3]. These approaches have limitations in terms of flexibility, accuracy, and efficiency. Visual inspections may overlook hidden or early-stage defects and are prone to human error and subjective judgment. Manual diagnostics are time-intensive, require specialized expertise, and may not be suitable for large-scale systems [4].

* Corresponding author.
E-mail: k.subhabalamurugan@gmail.com

DOI:10.25729/esr.2025.03.0008

Received June 27, 2025. Revised October 27, 2025. Accepted September 1, 2025. Available online November 28, 2025.

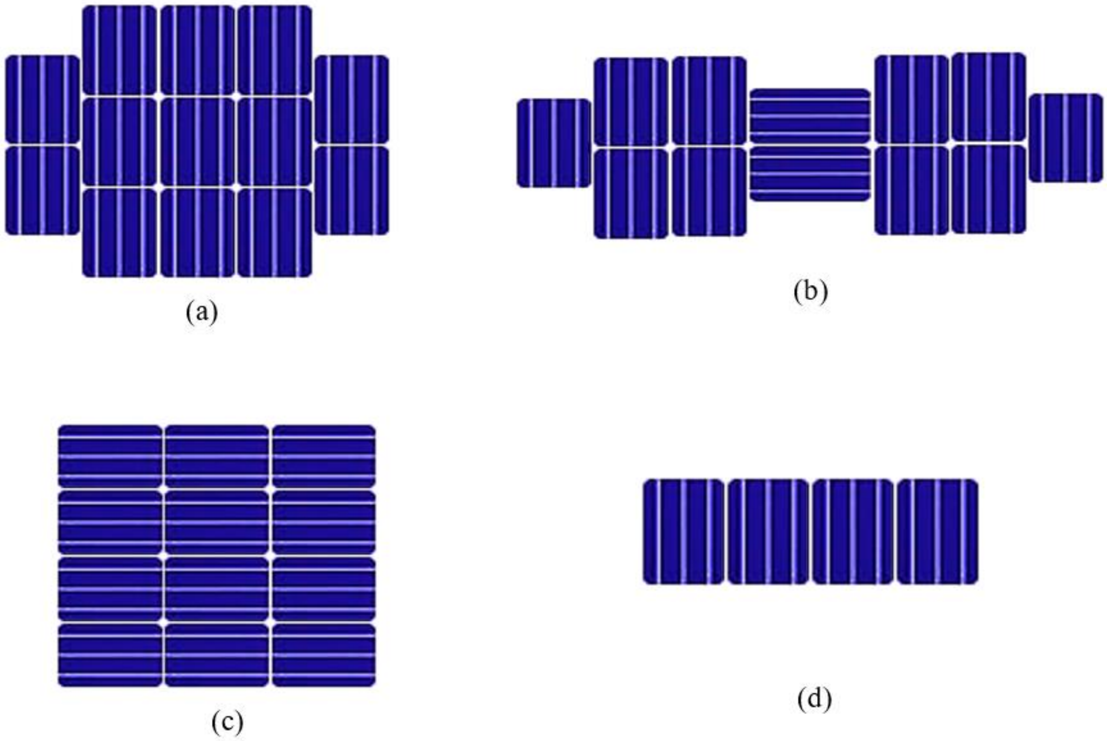

Fig. 1.Some PV solar tracker and panel setups.

To overcome these limitations, researchers and developers have turned to advanced techniques for improving the detection of faults in electrical system components. Infrared Thermography (IRT) is one such sophisticated method, which analyzes thermal characteristics by capturing thermal images of electrical system components. Abnormal temperature patterns or ranges can indicate potential component failures [5]. In addition to IRT, advanced data analysis methods, such as feature extraction and classification techniques, are employed to enhance fault detection accuracy and efficiency. These methods aim to classify collected thermal images into distinct fault categories and extract valuable insights from them. By leveraging data analysis and Artificial Intelligence (AI), the techniques automate the detection process, reducing human error, and managing large volumes of data in real time [6]. The growing demand for Renewable Energy Sources (RES), driven by ecological and climate concerns, along with the global economic recovery, poses significant challenges for the future. Reducing emissions and dependence on fossil fuels requires the adoption of alternative energy sources. Distributed PV plants are increasingly being deployed, and most of these systems are decentralized [7]. Europe has seen one of the most significant increases in this sector over the past five years, particularly in energy production from PV systems and RES. The importance of monitoring and maintaining PV plants grows, presenting challenges related to reliability, efficiency, durability, and safety. Several PV solar tracker and panel setups are depicted in Fig. 1 [8].

The durability and overall reliability of PV plants can significantly affect anticipated profits. The primary aim of this work is to address the fault identification challenge using the thermal images gathered through IRT. To achieve this, multiclass classification is employed for fault diagnosis, while binary classification is used for fault detection [9]. The literature indicates that various techniques were developed for this purpose. AI and advanced learning techniques are used to categorize typical red, green, blue (RGB) images of PV. Comparison of the *k*-nearest neighbors (kNN) classification algorithm with other classification methods demonstrates improved accuracy of up to 98.95% with a computation time of 0.04 seconds [10]. CNN-ML models are applied to identify PV issues by processing true-color images captured by Unmanned Aerial Vehicles (UAVs). The frameworks VGG16, GoogLeNet, AlexNet, and ResNet50 are evaluated in terms of their ability to extract relevant features. The study reveals that Support Vector Machine (SVM) classifiers exhibit the best performance for real-time classification in multi-class applications [11].

Information collected from two operational PV power plants in India facilitated the identification of specific connections between internal and external plant characteristic variables. Proposed IRT-based fault classification was used instead of signal processing for diagnosing PV failures [12]. The latest research in this area presents an automated defect identification system that leverages supervised machine learning techniques and texture feature extraction. To identify observable PV defects, a CNN-based deep learning framework with seven learned layers is employed. The study evaluates six common faults using an 8400-image dataset [13].

A. Problem Statement

Microcracks, electrical failures, and hotspots are among the issues that can significantly impair the efficiency of PV panels and reduce their lifespan. Existing analysis techniques such as electrical testing or manual visual inspections, are costly, time-consuming, and often ineffective at detecting minor or concealed flaws. Thermal imaging offers a non-invasive, efficient, and reliable method for identifying thermal anomalies caused by PV panel defects. Despite its potential, analyzing thermal images for fault diagnosis remains challenging due to complex, fluctuating climatic conditions and the precise, dynamic nature required for real-time fault detection in PV systems. Existing methods struggle to effectively evaluate temporal and spatial information, which is crucial for predicting the potential End-of-Life (EOL) for PV panels and detecting problems at an early stage. To facilitate preventive maintenance and enhance the reliability and longevity of solar energy systems, there is a need for an advanced, automated system capable of accurately detecting, categorizing, and predicting PV panel issues by using thermal imaging data.

B. Motivation

The increasing use of PV systems as an environmentally friendly energy source has highlighted the necessity of efficient and reliable maintenance processes to ensure their longevity and peak performance. Early failure detection is crucial for minimizing system downtime, reducing maintenance costs, and optimizing energy output as PV systems continue to proliferate. Existing defect detection techniques often require significant effort and are prone to human error, while struggling to keep pace with the growing complexity and scale of PV installations. Thermal

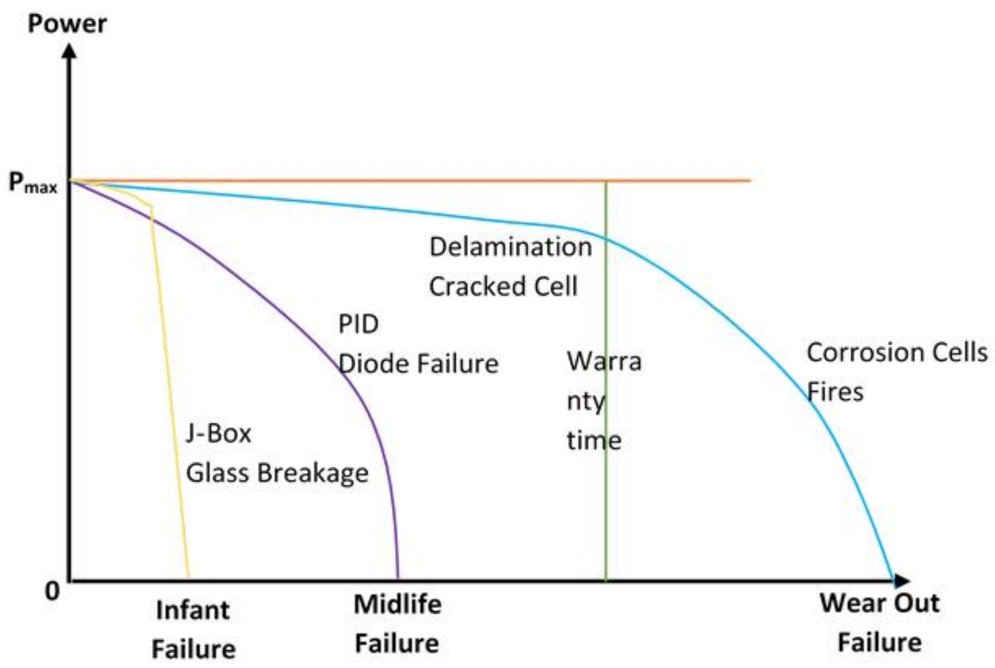

Fig. 2. Main categories of PV failures.

imaging provides a potential solution by enabling non-invasive, real-time identification of abnormalities that may indicate defects. The challenge lies in efficiently analyzing the vast amount of temperature data generated under varying external conditions. By addressing the limitations of existing techniques, this approach aims to provide a reliable, automated, proactive problem detection solution, thereby enhancing the efficiency, dependability, and management of PV systems.

II. RELATED WORKS

A research study on automated PV defect identification using realistically recorded IRT images in both indoor and outdoor settings is proposed in [14]. The study relies on deep learning approaches for independent ensemble transfer. The precision of a light CNN architecture-based, independently trained model achieved 98.67%. With independent and transferred learning systems, it took 13.12 ms and 13.07 ms, respectively, to generate an estimate for a single image. The computing cost required to achieve the model's effectiveness is not disclosed in the paper [15]. An IRT image-based method was developed that combined transfer learning with an Isolated Convolutional Neural Model (ICNM). Effectiveness indicators of the proposed multi-class classification method included validation loss, testing accuracy, training loss, training accuracy, and time to completion [16]. The PV health-based categorization findings were presented using the ICNM and publicly available pre-trained transfer learning models (SqueezeNet, GoogleNet, and ShuffleNet). Within the analysis, 695 images showed defects related to overheated regions, such as hotspots and overheating segments [17]. SC-DeepCNN was used to identify IRT images with hotspots. To recognize objects in hot areas an ROI-DeepCNN algorithm was created and applied in conjunction with joint learning. Thermal imaging provides a visual representation of the frequency patterns observed in the components. Various temperature indicators can be observed across different components, highlighting conditions such as normal operation, deterioration, soiling, fractures, short circuits, and other faults [18].

By analyzing the thermal properties of components, potential issues or abnormalities in PV systems can be detected at an early stage. Thermal imaging is a powerful tool that enables investigators to monitor the thermal behavior of components, revealing underlying problems or deviations from normal operations. A critical consideration in this process is the Field of View (FoV), which determines the spatial coverage of the thermal image, or the area captured by the thermal camera [19]. Choosing an appropriate FoV is therefore essential to ensure accurate data collection and processing. For instance, operational problems in PV modules can be categorized into three main groups based on the energy losses incurred: neonatal failures, midlife failures, and wear-out failures [20]. Neonatal failures occur during the initial operation of a PV system, often due to errors from manufacturers or installers, resulting in a rapid and significant decline in power output. In contrast, wear-out failures occur at the end of the PV module lifespan, typically when output drops to 80–70% of the initial energy, raising security and performance concerns [21]. The severity of PV defects further influences their categorization. Acute problems, such as short-circuit and open-circuit faults, are considered critical because they can cause complete shutdown of the energy system. On the other hand, chronic problems, often caused by partial shading or irregular light reception, are less severe but still impact overall efficiency [22]. Therefore, evaluating PV performance requires examining parameters such as light absorption, cell condition, and interconnections to promptly identify permanently defective components. Proper FoV selection is particularly important here, for thermal cameras to capture critical regions that are most likely to develop defects. This improves the reliability of datasets and strengthens fault diagnosis by covering both acute and chronic error regions [23].

Compared to existing methods, the proposed FoV-based thermal image collection framework emphasizes tailored data acquisition for PV systems. Existing approaches may overlook critical component regions or fail to adequately represent thermal behavior, thereby producing incomplete or less reliable data. By contrast, the FoV-based approach ensures a comprehensive and accurate representation of thermal properties, improving the precision of defect detection and analysis [24]. Researchers show that such targeted imaging significantly enhances fault identification, providing more representative datasets for training advanced models. Despite these improvements, several key limitations remain in current PV defect identification frameworks. Existing approaches often rely on shallow training algorithms or basic image-processing techniques, which lack the capability to capture the dynamic and complex nature of temperature anomalies in PV systems [25]. These methods are insufficient to detect subtle or evolving faults as they primarily exploit spatial

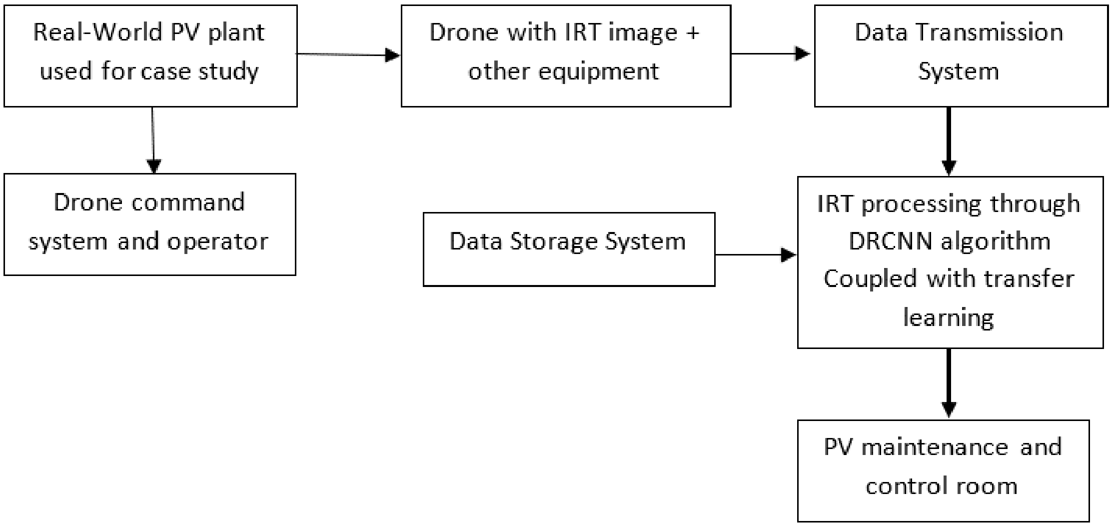

Fig. 3. Proposed architecture.

features while neglecting temporal dependencies critical for forecasting End-of-Life (EoL) states and tracking fault progression [26]. Thermal imaging data are highly sensitive to environmental factors such as fluctuating illumination and ambient temperature changes, yet existing systems are often not robust enough to address these variations [27]. This shortfall frequently results in delayed fault detection, reduced preventive maintenance capacity, and increased operational costs. To overcome these limitations, there is a need for a more integrated approach capable of handling both spatial and temporal dependencies, while accounting for environmental variations. Advanced deep learning architectures are well-suited to address these requirements. This study introduces a CNN designed to analyze thermal images comprehensively, track fault progression over time, and deliver early, accurate fault detection. By bridging spatial-temporal analysis with robust environmental adaptation, the proposed method addresses the gaps left by existing works and contributes to improving the long-term sustainability, reliability, and energy efficiency of PV systems [28,29].

III. Materials and Methods

The proposed method employs CNNs to identify abnormalities such as hot spots, microcracks, or overheated regions that may indicate issues by extracting spatial information from thermal images of PV panels shown in Fig. 3. Temporal analysis is crucial for understanding how defects develop, predicting their future impact, and determining the EoL of PV panels. The DRCNN technique is particularly beneficial for PV fault identification as it effectively handles the complexity of dynamic thermal images captured under varying environmental conditions, such as fluctuations in sunlight, temperature, or weather. By incorporating both spatial and temporal information, the DRCNN can detect faults at an early stage, including those that develop gradually or are difficult to identify in a single thermal image. This proposed system enhances the accuracy and efficiency of fault detection and enables proactive maintenance scheduling, reducing downtime, preventing severe malfunctions, and optimizing the overall efficiency of solar power systems. By integrating CNN and RNN methodologies, the proposed solution provides a robust, automated system for real-time fault detection in PV systems, thereby improving their operational lifespan and reliability.

A. Dataset Description

More than 10 000 thermal images taken by UAVs fitted with infrared thermographic cameras make up the dataset utilized for thermal imaging defect diagnosis in PV panels shown in Table 1. These images were taken from a variety of PV structures, such as rooftop and solar farm configurations, in a range of weather situations, including bright, overcast, and rainy ones, during the summer, fall, spring, and winter seasons. According to the recording device characteristics, the thermal images are available in a variety of formats (usually 640×480, 800×600, and 1024×768). Supervised training for fault identification is made possible by labeling the images into several fault

TABLE 1. Dataset Description

Dataset attribute	Description
Dataset Name	PV Thermal Imaging Fault Dataset
Data Source	UAV-based thermal images from PV panels, collected under diverse environmental conditions
Data Type	Thermal images (Infrared)
Resolution	Varies between 640×480, 800×600, and 1024×768 depending on the UAV camera used
Number of Images	10,000+ images
Fault Types	Hot spots, microcracks, electrical faults, and panel malfunctions
Image Format	JPEG, PNG, TIFF
Timeframe	Across all four seasons (spring, summer, fall, winter)
Environmental Conditions	Various lighting, temperature, and weather conditions (cloudy, sunny, rainy, etc.)
Annotation Type	Labelled for faults (e.g., hot spots, cracked cells, or no fault)
Data Collection Frequency	Regular intervals (e.g., every 5 minutes or hourly) depending on the setup
Data Augmentation	Includes flipping, rotating, and scaling to improve model robustness
Data Preprocessing	Normalization, noise reduction, and image resizing
Number of Classes	4 (Hot spot, Cracked cell, Electrical fault, No fault)
Data Collection Tool	UAV with infrared thermographic camera (e.g., FLIR, DJI)
Geographical Region	Various locations with diverse solar panel installations (e.g., rooftops, solar farms)
Temporal Data	Image sequences showing thermal dynamics over time (temporal sequence for fault progression analysis)
Labeling Method	Expert annotation based on thermal images and visual inspection

TABLE 2. Sample Data

Image ID	Fault Type	Resolution	Time of Capture	Environment	Temperature (°C)	Location	Annotations
001	Hot Spot	640×480	2024- 07-02 10:45 AM	Sunny	36ºC	Rooftop, City A	Hot spot in the middle of the panel
002	Cracked Cell	800×600	2024- 07-02 10:50 AM	Cloudy	29ºC	Rooftop, City B	Crack visible in top left corner
003	Electrical Fault	1024×768	2024- 07-02 10:55 AM	Sunny	36ºC	Solar Farm, City C	Electrical fault near junction box
004	No Fault	640×480	2024- 07-02 11:00 AM	Rainy	29ºC	Rooftop, City D	No anomalies detected
005	Hot Spot	800×600	2024- 07-02 11:05 AM	Sunny	37ºC	Solar Farm, City A	Hot spot near bottom right corner
006	Cracked Cell	640×480	2024- 07-02 11:10 AM	Cloudy	30ºC	Rooftop, City B	Crack visible in bottom right
007	Electrical Fault	1024×768	2024- 07-02 11:15 AM	Sunny	37ºC	Solar Farm, City C	Electrical fault along wiring

groupings, including electrical problems, hot spots, microcracks, and non-faulty panels (no fault).

The collection allows for longitudinal investigation of fault propagation since it contains both static thermal images and image sequences taken over time. Experts interpret the information according to discernible thermal anomalies in the images, and information enrichment methods like flipping, revolving, and scaling are used to improve the resilience of the mathematical framework. To get the images ready for deep learning, designs methods of preprocessing such as noise elimination and standardization are used. This dataset's mixture of time and space-based information enables the creation of deep learning examples. Notably, DRCNN efficiently detects and forecasts PV system errors, enhancing preservation and prolonging the panels' operational life. Sample data are shown in Table 2.

Deep learning models for PV panel defect diagnosis may be trained using this sample information, which offers an organized and transparent view of the characteristics linked to each thermal image in the dataset. An example of the gathered images is displayed in Fig. 4(a) and (b). The shading effect, shunted, dust-accumulated, and broken bypass diode are all normal problems seen in PV modules.

B. Image Pre-processing

Image preprocessing is an essential step in the analysis of PV panel defects using DRCNN. Enhancing image

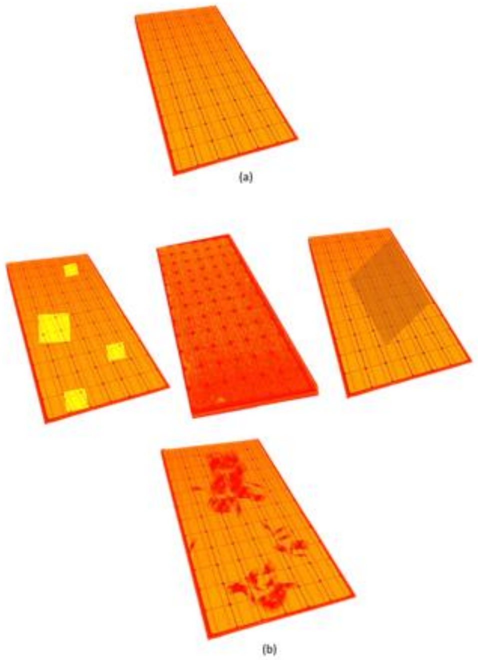

Fig. 4. Sample images of IRT: healthy(a) and faulty(b)

quality, lowering noise, normalizing the values of pixels, and preparing the information for neural networks to receive input are the objectives of image preprocessing.

1) Resizing

It is essential that all images have a uniform size for batch processing in deep learning models. Thermal images from UAVs may have different dimensions, and resizing is done to maintain consistency:

$$X_{resized} = f\left(X,(W,H)\right), \quad (1)$$

where *X* is the original image; *W*, *H* are the desired width and height, respectively; *f*(*X*, (*W*, *H*)) represents the resizing function.

2) Normalization

Normalization of pixel values is a technique to scale the values to a specific range, often between 0 and 1, which helps speed up the convergence of the model during training:

$$X_{norm}\left(i,j\right) = \frac{X\left(i,j\right) - X_{\min}}{X_{\max} - X_{\min}}, \quad (2)$$

where $X\left(i,j\right)$ is the pixel value at position $\left(i,j\right)$ in the image; $X_{\min}$ and $X_{\max}$ are the minimum and maximum pixel values in the image, respectively; $X_{norm}\left(i,j\right)$ is the normalized pixel value.

TABLE 3. Specifications of the Solar Power Grid

Power production rate in 2022	500 kW
Installation type	Ground mount
Panels type	Polycrystalline
Inverter type	String inverters
Commissioned	2019
CO_2 abated per year	747 tonnes
Equivalent to planting	12 910 Trees

3) Grayscale Conversion

Since thermal images are typically represented in grayscale, this step ensures that the image only contains intensity values, reducing computational complexity:

$$X_{grayscale}\left(i,j\right) = 0.2989R\left(i,j\right) + \\ +0.587G\left(i,j\right) + 0.114B\left(i,j\right), \quad (3)$$

where $X_{grayscale}\left(i,j\right)$ is the resulting grayscale intensity at pixel $\left(i,j\right)$.For thermal images, the RGB channels might already be collapsed into a single channel, so this step might be skipped.

4) Noise Reduction

Thermal images often contain noise due to environmental factors. A common method to reduce noise is applying Gaussian filtering, which smooths the image and removes high-frequency noise:

$$X_{filtered}\left(i,j\right) = \sum_{x=-k}^{k}\sum_{y=-k}^{k} G\left(x,y\right) X\left(i+x, j+y\right), \quad (4)$$

where $G\left(x,y\right)$ is the Gaussian kernel; $X\left(i+x, j+y\right)$ is the pixel value at the neighborhood of pixel $\left(x,y\right)$; k defines the size of the kernel (e.g., 3×3 or 5×5).

5) Data Augmentation

Rotation:

$$X_{rotated}\left(i',j'\right) = X\left(R^{-1}\left(i',j'\right)\right), \quad (5)$$

where R^{-1} is the inverse rotation matrix used to rotate the image by a certain angle.

Flipping:

$$X_{flipped}\left(i,j\right) = X\left(W-i,j\right), \quad (6)$$

where *W* is the width of the image.

Scaling:

$$X_{scaled}\left(i,j\right) = X\left(\alpha i, \alpha j\right), \quad (7)$$

where α is the scaling factor.

6) Edge Detection

It can be used to highlight important features such as cracks or hot spots. One of the most common techniques is

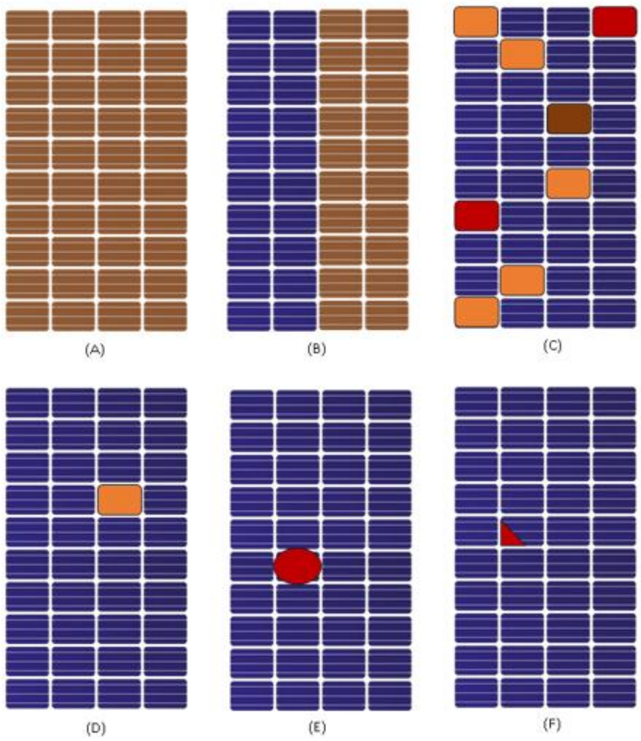

Fig.5.Different PV faults in thermography: Open circuit (offline)(a); Bypass diode short circuit panel (b); Shading represents wrong connection (c); Defect cell or shading (delamination) (d); Snail trails (Pointed heat) (e); Broken cell (f).

the Sobel operator:

$$X_{edge}\left(i,j\right)=\sqrt{\left(\frac{\partial X}{\partial x}\right)^{2}+\left(\frac{\partial X}{\partial j}\right)^{2}}, \tag{8}$$

where $\frac{\partial X}{\partial x}$ and $\frac{\partial X}{\partial j}$ are the gradients of the image in the x and y directions.

7) Final Preprocessed Image

After the preprocessing steps, the final preprocessed image is ready for input into the DRCNN model:

$$X_{final}\left(i,j\right)= = f_{final}\left(X_{resized}, X_{norm}, X_{grayscale}, X_{filtered}, X_{edge}\right), \tag{9}$$

where X_{final} denotes the composite function that applies all preprocessing steps in a sequence.

These preprocessing techniques help enhance the quality and consistency of the thermal images, which is crucial to identify faults in PV panels using the proposed DRCNN system.

C. Specifications

1) Solar Power Grid

The specifications of a 500 kW solar power grid, which occupies an area of around 1 200 m2, is shown in Table 3.

2) Thermal Camera Specifications

Large power plants frequently utilize IRT for non-contact temperature analysis and measurement. IR cameras offer several advantages over manual inspections, including the ability to record temperature data remotely and display temperature patterns instantly. When employing IRT for PV power plant analysis, certain requirements, limitations, and factors must be considered. The ability of an infrared camera to detect minute temperature variations is referred to as its sensitivity; higher sensitivity enables the detection of smaller temperature changes. In addition, the precision of a thermal imaging camera reflects its ability to provide consistent and accurate temperature readings under repeated measurements. The number of pixels in the camera's sensor, or resolution, also influences the quality of thermal images. Cameras with higher sensitivity, precision, and resolution provide more reliable and accurate temperature assessments.

D. Visual Thermal Methods (VTMs)

Figure 5(a)–(f) illustrates six distinct thermal signatures commonly observed in PV modules through thermographic inspection. These thermal images provide a visual representation of surface temperature variations, where color gradients indicate differences in heat distribution. Warmer zones typically appearing in red, orange, or brown, highlight the presence of faults or defects. Figure 5(a) displays a module that is uniformly warm, indicating an open circuit or offline status. Figure 5(b) presents a characteristic pattern caused by a short-circuited bypass diode that affects a defined section of cells. Figure 5(c) shows irregular warming attributed to shading effects or improper electrical connections. Figure 5(d) highlights an isolated hot spot, often linked to a single defective cell or delamination. Figure 5(e) captures localized heating associated with snail trails or concentrated pointed defects. Figure 5(f) depicts the triangular thermal pattern of a broken cell. These panels provide a practical reference for identifying and classifying PV module failures based on distinctive thermal signatures, thereby supporting fault detection and predictive maintenance strategies in solar energy systems.

E. Feature Extraction Using DRCNN

To prevent the explicit collection of characteristics, the DRCNN–a multilayer neural network –has demonstrated outstanding results in hyperspectral image recognition, as illustrated in the training data shown in Fig. 6. To improve the outcomes, the cross-entropy derived from gradient research and the loss function are analyzed simultaneously. MNIST and CIFAR-10 are two deep-learning benchmark datasets that were used in the studies. In both datasets, the proposed DRCNN produced useful outcomes. When it comes to illustrating and classifying the characteristics of images, they are unmatched.

Imperfection diagnosis and defect detection are the two primary tasks of the process shown in Fig. 7. Classifying

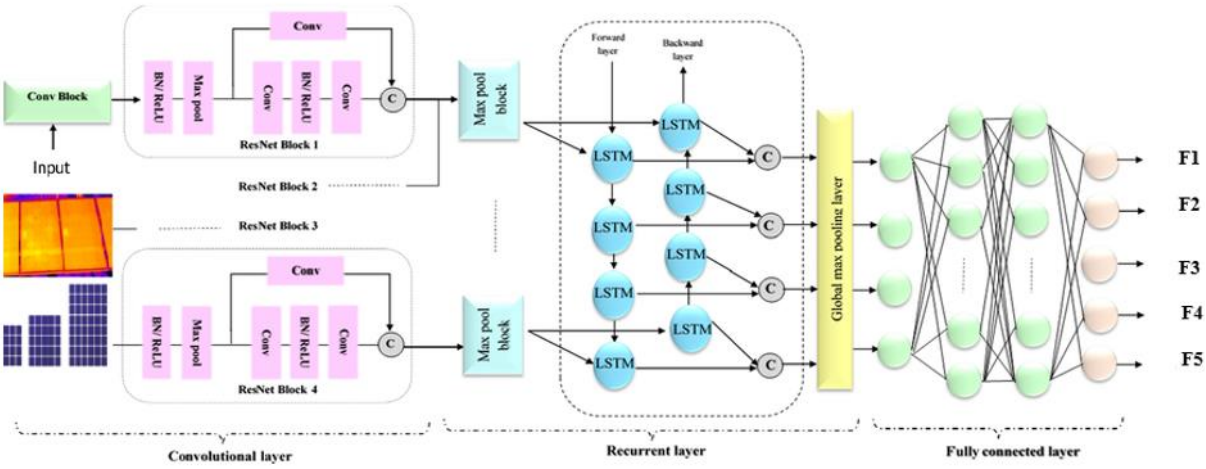

Fig. 6. DRCNN-based classification for fault identification in PV Panels using thermal imaging.

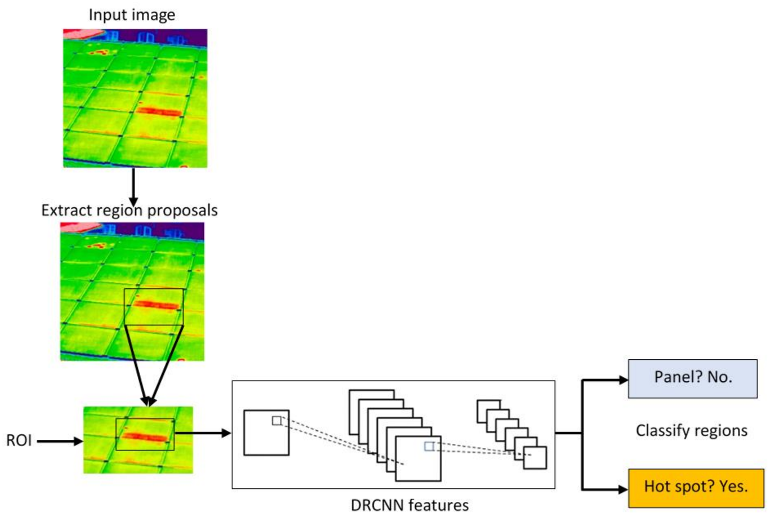

Fig.7.Fault identification using DRCNN. The DRCNN algorithm for identification of faults in photovoltaic panels through the use of thermal imaging.

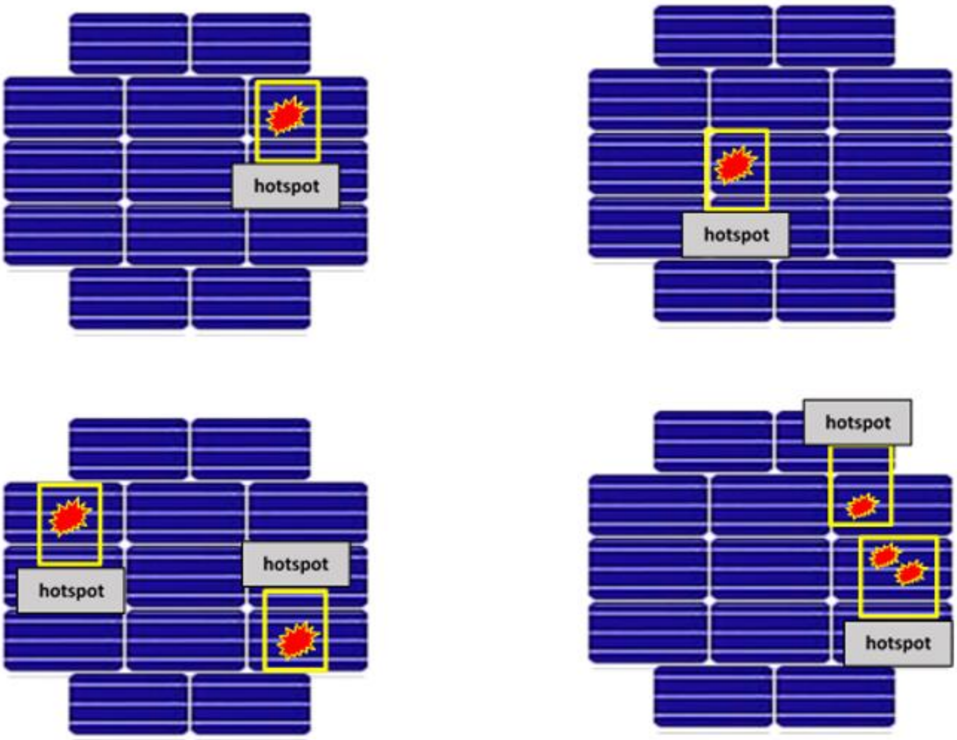

Fig. 8.Region of interest for DRCNN training.

the studied defects is the purpose of the fault diagnostic function, whereas fault detection seeks to identify abnormalities in the PV cells. Every defect has a unique temperature and this process is based on looking at the differences in the hotspot profile.

Step 1: Prepare input data

Thermal Image Acquisition. Collect thermal images of photovoltaic panels using UAVs under various environmental conditions.

Preprocessing. Enhance the images through resizing, normalization, noise reduction, and augmentation:

$$X_{preprocessed} = f\left(X\right), \tag{10}$$

where *X* is the original image, and f represents the sequence of preprocessing operations.

Step 2: Extract features using convolutional layers

Convolution Operation. Extract spatial features from the thermal images using convolutional filters:

$$F\left(i,j,k\right)=\sum_{x=1}^{m}\sum_{y=1}^{n}X\left(i+x,j+y\right)W(x,y,k)+b\left(k\right), \tag{11}$$

where $F\left(i,j,k\right)$ is the feature map at position (*i*, *j*) for filter *k*; $W\left(x,y,k\right)$ is the weight of the filter; *b*(*k*) is the bias term; *m* and *n* are the dimensions of the filter.

Activation Function. Apply a non-linear activation function, such as ReLU, to introduce non- linearity:

$$F_{activated}\left(i,j,k\right)=\max\left(0,F\left(i,j,k\right)\right). \tag{12}$$

Pooling Operation. Downsample the feature maps to reduce dimensionality and computational load:

$$P\left(i,j,k\right)=\max\left(F_{activated}\left(i',j',k\right)\right), \quad \forall\left(i',j'\right)\in pooling\ window, \tag{13}$$

where $P\left(i,j,k\right)$ is the pooled output value at position (*i*, *j*) for the feature map channel *k*. The $F_{activated}\left(i',j',k\right)$ represents the ReLU-activated feature values inside the pooling window corresponding to location (*i*, *j*). The operator max selects the maximum value within the pooling window.

Step 3: Extract temporal features using recurrent layers

Sequence Formation. Flatten spatial features into a sequence of feature vectors:

$$S_t = Flatten\left(P_t\right), \tag{14}$$

where S_t is the feature vector at time *t*, and P_t is the pooled feature map at time *t*.

Recurrent Neural Network (RNN) operation. Use Long Short-Term Memory (LSTM) units or Gated Recurrent Units (GRU) to capture temporal dependencies. LSTM cell

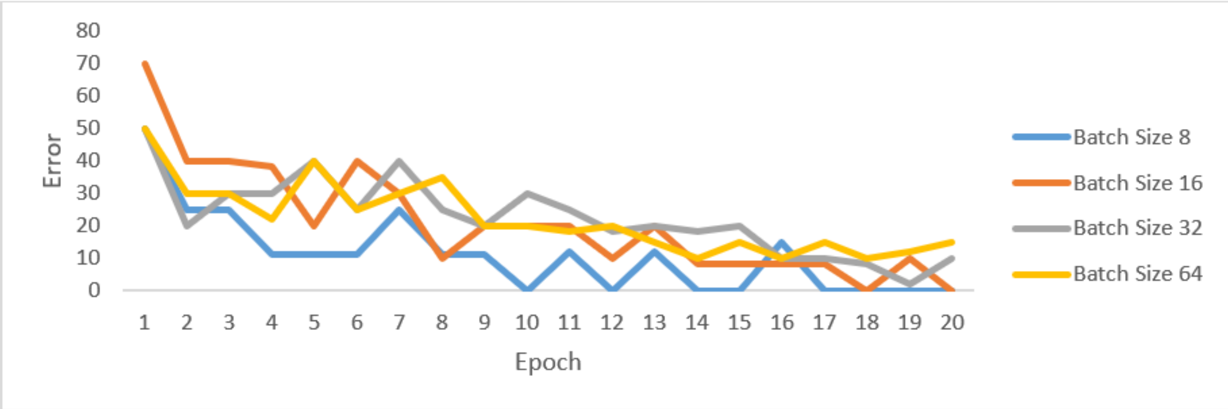

Fig. 9. Comparison of error vs maximum epoch during DRCNN validation.

equations:

$$f_t = \sigma\left(W_f\left[h_{t-1}, S_t\right] + b_f\right), \quad (15)$$

$$\tilde{C}_t = \tanh\left(W_C\left[h_{t-1}, S_t\right] + b_C\right), \quad (16)$$

$$C_t = f_t C_{t-1} + x_t \tilde{C}_t, \quad (17)$$

$$o_t = \sigma\left(W_o\left[h_{t-1}, S_t\right] + b_o\right), \quad (18)$$

$$h_t = o_t \tanh\left(C_t\right), \quad (19)$$

where f_t, x_t, o_t stand for the forget, input, and output gates, respectively; C_t is the cell state; h_t represents the hidden state; S_t is the input vector, W_f, b_f are the weight max and the bias term of the forget gate, respectively; σ is the sigmoid activation function, W_C, b_C are the weight matrix and the bias for a candidate cell state, respectively; $\tanh$ is the hyperbolic tangent activation function; W_o, b_o are the output gate values of the weight matrix and the bias, respectively; t–1 indicates the pervious state in relation to the current state; $\tilde{C}_t$ is the candidate new cell state.

Step 4: Classify

Fully connected layer. Map the extracted features to fault classes:

$$z = W_{fc} h_T + b_{fc}, \quad (20)$$

where h_T is the hidden state at the last time step; W_{fc} represents the weights of the fully connected layer; b_{fc} is the bias term.

Softmax Function. Compute the probabilities of fault categories:

$$p(c) = \frac{e^{z_c}}{\sum_y e^{z_y}}, \quad (21)$$

where $p(c)$ is the probability of class c; z_c is the output score for class c.

Step 5: Calculate loss function

Categorical Cross-Entropy Loss:

$$L = -\frac{1}{N}\sum_{x=1}^{N}\sum_{c=1}^{C} y_{x,c} \log\left(p_{x,c}\right), \quad (22)$$

where N is the number of samples; C is the number of classes; $y_{x,c}$ is the true label of sample i for class c; $p_{x,c}$ is the predicted probability of sample i for class c.

The proposed DRCNN algorithm is designed for automated fault identification in photovoltaic panels using thermal imaging. In the first stage, UAV-acquired thermal images are preprocessed through resizing, normalization, noise reduction, and augmentation to enhance data quality. Spatial features are then extracted using convolutional layers, where convolution, activation (ReLU), and pooling operations capture localized fault-related patterns while reducing dimensionality. These spatial features are flattened into sequential vectors and processed through recurrent layers, such as LSTM or GRU units, to model temporal dependencies and identify subtle variations in thermal signatures. The final hidden state is passed through a fully connected layer, and the Softmax function assigns probabilities to fault categories, enabling accurate classification of different defect types. Model learning is guided by categorical cross-entropy loss, ensuring optimized prediction accuracy across multiple fault classes. This integration of CNN-based spatial analysis with RNN-based temporal modeling ensures robust and precise detection of PV faults under diverse environmental conditions.

TABLE 4. Performance Measures

System	Accuracy (%)	Precision (%)	Recall (%)	F1-Score (%)
DRCNN	99.8	99.6	99.0	99.8
CNN-based approach	95.6	94.3	93.9	94.0
LSTM-based method	94.8	93.6	95.0	94.3
SVM with feature selection	92.5	91.9	90.1	91.4
RNN	96.9	96.0	96.4	96.2

TABLE 5. Performance Measures (Error)

System	MAE	MSE	RMSE
DRCNN	0.013	0.0016	0.040
CNN-Based Approach	0.026	0.0033	0.058
LSTM-Based Method	0.023	0.0029	0.054
SVM with Feature Selection	0.031	0.0046	0.068
RNN Model	0.019	0.0021	0.046

IV. RESULTS AND DISCUSSIONS

The GUI-powered system in the proposed studies for hotspot detection on electrical lines and fuses will look at two different kinds of faults: 1) excess temperatures in the fuse contact and 2) excessive temperatures in any one or two electrical segments.

320 hotspots are included in the 800 images that make up the training image set that is used. It is necessary to incorporate various panel kinds, forms, sizes, and alignments. In this study, the instruction procedure was carried out by identifying the Region of Interest (ROIs) within the selected frames of each subject. Two kinds of ROIs are examined: ROIs for a panel set and relative hot spots. The border-box and labeling must be defined before the ROIs may be created. The region of the image covered by the ROI is identified by the border-box. An illustration of the ROIs during the DRCNN training procedure is provided in Fig. 8.

Figure 9 illustrates the validation error across 20 epochs for the DRCNN algorithm, comparing the performance of four different batch sizes: 8, 16, 32, and 64. The general trend is that error decreases as the number of epochs increases, though all models exhibit significant volatility, particularly the Batch Size 8 model. The Batch Size 16 model demonstrates the lowest final error, while the Batch Size 32 model shows the least volatility after the initial epochs. The results are comparable based on the observation that the inaccuracy stabilizes for most models after approximately 15 epochs.

Figure 10(a) shows the original image. Figure 10(b) demonstrates the result of whatever process is described for 10(b) (e.g., edge detection, filtering, etc.). The current B&W image seems to be an edge detection output. Figure 10(c)definitively shows the rotated version of the image from 10(a) or the processed version from Fig. 10(b), depending on the workflow. Figures 10(d), 10(e), and 10(f) are unique representations of their specific processing step (panel detection, hot area detection, and final prediction), even if the differences are subtle (e.g., different bounding boxes, masks, or overlay colors). The image duplication invalidates the entire sequence.

The proposed DRCNN system achieves the highest performance across all metrics due to its integrated spatial and temporal feature extraction capabilities shown in Table 4. The RNN model performs well but slightly lags behind the proposed system, as it may not fully capture complex dependencies. Existing models, such as SVM, show the lowest performance indicating limitations in handling the large feature space and temporal dependencies. The proposed DRCNN system achieves the lowest errors (MAE, MSE, and RMSE), demonstrating superior prediction accuracy. The RNN model performs well but is slightly less effective than the proposed system. The SVM with feature selection has the highest errors, showing its limitations in capturing complex patterns in data.

The changes in the learning impairment and precision functions are displayed in Fig. 11(a). The degree of precision is very close to 1 and the loss is as low as 0.01. The matrix of confusion that was generated is shown in Fig. 11(b).

V. Conclusion

When employing IRT to detect faults in PV solar panels, the DRCNN demonstrates significant improvements in precision, recall, F1-score, and accuracy compared to existing techniques. The proposed model effectively captures the complex thermal characteristics of defective panels under various conditions by leveraging RCNN for temporal pattern recognition and CNN for spatial feature extraction. Superior performance metrics, such as reduced

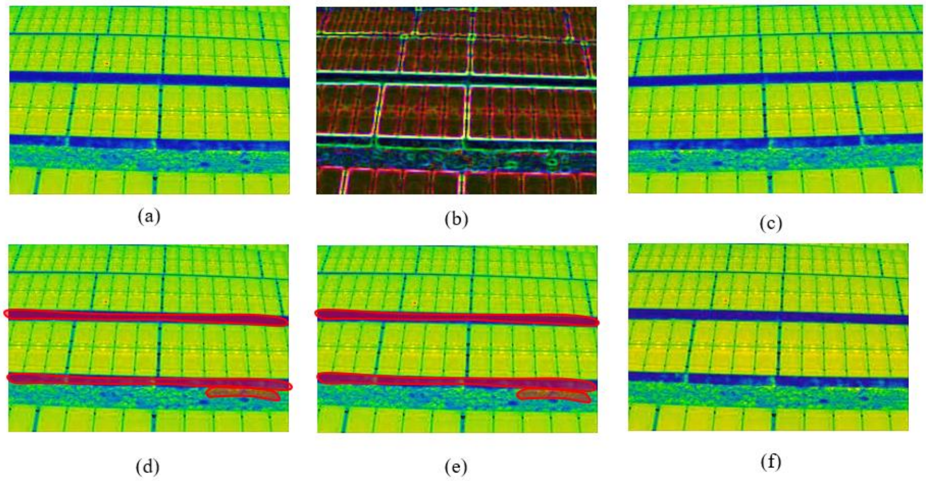

Fig. 10. IRT (a), Detection of contour (b); Image rotation (c), Panel detection (d); Detection of hot region (relative) (e); Location of relative hotter regions (f).

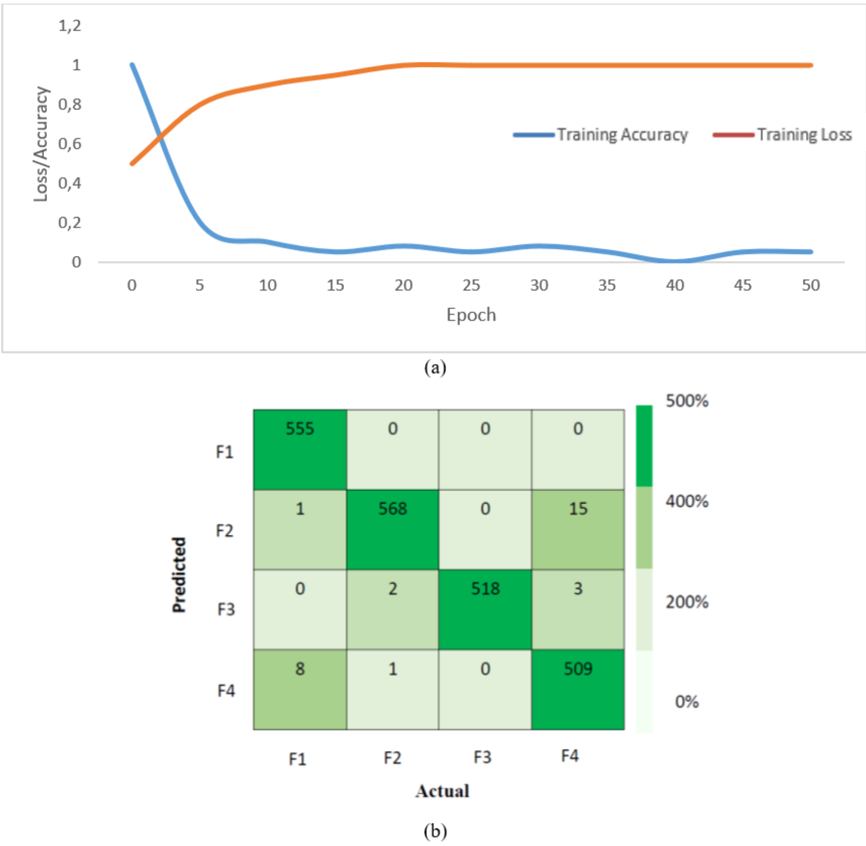

Fig. 11. Multiclass classification (fault diagnosis): training loss and accuracy functions (a); confusion matrix (b).

Mean Absolute Error (MAE), Mean Squared Error (MSE), and Root Mean Squared Error (RMSE), indicate that the integration of advanced preprocessing techniques with a robust architectural design minimizes error rates. This approach enhances defect detection, contributing to improved energy utilization and reduced operational costs. It offers a scalable solution for real-time solar system monitoring and maintenance. The results provide a solid foundation for future research in automated fault diagnostic systems and underscore the potential of deep learning frameworks in advancing green energy technology.

REFERENCES

[1] Ö.Baltacı, Z.Kıral, K.Dalkılınç, O.Karaman, "Thermal image and inverter data analysis for fault detection and diagnosis of PV systems,"Applied Sciences, vol. 14, no. 9, Art. no. 3671, 2024.

[2] S. Umar, M. S. Qureshi, M. U. Nawaz, "Thermal Imaging and AI in solar panel defect Identification," International Journal of Advanced Engineering Technologies and Innovations, vol. 1, no. 3, pp. 73–95, 2024.

[3] Z. Tang, X. Jian, "Thermal fault diagnosis of complex electrical equipment based on infrared image recognition," Scientific Reports, vol. 14, no. 1, Art. no. 5547, 2024.

[4] G. B.Balachandran, M.Devisridhivyadharshini, M. E.Ramachandran, R. Santhiya, "Comparative investigation of imaging techniques, pre-processing and visual fault diagnosis using artificial intelligence models for solar photovoltaic system–A comprehensive review," Measurement, vol. 232, Art. no. 114683, 2024.

[5] W. Zhang, G. Wang, G. Yao, C. Lu, Y. Liu, "Study on fault monitoring technology of photovoltaic panel based on thermal infrared and optical remote sensing," The International Archives of the Photogrammetry, Remote Sensing and Spatial Information Sciences, vol. 48, pp. 855–860, 2024.

[6] C. Yang, F. Sun, Y. Zou, Z. Lv, L. Xue, C. Jiang, H. Cui, "A survey of photovoltaic panel overlay and fault detection methods," Energies,vol. 17, no. 4, Art. no. 837, 2024.

[7] H. Yousif, Z. Al-Milaji, "Fault detection from PV images using hybrid deep learning model," Solar Energy, vol. 267, Art. no. 112207, 2024.

[8] Prakasam, K. R. Laxmikanth, P. Srinivasu, "Design and simulation of circular microstrip patch antenna with line feed wireless communication application," in 2020 4th International Conference on Intelligent Computing and Control Systems (ICICCS), Madurai, India, 2020, pp. 279–284.DOI: 10.1109/ICICCS48265.2020.9121162.

[9] S. Jaybhaye, V. Sirvi, S. Srivastava, V. Loya, V. Gujarathi, V. D. Jaybhaye, "Classification and early detection of solar panel faults with deep neural network using aerial and electroluminescence images," Journal of Failure Analysis and Prevention, vol. 24, pp. 1746–1758, 2024.

[10] X. Chao, L. Zhang, Y. Li, C. Huang, J. Li, "Photovoltaic fault detection based on infrared and visible image augmentation and fusion," Turkish Journal of Agriculture and Forestry, vol. 48, no. (3), pp. 430–442, 2024.

[11] U. Shafique, S. M. Alam, U. Rashid, W. Javed, H. Anwaar, M. S. Zeb, F. Nzanywayingoma, "Infrared thermography based insulator fault classification via unsupervised clustering and semi-supervised learning," IEEE Access, vol. 12, pp. 180781–180791,2024.

[12] X. Zhang, Y. Ge, Y. Wang, J. Wang, W. Wang, L. Lu, "Residual learning-based robotic image analysis model for low-voltage distributed photovoltaic fault identification and positioning," Frontiers in Neurorobotics, vol. 18, Art. no. 1396979, 2024.

[13] P. Garikapati, K. Balamurugan, T. P. Latchoumi, R. Malkapuram, "A cluster-profile comparative study on machining AlSi7/63% of SiC hybrid composite using agglomerative hierarchical clustering and K-means," Silicon, vol. 13, no. 4, pp. 961–972, 2021.

[14] P. Chandana, P. G. S. Ghantasala, J. Rethna Virgil Jeny, K. Sekaran, N. Deepika, Y. Nam, S. Kadry, "An effective identification of crop diseases using faster region-based convolutional neural network and expert systems,"International Journal of Electrical and Computer Engineering, vol.10, no. 6, pp. 6531–6540, 2020. DOI: 10.11591/IJECE.V10I6.PP6531-6540.

[15] M.Rama Krishna, K. R.Tej Kumar, G. Durga Sukumar, "Antireflection nanocomposite coating on PV panel to improve power at maximum power point,"Energy Sources, Part A: Recovery, Utilization and Environmental Effects, vol. 40, no. 21, pp. 2407–2414, 2018. DOI: 10.1080/15567036.2018.1496198.

[16] G. Tanda, M. Migliazzi, "Infrared thermography monitoring of solar photovoltaic systems: A comparison between UAV and aircraft remote sensing platforms," Thermal Science and Engineering Progress,vol. 48, Art. no. 102379, 2024.

[17] E. A.Ramadan, N. M.Moawad, B. A.Abouzalm, A. A.Sakr, W. F.Abouzaid, G. M. El-Banby, "An innovative transformer neural network for fault detection and classification for photovoltaic modules," Energy Conversion and Management,vol. 314, Art. no. 118718, 2024.

[18] C.Kim, S. Perilli, S. Sfarra, E. J. Kim, "Detection of the surface coating of photovoltaic panels using drone-acquired thermal image sequences," Journal of Thermal Analysis and Calorimetry,vol. 149, no. 8, pp. 3443–3452, 2024.

[19] E. K.Ukiwe, S. A. Adeshina, T.Jacob, B. B. Adetokun, "Deep learning model for detection of hotspots using infrared thermographic images of electrical installations," Journal of Electrical Systems and Information Technology,vol. 11, no. (1),Art. no. 24, 2024.

[20] R. Duan, Z. Ma, "A method for detecting photovoltaic panel faults using a drone equipped with a multispectral camera," ISPRS Annals of the Photogrammetry, Remote Sensing and Spatial Information Sciences, vol. 10, pp. 59–65, 2024.

[21] K. Awedat, G. Comert, M. Ayad, A. Mrebit, "Advanced fault detection in photovoltaic panels using enhanced U-Net architectures," Machine Learning with Applications, vol. 20, Art. no. 100636, 2025.

[22] U. R.Qureshi, A.Rashid, N.Altini, V.Bevilacqua, M. La Scala, "Radiometric infrared thermography of solar photovoltaic systems: An explainable predictive maintenance approach for remote aerial diagnostic monitoring," Smart Cities,vol. 7, no. 3, pp. 1261–1288, 2024.

[23] N. V.Sridharan, V.Sugumaran, "Visual fault detection in photovoltaic modules using decision tree algorithms with deep learning features," Energy Sources, Part A: Recovery, Utilization, and Environmental Effects,vol. 47, no. 2, Art. no. 2020379, 2025.

[24] D. Matusz-Kalász, I. Bodnár, M. Jobbágy, "An overview of CNN-based image analysis in solar cells, photovoltaic modules, and power plants," Applied Sciences,vol. 15, no. 10, Art. no. 5511, 2025.

[25] Cardoso, D. Jurado-Rodríguez, A. López, M. I. Ramos, J. M. Jurado, "Automated detection and tracking of photovoltaic modules from 3D remote sensing data," Applied Energy,vol. 367,Art. no. 123242, 2024.

[26] P. Sandeep, P. A. Harsha Vardhini, V. Prakasam, "SRAM utilization and power consumption analysis for low power applications," in 2020 International Conference on Recent Trends on Electronics, Information, Communication & Technology (RTEICT), Bangalore, India, 2020, pp. 227–231. DOI: 10.1109/RTEICT49044.2020.9315558.

[27] D. Suárez-Gómez, J. O. B. Quintero, "Integrated thermal monitoring system for solar PV panels: An approach based on TinyML and Edge Computing," in Workshops at the 7th International Conference on Applied Informatics 2024 (ICAIW 2024), Oct. 24–26, 2024, Viña del Mar, Chile, pp. 14–27.

[28] W. Yang, W. Wang, X. Wang, J. Gu, Z. Wang, "Fault diagnosis method of a cascaded H-bridge inverter based on a multisource adaptive fusion CNN-transformer," IET Power Electronics,2024, pp. 1–21.

[29] S. K.NB, S. Madichetty, S. S. Koduru, M. V. S. P. Chowdary, S. Mishra, "Finding a faulty/partially shaded panel in an solar photovoltaic array: A novel and instantaneous additional hardware module-based echnique," IEEE Industry Applications Magazine, vol. 31, no. 1, pp. 73–85, 2025.

Flat-Plate Solar Collectors: Development Methods and Challenges

A.A. Saad[1], M.H. Khaleel[2,*], A.M. Abdulwahaab[2], S.E. Kaska[1]

[1] Northern Technical University, Oil and Gas Engineering Techniques College, Iraq
[2] Northern Technical University, Kirkuk Technical Institute, Iraq

***Abstract* — One of the key technologies in the field of solar energy is the flat plate solar collector, recognized for its extensive applications. It is effective in meeting residential needs for heating and water, as well as the needs of various industrial processes. There are innovative solutions, such as the use of coatings and nanofluids, to enhance the efficiency of flat plate solar collectors. However, as advanced solutions arise, manufacturing and operational expenses, space availability, and material degradation continue to hinder their adoption. This study focuses on future research to enhance the thermal performance of flat plate solar collectors while addressing the challenges facing the global shift towards clean and sustainable energies**

***Index Terms* — Flat-plate solar collectors, development methods, challenges, thermal energy systems.**

I. INTRODUCTION

One of the prominent techniques in solar energy that shines the spotlight on the transition from conventional energy systems to sustainable and clean energy systems is solar collectors, specifically flat plate solar collectors. Their prominence is due to their diverse applications in water heating systems in home appliances, heating systems in conditioned places, and their industrial use, where solar energy is converted to thermal energy. Flat plate solar collectors are characterized by their simple design, durable structure, handy configuration, and affordable cost in comparison to other solar energy applications. Still, challenges and obstacles are present, such as overall system efficiency, initial and operational expenses, and maintenance. Environmental challenges, public preferences, and the availability of space on buildings should also be taken into account when utilizing flat plate solar collectors. This study puts a significant emphasis on developing innovative systems that align with the concept of sustainability [1].The necessity of employing sustainable energy, especially solar energy, has arisen due to the concerns over depleting fossil fuels. This sparked a worldwide shift towards the emerging renewable energy because of its abundancy and compatibility with climate change initiatives despite the rise of other competing renewable energy technologies [2]. Flat plate solar collectors (FPCs) are considered the major techniques for saving and supplying thermal energy in a wide range of home applications for hot water consumption and space heating systems and industrial applications with lower thermal energy requirements [3].FPCs are a widely preferred solution because they perform well in changing climates and offer low operational and maintenance costs. Moreover, they are suitable for broader use and on an international scale, which sets them apart from other developed systems such as concentrated photovoltaics. Yet, the presence of challenges and barriers underscores the need to improve their performance by using innovative materials and advanced production systems [4]. The primary challenges facing the conversion and storage of thermal energy from solar energy in FPCs are the heat loss from the solar collectors, which can be caused by components themselves, or environmental heat loss that occurs at night. Other problems are related to material corrosion in piping and performance degradation in harsh environments, alongside environmental cost issues. To address these issues and come up with sustainable solutions, a novel approach for designing solar collectors

* Corresponding author.
E-mail: mahmood.aboretag.husain@gmail.com

DOI:10.25729/esr.2025.03.0009

Received April 22, 2025. Revised August 20, 2025. Accepted September 2, 2025. Available online November 28, 2025.

should be provided [5].There can be new ideas in designing the external shape of solar collectors, such as the rhombus shape, or enhancing the efficiency that may reach 59% in March [6], or considering another design and operation analysis of an Integrated Collector Storage (ICS) solar water heater. The heater consists of an asymmetric compound parabolic concentrating reflector trough and two concentric cylinders. The environmental footprint is analyzed through Life Cycle Assessment (LCA) to evaluate environmentally friendly and cost-effective devices with improved thermal performance and offer new perspectives on ICS solar water heater design. Methods used to evaluate thermal energy, environmental impacts, and economic results of the ICS solar water heater include a multi-criteria optimization algorithm and Life Cycle Assessment (LCA), utilizing different configuration parameters [7].The dish-Stirling configuration is commonly used in small-scale concentrated solar power plants, but its high maintenance costs and reliability issues limit its market appeal. Micro gas turbines, which are cheap, reliable, and widely available, are a promising solution. A plant simulator is crucial for predicting performance and optimizing plant operations under different conditions. This method is employed to develop a simulation tool for solar dish-micro gas turbine applications and model the solar concentrator, receiver/absorber, micro gas turbine, high-speed generator, and power electronic systems. The simulator uses quadratic programming technique and performs steady-state simulations to predict performance and ensure safe and reliable power plant operation. The results show a nominal peak efficiency of about 10% for a net generated power of about 6 kW [8]. Concentrating the solar radiation falling on the system, focusing on a specific point to collect solar radiation is considered one of the methods that concern enhancing the performance, where the part that receives the rays is fixed at a distance of 3 meters and the performance is noticeably activated for an amount of solar radiation falling with a value of 700 W/m^2 and above [9]. Another avenue to develop the solar collector system is to add inter-heat exchangers that use different fluids, in which the performance efficiency of the solar collector may reach 64% at a 1 L/min flow rate over a working period of 15 hours [10].To handle the issues facing these systems, a profound awareness and understanding is required, which can be achieved through a thorough study of the factors affecting the performance of FPCs [11]. This research analyzes the techniques that can enhance the thermal performance of solar collectors, providing valuable insights into potential solutions to overcome the obstacles [12]. This work focuses on solar collectors being an essential component of the transition to renewable energy by delivering an engineering assessment of challenges, drawbacks, and advantages.

A. Scope and Review Contributions

This paper provides an overall review of recent technologies applied in flat plate solar collectors, focusing on smart materials, environmentally friendly designs, and AI technologies. Although numerous previous studies overview these critical points, this review presents a comprehensive approach that links the developments in materials, such as nanofluids and coatings. It also addresses design improvements, such as optimal angles and improved flow pathways, alongside their integration with hybrid PV-T collectors.

The areas highlighted in this paper are as follows:

- Design adaptability, especially in regions with low solar irradiation.
- Important aspects of employing AI technologies in improving the data analysis and operations of flat plate solar collectors.
- Directions for the future research provided with overall review of nanomaterials and affordable sustainable designs.
- Critical analysis of PV-T bifacial systems, clarifying their advantages compared to conventional systems.

Thus, this review provides an important roadmap in enhancing the efficiency of thermal solar systems in the context of the transition to sustainable energies.

II. Flat-Plate Solar Collectors: Development Strategies

A. Improvement in Components and Materials

To improve the solar radiation absorption and reduce heat losses and material resistance, it is crucial to consider the components and material structure for constructing flat-plate solar collectors.

Choosing the right material for absorber plate enhances the overall efficiency. The high heat conductivity of aluminum and copper make them common in manufacturing absorber plates. This is because higher conductivity means faster heat transfer from the absorber plate to the working fluid, thus increasing the efficiency. Modern developments mostly concentrate on selective surfaces and nanocoating to reduce heat loss and improve absorption. Methods like black chrome, titanium nitride oxide, and new multilayer coatings lower emissivity and increase absorptivity. Selective coatings are shown to increase thermal efficiency by up to 10%. Clear covering that protects the absorber plate while reducing heat loss depends critically on transparency of the glass and polymer used [13]. Transparent covers in flat-plate solar collectors are of great importance in minimizing heat losses. Low-iron glass and anti-reflective coatings to improve transmittance are among recent advances. Furthermore, double or triple glazing reduces convective heat loss.

Materials for insulation, such as polyurethane foam, fiberglass, and vacuum insulation panels, are among the upgraded insulating materials used to lower heat losses from the back and sides of collectors. These materials guarantee that the system keeps more heat inside, thus improving general efficiency.

Development of improved heat transfer fluids, including nanofluids with increased thermal conductivity and stability, is the main emphasis of research here. The findings reveal that adding nanoparticles, such as $TiO_2$and Al_2O_3, to base fluids greatly increases heat transfer capability [14, 15]. The hybrid solar systems may include a porous cushion and a spiral tube designed for use with a $CuFe_2O_4$/water nanofluid motor. Experimental and numerical modeling for the system demonstrates a 22% improvement in thermal transfer (Nusselt) and nearly a 20% increase in heat flux compared to water [16].

B. Design Improvement

The efficiency of flat-plate collectors is largely influenced by their geometric arrangement. Recent research has identified ideal proportions and layouts for reducing heat losses and optimizing solar absorption through the use of computational fluid dynamics (CFD) simulations. Varied tilt angles coupled with adjusted seasonal sun angles show better energy collection in many different climatic settings. The FPC performance is evaluated using CFD analysis based on the model proposed for predicting the energy yield of south and east-west facing bifacial PV system compared with south facing monofacial system [17]. The study shows that the accuracy in the model is highest when predicting the energy yield of south facing inclined bifacial PV system. Such models can guide the deployment of bifacial PV systems.

Enhanced flow patterns like meandering and bifurcation channels are replacing conventional flow designs like serpentine and parallel flow to improve heat transfer rates and guarantee homogeneous fluid temperature distribution. Incorporating turbulators or vortex generators into flow channels leads to an increase in thermal efficiency, as convective heat transfer rises without an appreciable increase in pressure drop.

Combining flat-plate collectors with phase-change material (PCM) thermal energy storage provides constant output independent of changing solar irradiation. Together, these help reduce reliance on supplemental heating systems [18]. For example, a numerical model using ANSYS was employed to simulate a flat collector incorporating a nano-coated octadecane PCM behind the absorber plate. Results indicated better performance at a 5% nano concentration, which improved morning heat output but did not fully dissolve at night, demonstrating a mixed effect on performance [19].

Embedded storage units in modular designs allow residential and commercial applications to have better scalability and flexibility. Enhancement of optical designs and reflections by adding exterior or internal reflectors such as Compound Parabolic Concentrators (CPCs), markedly improves solar energy collection, particularly in low-sunlight hours. Improvements in anti-reflective and self-cleaning coatings help to further increase light transmission through transparent coverings, hence lowering maintenance needs.

Hybrid PVT systems, combining flat-plate collectors with photovoltaic panels simultaneously generate thermal and electrical energy [20]. This two-fold utilization maximizes land use and increases general energy output. Real-time performance monitoring and adaptive operation offered by hybrid systems coupled with IoT-enabled sensors and smart controllers facilitate maximizing the efficiency.

Applications in both urban and rural locations will find modular collector units fit as they enable simple assembly, transportation, and scalability. Flexible mounting methods combined with plug-and-play designs help to reduce system downtime by reducing the time of installation and simplifying maintenance [21, 22].

C. Improved Hybrid PVT Compounds — Bifacial PVT Compounds

Hybrid PVT systems are solar PV collectors that generate simultaneously both heat energy and electricity. Bifacial PVT system, being one of them, is a dual-sided PVT system that produces electricity from both sides of the panel. One type of these systems is equipped with a mirror reflector where air can be used as a cooling fluid. For example, there is a design of this system with a V-shaped groove that has a mirror serving as a reflector, in which air is used to cool the fluid and to enhance the heat transfer efficiency.

To study and evaluate the performance of these systems, mathematical modeling is considered as one of the critical methods. A mathematical model was applied using the first and second laws of thermodynamics to predict the energy output [23]. Data on energy yield from bifacial PV module were examined and compared to those for monofacial PV systems under the climate conditions of west Africa [17].The study utilizes an analytical mathematical model, which relies on energy balance equations. This model uses real data from Ghana in Africa in the prediction of energy yield. The model reveals that the bifacial PV system oriented to the south outperforms the monofacial PV systems. Experimental studies report that the photovoltaic thermal collector achieves an operating efficiency of 57% at a solar radiation of 863 W/m² at a mass flow rate ranging from 0.02 kg/s to 0.08 kg/s[24]. By comparison, the double-sided photovoltaic thermal collector operates at an efficiency of 70% versus 50% for the single-sided type[25].

Another study on a water based photovoltaic thermal collector is based on experimental and theoretical analysis [26].It involves physical testing and MATLAB simulations to investigate hybrid photovoltaic thermal collector that utilizes water as a working fluid and introduces a new absorber pipe design. The key findings of the work indicate a total efficiency obtained of approximately 67% [27]. The studies aim to employ the hybrid PVT collector type of solar collectors, in particular a solar-thermal collector, to cool photovoltaic cells with fluids that transfer thermal energy effectively. In some PVT designs, nanofluids are used to boost photovoltaic cell efficiency and simultaneously produce thermal energy through a hybrid method.

Integrating photovoltaic and thermal energy technologies results in a greater increase in overall efficiency when compared to two systems operating separately. This work is classified as an advanced pathway, addressing the significantly growing importance of solar energy and its role in clean renewable energies. Additionally, this field of research highlights a large group of factors, such as cell temperature and thermal energy transfer mechanisms, to enhance the efficiency and thermal performance of these systems [28].

III. FLAT-PLATE SOLAR COLLECTOR CHALLENGES

A. *Limitations in Performance and Efficiency*

Loss of heat through conduction, convection, and radiation lowers the general efficiency. A smaller temperature difference between the absorber plate and the inlet fluid caused by the increasing temperature as the fluid enters is a major cause of the dropping thermal efficiency [29]. As the inlet fluid temperature rises, the difference in temperature between the absorber plate and fluid decreases. This leads to the reduction in heat transfer to the fluid. As a result, the absorber plate gets hotter and therefore loses more heat to the surrounding via conduction, convection, and radiation. Developing materials with low thermal emissivity and designing sophisticated insulating methods remain difficult. However, expensive, multi-layer transparent coverings with vacuum sealing demonstrate promise. Performance is somewhat reliant on the state of the weather, especially in areas with little sun irradiation or high ambient temperatures. Adaptive solutions using angle-adjustable collectors can address this restriction [30, 31].

B. *Material Degradation and Durability*

Harsh environments, such as extreme temperatures and humidity can affect material durability and cause degradation. Metals like copper and aluminum are easily corroded, particularly in humid and saline conditions. Important solutions to this problem include protective coatings, anti-corrosion treatments, and non-metallic substitutes, such as polymer composites. The durability of flat-plate solar collectors with Ni-Co coating and without coatings is examined in [32]. The results reveal that the coated Ni-Co collector is about 50% more efficient than the uncoated one, with this enhanced efficiency maintained throughout the day and evening regardless of a decline in solar irradiance in the evening. This demonstrates the durability of this coating for flat plate solar collectors.

C. *Environmental and Financial Difficulties*

Carbon footprint, particularly for metals, coatings, and manufacturing techniques, may have a major environmental effect. Carbon impact of FPCs systems can be minimized by means of lifecycle assessment (LCA).Long payback times and high starting expenses might make broad adoption difficult in underdeveloped areas. To make FPCs more accessible, governments and companies are looking at subsidies and incentives. The End-of-Life management and recycling of polymers and coatings remain a significant challenge for sustainable FPCs deployment. Innovative recycling techniques and eco-design principles gain traction in addressing this issue [33, 34].

D. Fluid Usage and Climate

There are significant challenges related to heat transfer fluids in FPCs, particularly in cold climates and hard water areas. The main of them are outlined below:

One challenge facing specialists and researchers in this field is the type of fluid used in flat-plate solar collectors and the climate conditions to which these fluids are exposed, particularly in areas with hard water. A significant concern is the freezing of these fluids in cold weather. When these fluids freeze, they expand, which can damage the pipes that transport them, potentially leading to a system failure. To mitigate this issue, some studies suggest using antifreeze agents, such as propylene and ethylene glycol, which lower the freezing point of water and enable the system to function under moderately cold conditions without freezing. However, these antifreeze fluids increase maintenance costs, as they lose their effectiveness over time and need replacing.

Sedimentation and contamination are additional challenges in areas with hard water. The presence of minerals, like magnesium and calcium, can lead to scaling inside the fluid transport pipes, hindering fluid movement and reducing the efficiency of thermal energy transfer. The accumulation of pollutants, such as biofilms, can further exacerbate the contamination issue. Some studies propose implementing cleaning programs, treating the fluids, or introducing measures to prevent sedimentation.

As these fluids are used over time, another issue arises: they may lose some of their beneficial properties due to mixing with antifreezes like glycol or fail to prevent sedimentation due to exposure to high temperatures or UV radiation. Additionally, these fluids can produce acidic byproducts that may erode certain metals in the system's structure. The viscosity of the fluids, particularly those containing glycol, can also increase, especially in frigid climates. This problem can be addressed by regularly monitoring the acidity of the fluids, scheduling timely replacements, and carefully selecting the appropriate fluid type, especially for systems operating in low-temperature environments [35–38].

IV. Future Research Approaches

Although there are numerous studies on PVT collectors, the future trend should focus closely on cost-effective advanced materials integrated with smart technologies that improve the overall performance efficiency.

A. Novel Materials

The development of lower-emissivity and higher-absorptivity nanostructured coatings, for example, graphene, carbon-based nanomaterials, and biopolymers, show a promising potential for improving thermal qualities. Investigation of transparent coverings based on biopolymers will aid in increasing the sustainability and lessening the reliance on fossil fuels. Research of self-cleaning coatings is crucial to lower maintenance needs and enhance performance in dusty surroundings [39, 40].

B. Compatibility with Novel Technologies

1) Hybrid Solar Systems

The studies explore combining FPCs with hybrid PVT collector systems for simultaneous thermal and electric energy production. Applications demanding both heat and electricity find hybrid systems especially appealing. Integration with Internet of Things (IoT) is one of the strategies for real-time collector performance enhancement. By means of temperature, fluid flow, and weather condition data offered by IoT-enabled devices, proactive maintenance, and efficiency enhancements are made possible [41, 42].

2) Nanofluids

The studies demonstrate that flat-plate solar collectors are highly effective with a variety of developed fluids, particularly nanofluids. Nanofluids consist of tiny particles that disperse evenly within the fluid, enhancing heat transfer efficiency. These fluids possess higher thermal conductivity and heat capacity compared to other fluids commonly used in solar collectors. However, it is crucial to handle them carefully to prevent sedimentation and corrosion problems over time [43, 44].

3) AI Integration in Solar Collectors

The integration of AI in the development of solar collectors enhances both the operating and control systems. AI algorithms can accurately predict optimal flow rates based on operating conditions, maximizing thermal efficiency. Additionally, these algorithms can forecast maintenance needs and potential malfunctions, allowing for proactive measures to prevent issues before they arise [45, 46].A study confirms the effectiveness of applying artificial intelligence (AI) as a promising method through studying the electrical and thermal efficiency of PVT collectors operating with nanofluids [47]. The accuracy of the AI generated models in predicting thermal and electrical efficiency is assessed by introducing a value of correlation coefficient (R2). Three models were generated namely, extreme gradient boosting (XGB), extra tree

TABLE 1. Comparative Efficiency

Collector Type	Average Thermal Efficiency (%)	Operation Conditions	Notes
Flat Plate Collectors (FPCs)	45–70	Standard outdoor testing	Low cost, widely available
Evacuated Tube Collector (ETC)	60–75	Cold climates	Better for diffuse radiation
PVT Hybrid Collector	50–65 (thermal) 10–20 (electrical)	Under sunlight + cooling	Combines heat and power
CSP with PCM	70–85	Concentrated solar input	High cost, stable storage

regression (ETR), and k-nearest Neighbor (KNN). The XGB model accuracy reached 0.99997 and 0.99995 for electrical and thermal efficiency, respectively. The ETR model accuracy stood at 0.99999 and 0.99999 for electrical and thermal efficiency, respectively. The KNN model accuracy was 0.92682 and 0.94726 for electrical and thermal efficiency, respectively. These results indicate that integrating AI models into renewable energy technologies is a promising way for parameter prediction. Another study demonstrates the high accuracy of AI models predicting the electrical efficiency of solar PVT systems [48]. The researchers generated a model that used over 350 data samples from literature on PVT systems using water as a working fluid. The results show that the models can be applied to improve the efficiency prediction of solar PVT collectors.

4) Coatings and Advanced Materials

The development of materials and coatings with superior thermal properties increases the heat absorption from radiation on solar collectors. This improvement enhances the efficiency of solar collectors, particularly in colder regions where solar radiation is weaker. Importantly, applying these coatings to the absorbing panels of solar collectors does not involve complex techniques. In contrast, effective solutions can be achieved through simple and straightforward methods [49, 50].

Consideration is also given to the cost reduction strategies proposed in the studies on reasonably priced substitutes for coatings and absorber materials. Investigating composite materials with thermal performance comparable to metals, for instance, manufacturing process optimization, enables the improvement in price and scalability. Additive manufacturing (3D printing) is explored as a possible alternative for manufacturing intricate components with little waste [53].

C. Climate– Adapted Designs

The studies focus on the creation of regionally tailored designs to handle different climatic conditions, including desert regions or those with excessive humidity. These designs include improved cooling systems and anti-condensation strategies. Ideas on modular construction are proposed, providing simple transit and installation at far-off locations [51, 52].

D. Policy and Regulatory

Support is needed in creating regulations that foster the adoption of FPCs through subsidies, tax incentives, and mandatory renewable energy goals. Development of criteria for certification and performance tests is key to guaranteeing dependability and quality [54].

V. COMPARISON OF CATEGORIES AND OPERATORS

A comprehensive scientific comparison of some types of solar collectors included in previous studies can be made in terms of thermal performance, operating factors, and variables. Table 1 compares various types of solar collectors in terms of thermal efficiency, operational variables, and technical characteristics. As seen in the Table, the flat-plate collectors (FPCs) have an efficiency ranging from 45% to 70% and is a low-cost and widely used option. The evacuated tube collector (ETC) achieves higher efficiency in cold climates due to its ability to absorb diffuse radiation. The hybrid PVT collector combines thermal (50–65%) and electrical (10–20%) efficiencies, enhancing the overall system benefit. Finally, the concentrated solar power (CSP) collector supported by phase-change storage materials (PCM) stands out with its high efficiency of up to 85%. High radiation concentration and high operating costs are necessary, but advanced storage technologies allow for high thermal stability.

VI. INCONSISTENCIES AND UNRESOLVED DISPUTES IN THE LITERATURE

The following key points summarize some of the conflicting issues related to the studies:

- Contradiction remains regarding whether nanofluids have a positive effect on improving the thermal efficiency of solar collectors or whether the effect is negative due to obstruction.
- Scientific opinion differs regarding the performance of photovoltaic/thermal cells when operating under partial shade conditions.
- There is no clear consensus in researchers' conclusions regarding the best type of material to use in PCM applications in specific climate zones.

VII. FUTURE TECHNOLOGICAL DEVELOPMENT PATH IN THE ENERGY SECTOR

The evolutionary diagram (Fig. 1) compellingly shows the significant strides made in solar thermal energy technology over the years in four major areas: enhancing coating technologies, which progressed from standard black paint to selective coatings and finally to innovative nanocoatings; evolving systems from single collectors to hybrid photovoltaic/thermal (PVT) systems, and subsequently to intelligent systems utilizing artificial intelligence; advancing storage technologies from basic thermal storage to phase-change materials, culminating in efficient chemical storage; and revolutionizing control systems from manual operations to automated tracking, ultimately integrating IoT and machine learning systems.

VIII. PRINCIPAL CONSTRAINTS IN EXISTING STUDIES

A thorough review of the studies reveals the following limitations and weaknesses:

- The data available from the studies are limited to short-term observations and are considered as weak regarding nanoscale thermal absorption materials.
- The scientific analysis of the scalability of solar collectors, especially hybrid ones, is quite inadequate with multi-layer collectors facing even greater deficiency in research.
- Most studies that focus on practical applications do not fully model performance, operation, and maintenance costs.

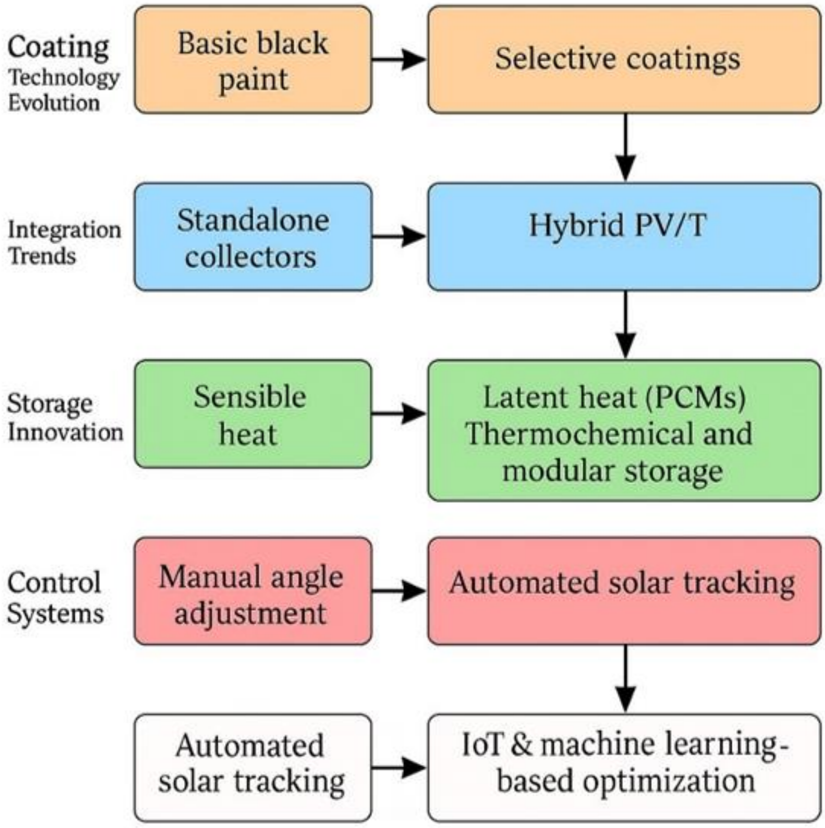

Fig. 1. Conceptual map of technological development.

- The evaluation of the thermal performance of solar collectors in terms of weather factors and geographical diversity is insufficient and requires enhancement.

IX. Future Pathways of Addressing Key Challenges

Based on a review of previous research addressed in this study, the following innovations are expected to address key issues in solar photovoltaic and thermal (PVT) systems:

- Adopting nanoscale coatings to reduce the degradation of materials exposed to high thermal energy, especially ultraviolet radiation.
- Using phase-change materials (PCMs) and combining them with solar collectors to better control and improve thermal energy and performance.
- Leveraging artificial intelligence, smart tracking systems, and intelligent operation to increase the efficiency of solar collectors.
- Developing hybrid systems, such as solar thermal systems integrated with photovoltaics, as well as concentrated solar power systems integrated with energy storage systems, to provide more realistic and scalable options and solutions.

X. Conclusion

Flat-plate solar collectors are still an essential component of the worldwide transition to renewable energy. Their simplicity, cost-efficiency, and adaptability make them suitable for diverse applications spanning industrial thermal energy systems and home water heating. Improvements in materials, design optimization, and integration with contemporary technology over years have greatly improved their performance and expanded their use.

To fully utilize these potential benefits, however, it is essential to tackle persistent challenges like heat losses, material deterioration, and financial constraints. Promising avenues to overcome them include innovations in advanced materials, hybrid system integration, and climate-specific designs. Furthermore, adopting smart technology and using sustainable manufacturing techniques will be crucial for increasing the lifetime and efficiency of flat-plate solar collectors.

Future studies should concentrate on designing affordable and sustainable methods to raise the acceptance of FPCs across many uses and areas. Scaling up these technologies and reaching worldwide renewable energy objectives would depend much on cooperation among academics, legislators, and businesses. Flat-plate solar collectors can greatly contribute to building a sustainable and energy-efficient future by addressing current problems while taking advantage of the possibilities offered by contemporary advancements.

References

[1] J. A. Duffie, W. A. Beckman, Solar engineering of thermal processes. New York, NY, USA: Wiley, 1980. DOI: 10.1002/9781118671603.

[2] M. R. Rahi, S. Ostadi, A. Rahmani, M. Dibaj, M. Akrami, “Studying the improvement of solar collector mechanism with phase-change materials,” Energies, vol. 17, no. 6, 2024.DOI: 10.3390/en17061432.

[3] S. A. Kalogirou, “Solar thermal collectors and applications,” Prog. energy Combust. Sci., vol. 30, no. 3, pp. 231–295, 2004.DOI: 10.1016/j.pecs.2004.02.001.

[4] Y. Tian, C.-Y. Zhao, “A review of solar collectors and thermal energy storage in solar thermal applications,” Appl. Energy, vol. 104, pp. 538–553, 2013.

[5] W. Gu, “Research on strategy optimization of sustainable development towards green consumption of eco-friendly materials,” J. King Saud Univ.-Sci., vol. 36, no. 6, Art. no. 103190, 2024.DOI: 10.1016/j.jksus.2024.103190.

[6] A. S. Al-jerjery, O. K. Ahmed, “Experimental investigation of thermal performance for novel integrated collector storage,” NTU J. Renew. Energy, vol. 7, no. 1, pp. 22–33, 2024.DOI: https://doi.org/10.56286/ntujre.v4i1.456.

[7] N. Arnaoutakis et al., “Design, energy, environmental and cost analysis of an integrated collector storage solar water heater based on multi-criteria methodology,” Energies, vol. 15, no. 5, Art. no.1673, 2022.DOI: 10.3390/en15051673.

[8] S. Mazzoni, G. Cerri, L. Chennaoui, “A simulation tool for concentrated solar power based on micro gas turbine engines,” Energy Convers. Manag., vol. 174, pp. 844–854, 2018.DOI: 10.1016/j.enconman.2018.08.059.

[9] M. Aidi Sharif, K. Sabah Khalaf, M. Anwar Omer, “A simulation model of a system-based concentrated solar power system (CSP) by using COMSOL software,” NTU J. Renew. Energy, vol. 4, no. 1, pp. 26–35, 2023.DOI: 10.56286/ntujre.v4i1.410.

[10] G. A. Baker, O. K. Ahmed, A. H. Ahmed, “An experimental study to improve the performance of a solar still using solar collectors and heat exchanger,” NTU J. Renew. Energy, vol. 4, no. 1, pp. 47–56, 2023.DOI:10.56286/ntujre.v4i1.417.

[11] V. V Tyagi, S. C. Kaushik, S. K. Tyagi, “Advancement in solar photovoltaic/thermal (PVT) hybrid collector technology,” Renew. Sustain. Energy Rev., vol. 16, no. 3, pp. 1383–1398, 2012.DOI: 10.1016/j.rser.2011.12.013.

[12] A. Ibrahim, M. Othman, M. H. Ruslan, M. Sohif, K. Sopian, “Recent advances in flat plate photovoltaic/thermal (PVT) solar collectors,” Renew. Sustain. Energy Rev., vol. 15, pp. 352–365, 2011.DOI: 10.1016/j.rser.2010.09.024.

[13] L. Fernandes, P. B. Tavares, "A review on solar drying devices: heat transfer, air movement and type of chambers," Solar, vol. 4, no. 1, pp. 15–42, 2024.DOI: 10.3390/solar4010002.

[14] W. Carrión-Chamba, W. Murillo-Torres, A. Montero-Izquierdo, "A review of the state of the art of solar thermal collectors applied in the industry," Ingenius, pp. 59–73, 2022.DOI: 10.17163/ings.n27.2022.06.

[15] R. Kumar, M. A. Rosen, "A critical review of photovoltaic--thermal solar collectors for air heating," Appl. Energy, vol. 88, no. 11, pp. 3603–3614, 2011. DOI: 10.1016/j.apenergy.2011.04.044.

[16] N. Q. Shary, H. A. A. Wahhab, A. Mola, Sahira, H. Ibrahim, "Performance analysis of solar porous media collector integrated with thermal energy storage charged by CuFe2O4/water nanofluids coil tubes," Energy Eng., vol. 122, no. 6, pp. 2239–2255, 2025.DOI: 10.32604/ee.2025.061590.

[17] R. O. Yakubu, M. T. Ankoh, L. D. Mensah, D. A. Quansah, M. S. Adaramola, "Predicting the potential energy yield of bifacial solar PV systems in low-latitude region," Energies, vol. 15, no. 22. 2022. DOI: 10.3390/en15228510.

[18] K. Kumar, "Performance analysis of flat plate solar collector," Int. J. Appl. Eng. Res., vol. 10, pp. 997–1002, 2015.

[19] A. S. Malik, A. Faisal, "Numerical investigation to enhance the solar collector performance using nano-encapsulated octadecane organic paraffin PCM," Energy Eng., vol. 122, no. 5, pp. 2099–2117, 2025.DOI: 10.32604/ee.2025.061569.

[20] P. K. Nagarajan, J. Subramani, S. Suyambazhahan, R. Sathyamurthy, "Nanofluids for solar collector applications: A Review," Energy Procedia, vol. 61, pp. 2416–2434, 2014.DOI: 10.1016/j.egypro.2014.12.017.

[21] M. Samykano, "Role of phase change materials in thermal energy storage: Potential, recent progress and technical challenges," Sustain. Energy Technol. Assessments, vol. 52, Art. no. 102234, 2022.DOI: 10.1016/j.seta.2022.102234.

[22] M. Ghofrani, N. N. Hosseini, "Optimizing hybrid renewable energy systems: A review," in Sustainable Energy, A. F. Zobaa, S. N. Afifi, and I. Pisica, Eds. Rijeka: IntechOpen, 2016. DOI: 10.5772/65971.

[23] R. Rawat, R. Lamba, S. C. Kaushik, "Thermodynamic study of solar photovoltaic energy conversion: An overview," Renew. Sustain. Energy Rev., vol. 71, pp. 630–638, 2017.DOI: 10.1016/j.rser.2016.12.089.

[24] N. S. B. Rukman et al., "Thermal efficiencies of photovoltaic thermal (PVT) with bi-fluid cooling system," Int. J. Heat Technol., vol. 40, no. 2, pp. 423–428, 2022.DOI: 10.18280/ijht.400209.

[25] A. Fudholi, M. Mustapha, "Mathematical modelling of bifacial photovoltaic-thermal (BPVT) collector with mirror reflector," Int. J. Renew. Energy Res., vol. 10, no. 2, pp. 654–662, 2020.DOI: 10.1016/j.csite.2023.102800.

[26] S. D. Prasetyo, A. R. Prabowo, Z. Arifin, "The use of a hybrid photovoltaic/thermal (PVT) collector system as a sustainable energy-harvest instrument in urban technology," Heliyon, vol. 9, no. 2, Art. no. e13390, 2023.DOI: 10.1016/j.heliyon.2023.e13390.

[27] A. L. Abdullah, S. Misha, N. Tamaldin, M. A. M. Rosli, F. A. Sachit, "Theoretical study and indoor experimental validation of performance of the new photovoltaic thermal solar collector (PVT) based water system," Case Stud. Therm. Eng., vol. 18, Art. no. 100595, 2020.DOI: 10.1016/j.csite.2020.100595.

[28] M. T. Ahmed, M. R. Rashel, M. Islam, A. K. M. K. Islam, M. Tlemcani, "Classification and parametric analysis of solar hybrid PVT system: A review," Energies, vol. 17, no. 3, Art. no. 588, 2024.

[29] S. Hamidi, "An experimental investigation on thermal efficiency of flat plate tube solar collector using nanofluid with solar tracking mechanism," Eng. Technol. J., vol. 37, no. 11A, pp. 475–487, 2019.DOI: 10.30684/etj.37.11A.5.

[30] S. Odeh, M. Behnia, G. Morrison, "Performance evaluation of solar thermal generation systems," Energy Convers. Manag., vol. 44, pp. 2425–2443, 2003.DOI: 10.1016/S0196-8904(03)00011-6.

[31] A. Cotorcea, M. Ristea, I. Visa, N. Florin, "CFD simulation of heat transfoer process for a solar thermla collector," Renewable Energy Sources and Clean Technologies, 2014. DOI: 10.5593/SGEM2014/B41/S17.012.

[32] S. O. Giwa, M. Sharifpur, M. H. Ahmadi, J. P. Meyer, "Magnetohydrodynamic convection behaviours of nanofluids in non-square enclosures: A comprehensive review," Math. Methods Appl. Sci., 2020. DOI: 10.1002/mma.6424.

[33] A. B. Boukadoum, A. Bourabaa, S. El Mokretar, H. Semai, A. Amari, "Numerical study of sensible thermal storage in solar collectors for air heating applications," in *2023 14th International Renewable Energy Congress (IREC)*, Sousse, Tunisia, 2023, pp. 1–6. DOI: 10.1109/IREC59750.2023.10389286.

[34] D. Y. Goswami, F. Kreith, Handbook of energy efficiency and renewable energy. Boca Raton, USA: Crc Press, 2007. DOI: 10.1201/9781420003482.

[35] H. Lugo-Granados, L. Canizalez-Dávalos, M. Picón-Núñez, "Thermohydraulic effects of scaling in flat plate solar collector networks," Chem. Eng. Trans., vol. 103, pp. 421–426, 2023.DOI: 10.3303/CET23103071.

[36] J. Shandal, Q. A. Abed, "A review on development of solar thermal flat plate collector," IOP Conf. Ser. Mater. Sci. Eng., vol. 928, no. 2, Art. no. 22051, 2020.DOI: 10.1088/1757-899X/928/2/022051.

[37] W. A. Fadzlin, M. Hasanuzzaman, N. A. Rahim, N. Amin, Z. Said, "Global challenges of current building-integrated solar water heating technologies and its prospects: A comprehensive review," Energies, vol. 15, no. 14, Art. no.5125, 2022.DOI: 10.3390/en15145125.

[38] A. Greco, E. Gundabattini, D. S. Gnanaraj, C. Masselli, “A comparative study on the performances of flat plate and evacuated tube collectors deployable in domestic solar water heating systems in different climate areas,” Climate, vol. 8, no. 6, Art. no.78, 2020.DOI: 10.3390/cli8060078.

[39] N. Amrizal, D. Chemisana, J. I. Rosell, “Hybrid photovoltaic–thermal solar collectors dynamic modeling,” Appl. Energy, vol. 101, pp. 797–807, 2013.DOI: 10.1016/j.apenergy.2012.08.020.

[40] R. P. M. Lotilla, “The efficacy of the anti-pollution legislation provisions of the 1982 Law of the Sea Convention: A view from South East Asia,” Int. Comp. Law Q., vol. 41, no. 1, pp. 137–151, 1992.DOI: 10.1093/iclqaj/41.1.137.

[41] D. Nath et al., “Internet of Things integrated with solar energy applications: a state-of-the-art review,” Environ. Dev. Sustain., vol. 26, pp. 24597–24652, 2023.DOI: 10.1007/s10668-023-03691-2.

[42] Y. Qiu, Y. Xu, Q. Li, J. Wang, Q. Wang, B. Liu, “Efficiency enhancement of a solar trough collector by combining solar and hot mirrors,” Appl. Energy, vol. 299, Art. no.117290, 2021.DOI: 10.1016/j.apenergy.2021.117290.

[43] R. Saidur, K. Y. Leong, H. A. Mohammed, “A review on applications and challenges of nanofluids,” Renew. Sustain. energy Rev., vol. 15, no. 3, pp. 1646–1668, 2011.DOI: 10.1016/j.rser.2010.11.035.

[44] R. F. Garcia, J. C. Carril, J. R. Gomez, M. R. Gomez, “Energy and entropy analysis of closed adiabatic expansion based trilateral cycles,” Energy Convers. Manag., vol. 119, pp. 49–59, 2016.DOI: 10.1016/j.enconman.2016.04.031.

[45] A. S. Kazsoki, B. Hartmann et al., “Methodology for the formulation of medium voltage representative networks in three DSO areas,” Renew. Energy Power Qual. J., vol. 18, no. 1, 2020.DOI: 10.24084/repqj18.275.

[46] P. Upadhyay, R. Kumar, “A ZVS-ZCS quadratic boost converter to utilize the energy of PV irrigation system for electric vehicle charging application,” Sol. Energy, vol. 206, pp. 106–119, 2020.DOI: 10.1016/j.solener.2020.05.068.

[47] S. Margoum, B. Hajji, S. Aneli, G. M. Tina, A. Gagliano, “Optimizing nanofluid hybrid solar collectors through artificial intelligence models,” Energies, vol. 17, no. 10, Art. no. 2307, 2024.DOI: 10.3390/en17102307.

[48] H. Gharaee, M. Erfanimatin, A. M. Bahman, “Machine learning development to predict the electrical efficiency of photovoltaic-thermal (PVT) collector systems,” Energy Convers. Manag., vol. 315, Art. no. 118808, 2024.DOI: 10.1016/j.enconman.2024.118808.

[49] L. M. Panggabean, “Four years Sukatani,‘the solar village Indonesia,” Sol. energy Mater. Sol. cells, vol. 35, pp. 387–394, 1994.DOI: 10.1016/0927-0248(94)90165-1.

[50] Y. Qiu, P. Zhang, Q. Li, Y. Zhang, W. Li, “A perfect selective metamaterial absorber for high-temperature solar energy harvesting,” Sol. Energy, vol. 230, pp. 1165–1174, 2021.DOI: 10.1016/j.solener.2021.11.034.

[51] [J. Lizana, R. Chacartegui, A. Barrios-Padura, J. M. Valverde, “Advances in thermal energy storage materials and their applications towards zero energy buildings: A critical review,” Appl. Energy, vol. 203, pp. 219–239, 2017.DOI: 10.1016/j.apenergy.2017.06.008.

[52] F. Cavallaro, L. Ciraolo, “Sustainability assessment of solar technologies based on linguistic information,” in Green Energy and Technology, vol. 129, 2013, pp. 3–25. DOI: 10.1007/978-1-4471-5143-2_1.

[53] A. Al-Mamun et al., “Design and development of a low cost solar energy system for the rural area,” in 2013 IEEE Conference on Systems, Process & Control (ICSPC), Kuala Lumpur, Malaysia, 2013, pp. 31–35. DOI: 10.1109/SPC.2013.6735098.

[54] B.-H. Truong, T. T. Van, T. V. Minh, T. D. Van, D. V. Ngoc, “Multiobjective optimization of solar flat plate collector using water cycle algorithm,” GMSARN Int J, vol. 16, pp. 106–114, 2022.[Online]. Available:https://gmsarnjournal.com/home/wp-content/uploads/2021/05/vol16no1-12.pdf.Accessed on: Aug. 5, 2025.

Aya A. Saad, born in Baghdad in 1995, holding B.Sc. in Energy Engineering from the American University of Iraq Sulaimaniyah in 2019, and MSc in Energy Engineering from University of Baghdad in 2023, current job is lecturer at the Middle Technical University of Baghdad/ Department of Artificial Intelligence Engineering Techniques. My research interest is on energy engineering, specifically renewable energies including solar and wind energies, and the production of hydrogen fuel from renewable energy resources.

Mahmood H. Khaleel, born in Baghdad in 1983, holds a B.Sc. in Refrigeration and Air Conditioning Engineering Techniques from the Northern Technical University in Kirkuk, Iraq (2007), and an M.Sc. in Thermal Engineering Techniques from the Middle Technical University in Baghdad, Iraq (2014). He is an assistant professor and currently serves as the head of the Mechanical Techniques Department at Kirkuk Technical College of Polytechnic, Northern Technical University, Kirkuk, Iraq. His main fields of specialization include building thermal performance, building envelope technologies, refrigeration systems, air-conditioning systems, solar collectors, and the utilization of clean and renewable energy sources.

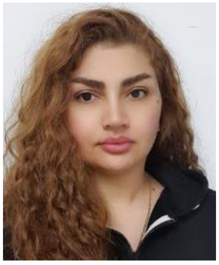

Aveen M. Abdulwahaab, born in 1986 in Kirkuk, holds a B.Sc. in Petroleum Engineering from Kirkuk University in Kirkuk, Iraq (2009), and an M.Sc. in Engineering Management from Gedik University in Istanbul, Turkey (2021). She is a teaching assistant and currently serves as the department head deputy in the Mechanical Techniques Department at Kirkuk Technical College of Polytechnic, Northern Technical University, Kirkuk, Iraq. Her main fields of specialization include petroleum engineering, engineering management.

Shereen E. Kaska, born in 1973 in Iraq, holds a B.Sc. in Mechanical Engineering (University of Technology, Baghdad, 2004) and an M.Sc. in Thermal Engineering (Technical College, Baghdad, 2012). She previously worked as a laboratory engineer and assistant lecturer in the fields of mechanical engineering, refrigeration and air conditioning, and fuel and energy engineering at technical colleges in Baghdad and Kirkuk. She also gained industrial experience as a mechanical engineer at Bluefiregas Company in Sulaymaniyah. Her main fields of interest include thermal engineering,